EARTHING PERFORMANCE OF TRANSMISSION LINE TOWERS

MOHAMMAD AHMEDA

Thesis submitted to Cardiff University in candidature for the degree of Doctor of Philosophy.

School of Engineering

Cardiff University

2012

ABSTRACT

This work is primarily concerned with the performance of tower base earthing systems under AC variable frequency and transient conditions. The work has involved the investigation into the performance of practical earthing systems including tests on a full-size 275kV transmission tower base and corresponding calculation and numerical simulations.

An extensive literature review of the performance of various types of electrodes under dc, ac and impulse currents is presented. In addition, a critical review of electrocution hazards from earthing systems was achieved.

A full 275 kV tower base, built for the purpose of earthing performance investigations, was used to evaluate the potentials around the tower footings and at the ground surface in the vicinity of the tower base.

Using low magnitude variable frequency AC current injection, it was demonstrated experimentally that the surface potential around the tower base falls rapidly which may result in high step and touch voltages. This behaviour is verified by using CEDEGS software. The ground potential of the concrete and soil at different depths has been investigated and revealed that the potentials generated decrease with depth. In addition, DC earth resistance are carried out on earthing system components using 61.8 rule and their seasonal variation recorded. To mitigate the touch and step voltages in the vicinity of tower base, a voltage control ring applied. The investigation was computed where several parameters including such as, number and depth of the rings, the soil resistivity and the frequency.

As for the low magnitude impulse current injection, it was demonstrated experimentally that the surface potential around the tower base falls rapidly along the four diagonal profiles which may result in high step and touch voltages. The ground potential distribution into the concrete and the soil at different depths under impulse energisation is investigated experimentally and revealed that the potentials generated decrease with depth. The current distributions into the tower base and one of the tower footings are also investigated. It was found that majority of the current dissipated into the footing.

The experimental work with high impulse current injections up to 9kA was achieved. Soil ionisation in the ground around the tower footings was obtained experimentally. It was observed that when a sufficiently high current is injected through one tower foot, a sudden increase in current together with a sudden fall of voltage is observed which is indicative of soil ionisation**.** Such phenomenon does not occur when the full tower base is tested, where the current through individual tower footings is smaller. The initial ionisation inception current was not constant but increased with the rate of rise of the applied current.

The concept of effective length of horizontal electrodes under impulse current energisation, used for the mitigation of rise of earth potentials around tower base, was demonstrated experimentally and the measured results compare well with empirical formula predictions. The voltage and current distributions along the horizontal electrode were investigated experimentally and verified by the simulation where a close agreement obtained between the measured and computed voltages.

LIST OF PUBLICATION

M. Ahmeda, N. Harid, H. Griffiths, and A. Haddad: ‘‘Earth surface potential in the vicinity of transmission tower under low frequency and transient currents’’ 17th International Symposium on High Voltage Engineering (ISH), Hannover, Germany, August 22-26, 2011.

M. Ahmeda, N. Ullah, N. Harid, H. Griffiths and A. Haddad: ‘‘Current and Voltage Distribution in a Horizontal Earth Electrode under Impulse Conditions’’ 44th Universities Power Engineering Conference (UPEC), Glasgow, UK, 1-4 September 2009.

N. Harid, N. Ullah, **M. Ahmeda**, H. Griffiths and A. Haddad: ‘‘Experimental Evaluation of Potential Rise and Step and Touch Voltages at High Voltage Towers under Lightning Impulse’’ 16th International Symposium on High Voltage Engineering (ISH), pp. 1651-1656, Cape town South Africa, 24-28 August 2009.

A. Haddad, H. Griffiths, **M. Ahmeda** and N. Harid: ‘‘Experimental Investigation of the Impulse Characteristics of Practical Ground Electrodes Systems’’ International Conference on High Voltage Engineering and Application (ICHVE), New Orleans USA, 11-14 October 2010.

Elmghairbi A., **Ahmeda M.**, Harid, N., Griffiths H., and Haddad, A.: “Current and Voltage Distribution in Horizontal Earth Electrodes and a Technique to Increase Effective Length," 17th International Symposium on High Voltage Engineering (ISH), Hannover, Germany, August 22-26, 2011.

N. Harid, H. Griffiths, N. Ullah, **M. Ahmeda** and A. Haddad: ‘‘Experimental Investigation of Impulse Characteristics of Transmission Line Tower Footings’’ Journal of Lightning Research, 2012, 4, (Suppl 1: M6) 36-44.

Harid N, **Ahmeda M**, Griffiths H, and Haddad A: ‘Experimental Investigation of The Impulse Characteristics of Practical Ground Electrode Systems’, High Voltage Engineering Journal, Vol. 37, No. 11, 11500-11505, November 30 (2011), ISSN 1003-6520.

Elmghairbi, A., **Ahmeda M**., Harid N., Griffiths, H., Haddad, A.: ‘‘Technique to increase the effective length of practical earth electrodes: Simulation and field test results’’ Electric Power Systems Research, Vol. 94, pp. 99-105, January 2013.

M. Ahmeda, N. Ullah, N. Harid, H. Griffiths, and A. Haddad: ‘‘Effective length of a horizontal electrode under impulse conditions’’, 3rd UHVNet Colloquium on Technologies for Future High Voltage Infrastructure, University of Manchester, 19& 20 January 2010.

M. Ahmeda, N. Harid, H. Griffiths, and A. Haddad: ‘‘Performance of tower footing earth resistance under high impulse current’’, 3th UHVnet Colloquium Winchester, UK, January 18th-19th 2011.

DECLARATION

This work has not previously been accepted in substance for any degree and is not concurrently submitted in candidature for any degree.

Signed …… (candidate) Date ….....

STATEMENT 1

This thesis is being submitted in partial fulfilment of the requirements for the degree of PhD

Signed …… (candidate) Date ….....

STATEMENT 2

This thesis is the result of my own work/investigation, except where otherwise stated. Other sources are acknowledged by explicit references.

Signed …… (candidate) Date ….....

STATEMENT 3

I hereby give consent for my thesis, if accepted, to be available for photocopying and for inter-library loan, and for the title and summary to be made available to outside organisations.

Signed …… (candidate) Date ….....

STATEMENT 4

I hereby give consent for my thesis, if accepted, to be available for photocopying and for inter-library loans after expiry of a bar on access previously approved by the Graduate Development Committee.

Signed …… (candidate) Date ….....

ACKNOWLEDGEMENTS

First, I would like to give thanks to Allah (My Lord) the almighty, the all great without whom I could not have completed this educational endeavour.

I would like to extend special thanks and gratitude to my supervisors Professor A. Haddad and Dr. Huw Griffiths. Thanks for their inspiration, guidance, encouragement and invaluable advice throughout my stay at Cardiff University. Also, I am deeply grateful to Dr. Noureddine Harid, for all his expert insight which he has shared with me and supported me during my study.

In addition, I would like to express my gratitude to my colleague, the former researcher in the High Voltage Group, Dr Dongsheng Guo for his support.

Grateful acknowledgment of my funding and support must be made to my home country Libya and the Libyan Ministry of Higher Education. Also, my sincere thanks go to the Libyan Cultural Bureau in London and all of its members for their advice and support.

My most sincere gratitude and appreciation go to my wife for her patience, continuous encouragement and support over the past difficult years. Thanks as well to Allah for his gifts; my beloved kids ‘‘Safiyah’’, ‘‘Ammar’’, ‘‘Ghyaheb’’ and ‘‘Suhayel’’.

I am deeply indebted to my parents, sisters and brothers who gave me continuous support and encouragement throughout my life.

TABLE OF CONTENTS

CHAPTER ONE

Introduction

1.1 Introduction

During a lightning strike, the electrical power system is subjected to a very large current with a fast rise time. Lightning strikes to tall structures such as transmission towers can produce voltages so high that insulation fails and electrical equipment can be destroyed. Such strikes produce an earth potential rise in the surrounding soil which can endanger persons who happened to there at the time. Thus, high voltage transmission and distribution systems require lightning protection and insulation co-ordination schemes to protect personnel and power system equipment from danger and damage. A fundamental factor that determines the effectiveness of these schemes is an efficient connection to earth. For safety, an appropriate design of earthing system limits the step and touch voltages to be within the values permitted by national and international standards.

In this thesis, the performance of a full scale 275kV transmission tower base is investigated under DC, AC variable frequency and low and high impulse voltages. The behaviour of an enhanced earthing system in the form of a horizontal electrode under low impulse current is also studied.

In this chapter, a brief introduction of the role of earthing systems and components is provided together with a resume of key earthing standards.

1.2 Earthing systems

The earthing system of electricity substations and transmission lines is required to ensure (i) electrical safety for persons working within or near the substation or in proximity of transmission towers and (ii) reduce damage to equipment while reducing

disturbances to power system operations. Though high voltage transmission and distribution systems are protected from lightning strikes, the effectiveness of the lightning protection depends very much on its connection to earth.

1.2.1 Earthing system components

The earthing system at transmission level comprises two main components: the earth grid and an extension of the earth electrode system which is determined by the transmission tower lines [1.1]. There are outdoor transmission substation earthing grids which can encompass large areas reaching more than 30,000 m^2, while indoor substations are more compact with smaller earth grids. The earth wire (shielding wire) forms an important part in transmission earthing systems, quite apart from its main role in shielding the conductor wire against lightning strikes. This earth connection is provided by bonding the earth wire to every latticed steel tower carrying the transmission line, and at both ends of the transmission line, the terminals of the earth wire is connected to the main earthing system (earthing grid) of each of the substations at the beginning and end of the transmission line. Thereby, the earthing grids and the tower footings along the transmission line interconnected by the earth wire form an extended earthing system. Consequently, the earth impedance of the substations' earthing grids and any earth impedance along the transmission path will be reduced by virtue of this interconnection. As a result, this will decrease the step and touch voltages in the vicinity of the transmission line towers. However, any earth potential rise in the main earthing system of the substation will be transferred to the transmission towers.

The earth wire has a significant influence on the overhead line outage rate. Where there is no earth wire, single circuit steel lines have an outage rate due to lightning strikes about 29.8 outages per hundred miles of line per year [1.2]. When one earth wire is connected the outage rate falls to 9.8, and in the case of two earth wires, the outage becomes 7.0, as shown in Figure 1.1.

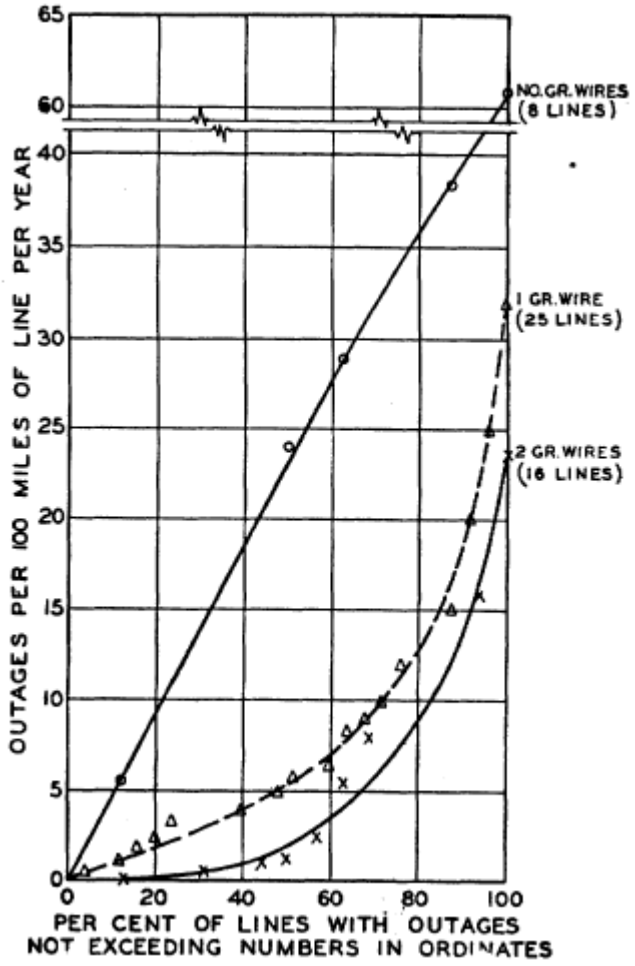

Figure 1.1: Effect of earth wire on lightning outages of 165-110 kV single circuit lines (Reproduced from [1.2])

1.2.2 Standards applicable to earthing systems

Standards applicable to earthing systems have been examined for earthing requirements under fast transients and their recommendations are presented.

BS EN 50522:2008 Earthing of Power Installations Exceeding 1 kV AC [1.3], recommends measures to reduce interference to control and protection devices caused by high frequency current as it is dissipated into earthing systems. Such measures include (i) current paths being of as low an inductance as possible, (ii) earth electrodes and earthing conductors to be meshed, (iii) the more likely a high transient current is to

occur at the location, the higher the density of the earthing mat mesh in that area, and (iv) connections to the earthing system should be as short a length as possible.

BS EN 62305-3:2011 Code of Practice for Protection of Structures against Lightning [1.4] recommends that the designing of earthing system intended to protect against lightning strikes should have an earthing resistance not exceeding 10Ω. This seems to be the only transient earthing system design limit specified and has been adopted by most of electricity companies in the UK. Although the standard recognises the importance of the inductive effects, the design limit appears to be based on resistance. The standard also recommends that the down conductor should be directly routed to the earth electrode.

The UK earthing standard EA TS 41-24 Guidelines for the Design, Installation, Testing and Maintenance of Main Earthing Systems in Substations [1.5], recognises that '*equipment such as surge arresters and CVTs are more likely to pass high frequency current due to the low impedance they present to steep fronted surges*' and suggests that '*unless a low impedance earth connection is provided, the effectiveness of the surge arrester could be impaired*'.

This standard also recommends that the connection from the equipment to earth should be '*as short, and as free from changes in direction, as is practicable*' and that the effectiveness of the arrester can be improved by connecting it to an earth electrode in the immediate vicinity, for example an earth rod (normally 5m long).

Similarly, BS 7430:1998 Code of Practice for Protective Earthing of Electrical Installations [1.6] is in conformity with EA TS 41-24 that the earth connection should be as close as practicable to a surge arrester and as straight and short as possible.

IEEE Std. 80-2000, the IEEE Guide for Safety in AC Substation Grounding [1.7], does not give direct guidance on the design of earthing for systems likely to be subjected to

lightning strikes but, in common with other relevant standards, it does recommend that surge arresters should '*always be provided with a reliable low resistance ground connection*' and have as '*short and direct a path to the grounding system as practical'*. It also suggests the design of grounding systems be carried out according to the principles used in the design of power frequency systems which, it considers, will '*provide a high degree of protection against steep wave front surges*'. The standard recognises the capacity of the human body to withstand high magnitude transient currents for very short periods.

1.3 Lightning parameter data

Figure 1.2 presents the cumulative frequency distribution of lightning current amplitudes. The data was obtained from lightning discharges (26 positive and 101 negative lightning strokes) onto a tower on Mount San Salvatore, Switzerland [1.8]. For negative strokes lightning current, the maximum recorded magnitude was in excess of 80 kA and the mean was 30 kA. The corresponding values for positive stroke currents are significantly higher with a maximum that exceeds 250 kA and a mean value of 35 kA. However, positive stroke ground flashes form less than 10% of the total while negative strokes represent more than 90% [1.9]. The lightning impulse is generally specified by two parameters, the value of the peak current, $I_{p,}$ and the impulse shape which is characterized by rise time (front time also called rise time) and tail time. The rise time is defined as the time which takes it the current from zero to its peak value and the tail time is defined as the time which current takes to decay to its half peak value. Tail time is invariably longer than rise time.

The standard lightning impulse shape is generally expressed by the peak current (or voltage) and by the front and tail times T1 and T2 written as T1/T2. T1 and T2 are usually measured in μs, in which case T1/T2 is unit less. Typical lightning impulse

curves are shown in Figure 1.3. T1 is the current rises from zero to its peak value (I_p), afterward it is decay to its half value ($I_P/2$) in time T2.

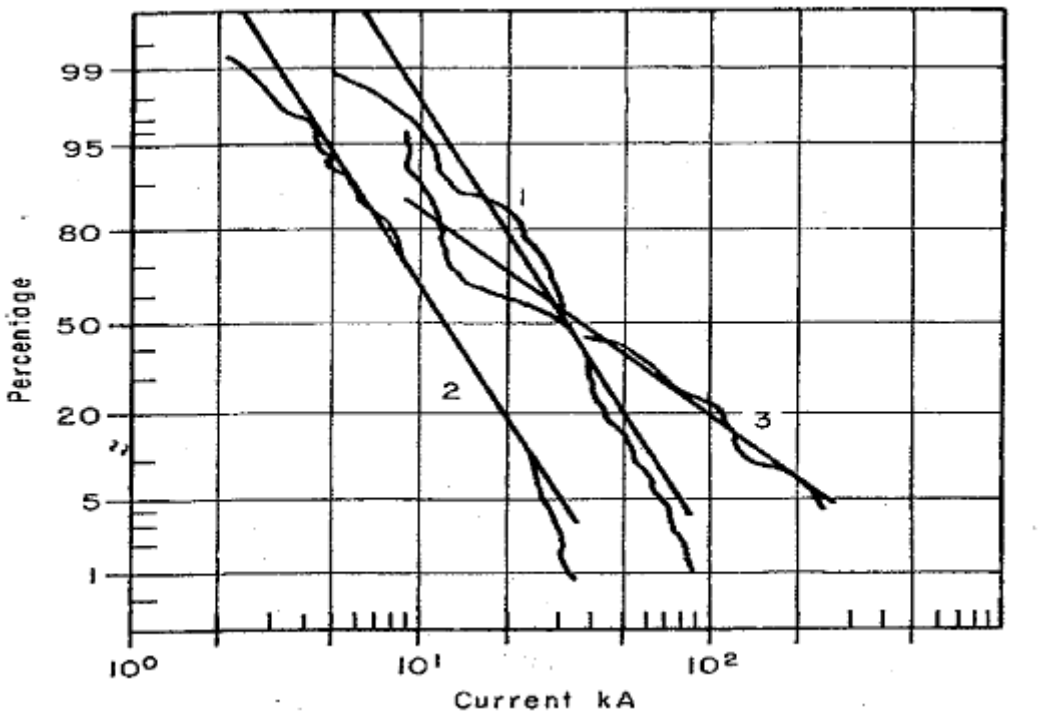

Figure 1.2: Cumulative frequency distribution of lightning current amplitudes

1. Negative first strokes 2. Negative subsequent strokes 3. Positive strokes [1.8]

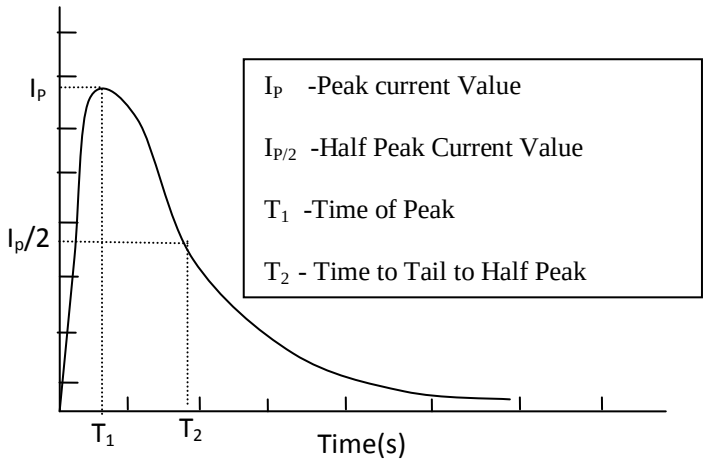

Figure 1.3: Standard lightning impulse voltage (T_1=1.2μs, T_2=50μs)

For lightning impulse current (T_1=8μs, T_2=20μs)

1.4 Aims and objects

The aims and objectives of this thesis are;

1. To investigate the ground surface potential in the vicinity of the base of a 275kV high voltage transmission line tower energised by an AC power current. The effect of profile route and influence of the frequency on the current also to be investigated, and the field results to be verified by the results obtained using a computer model (Chapter 3).

2. To examine the frequency response of potential of a tower footing and surrounding soil by mean of probes embedded at different depths in the tower footing and surrounding soil (Chapter 3).

3. To compare the measured and computed DC earthing resistance of the earthing system and observe the influence of seasonal variation on that system for a whole year (Chapter 3).

4. To investigate the ground surface potential in proximity of the base of the high voltage transmission line tower when energised by low impulse currents at different rise times. These results to be compared with resultant ac profiles (Chapter 4).

5. To investigate the vital role of the tower footing in dissipating impulse currents of different impulse shapes (Chapter 4).

6. To examine the transient response of the earthing system as measured by the set of probes buried in and around the tower base for different rise times (Chapter 4).

7. To perform high voltage impulse tests on a full scale transmission tower base and its footing and examine non-linear behaviour for high amplitude impulse currents (Chapter 5).

8. To carry out an impulse test of low amplitude on a horizontal electrode and investigate the effective length, injection point and rise time (Chapter 6).

1.5 Contribution of this research

1. Contribution to a better understanding of earth surface potential, especially close to the tower footing and in the vicinity of the tower base.

2. Developed a better understanding of the ground potential at different depths in the concrete base of the tower footing and soil for low amplitude impulses and AC sources.

3. Provided a better understanding of the role of the tower footing in the dissipation of impulse current, and the influence of the rise time on that dissipation.

4. Improved knowledge of effects of different parameters, such as rise time and injection point on horizontal electrode buried in soil of low resistivity.

5. Contributed to the design and construction of a high magnitude impulse test facility to study the transient performance of transmission tower base earthing systems.

1.6 Thesis layout

The thesis is divided into seven chapters.

Chapter one: the introduction chapter set the scene and introduces the thesis.

Chapter two: gives an overview of the literature including: tower footing earthing systems under high impulse current, and effect of the tower footing resistance on the reliability of the high voltage transmission network.

Chapter three: presents an experimental investigation of the earth surface potential in the proximity of the transmission line tower base when the tower is energized with AC

current at low and higher frequencies. Further, the frequency response of the tower legs at different depths of the concrete footing and the adjacent soil has been measured. The DC earth resistance of the components of the electrode under test and the current return electrode were measured and then compared with their calculated and computed values. In addition, these DC earth resistances were monitored over a one year period to investigate the influence of seasonal variation on their magnitudes. In this chapter, a new proposed method to mitigate the step and touch voltages was investigated. The effects of parameters such as depth and number of rings around the leg on the mitigation were examined.

Chapter four: deals with the safety performance evaluation of the tower base. In this chapter, field measurements of the earth surface potential along the four diagonal profiles was measured under impulse energisation, and the resulting step and touch voltage were computed. These voltages were measured using two methods; direct and indirect. A number of factors which have influence on these hazardous voltages were investigated, such as the injection point and rise time. The impulse current distribution amongst the legs was studied. The potential at a different depths of the in tower footing and the surrounding soil were also measured under impulse conditions.

Chapter five: involves Investigation of earthing characteristics of a tower base under high impulse current. In this section, high impulse current is injected into the tower base and its individual legs, and the impulse resistance was determined as a function current. The soil ionisation phenomenon around the tower legs was demonstrated on the recorded voltage and current traces.

Chapter six: addresses the enhancement of the tower base earthing system by mean of installing counterpoise near the installation. A number of parameters that have an effect on the performance of the electrode under impulse condition have been

investigated. These include the rise time of the impulse current and the injection point. Furthermore, voltage and current attenuation and distortion during propagation along the electrode were examined. The effective length of the electrode was determined and found to match the length calculated by using empirical formulae.

Chapter seven: gives the overall conclusions and makes suggestions for further work.

CHAPTER TWO: TOWER FOOTING EARTH RESISTANCE UNDER HIGH IMPULSE CURRENTS: LITERATURE REVIEW

2.1 Introduction

Earthing systems for high voltage transmission lines are important for the security of the power system and safety of personal in and around the structures associated with the transmission lines. The effects of lightning strikes on the performance of transmission lines are influenced by factors such as route location, shielding, insulation and tower footing resistance. In this chapter, the investigation focuses on the performance of earth electrodes and, in particular, the tower footing under high impulse currents.

When a lightning strike terminates on an overhead ground wire (OHGW), a high impulse current will flow to the ground, transmitted through the tower footing. Such currents produce a high impulse voltage on the tower structure and nearby ground surface with respect to a remote earth, and this may endanger the life of people close to the line or its towers. To reduce outage rates and exposure of human life to danger due to lightning strikes, the tower footing impedance must be kept to a minimum. In cases where the tower footing resistance is higher than the standards value (10Ω or less), additional measures may be considered to lower the resistance. Such measures may include use of a vertical or horizontal electrode or even using a special resistance reducing material to achieve a lower tower footing resistance [2.1].

In this chapter, a review of the published literature on tower footing earthing under high impulse currents is carried out. The review is extended to consider simple vertical and horizontal earth electrodes, as these are sometimes used as supplementary electrodes to enhance tower earthing. Laboratory test results on small-scale earth

electrodes are reviewed which lead to the formation of models describing the electrodes' non-linear behaviour under high current impulses. Finally, electrical safety is considered with reference to international standards.

2.2 Description of general practical earth electrodes

An earthing system refers to metallic wire(s) of various geometrical shapes and sizes acting as electrodes and buried in the soil. The commonly used earthing electrodes are the vertical rod, horizontal electrode, ring electrode and earthing grid as illustrated in Figure 2.1. The vertical rod is the simplest and most economical form of earth electrode. It is highly effective for small installations especially when the bottom layer of soil penetrated has a lower resistivity than that of the upper strata [2.2]. However, in general, the resistance of a single rod is not sufficiently low, and it is necessary to use a number of rods connected in parallel. For large electrical installations, however, the horizontal earth is mainly used and is normally buried at a shallow or moderate depth where there is no significant effect of the depth on the earth resistance if the electrode length is more than about 10m and 50m in the case of transient and steady state conditions respectively [2.3]. The ring electrode is a type of horizontal earthing grid and is sometimes used as peripheral earth conductors around structures e.g. wind turbines. To obtain even lower earth resistance, the horizontal earth grid can be augmented with vertical rods which are normally inserted at the periphery of the earthing grid.

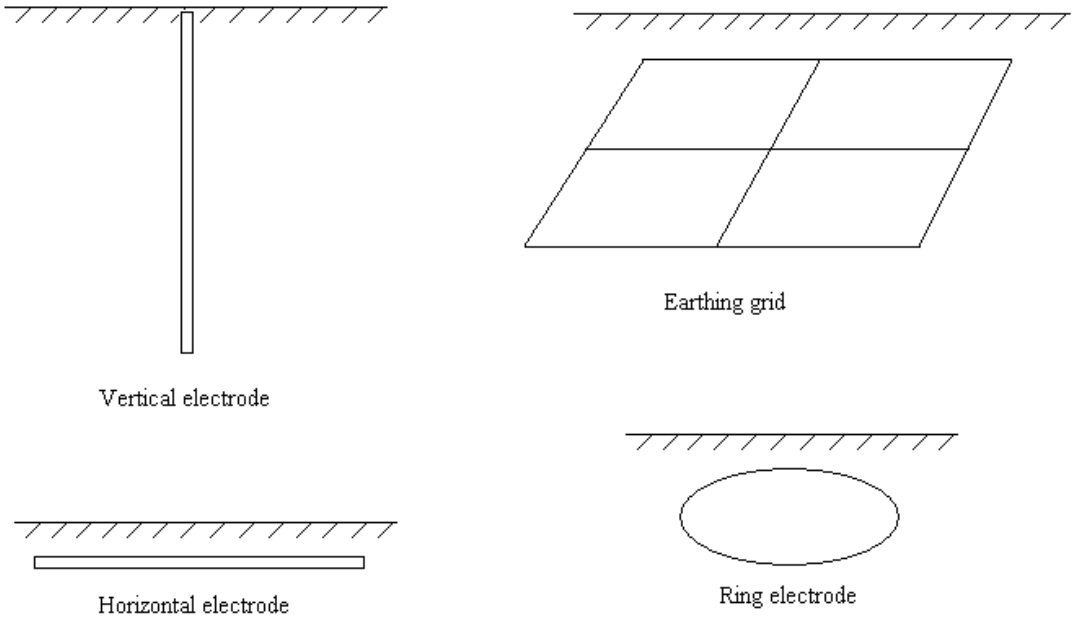

Figure 2.1: Different types of earth electrodes

2.3 Transmission line structure earthing systems

The earthing systems of transmission line structures fall into two categories; (i) the tower footing which includes the metallic part of the tower surrounded by its concrete foundation in soil, and (ii) supplementary earthing electrodes such as vertical rods, etc. which are selected depending on the conditions and nature of the earth around each individual transmission tower.

2.3.1 Tower footing earthing and performance under high current impulse

If a transmission line tower is struck by lightning and the potential of the tower is raised above the voltage impulse strength of the insulator string, a flashover will occur from the tower to a phase conductor which may lead to serious outages of the system. This type of flashover is called backflashover. The electrical resistance of the tower footing is a significant parameter affecting backflashover voltage across the insulator(s) in transmission systems (IEEE Std. 1313.2-1999) [2.4]. According to IEEE Std. 1243-1997 [2.5], the individual performance of each tower is important in

determining the lightning performance of the transmission line. ‘‘*The overall performance of an entire transmission line is influenced by the individual performance of the towers rather than by the average performance of all the towers together’’* [2.6].

To investigate the effect of the average tower footing resistance on the lightning outage rate, a study carried out by Whitehead [2.7] on a 500 kV transmission line showed that the outage rate was approximately proportional to the average tower footing resistance as can be seen in Figure 2.2. For an average tower footing resistance of 30 Ω, the lightning outage rate was 1.0 per 100 km per year. The findings confirmed results obtained by Chisholm and Chow [2.8]. The influence of the tower footing resistance on the lightning fault rate was also studied by Tomohiro et al. [2.9], as shown Figure 2.3, where it is shown that the lightning fault rate increased with the increase in tower footing resistance.

As a result of the important effect that the tower footing resistance has on the lightning performance of transmissions lines, a design standard for footing resistance against system voltage, isokeraunic level and importance of the line has been published by a Japanese power company [2.9], as shown in Table 2.1. In many other countries, the target level of tower footing resistance is taken as 10Ω or less to give protection from backflashover, and it is considered more economical than adding extra insulation to increase the capacity of the insulators to withstand lightning strikes [2.10-2.12]. However, the higher footing resistance, for example 50Ω, may cause outage rate of the shielded transmission line higher than that of the unshielded one [2.13].

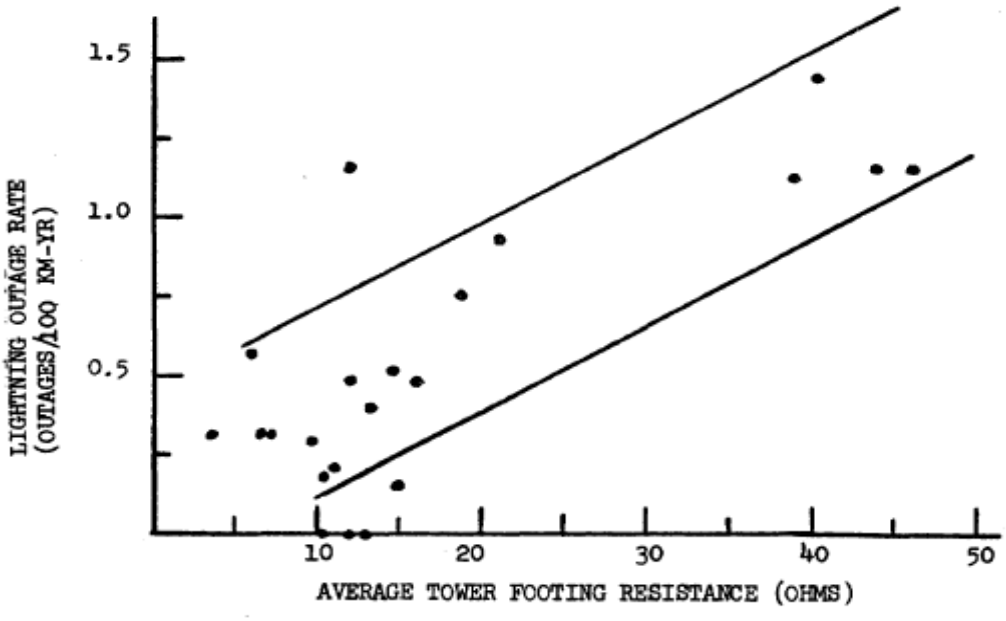

Figure 2.2: Lightning outage rate vs tower footing resistance for a 500 kV line

(Reproduced from reference [2.7])

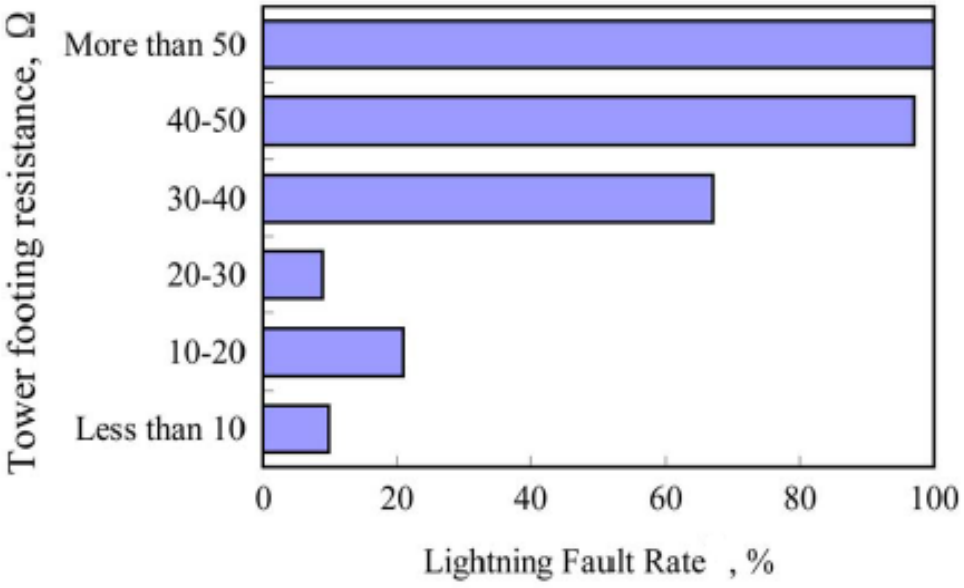

Figure 2.3: Tower footing resistance vs. lightning fault rate

(Reproduced from reference [2.9])

Table 2.1: Design values of tower footing resistance (Reproduced from reference [2.9])

System voltage, kV	Design value of tower footing resistance, Ω		
	I	II	III
500	13		
275	13		
154	15		20
77	13		20
33	20		

IKL: Isokeraunic level, thunder storm days per year

I : IKL more than 30 and important lines.

II : IKL from 20 to 30.

III : IKL less than 20.

In the literature, very few experimental field studies are reported on tower footing impulse resistance under high impulse currents. A limited number of investigations have been conducted on a full scale tower footing and tower base [2.11, 2.14 and 2.15]. Kosztaluk et al. [2.15] carried out a series of field tests to determine the transient behaviour of tower footing earthing resistances. A current of 24 kA with rise time in the range between 3 and 12 μs was injected into the tower footing. The dynamic resistance was defined as $R_i = \frac{v(t)}{i(t)}$. Figure 2.4 shows the measured dynamic resistance as a function of the impulse current, the numbers on the curves refer to the time in μs. The resistance was close to low frequency resistance as the current first starts to rise at 1μs. However, after approximately 1μs when the current exceeds 2 kA, which corresponds to a current density on the electrode of 0.3 A/cm^2, the decrease in the impulse resistance was noticeable, and it was attributed to soil ionization. After the current reach the maximum value, a slight decrease in the resistance observed which

was attributed to the tail of the current.

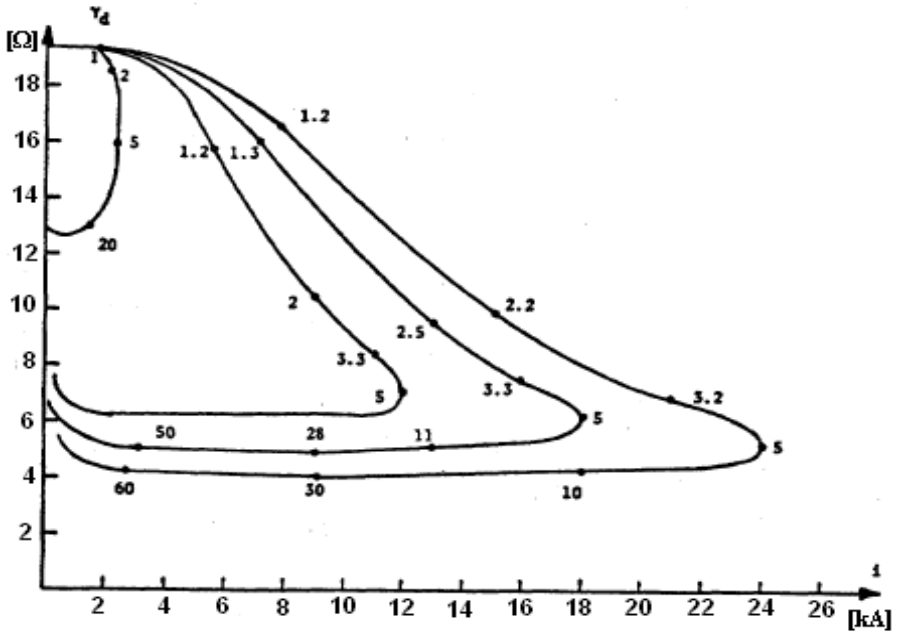

Figure 2.4: Dynamic resistance against impulse current. (Reproduced fromreference [2.14])

Similar tests were performed by Makoto et al. [2.11] investigating the impulse impedance of a tower footing base and other electrodes including rods, a grounding sheet and crow's foot electrode under high impulse current. The tower footing base was erected in soil with resistivity of 250Ωm. A high impulse current of up to 30 kA with front time 3.5μs was injected into the test electrodes. The impulse resistance was defined as crest voltage to crest current. In this investigation, two cases were considered; (i) the current was applied to the independent earthing system (no additional earthing arrangements) (ii) the tower footing was connected to different auxiliary electrode systems one at a time. Figure 2.5 shows the results of the tests on the individual electrodes. It can be seen that as the impulse current increases, the impulse resistance decreases. The relationship is most pronounced for the short rod. In the case of the tower base, the decrease is marginal. Figure 2.6 shows that adding electrodes to the tower base reduces the impulse resistance. However, for the combined systems the resistance is practically constant with impulse current, and this

was explained by the fact that the current density on the lateral surface of the tower footing base was less than the critical ionization level of the soil.

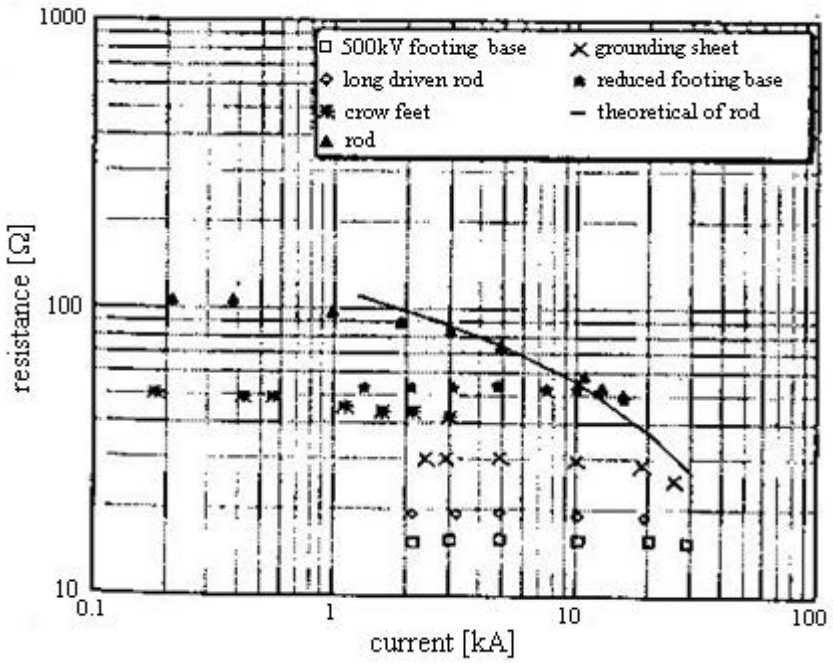

Figure 2.5: Current-dependent characteristics of resistances for various earthing electrodes. (Reproduced from reference [2.11])

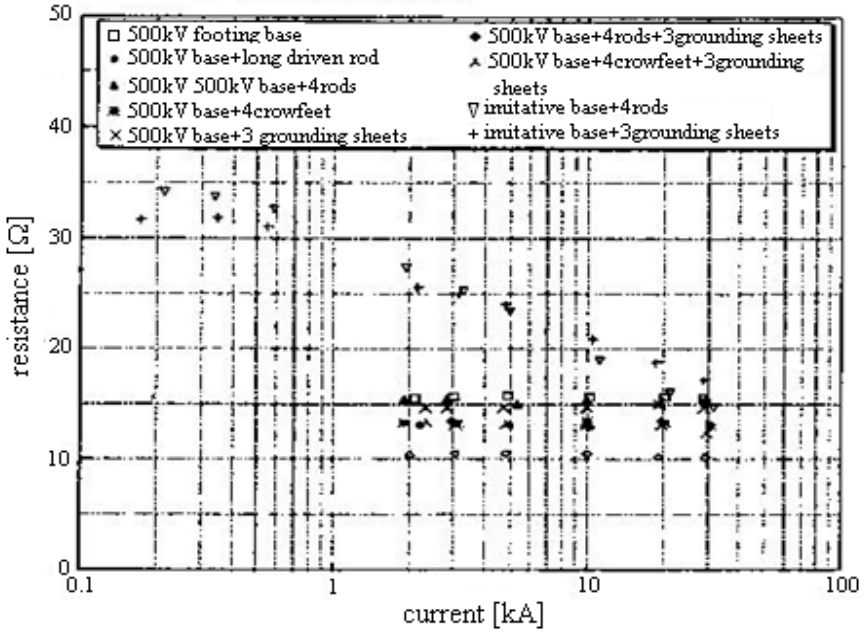

Figure 2.6: Current-dependent characteristics of resistances for composite grounding systems. (Reproduced from reference [2.11])

Harid et al. [2.15] carried out an experimental field tests to investigate the lightning characteristics of an actual 275 kV tower base (without the above-ground structure being erected) in soil of low resistivity at Cardiff University's test site in Llanrumney, Cardiff. A high current of the order of 2.75 kA with fast rise time of 1/5 μs was injected into the base. The authors found that the measured impulse resistance decreased with increasing surge current; the impulse resistance reduced by 20% as the current is increased by approximately five-folds, as can be seen in Figure 2.7. This reduction was attributed to non-linear conduction phenomena occurring in the soil (thermal conduction and/or soil ionization).

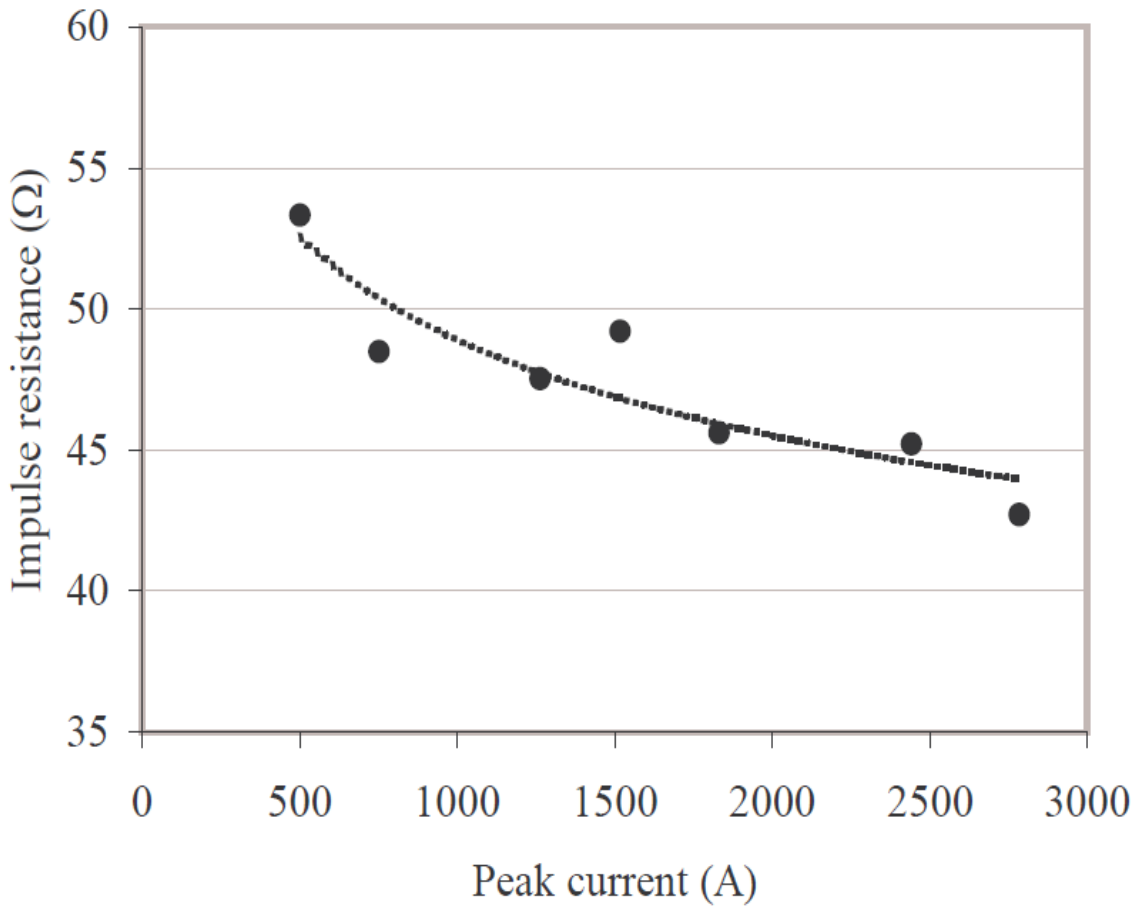

Figure 2.7: Variation of impulse resistance with applied peak current for rise time of 0.2 μs. (Reproduced from reference [2.15])

According to the IEEE Working Group on Modelling Guidelines for Fast Front Transients [2.16], the current dependent tower footing resistance (R_T) can be estimated using:

$$R_T = \frac{R_0}{\sqrt{1+\frac{I}{I_g}}} \qquad (1)$$

Where:

R_0 is the low frequency tower footing resistance, Ω

I is the lightning current through the footing resistance, A

I_g is the soil ionisation current and is given by Equation 2:

$$I_g = \frac{1}{2\pi}\frac{E_0\rho}{R_0^2} \quad \text{A} \qquad (2)$$

Where:

ρ is the soil resistivity, Ω.m, and E_0 is the soil ionisation gradient, kV/m.

2.3.2 Supplemental earthing electrodes

When the transmission line tower is erected in sand or rocky terrain of high soil resistivity, the tower footing may require supplemental electrodes to reduce the overall earth resistance. In such circumstances, various kinds of earthing electrodes have been used. The most commonly used electrodes for this purpose are the vertical and horizontal electrodes.

2.3.2.1 Vertical earth electrodes

The vertical earth electrodes are the most common type of electrodes in earthing systems and usually the most economic to install. To reach a low earth resistance in high resistivity soil (ρ>300 Ωm), long vertical electrodes can be used and are driven to a few meters depth when soil conditions permit. Experimental field tests have been conducted on the vertical electrode to investigate its behaviour when subjected to transient conditions [2.17-2.20].

The phenomenon of reduction in the electrode's earth resistance under lightning current was first reported by Towne [2.17] nearly one hundred years ago. During his work, in the Lightning Arrester Engineering Department within the General Electric Company, he deduced from previously inconclusive tests that the majority of the results for earthing resistance of arresters had similar trends under high impulse current conditions; the impulse resistance was considerably less than the low frequency resistance; between 34% to 80% of the measured steady state resistance. The impulse resistance was found to decrease with increasing current magnitude, and this was attributed to a soil ionisation process. The impulse resistance was defined by Towne as peak voltage to peak current and was shown to be dependent on current magnitude, rise time as well as earth electrode configuration and the soil's electrical properties.

A series of high impulse current tests were conducted on four vertical earth electrodes in different soils (shale, clay, gravel, sand) in late 1939-early 1940 by Bellaschi [2.18]. The current range was from 2 kA to 8 kA and rise times varied from 6μs to 13μs. Again, the impulse resistance was obtained as the ratio of peak voltage to peak current and, in agreement with previous work, a fall of impulse resistance with increase of current was observed. The impulse resistance dropped below the low frequency resistance, and this characteristics was attributed to the soil's electrical breakdown. It

was confirmed that the size, shape and the arrangement of the earth electrode(s) were factors contributing to the earthing characteristics. The impulse resistance was determined for both positive and negative polarities; the difference was found to be very small.

Bellashi and his colleagues followed their initial investigation by an extensive study on soil breakdown for different soils and electrode arrangements [2.19]. The current magnitude was increased to 15.5 kA with impulse shapes ranging from 6/13μs to 20/120μs. In this study, impulse characteristic curves were obtained for different types of ground electrode and soil. The apparent resistance was defined as the peak impulse voltage to the peak impulse current. The curves were expressed as a ratio of apparent impulse resistance to 60-cycle resistance as a function of peak applied current. The influence of soil type and dimension of the electrode on the impulse characteristics of the ground is shown in Figure 2.8. It was found that the percentage decrease in resistance with current was greater for electrodes embedded in high resistivity soil than in low resistivity soil and the two electrodes of different length such as electrode P (29ft) and F (10ft), which were imbedded in the clay with same soil resistivity, the higher fall off in the impulse characteristic curve was noted in electrode F due to higher current intensity on its surface. Figure 2.9 shows a comparison between individual's rods and four parallel rods (representing the four footings of tower base) dug in clay. It was observed that the percentage decrease in resistance was less when the electrodes were connected in parallel.

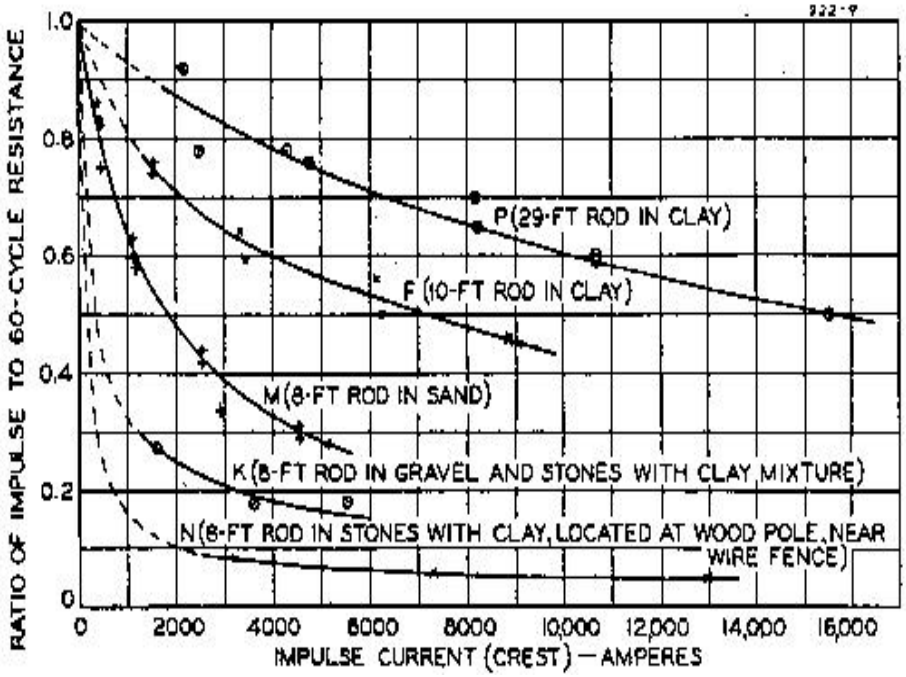

Figure 2.8: Impulse characteristics for various soils and grounds. (Reproduced from reference [2.19]).

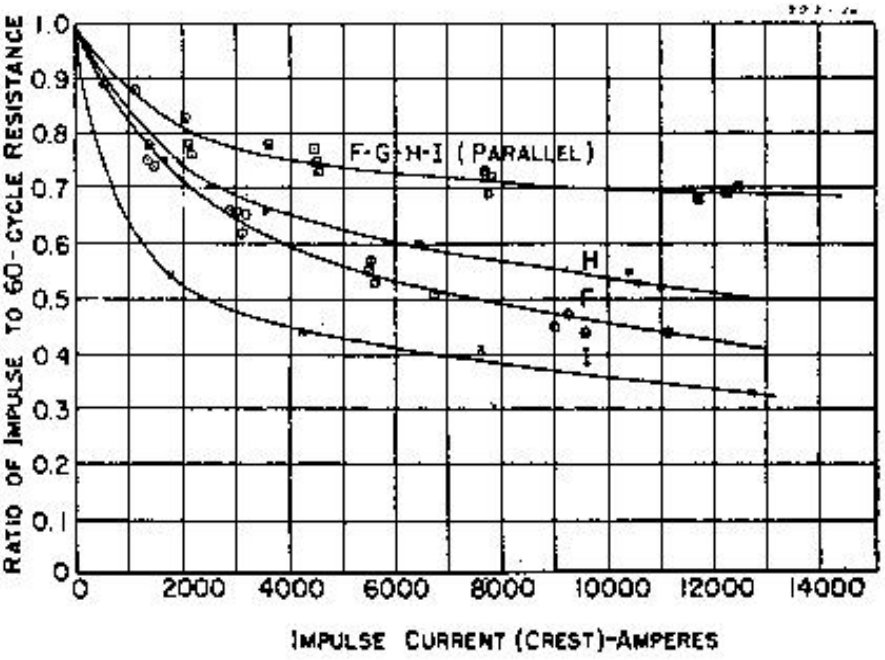

Figure 2.9: Impulse characteristics for single and parallel vertical earthing electrodes. Rods F, G, H and I of 10ft length embedded in clay soil (Reproduced from reference [2.19]).

Similar tests were conducted by Liew and Darveniza [2.20] on different arrangements of vertical electrodes to investigate the influence of high lightning current on impulse resistance. The tests were performed on electrodes in a sand and gravel mix soil with a resistivity of 5000 Ωcm. Impulse currents up to 13 kA magnitude and with rise times in the range 6μs -18μs were applied. The impulse resistance was defined as the instantaneous ratio of voltage to current with time. A significant reduction of earth impulse resistances with increasing impulse current was observed and attributed to ionization processes in the soil. The authors found that the electrode impulse resistance was dependent on rise time.

Vainer and Floru [2.21] carried out tests to show influence of depth on the performance of a number of earth electrodes, placed in a ground over a period of 11 years. These experiments were conducted with high discharging currents of up to 12 kA. Figure 2.10 shows the non-linear volt-ampere characteristics of vertical earth electrodes buried to depths of 3.6m, 38m and 44.2m. In particular, the rise time of the current was longer for deeper driven electrodes. This was ascribed to an inductive effect.

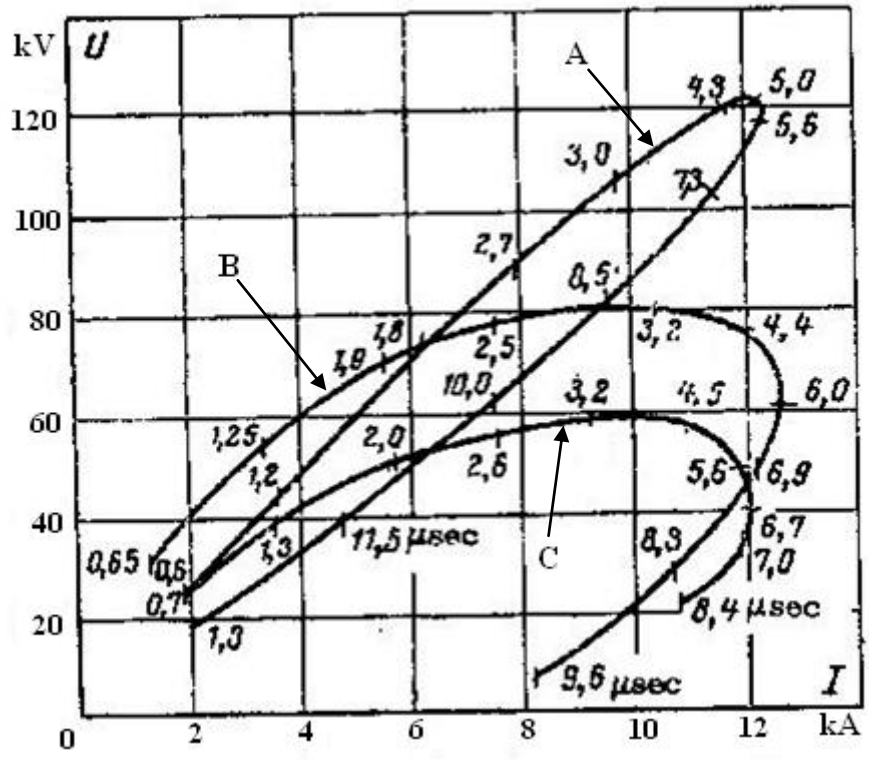

Figure 2.10: V-I characteristics for deep earth electrodes.

Electrode A- 3.6m Electrode B- 38m Electrode C- 44.2m (Reproduced from reference [2.21]).

2.3.2.2 Horizontal earth electrodes

Horizontal earth electrodes can be used to reduce the earth resistance of a substation or a tower base footing. The horizontal earth electrode applied to tower lines may be continuous or non-continuous and laid between towers and parallel to the line conductors. Alternatively, conductors may be laid perpendicular to the transmission line and enhanced arrangements using 4 point, 6 point or 8 point star can be used.

Tests were carried out by Bewley [2.22] on 0.25 ft diameter horizontal steel wire electrodes of lengths 200, 500 and 925 ft buried to a depth of 1 foot in earth of low soil resistivity. Impulse voltages of 15 kV and 90 kV were applied with front times less than 1.5 µs. The impulse impedance was found to be defined as the ratio of

instantaneous voltage and current, starting at a magnitude equal to the surge impedance and ending at a value equal to the leakage resistance. The author observed that the effective length of the horizontal electrode was no more than 200 ft as a result that no further benefit was obtained by extending electrodes beyond this length.

Geri and Garbagnati [2.23] conducted field tests on a horizontal steel earth electrode to investigate its impulse response. Impulse currents with magnitudes from 5 to 26 kA and a rise time of 2.5 μs were injected into the 5m long electrode. The impulse resistance was observed to decrease as the current peak increased, and this reduction was attributed to the non-linear ionisation phenomenon on the soil.

Similar investigations on three different lengths of horizontal electrodes buried in soil with a resistivity of 200 Ωm were carried out by Sekioka et al. [2.24]. Currents up to 40 kA magnitude with rise times less than 4 μs were injected into the electrodes of different lengths; 8.1 m, 17 m and 34 m. From Figure 2.11, it is clear that the impulse resistance of the shortest electrode of 8.1m has the greatest current dependency, although lower resistance values were obtained with the longer electrodes.

To clarify the dependency of impulse resistance of the horizontal electrode under high impulse current, Sonoda et al. [2.25] used impulse voltages up to 3 MV and impulse currents up to 32.2 kA on two horizontal electrodes of lengths 5 m and 20 m, and two horizontal square grids of areas 10 m^2 (grid I) and 20 m^2 (grid II). The two horizontal electrodes showed strong current dependency where this behaviour was attributed to soil ionization, as shown in Figure 2.12a. However, in the case of the earth grids, the current dependence on impulse resistance was not so pronounced, see Figure 2.12b. These findings are in agreement with those of Sekioka [2.24].

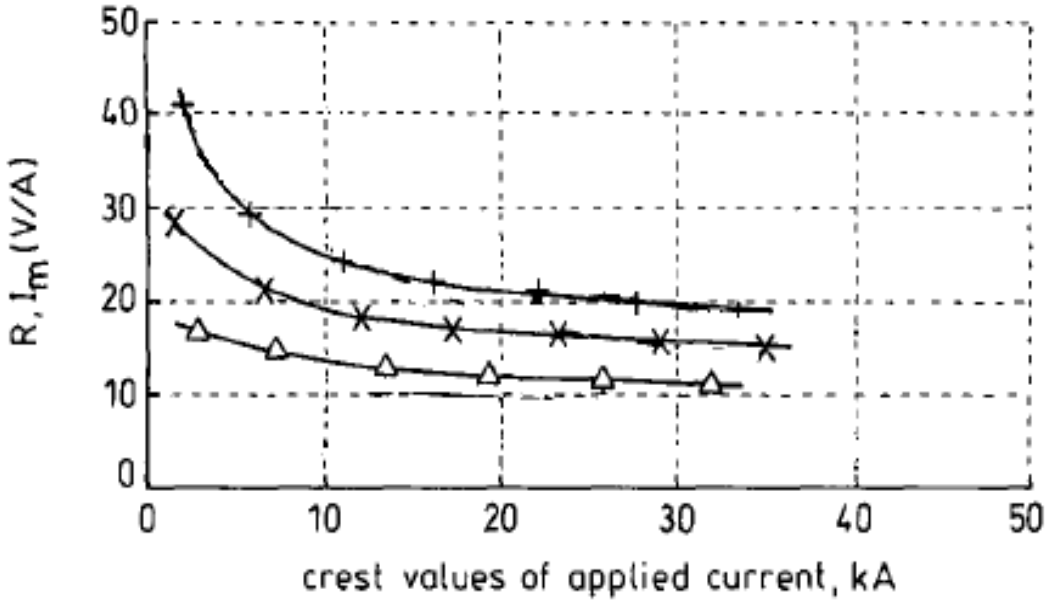

Figure 2.11: Earth resistance characteristics vs crest current. + 8.1 m horizontal electrode, x 17 m horizontal electrode,△17m buried conductor. (Reproduced from reference [2.24])

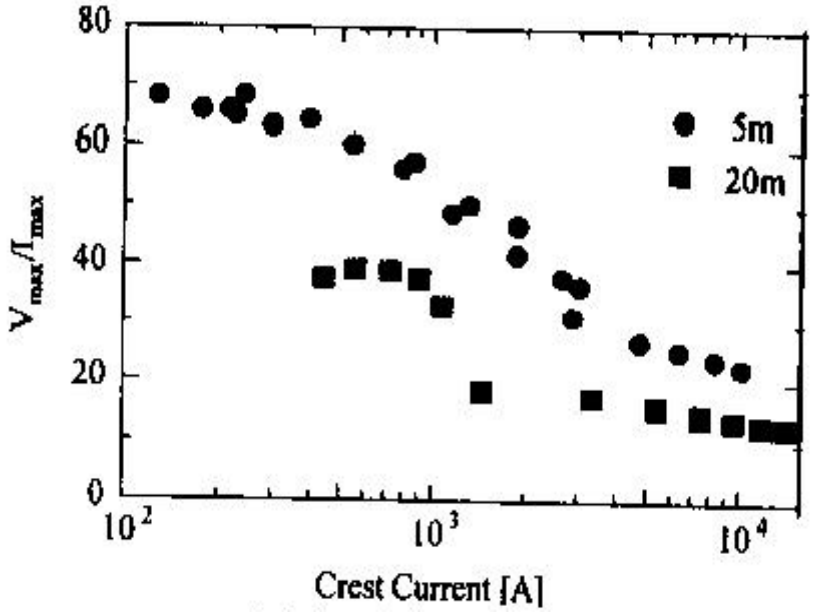

(a)

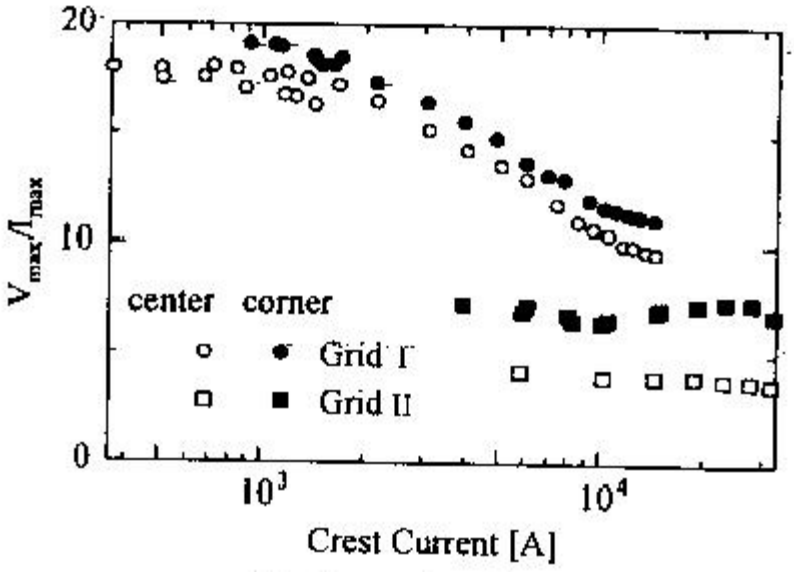

(b)

Figure 2.12: Impulse resistance as a function of peak current. (a) horizontal electrode, (b) earthing grid. (Reproduced from reference [2.25]).

2.3.3 Laboratory test on earth electrode systems

To predict the behaviour of real earth electrodes under lightning strikes, laboratory tests on reduced scale models are carried out in similar conditions to those found in the field. Such tests are a practical alternative solution to field tests to investigate earthing systems. In addition, in laboratory tests, the soil resistivity value can be more easily controlled. Hemispherical and cylindrical test cells are commonly used in high voltage laboratories for different kinds of electrodes.

2.3.3.1 Hemispherical test geometry

Many published studies [2.26-2.28] have adopted hemispherical test geometries in investigating soil characteristics under high impulse currents in the laboratory. Berger in 1946 [2.26] conducted laboratory tests on spherical earth electrodes half buried in the soil in a hemispherical tank. The tests were carried out on different sizes of electrodes and in various types of soil. The impulse current was in the range from 3 kA

to 11.4 kA with a front time 3-30 μs. It was observed that in a lower current range the impulse resistance was linear with current and equivalent to the resistance measured at 60 Hz. At high currents, the v-i curves exhibited hysteresis due to non-linear soil behaviour, see Figure 2.13. The figure shows that when the current density exceeds the critical value on the electrode surface the electrode earth resistance starts to decrease due to soil ionisation. Figure 2.14 shows the impulse resistance as a function of time for different current magnitudes where the higher decrease in the resistance observed with higher current magnitude.

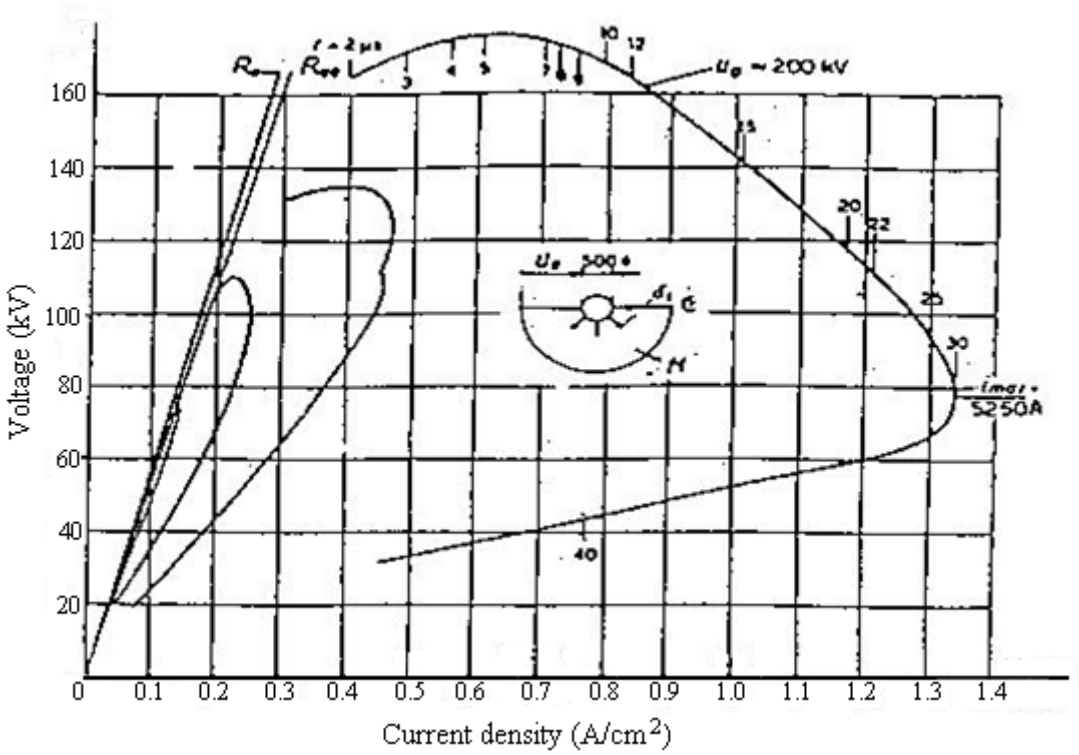

Figure 2.13: Voltage-current density to a mixture of sand, gravel and humus. (Reproduced from reference [2.26])

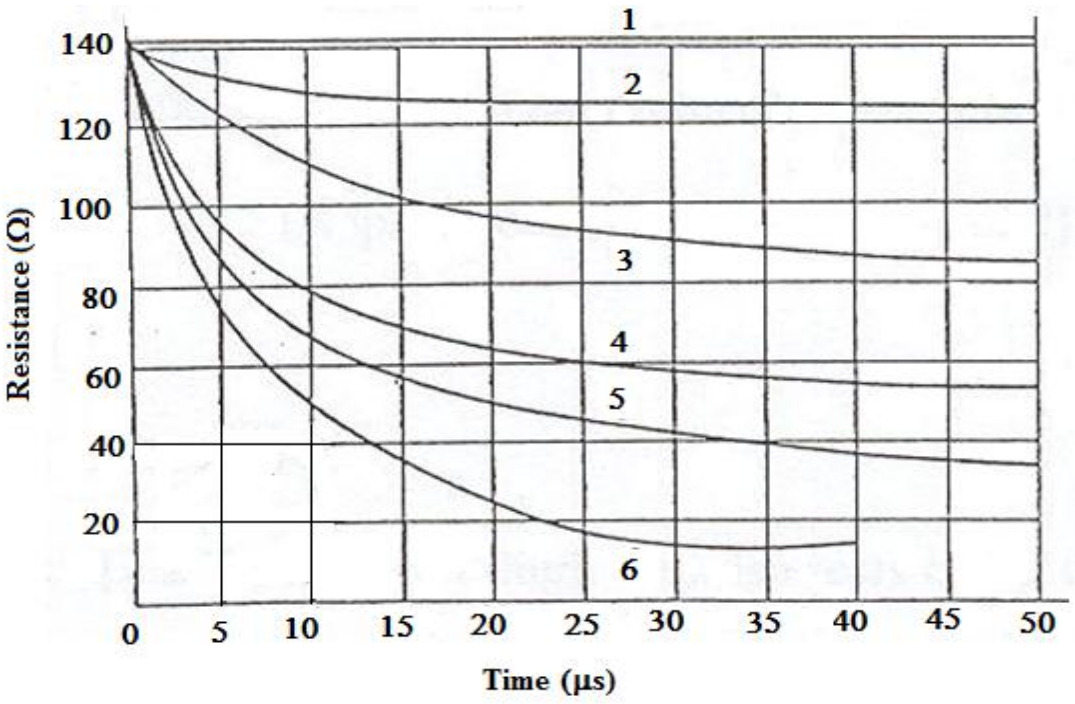

1, i_{max}=250A 2, i_{max}=560A 3, i_{max}=975A

4, i_{max}=1800A 5, i_{max}=2400A 6, i_{max}=5300A

Figure 2.14: Impulse resistance as a function of time for different current magnitudes.

(Reproduced from reference [2.26])

A similar experimental setup was adopted by Petropoulos [2.27] to estimate cell voltage breakdown. Tests were carried out with impulse voltages up to 52kV. They were conducted on plain spherical electrodes and spherical electrodes with spikes embedded in soil. The impulse resistance was found to decrease with increasing impulse voltage. This reduction was always larger for the spherical electrodes with spikes than for the plain one. The decrease in resistance for the spiked electrodes started decreasing from the lowest voltage level used while the resistance of the plain electrode began to fall only after the voltage had exceeded the so-called 'starting voltage' of 16 kV as shown in Figure 2.15. The 'starting gradient' in these tests was 8.3kV/cm. The high field intensity at the end of the points, which was present at very low voltages accounted for the immediate reduction in impulse resistance for the spiked electrodes.

Similarly, Cotton [2.28] adopted hemispherical model in order to describe the process of soil ionisation. A 75cm diameter inverted hemisphere was constructed out of concrete with two hemispherical electrodes 2.4 cm and 5 cm in diameter. A ten stage impulse generator with a maximum output voltage of 2 MV and current that reached 3.25 kA with rise times of between 4 and 10μs was used. The results showed a decrease in the instantaneous resistance of the earthing system as the applied voltage increases, except in the case of the lowest applied voltage which did not appear to cause any soil ionisation, see Figure 2.16. However, similar levels of voltages applied to the larger hemispherical electrode gave no evidence of significant soil ionisation since the electric field levels at the surface of the electrode were lower than the critical soil ionisation gradient, which was estimated to be 450kV/m. No significant difference was observed between fast and slow rise times on the impulse resistance.

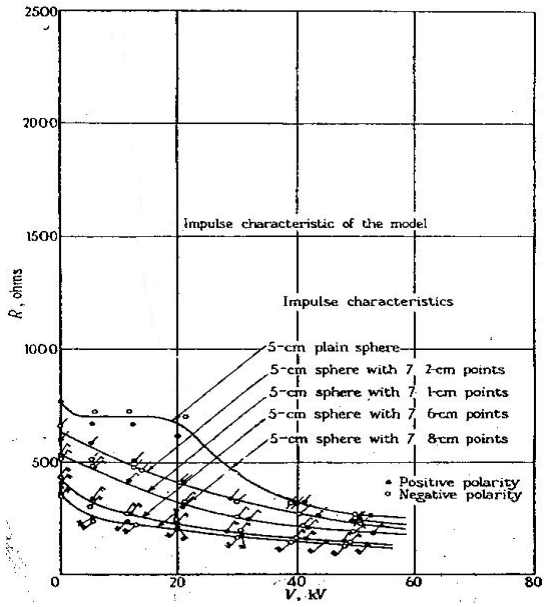

Figure 2.15: Impulse impedance vs applied voltage for plain and sphere with points electrodes. (Reproduced from reference [2.27])

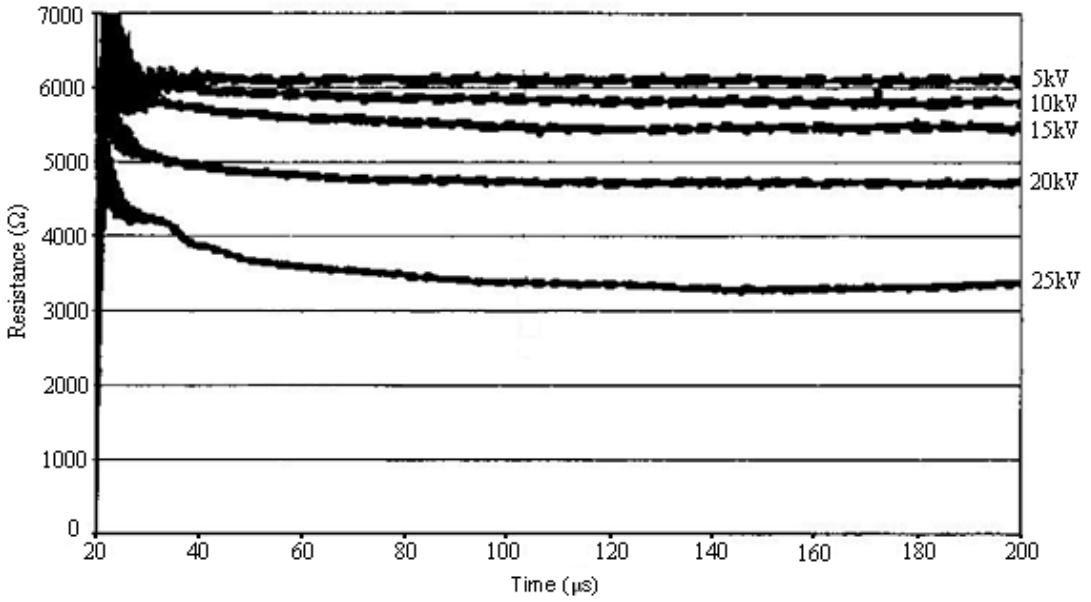

Figure 2.16: Resistance of electrode system under long tail impulses.

(Reproduced from reference [2.28]).

2.3.3.2 Cylindrical electrode geometry

This test cell geometry consists of a vertical rod placed into a coaxial cylinder test cell. A simple expression for the resistance for this test geometry with homogenous soil is [2.29]:

$$R = \frac{\rho}{2\pi l} \ln\left(\frac{r_{out}}{r_{in}}\right) \tag{2.3}$$

Where r_{in} is the radius of the central conductor, r_{out} is outer cylinder radius and l is effective length of the cylinder.

Cabrera et al. [2.29] conducted impulse tests on sands with different grain sizes using a coaxial cylindrical test cell with an outer cylinder radius of diameter 100mm and a central conductor radius of 2.5mm. Test voltages were applied up to 34.7kV with rise times less than 6 μs and sample with sand of resistivity 6.5 kΩm as shown in Figure 2.17. The arc resistance was the parameter used to describe the ionization process,

which was measured as the voltage drop per unit current at the second peak of the current and occurring at about 1 μs after breakdown. The study found that the arc resistance was higher for sand composed of small grains than sand with large grains. This was attributed to the smaller particles having a larger contact area between the arc channel and the particles. It was also observed that, with large grain sand, the breakdown voltage with positive polarity was lower than that for negative voltage. However, in fine grain sand, negative breakdown voltages were always lower than or equal to the positive ones.

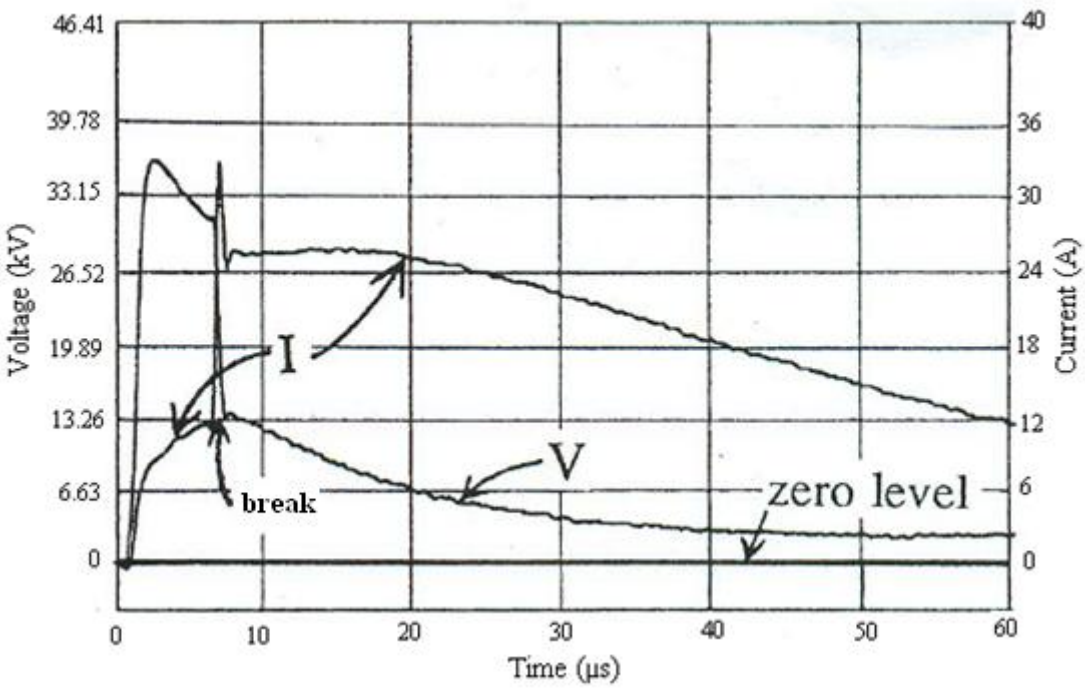

Figure 2.17: Lightning impulses in fine sample above the break down voltage (Reproduced from reference [2.29])

2.4 Soil conduction mechanisms

Much research has taken place into understanding the mechanisms by which the arc in soil breakdown is initiate. Thermal processes and soil ionisation are two possible explanations that have emerged to explain the initiation of the process.

2.4.1 Thermal process

During the thermal process, when the current starts to flow into the soil, the water film which coats the soil particles plays a primary role. Due to the consequent heating effect, the temperature of the water and soil increases and the resistivity of the bulk of the soil decreases. The thermal process in soils could be enhanced by ionic conduction which will depend on the amount of water and types of salts and composites present, as described by Schon [2.30].

Snowden and Erler [2.31] suggest that vapourization could occur if the water content is heated sufficiently. This vaporization causing its electrical resistance to increase greatly and this leads to breakdown. In 1982, Vanlint and Erler [2.32] investigated breakdown in earth samples under high electric field stress using coaxial test rigs. They found that there was an initiation delay before a streamer is formed at the high field electrode. This delay decreased with increasing electrode area and/or increasing electric field. Srisakot et al. [2.33] showed that the delay also decreases with the increase of the magnitude of the applied voltage and water content, according to an experimental study based on fast impulses on a hemispherical test cell filled with sand. These authors proposed that two distinct conduction phases could be identified; the first associated with thermal effects and the second due to soil ionisation.

2.4.2 Soil ionization

In most publications, the initiation of the breakdown process in the soil under impulse test is considered to be mainly due to electrical considerations. This initiation begins when the electric field magnitude in the voids between the soil grains becomes high enough to ionize the air in the voids [2.34-2.36]. Snowden et al. [2.34] conducted AC parallel plate tests to measure the relative dielectric constant for wet and dry soils. It

was found that at 50 Hz, the relative dielectric constant for the soil with 4% water content was higher than for the dry soil and depends on frequency.

A series of tests on samples of very fine sand filling a cylindrical chamber were carried out by Flanagan et al. [2.35] using impulse sources of up to 100 kV with a rise time of 17 ns. It was observed that when the sample was immersed in sulphur hexafluoride (SF6), the breakdown threshold field was in the order of 2.5 times higher than the threshold field for air at one atmosphere. The threshold field for dry soil was found to be approximately 2.5 times the threshold field for soil with a moisture content of 4.5%. Further experiments were conducted by Leadon et al. [2.36] on relatively coarse sand to prove that the arc initiation process is due to ionisation of gas between soil particles. When the air voids in the soil were filled with SF6 instead of air, the break down required a higher electric field. Mousa [2.37] performed a critical review of the most important studies published on impulse resistance and its drop when subjected to high currents due to lightning strikes. He concluded that the ionisation of the air trapped between the soil particles is responsible for the resistance reduction.

A recent laboratory experiments investigation to study the ionisation phenomenon in soil was carried out by Nor et al. [2.38]. In these experiments, a hemispherical electrode placed in a hemispherical container and medium grain soil used. When high impulse voltage applied, two peaks of current occur which reflects the non linear behaviour. The first peak attributed to the thermal effects while the second one is thought to be caused by soil ionisation.

Liew and Darveniza [2.20] proposed a dynamic model of impulse characteristics of concentrated earths to explain the behaviour of earth electrode subjected to high impulse current. The model, consisting of three zones: ‘no-ionisation, ionisation and de-ionisation zones’. The no-ionisation zone represents a condition of constant

resistivity with increasing current density and the ionisation zone represents the condition when the current exceeds the critical current density where the break down occur together with resistivity decreases exponentially and the deionisation zone represents the soil resistivity increase toward its steady state value exponentially as illustrated in Figure 2.18. An elemental shell model consisting of layers was used to simulate the three zones for a single rod, as shown in Figure 2.19. In this model, the non-linear soil resistivity parameter is represented as a function of time and radius of the electrode. An extension of Liew and Darveniza's model was introduced to account for the impulse behaviour of concentrated earth over a much wider range of current densities by Junping et al. [2.39]. Here, besides the three regions in Liew and Darveniza's model, a new region called the sparking region was introduced, see Figure 2.20. In the sparking region, it is proposed that another form of breakdown called sparking breakdown occurs, when current density exceeds sparking density current, Js, and the resistivity in this region drops to zero.

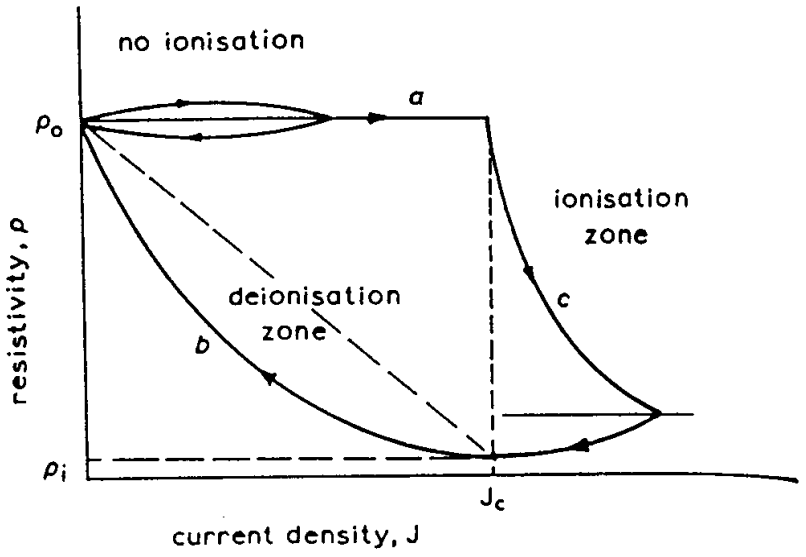

Figure 2.18: Resistivity profiles in dynamic-impulse resistance model.

(Reproduced from reference [2.20])

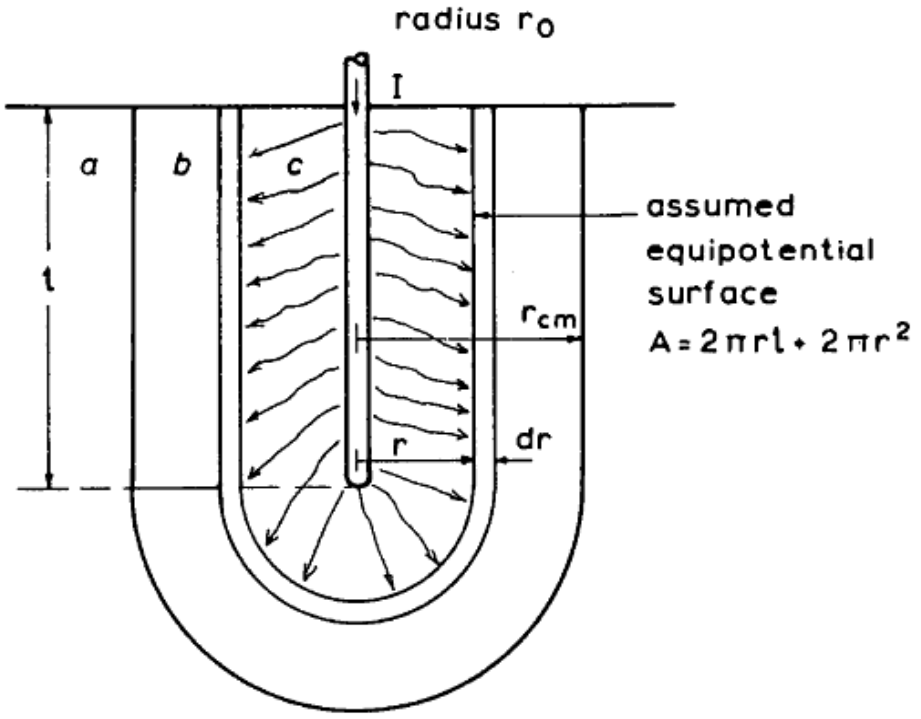

Figure 2.19: Simplified model for the resistance of a single driven rod

(Reproduced from reference [2.20])

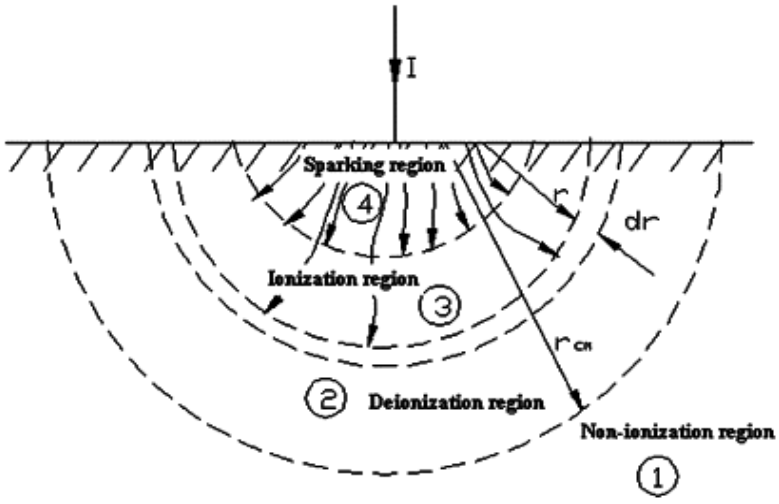

Figure 2.20: Hemispherical model for a direct sparking connection

(Reproduced from reference [2.39])

Almeida and Barros [2.40] proposed a soil ionization model based on the variable resistivity approach. In their computed results, the ionisation occurs in the soil surrounding the earth electrode, as the electric field at the electrode surface shows a value higher than the critical field and the area around the electrode is equifield region. Figure 2.21 shows the impulse resistance as a function of high impulse current obtained with the proposed model. The model shows that the resistance is constant until reach the critical current (1000A), after the critical point the breakdown occurs. Above this value of current, the electrode exhibited a decrease in soil resistivity.This model is in close agreement with Liew and Darvenizas' model [2.20].

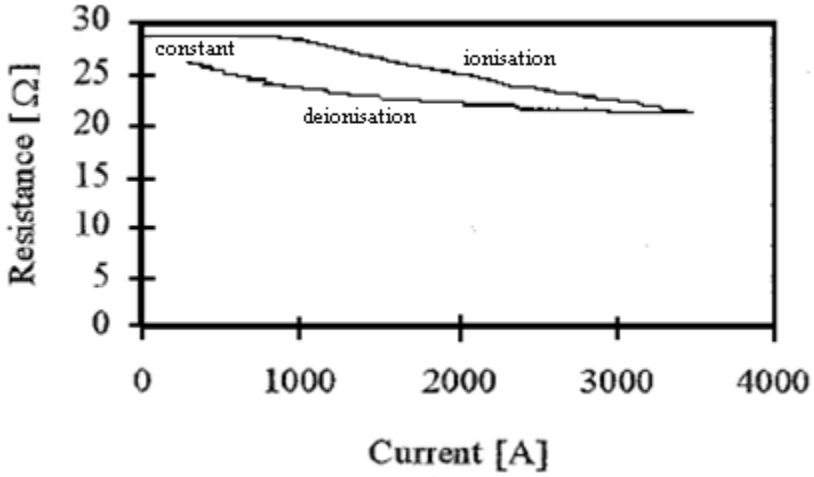

Figure 2.21: Impulse resistance as a function of current

(Reproduced from reference [2.40])

2.4.3 Evaluation of critical electric field intensity (E_c)

A key parameter in representing the ionization threshold level in soils is the critical field intensity, E_c. It is the product of the measured soil resistivity (ρ) and current density (J) at the electrode surface assuming uniform current distribution, where $E_c=\rho J$. This parameter has been measured by observing the breakdown of soil between two electrodes [2.41], but it depends upon the size and shape of the electrodes as well as the composition of the soil. A large number of studies [2.26, 2.27, 2.28, 2.39, 2.19,

2.20, 2.42 and 2.43] were carried out to determine the value of E_c and these studies produced values in the range of 1.3 to 18.5 kV/cm. E_c is generally taken as the amplitude at the instant when the i-v characteristic starts to become a nonlinear.

Berger [2.26] carried out an impulse tests on spherical electrodes in several types of soil, the critical field intensity was found to be in the range of 2.5 to 3kV/cm. However, a new general estimation curve for predicting the impulse impedance of concentrated earth electrodes in several types of soil has been published by Oettle [2.42]. The critical soil ionisation gradient was found to be between 6 and 18.5 kV/cm for wet and dry soil respectively.

For similar hemispherical electrodes, Petropoulous [2.27] also found the critical electric field as a function of dimensions of the electrode and the vessel and the 'starting voltage' which was the point at which the impulse resistance of the electrode starts to decrease, e.g. as soon as the breakdown occurs under its steady state resistance. E_c was calculated as 8.3kV/cm. The hemispherical electrodes, of diameter 5cm and 3cm were placed in a hemispherical copper vessel, radius 30cm, and filled with sifted soil with grains of maximum diameter 2 mm, the water content was 5.9% and resistivity was 132 Ωm. When spikes of 20, 40, 60, 80 mm length were added to hemispherical electrodes there was a strong electric field at the ends of the spikes, which was present even for very low voltages. In this case the drop in resistance begins with the lowest voltage used, while in the case of plain sphere the resistance began to fall only after the voltage exceeded the starting-voltage value.

Loboda and Scuka [2.43], based on their own experimental studies, considered that streamers played an influential role in the soil ionisation process and demonstrated that the calculated values of Ec could be up to 70% higher than those determined by assuming a uniform and perfectly conducting ionized zone.

Laboratory experiments of high voltage impulse test were performed to determine the critical value of the electric field in the soil by Srisakot et al. [2.44]. The test cell consists of a hemispherical container filled with medium soil grain with different soil water contents and the active hemispherical electrode placed in the middle. The critical electric field was 5.6kV/cm. This critical value was taken when the second current peak started to occur. This peak is due to soil ionisation. There is some time delay since the second current peak initiated in which the delay decrease with increasing the applied voltage and water contents.

2.5 Transmission Line Earthing Considerations

As described in section 2.1, the safety of people in and around transmission lines is important due to the presence of potentially danger voltages under fault conditions. In this section, the tolerated limits of body current are reviewed under typical electrocution scenarios.

2.5.1 Tolerable Body Currents

The effects of an electric current passing through the vital parts of a human body depend upon several factors, the most important being the magnitude, shock duration, frequency and physical condition of the victim. The worst outcome of the flow the electric current through the body is an induced heart condition known as ventricular fibrillation which causes an erratic pulse and an arrest of the blood circulation that is potentially life threatening. Thus, establishing the threshold fibrillating current is of particular importance for formulating safety requirements in the design of earthing systems and avoiding fatalities.

Humans seem to be particularly vulnerable to the effects of electric current of between 50 Hz and 60 Hz frequency range, [2.45]. Under DC, the body can tolerate up to five times higher current [2.46]. In the case of higher frequencies, from 3 kHz to 10 kHz,

even larger currents can be tolerated. Figure 2.22 taken from IEC 479-1 [2.47] shows the current magnitudes and durations which are particularly dangerous to humans over the frequency range 15 Hz to 100 Hz. From the graph it can be seen that human beings can tolerate higher currents of lower durations. Curve C, known as the safety curve, defines the current time curve where points to the safety of the curve will not produce ventricular fibrillation. Curve C2 represents a 5% risk and curve C3 a 50% risk.

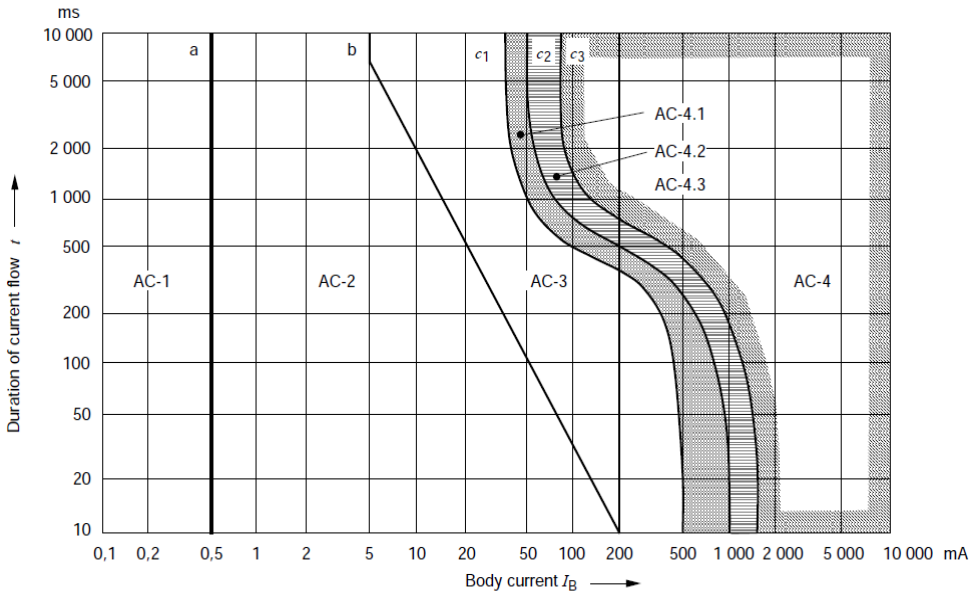

Figure 2.22: Time/current zones of effects of AC currents (15 Hz - 100 Hz) on humans (Reproduced from reference [2.47])

One series of tests were carried out by Charles Dalziel [2.48-2.52] who performed investigations on both animals and humans to study the effect of electric current flowing through the chest of the body. In these tests, he focused on the ‘let go’ current for humans. The term ‘let go’ current is defined as the maximum current a person can hold and release using the affected muscles when holding an energized copper conductor.

Dalziel et al [2.48] carried out experiments on 134 male and 28 female volunteers in an attempt to determine the let go current. The reasonably safe current was taken as the safe value for 99.5% of the group. From these series of tests, the let go current for men was 16 mA, and 66% of it for women with10.5 mA. The let go current for children was chosen as 50% of the let go current for men.

Dalziel suggested that the maximum tolerable current for a human, without risk of ventricular fibrillation, is approximately proportional to the body mass and inversely proportional to the shock duration. He concluded that for 99.5% of all the human subjects tested, the maximum tolerable body current for a 50 kg person can be determined from Equation (4).

$$I_{B(MAX)} = \frac{0.116}{\sqrt{t_s}} \tag{4}$$

Where $I_{B(MAX)}$ is the maximum tolerable current (A) and t_s is the electric shock duration (s).

For a 70 kg person, Equation 5 can be used.

$$I_{B(MAX)} = \frac{0.157}{\sqrt{t_s}} \tag{5}$$

As regard the IEC 479-1 (2005) [2.47], it is generally accepted that there is a decrease in the threshold of fibrillation if the sinusoidal AC current (50 Hz or 60 Hz) persists for more than one cardiac cycle. For a shock period less than one cardiac cycle, the threshold is nearly constant due to the very short time interval. This is the cause of the "twist" in the curve current/maximum disconnection time curve shown in Figure 2.23, which takes around 500 ms, about the duration of a human heart beat. It is worth noting that death is less likely for high currents of very short durations. This is

attributed to the reason that ventricular fibrillation will not occur unless the shock current passes during the vulnerable period in the (T) phase of cardiac cycle which occupies about 10% to 20% of the whole cardiac cycle, as illustrated in Figure 2.23. The cardiac cycle takes a 800ms long [2.53]

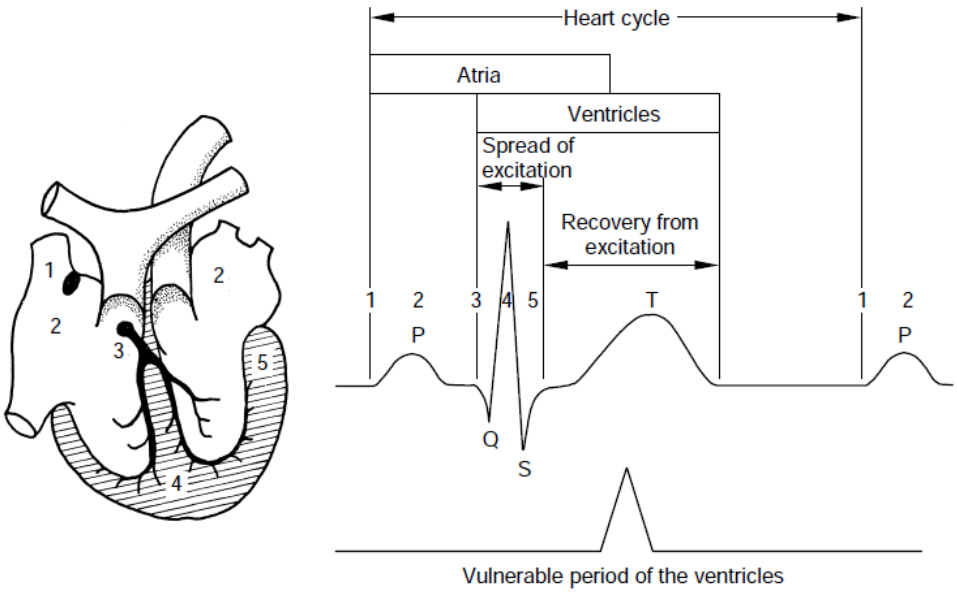

Figure 2.23: Typical human heart cycle

(Reproduced from reference [2.45])

Table 2.2: Time/current zones for 15 Hz to 100 Hz for hand to feet pathway

Zones	**Physiology effects.**
1	Perception but fibrillation not likely to occur.
2	No harmful physiological effects but in addition to perception, involuntary muscular contractions may occur.
3	Ventricular fibrillation is unlikely to occur. Involuntary muscular contractions become strong in this region combined with difficulty in breathing, reversible disturbances of formation and conduction of impulses in the heart. This effect increases with current magnitude.
4	Further to the effects in zone 3, the probability of ventricular fibrillation increases up to about 5% (C_1-C_2, Figure 2.22), up to about 50% (C_2-C_3) and above 50% beyond curve C_3. Also pathophysiological effects such as cardiac arrest, breathing arrest and heavy bums may occur with increase in magnitude and time.

2.5.2 Safety voltages

The earth surface potential is defined as the potential attained by the earth as the current is dissipated into the earth via an earth electrode, e.g. a tower foundation. It is measured in relation to a remote earth point which is assumed to have a potential of 0V.

The earth potential rise for steel transmission towers and substation earthed metal work is defined as the voltage that the metal wall may attain with respect the potential of a remote earth. This earth potential rise is proportional to the magnitude of the fault or lightning current which flows via the earthing system to the earth and the magnitude of the earthing system impedance.

2.5.2.1 Touch Voltage

The touch voltage is regarded as the difference between the earth potential rise and the earth surface potential at the point where the person stands 1m from the earthed structure and at same time touches that structure. The route of the current due to the touch voltage circuit is passing from the hands to the feet (in parallel and in contact with soil).

Guidance on the requirements for the earthing systems for overhead lines exceeding 45 kV is provided in BS EN 50341-1 [2.54]. In this standard, there is a requirement to ensure safety for persons coming into contact with earthed metal work of lines under earth fault conditions. The procedure for establishing safety is based on tolerable body current values given in Figure 2.22 (Curve C2) reproduced from standard IEC60479-1. Parameters of the electrocution circuit, made up of human body resistance and additional resistances such as footwear, are suggested for different scenarios. Importantly, consideration of the touch voltage scenario is restricted to towers which

are freely accessible and defined as frequently occupied. The permissible voltage against fault duration for an electrocution current with assumed typical resistances is based on hand to feet or hand to hand contact (without taking into consideration footwear or shallow material of high resistivity) and is shown in Figure 2.24 [2.55].

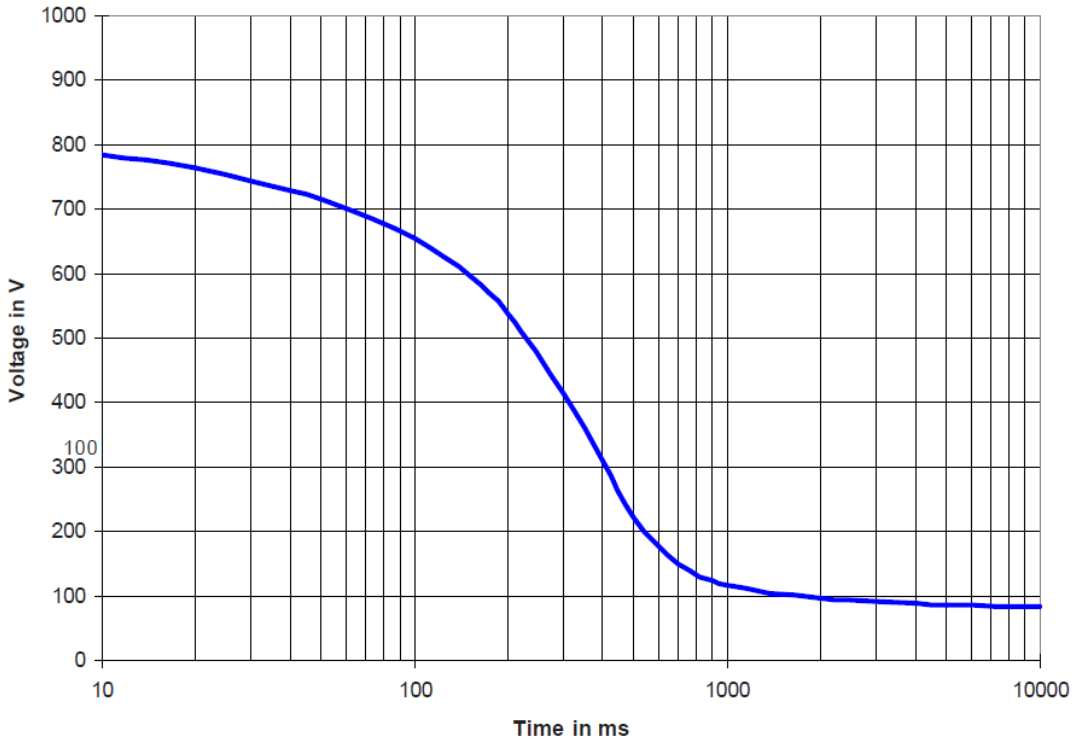

Figure 2.24: Tolerable touch voltage [Reproduced from (2.54)]

2.5.2.2 Step voltage

According to IEEE Std. 80 [2.56], the step voltage is the difference in earth surface potential experienced by a person bridging a distance of 1m with his/her feet without contacting any other grounded structure. In such circumstances, the current enters the body through one foot and leaves from the other. The body resistance when the current passes between extremities is conservatively considered to be 1000 Ω [2.56].

Step voltages are usually considered less hazardous than touch voltages. This is because the human body can tolerate higher currents for a path from foot to foot than

current from hand to feet which passes through the chest, as described in IEC 479-1 [2.47]. Given the step voltage is lower than the touch voltage, if a system is safe for touch scenarios, it should also be considered safe for step scenarios.

2.6 Discussion

Practical earth electrodes have been described and the components of a tower line earthing system identified. It is noted that tower footing earths may be enhanced using horizontal and vertical electrodes. Investigations into the performance of transmission lines tower earths have been reported, and extensive tests on horizontal and vertical electrodes reviewed. The non-linear behaviour of earth electrodes under high current impulse was described with reference to extensive laboratory investigations to characterise the impulse resistance and the critical electric field ionisation threshold. Further, aspects of human safety in the vicinity of tower lines were described.

CHAPTER THREE: CHARACTERISATION OF TOWER BASE EARTHING UNDER LOW DIRECT AND ALTERNATING VOLTAGES

3.1 Introduction

Earthing systems are designed to dissipate large fault currents to ground and protect persons working in or living near power system installations. To dissipate currents effectively under both power frequency and transient fault conditions, the earthing system should have low earthing impedance. When large currents disperse into the surrounding earth under earth faults, earth surface potentials develop around the grounded structures and present touch and step voltage hazards in the immediate vicinity of the structure [3.1, 3.2]. These potentials may be of sufficient magnitude to endanger human life. Thus, extra measures may be needed to minimise their magnitudes when designing earthing systems.

The measurement of the earth resistance of electrodes is important for new installations to verify the design and, for existing installations, to ensure continued integrity.

If enhancement of the earthing system of steel transmission lines is required, single earth rods or ring electrodes can be used; alternatively or additionally horizontal electrodes may also be employed.

In this chapter, the earth surface potential in the vicinity of a tower base under low voltage AC will be investigated. The earth surface potential profiles are compared with computer simulation using CDEGS-HIFREQ software [3.3]. In addition to the earth surface potential survey, an examination of the ground potential of both the tower footing and soil at different depth through the use of buried probes. DC earth resistance measurements of earthing system components are presented based on the

61.8% rule. Further, the values obtained by measurements are compared with analytical formulae.

3.2 Description of test set with tower base earth electrode

A satellite image of Cardiff University's Llanrumney field test site is shown in Figure 3.1.The figure highlights the positions of the four reinforced concrete tower footings forming the tower base. Each individual footing has a depth of 3m and the four footings are arranged at the corners of a 7.25 m x 7.25 m square. The construction detail of a footing is shown in Figure 3.2. A ring formation current return electrode surrounds the tower base and consists of eight 16 mm diameter copper rods, each driven to a depth of 2.4 m in a circle of 30 m radius. The rods are interconnected by sections of both bare and insulated copper conductors, to form a ring electrode. These conductors are buried at a depth of 30 cm, and junction boxes are located above the rods to allow connection/disconnection of components and facilitate measurement of current and voltage at each position.

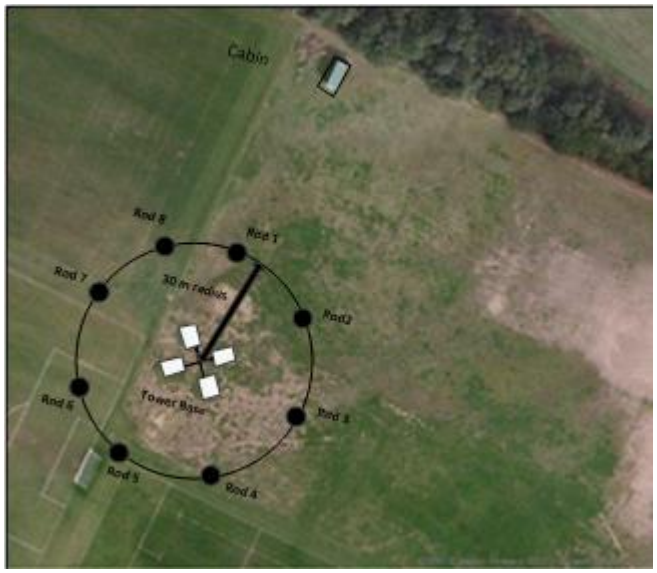

Figure 3.1: Satellite image of tower base at Cardiff University Llanrumney test site

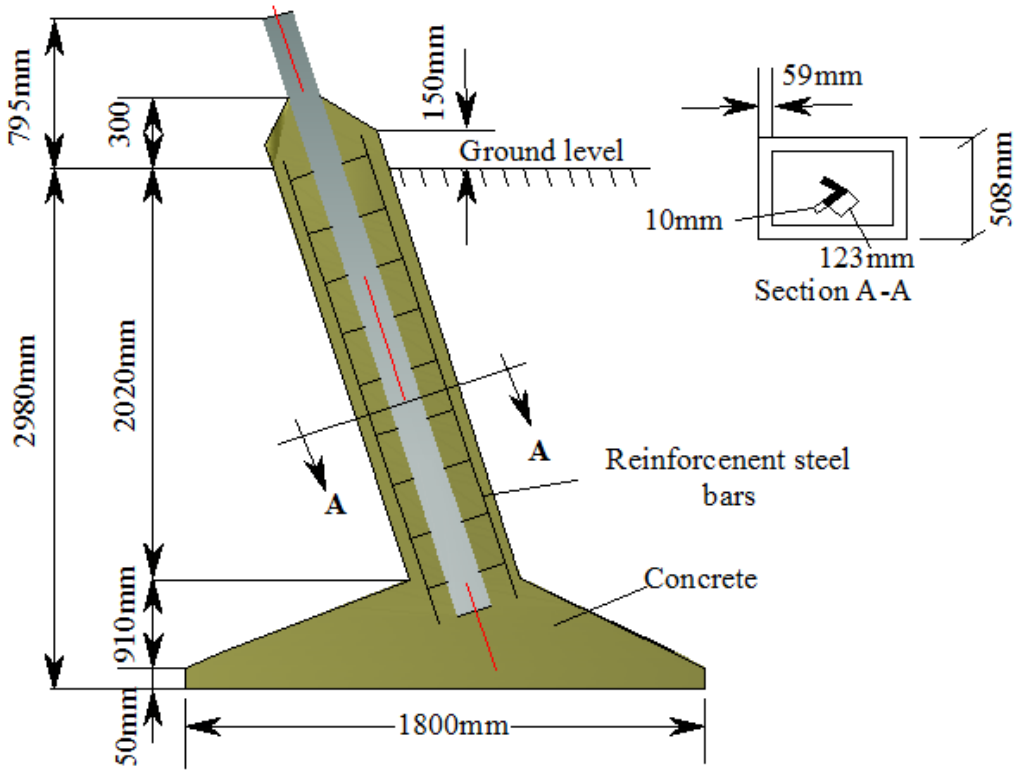

Figure 3.2: Tower footing construction

3.3 Test setup and measurement locations

The test circuit, depicted in Figure 3.3, shows the current source, the electrode under consideration (tower base), the current return electrode (ring) and the remote reference potential electrode and cable. The AC source is a variable frequency impedance measurement system (IMS) developed for this type of test [3.4]. The IMS consists, essentially, of two parts: an EG&G Model 7260 lock-in Amplifier and QSC Audio Power Amplifier. The lock-in amplifier is an instrument with a dual capability. It can recover signals in the presence of an overwhelmingly noisy background and it can provide high resolution measurements of relatively clean signals over several orders of magnitude and frequency. The dimension of the tower base and the ring electrode is described in the previous section. The earth surface potential (ESP) distribution was measured over one diagonal (profile 4) and two median profiles (profile 5 and 6), which are each 35 m long. The 'test probe' method was used to measure earth potentials and the step and touch voltages [3.5]. In this method, rods of 53 cm length,

located at equal intervals along the profile, were driven to a 20 cm depth [3.6 and 3.7]. A wide band current transformer having a frequency range from 1.5 Hz to 20 MHz with sensitivity 0.1V/A, and a high-bandwidth differential probe were used for these measurements. To eliminate interference including mutual coupling effects, a Nicolet fibre optic system was used to transmit the measurement signals to the recording instruments.

Figure 3.4 shows an example of the applied low frequency AC current (2.5A) and the corresponding earth potential rise (EPR) of 65.8V at the injection point, measured with reference to a remote ground rod placed 100 m away in a direction perpendicular to the return current line. As can be seen from the figure, the current and the earth potential rise are in phase, and the low frequency resistance of the tower base, (EPR/I_{rms}) = 26.3Ω.

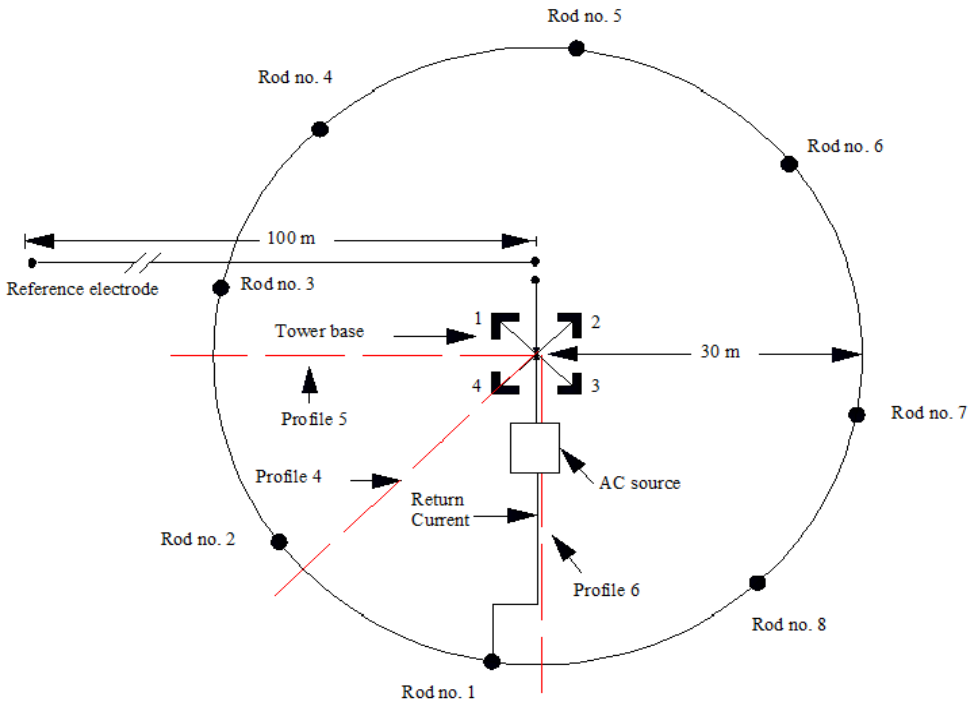

Figure 3.3: Experimental setup and detailed plan view of tower base foundation and arrangement of circular return ring electrode

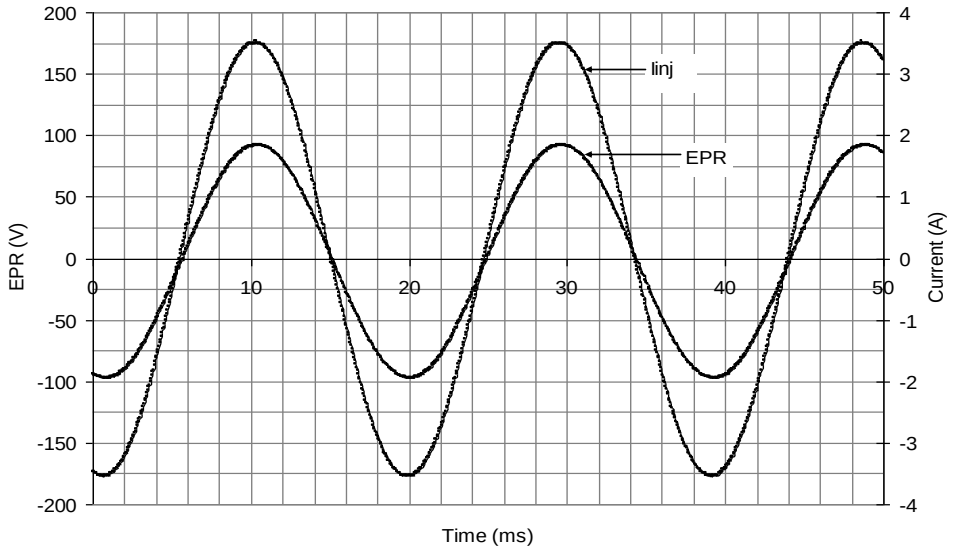

Figure 3.4: Injected AC current and tower base EPR (f=52Hz)

3.4 Low frequency AC voltage profiles

Figure 3.5 shows the earth surface potentials along the profiles P4, P5 and P6 with respect to the remote reference electrode. As can be seen from Figure 3.5.a, there is a marked difference in potential distribution near the tower base between the mutually perpendicular median profiles (P5, P6) and the diagonal (P4). With profile P4, the ESP reaches a well defined maximum of 83% of the tower earth potential (EPR) rise at a distance of about 5.5 m from the tower centre (10 cm from the tower footing). With this profile, P4, the earth surface potential increases sharply with distance for the first 6 meters of the profile. Beyond this distance, its value decreases sharply, and after about 15 m, it is about 5% of EPR.

For the median profiles P5 and P6, the maximum ESP magnitudes are only 16% and 19.5% of the EPR, respectively. The small difference between the P5 and P6 profiles is due to variations in local soil resistivity.

For distances greater than 12 m, the three potential distributions practically coincide, and decrease steadily to a minimum value at about 22 m from the tower centre. At this distance, the potential due to the current entering the tower base is equal and opposite

that due to the current leaving the return electrode. The effect of the ring electrode is indicated by the small rise in potential at a distance of 30m. Figure 3.5b shows the potential phase angle reversing at the location of minimum potential magnitude (22m) for all three profiles. Figure 3.6 displays ESP waveforms with for selected points along profile P5 as indicated.

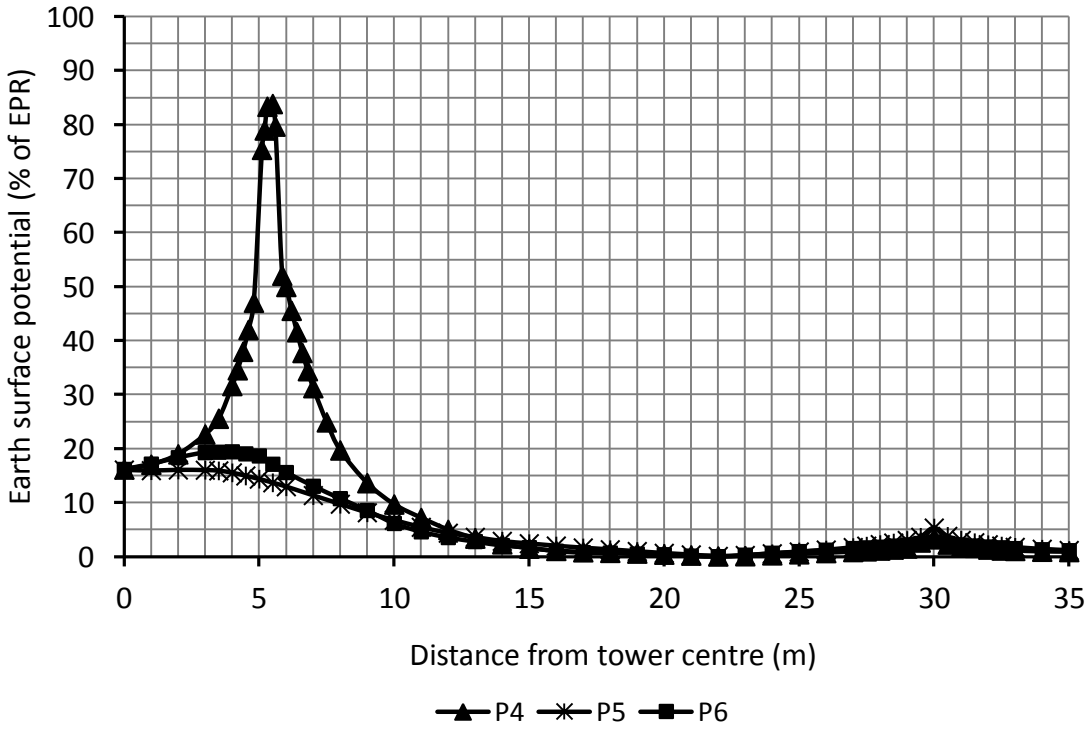

(a)

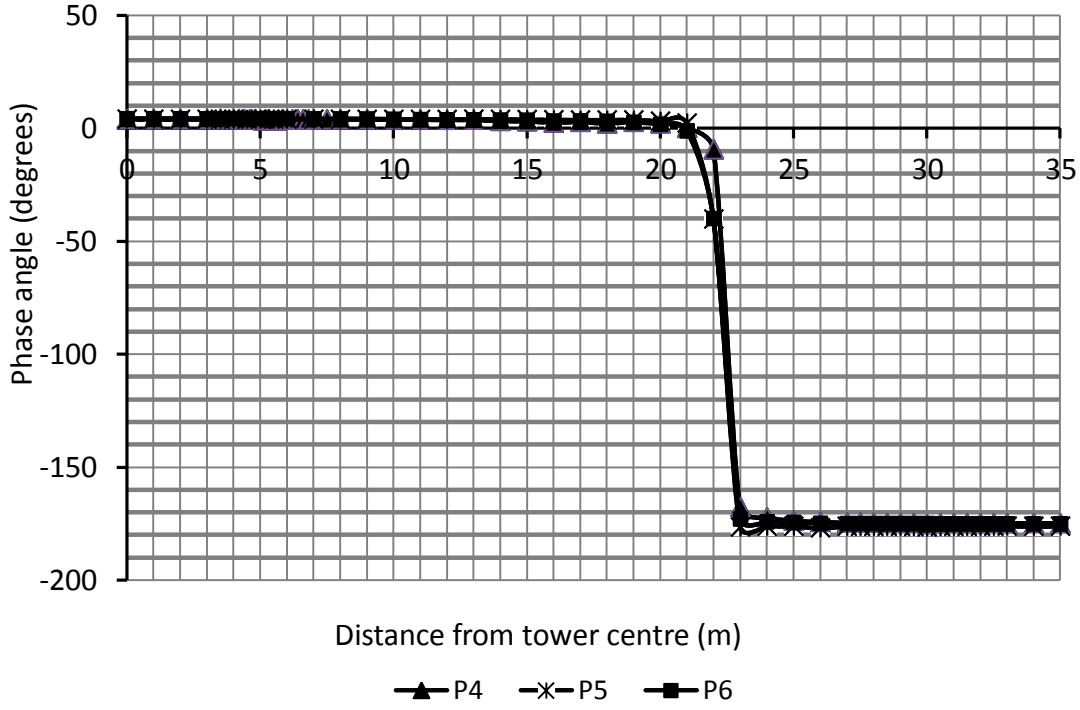

(b)

Figure 3.5: ESP distribution for low frequency AC current injection; (a) magnitude and (b) phase angle

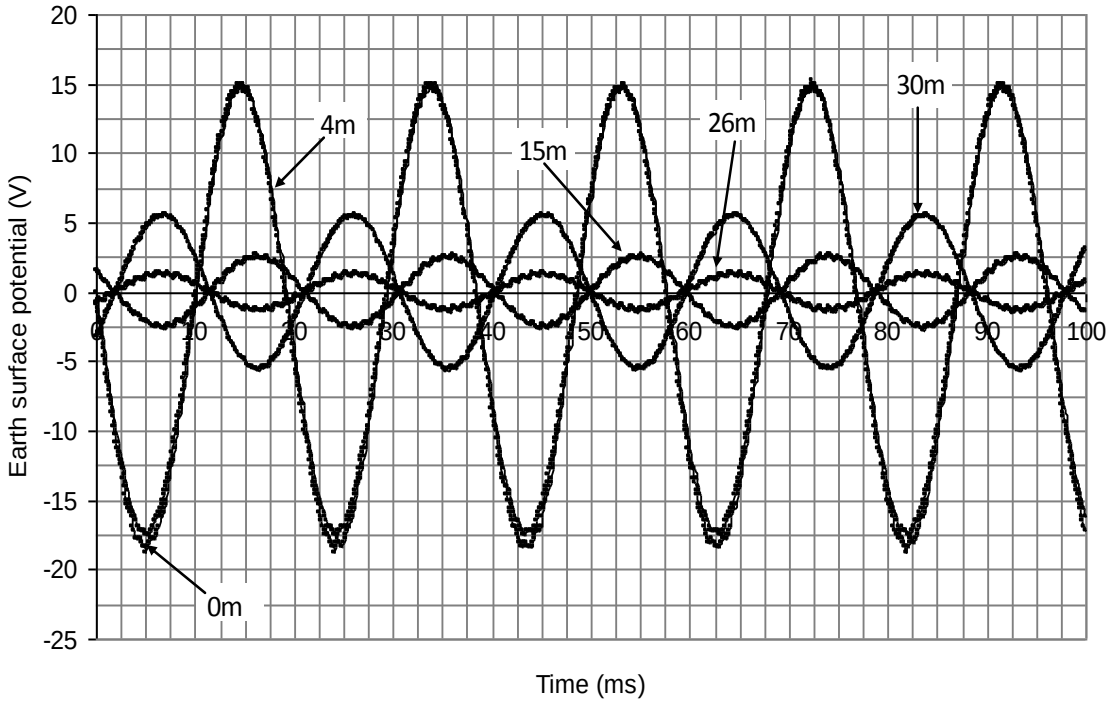

Figure 3.6: ESP waveforms along profile P5 with injection of AC current of 52 Hz

3.4.1 Effect of frequency on ESP

The ESP measured, on the critical profile (P4), at three different frequencies (52 Hz, 60 kHz and 120 kHz) is shown in Figure 3.7(a). As can be seen, from the figure, a similar trend is seen for all frequencies. However, the magnitude of the ESP falls off less rapidly (as a percentage of EPR) at high frequency compared with 52 Hz, on the inner region of the tower base (0-5m). The effect of a higher earth surface potential as a percentage of EPR on the return electrode at high frequencies can be seen by elevated ESPs in the range 15-35m. As can be seen from the figure, the influence of return electrode becomes more influential with increase the frequency. This can be confirmed in Figure 3.7(b) which present that the mass of the earth which form the resistance of the tower base decreases with increasing the frequency.

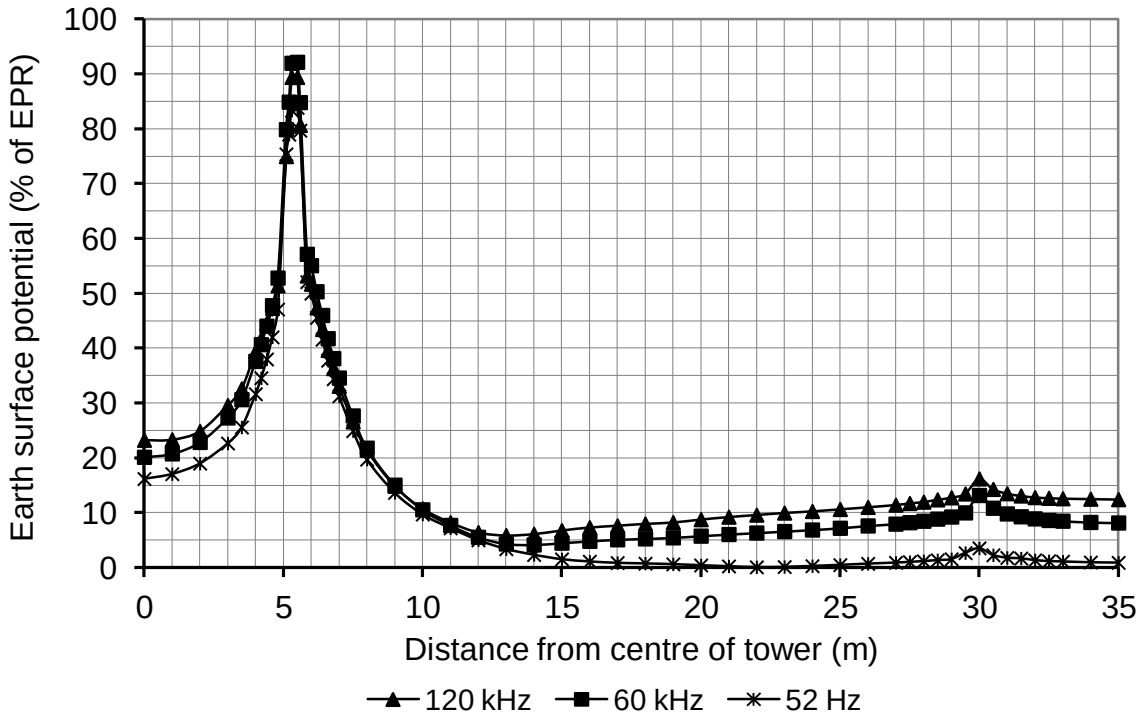

(a)

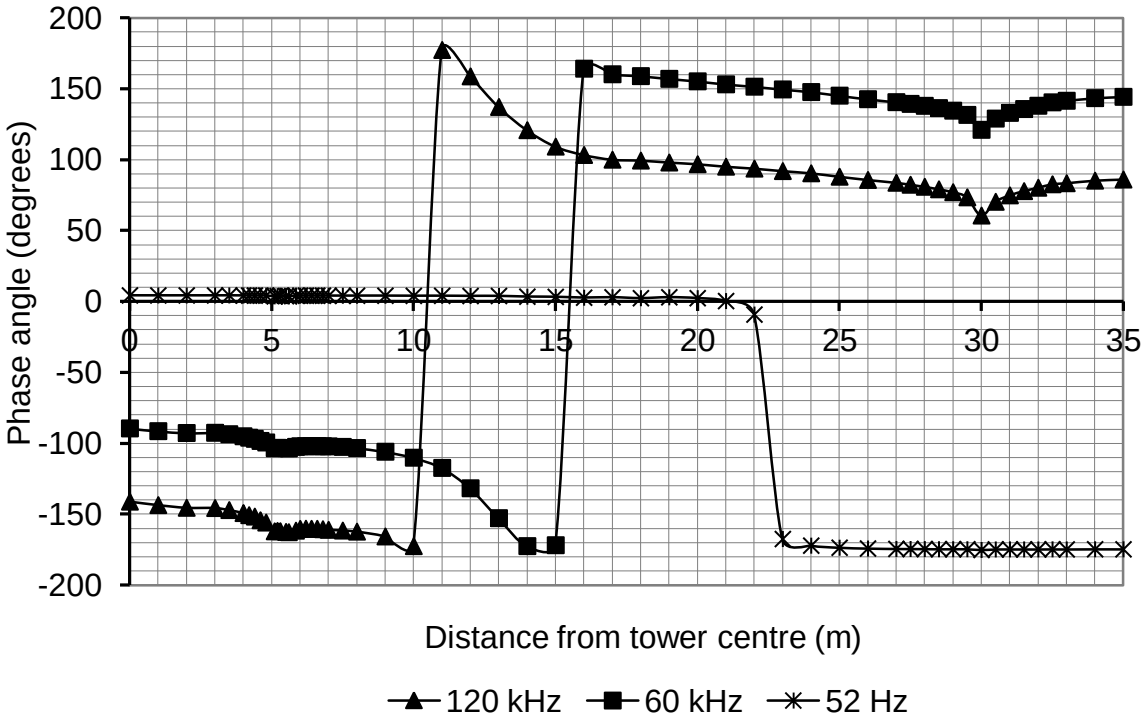

(b)

Figure 3.7: Measured ESP along profile P4 for frequencies of 120 kHz, 60 kHz and 52 Hz with distance from the centre of the tower (a) magnitude (b) phase angle.

3.4.2 Computer simulations of ESP

The geometrical test configuration of Figure 3.3 was simulated using the HIFREQ module of the CDEGS software [3.3]. The simulation requires all electrodes to be modelled as cylindrical conductors with radii much smaller than length. A two-layer soil model was used based on extensive soil resistivity measurements in the vicinity of the tower base. The soil model comprised an upper layer of resistivity 200Ωm with a depth of 8m and a lower layer of resistivity 30Ωm to enfinity.

AC current energisation with three different frequencies (52 Hz, 60 kHz and 120 kHz) was assumed. Figure 3.8 shows the results of the computation of ESP along the diagonal profile P4. The results from this computer model predict the ESP profiles which follow the same general trends as the measured values shown in Figure 3.7. The

amplitude of the initial peak occurs at the same distance from the centre of the tower but the predicted amplitude is slightly lower than the measured, 83% EPR compared to 92%. In the range 0-5m, the simulated profiles do not show a different rate of fall off as seen with the measured values. It is possible that inductance coupling in the test circuit may be responsible for higher potentials and a consequently lower rate of fall at the higher frequencies.

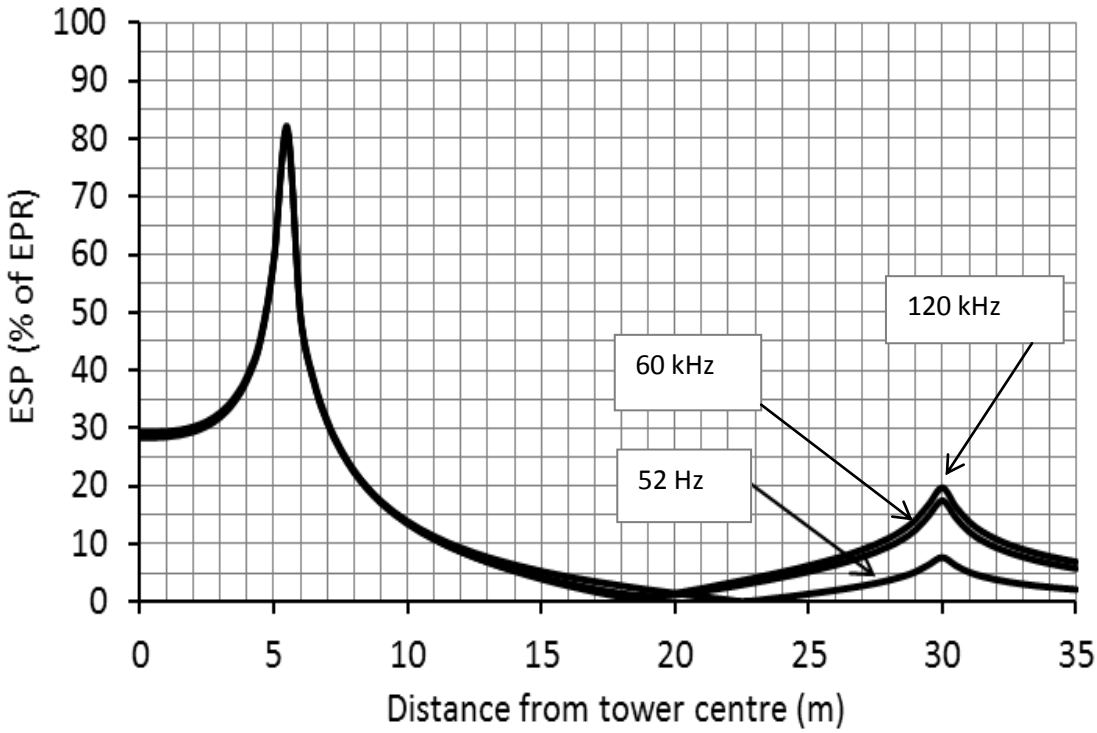

Figure 3.8: Computed ESP profiles for AC current injection at 52 Hz, 60 kHz and 120 kHz.

A detailed comparison between measured and computed ESP profiles for the 52 Hz energising current is shown in Figure 3.9. As can be seen from the figure, a quite close agreement between the measured and computed of ESP profiles is obtained. The differences can be attributed to the use of a simplified laterally homogeneous soil model in case of the simulation, which is due to a restriction inherited in software

package. It is known that significant lateral as well a vertical, variations in soil are present.

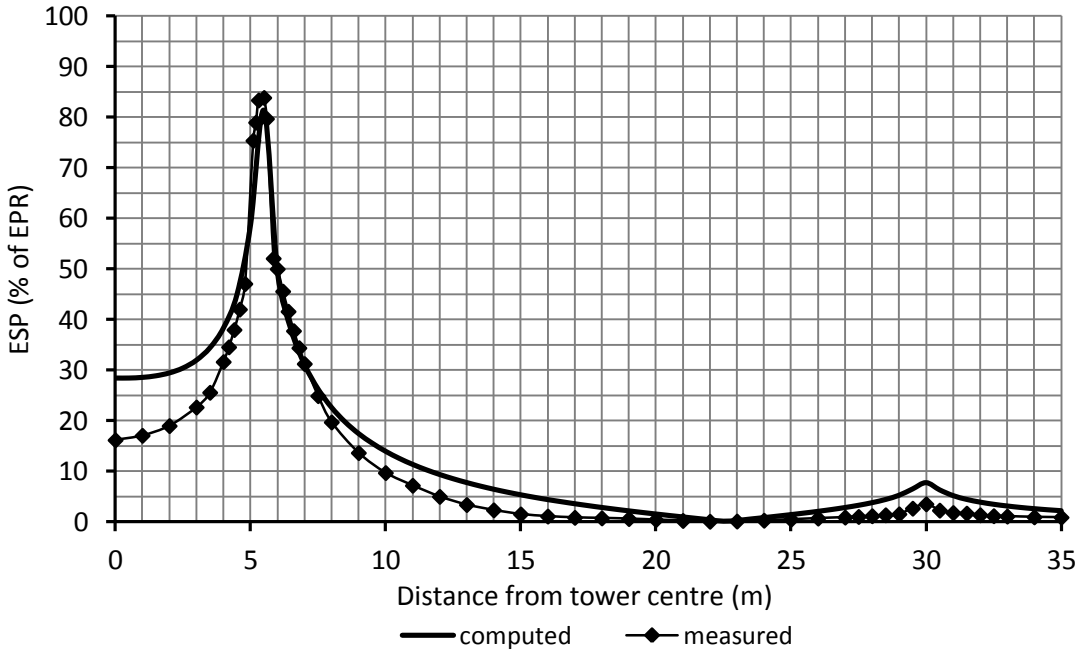

(a)

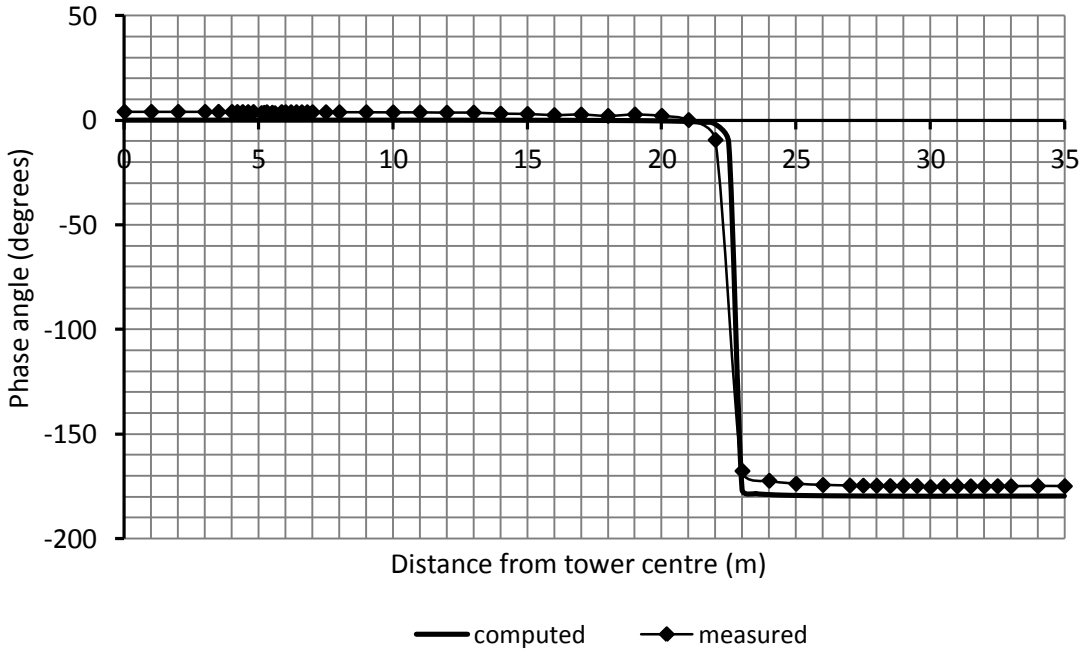

(b)

Figure 3.9: Computed and measured ESP and phase angles for AC current (52 Hz)

(a) ESP magnitude (b) ESP phase angle

3.5 Ground potential distribution inside the tower footing and soil

The potential gradient developed due to the flow of a current in a transmission tower has its largest magnitude in the area close to the tower footing. To investigate further the ground potential distribution at the tower footing and soil surrounding the footing, three sets of metal probes (a, b and c) were set orthogonally to each other as seen in Figure 3.10, and embedded in the footing concrete at different depths (1m, 2m and 3m). Similarly, a further set of three probes were also buried at depths (1m, 2m and 3m) in soil 1m away from the tower footing.

Experimental studies were carried out using an IMS (Impedance Measurement System) low AC current source of a variable frequency from 20 Hz to 120 kHz. Amplitudes and phase angles were recorded directly from the IMS. A differential probe with attenuation ratios of 20:1, 50:1 and 200:1 provided the voltage signal, and the current was obtained by means of a current transformer with a sensitivity of 0.1V/A.

3.5.1 Ground potential distribution in the tower footing

To investigate the frequency response of the ground potential distribution into the tower footing, a current of 107.2 mA was injected into Footing No.1 for frequencies ranging from 20 Hz to 120 kHz. These high frequencies represent the frequency content of an initial lightning stroke (100 kHz) [3.2].

The probes b, c, a in the concrete were placed in x, y, z coordination as depicted in Figure 311. Figure 3.12 shows the frequency response of the tower footing. As can be seen from the figure, the magnitude of the earth potential rise is 18Vat 52 Hz and falls gradually with frequency up to 100 kHz. The fall in earth potential rise may be due to capacitive effects. Similar trend obtained for the earth impedance which is 172.5Ω at the low frequency as show in Figure 3.13. The impedance angle decreases to -18^{o} this may indicate that capacitive effect could be important.

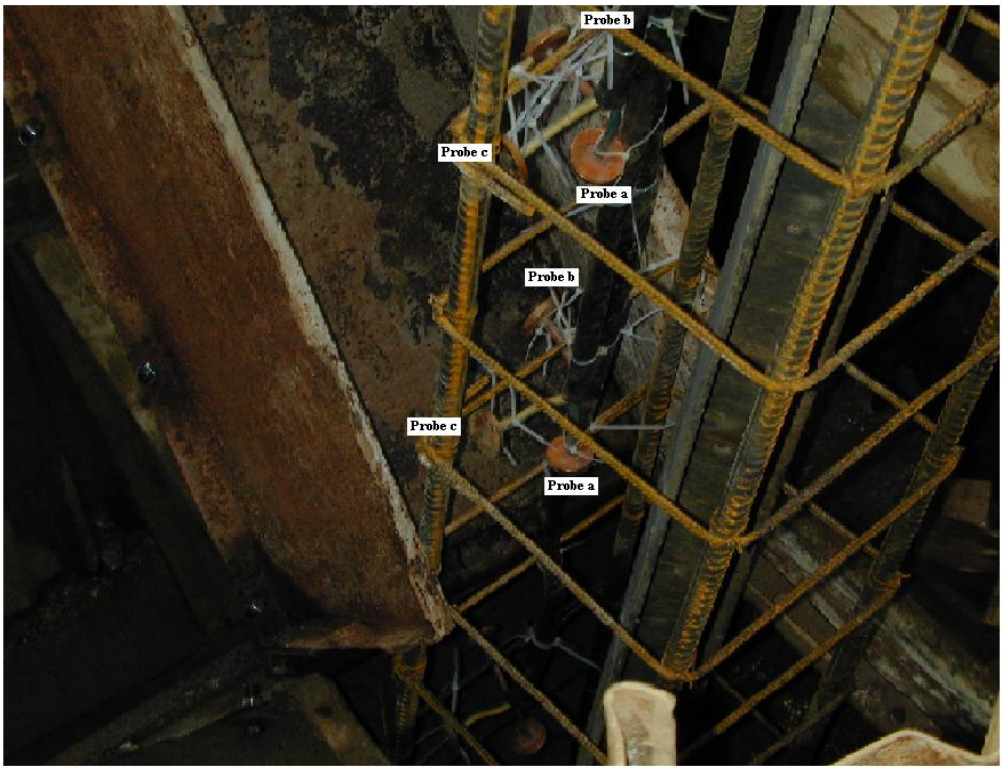

Figure 3.10: Probes embedded in concrete at different depths and directions

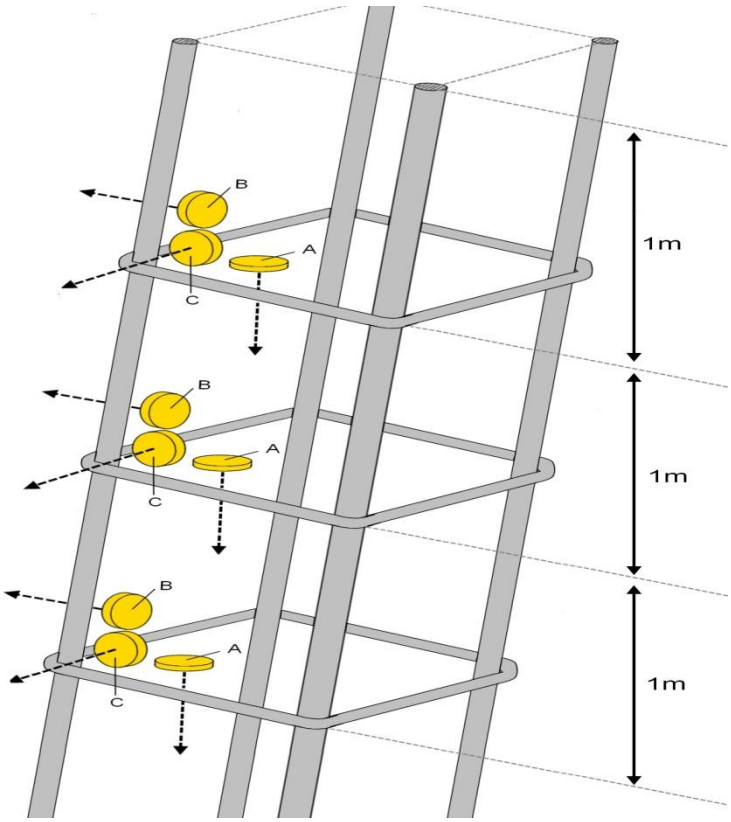

Figure 3.11: Three dimensions view of the embedded probes in concrete

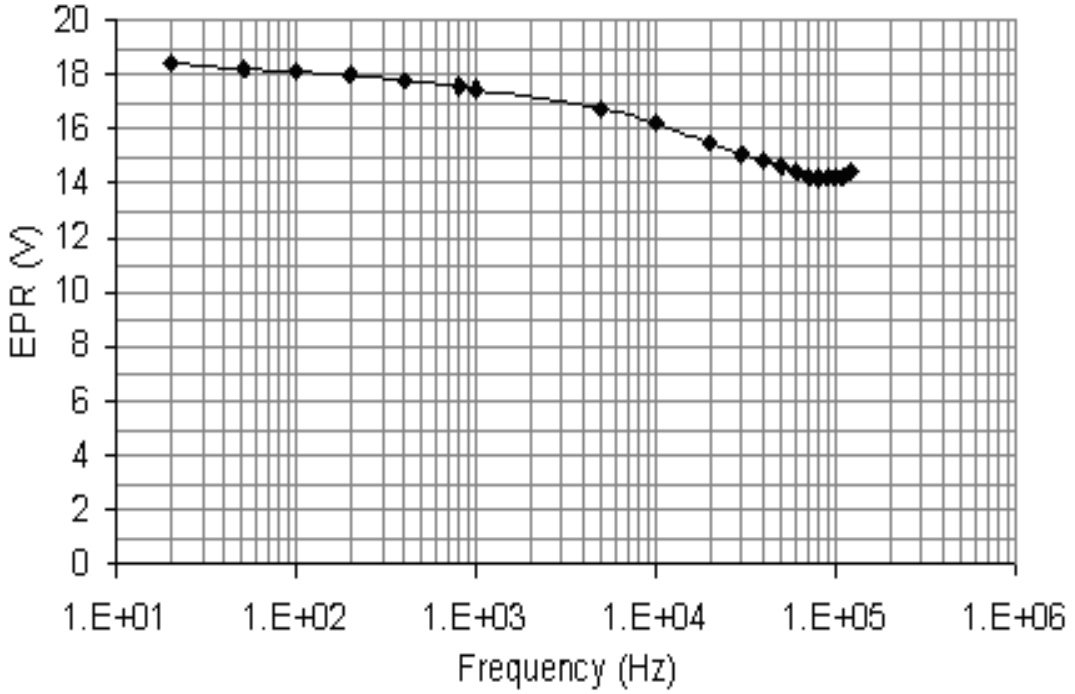

(a)

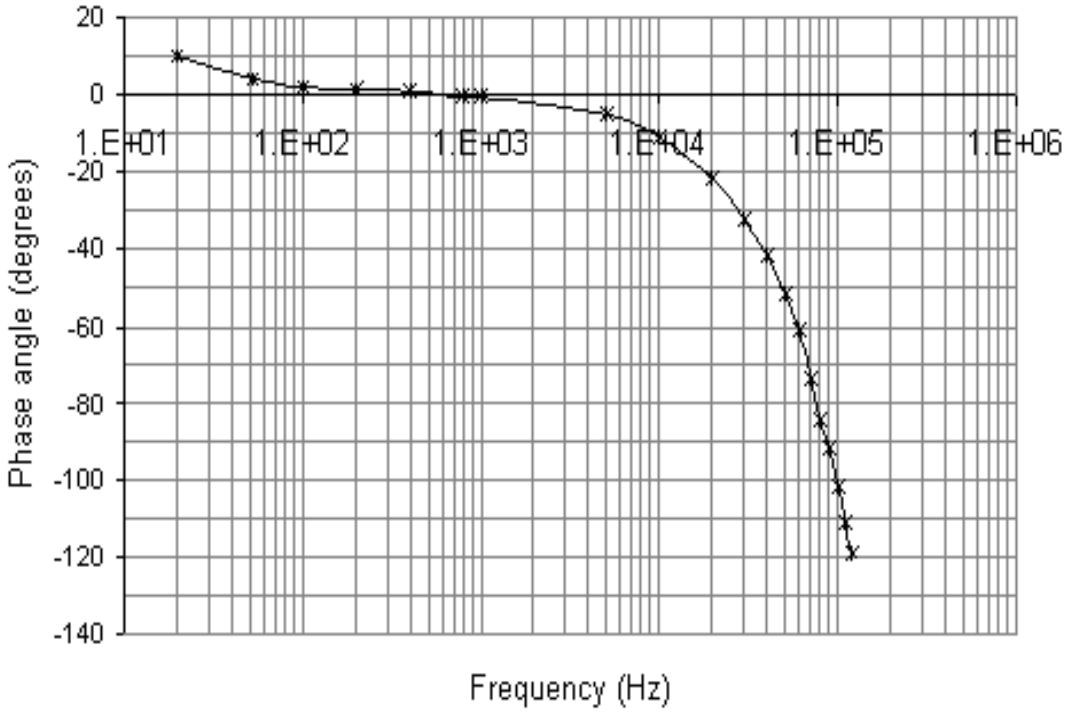

(b)

Figure 3.12: Frequency response of EPR of tower footing No.1, showing

(a) EPR magnitude and (b) EPR phase angle

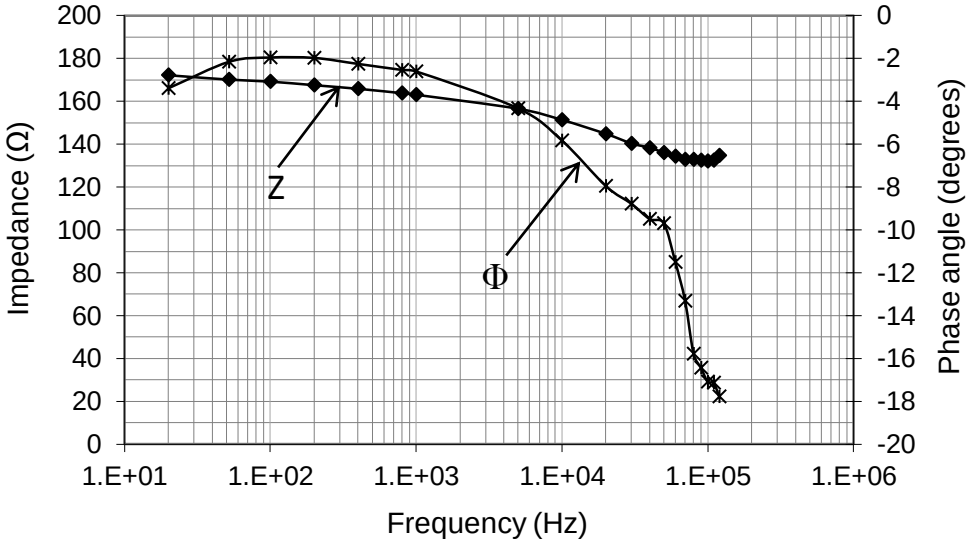

Figure 3.13: Frequency response of impedance of tower footing showing and impedance phase angle

3.5.1.1 Ground potential measured by the probes within concrete footing

The results presented in Figure 3.14 show the frequency response of the potential measured by probes a, b and c buried at a 1m depth in the concrete of the footing. It can be seen that the potential decreases with frequency up to 110 kHz following a similar trend to that seen for the impedance of the footing. Furthermore, at lower frequencies probe b has a significantly higher voltage compared with probes a and c. It is interesting to note that the measured potentials by the three probes converge at high frequency. The differences in potential measured by probes a, b and c indicate significant potential differences over relatively short distances within the concrete of the footing. Due to the construction process including the concrete pouring, it is not possible to identify accurately the orientation of the probes, and hence their relative distance from the tower footing metalwork.

For the set of probes at depths of 2m and 3m, similar trends were observed. Figures 3.15 and 3.16 show the ground potential at 2m and 3m depth, respectively.

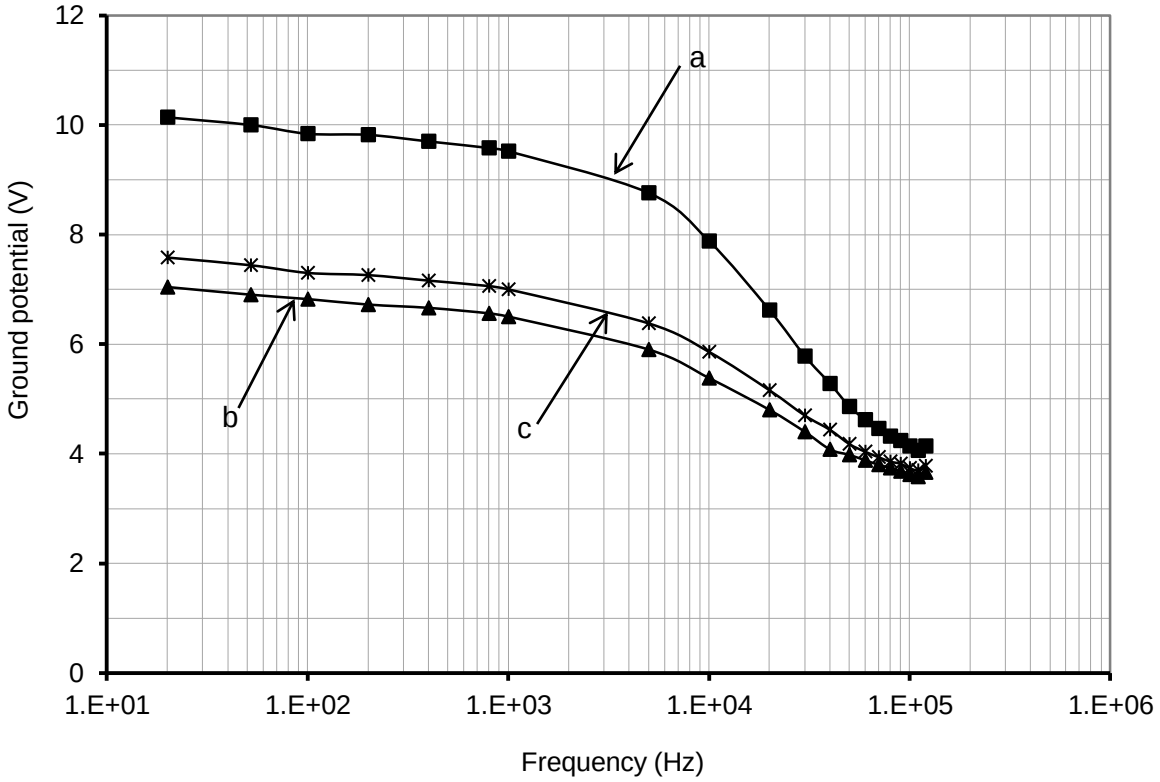

Figure 3.14: Frequency response of the magnitude of ground potential as measured by probes (a, b, c) at 1m depth

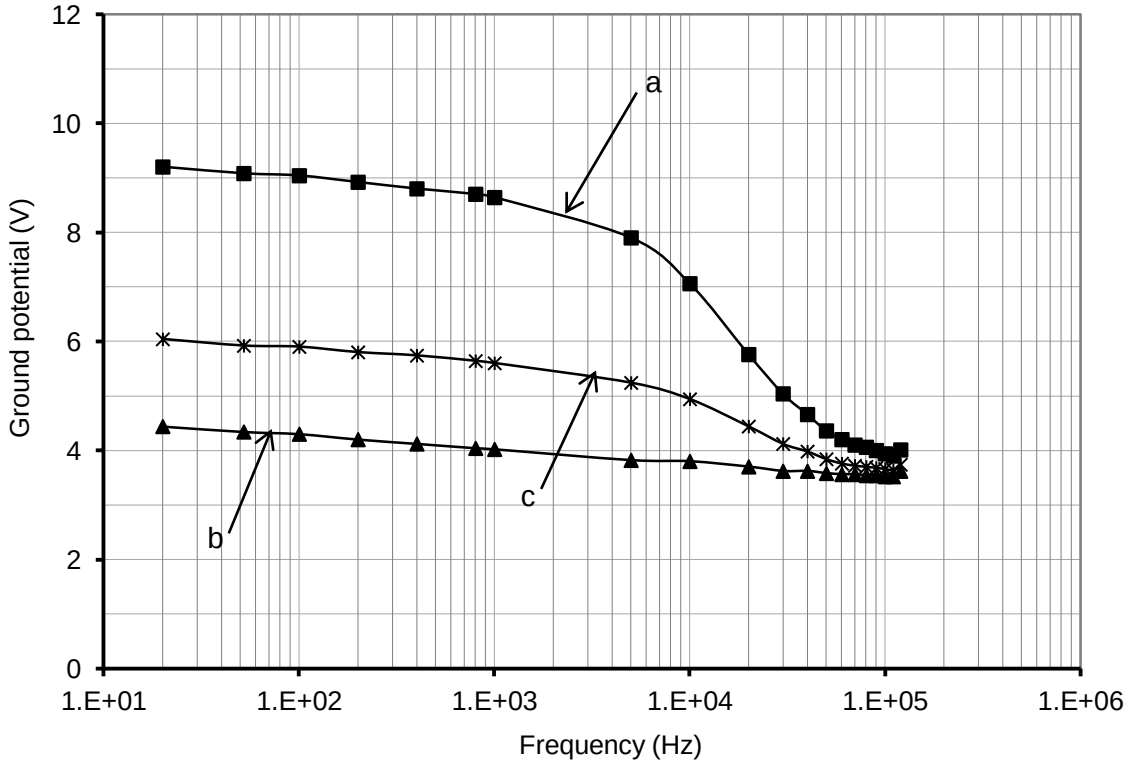

Figure 3.15: Frequency response of the magnitude of ground potential as measured by probes (a, b, c) at 2m depth

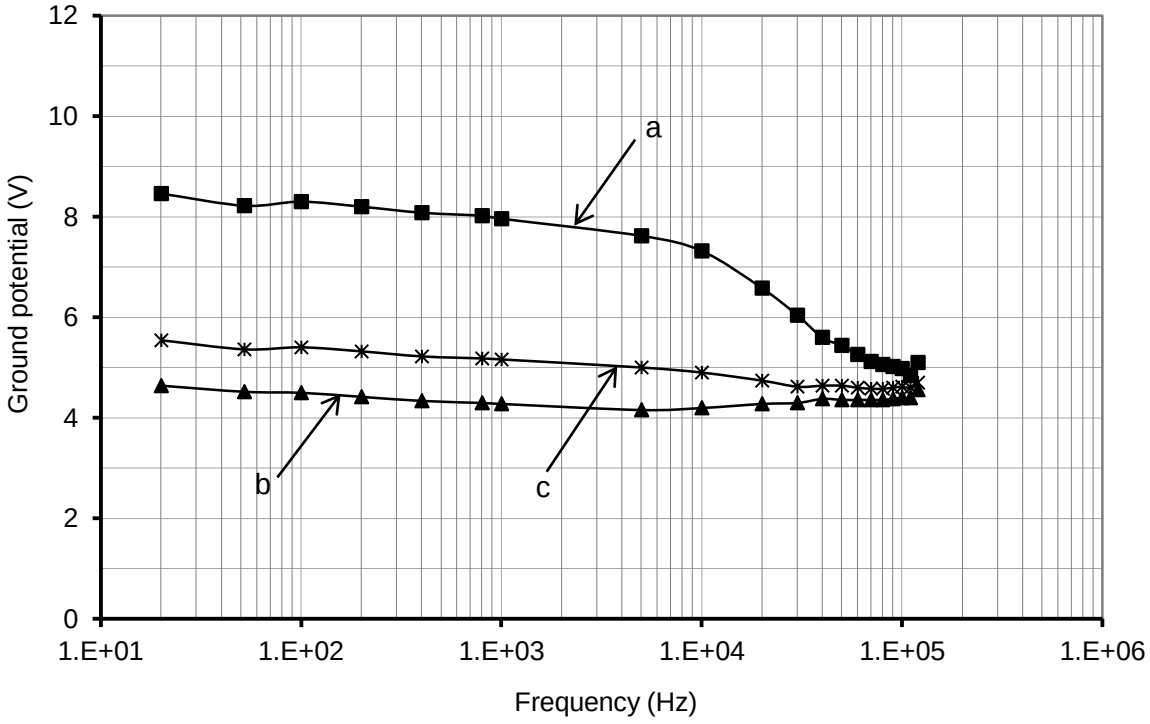

Figure 3.16: Frequency response of the magnitude of ground potential as measured by probes (a, b, c) at 3m depth

3.5.1.2 Ground potential within tower footing concrete at different depths

Figures 3.17-3.19 set out the characteristic responses of probes a, b and c, and show the measured potentials as a function of frequency at different depths. From Figure 3.17, for a depth of 1m, probe a (probe nearest the injection point) shows a higher potential than corresponding probes at 2 m and 3 m. Unexpectedly, the probe at 2 m has a lower ground potential than the probe at 3 m. Inductive effects becoming significant in the frequency range from 5 kHz up to 120 kHz for probe b at 3m depth. Figures 3.18 and 3.19 show a more consistent pattern in magnitude of measured potential with depth; generally as the probe depth increases its potential decreases. However, above about 10 kHz, the value of potential for all the probes (a, b and c) which were located at 3m depth increases relative to the other two locations. Above about 40 kHz, it records the highest value.

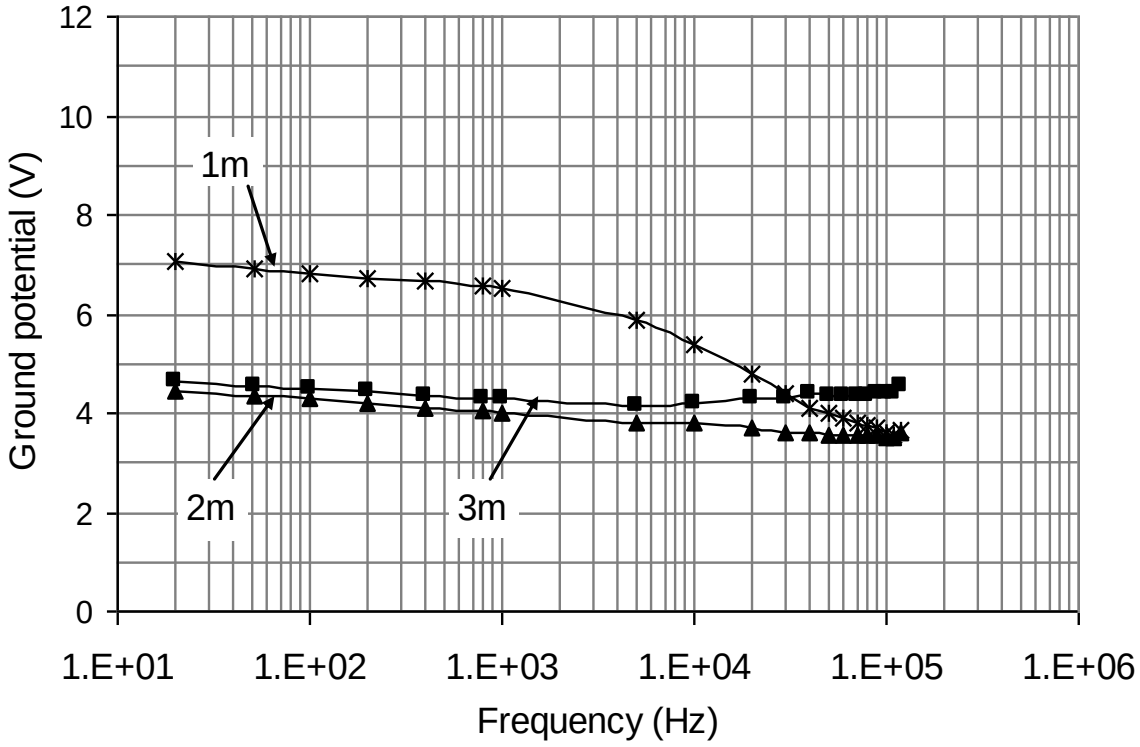

Figure 3.17: Probe b: Potential as a function of frequency at depths of 1 m, 2 m and 3 m

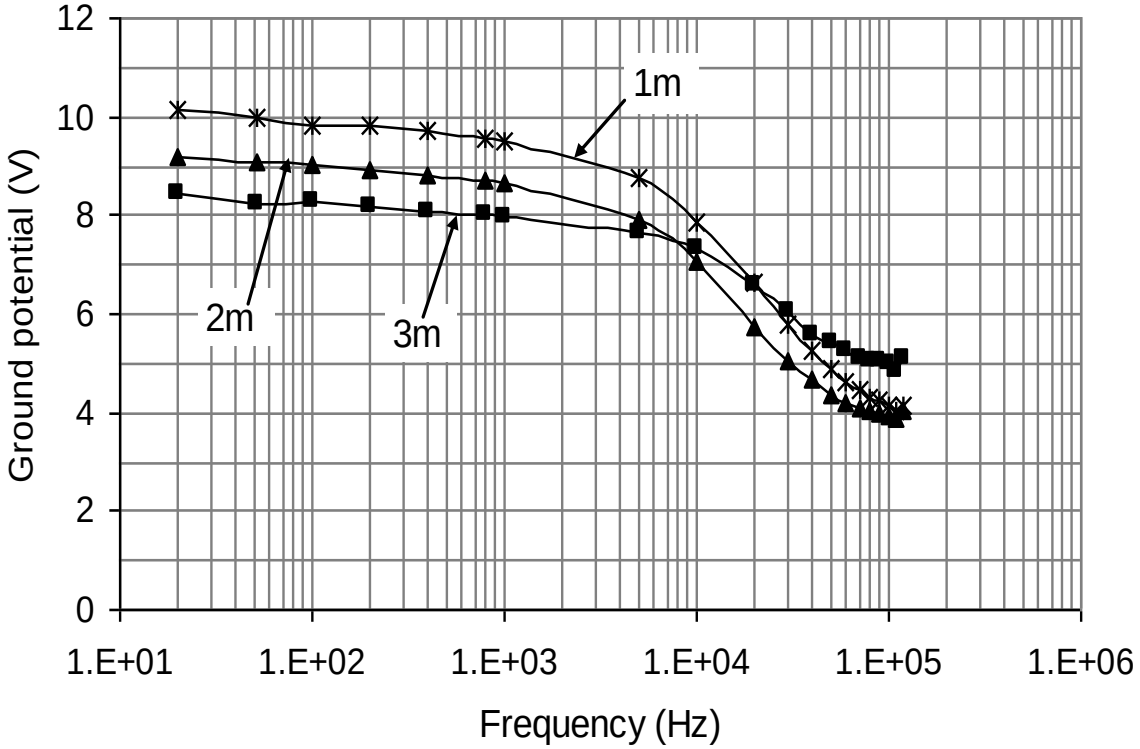

Figure 3.18: Probe a: Potential as a function of frequency at depths of 1 m, 2 m and 3 m

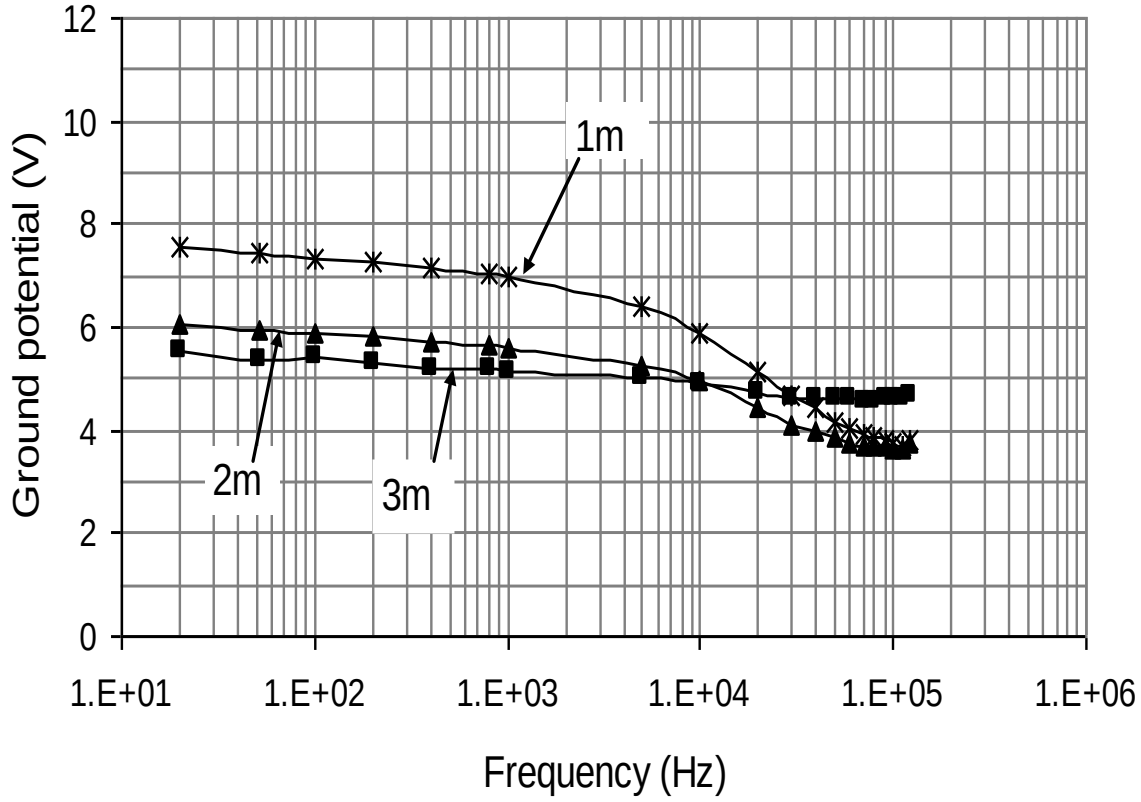

Figure 3.19: Probe c: Potential as a function of frequency at depths of 1 m, 2 m and 3 m

3.5.2 Ground potential distribution in soil adjacent to the tower footing

For measuring the ground potential in soil close to the tower footing similar metal probes to those described in section 3.51 were used. To examine the frequency response of the potential distribution into the soil, an AC current of 107.2 mA was injected into tower footing No. 2 with a frequency range from 20 Hz to 120 kHz. These probes, as shown in Figures 3.20 and 3.21, were buried at depths of 1 m, 2 m and 3 m, and placed approximately at a 1m distance from the central metal reinforcing structure tower footing No. 2. Figure 3.21 shows the detailed orthogonal arrangement of the three probes.

Figure 3.20: Preparation of probes in soil at different depths and 1m distance from footing No. 2 for measurement of potential (pre-installation)

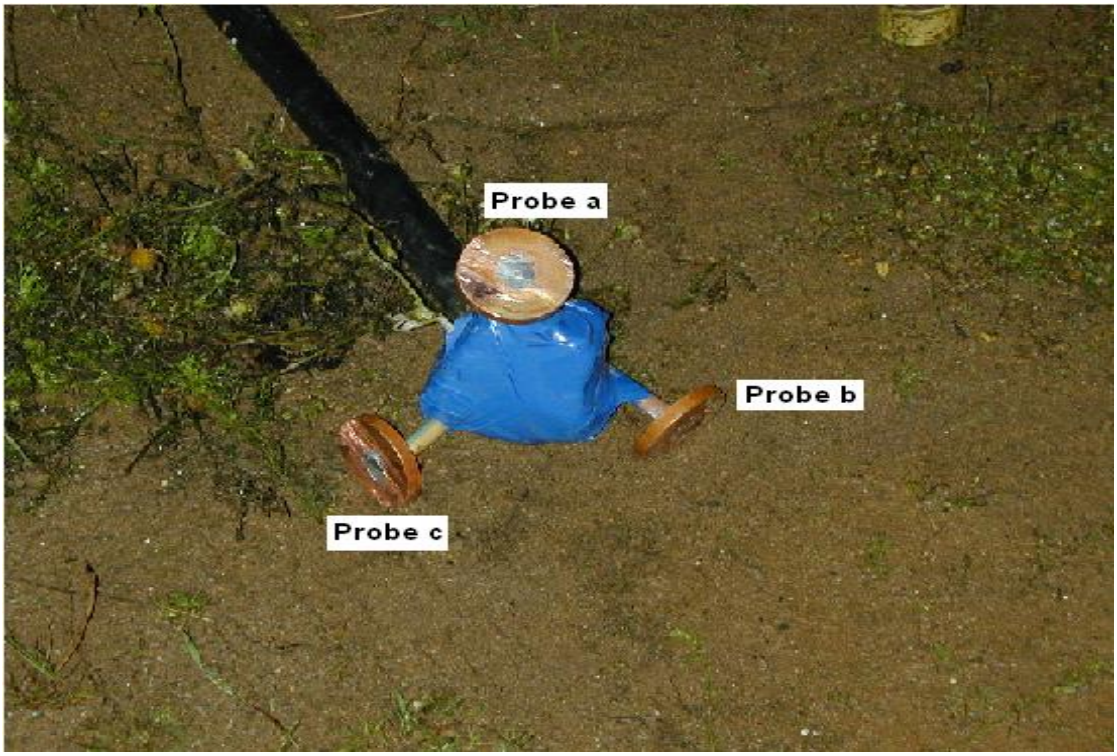

Figure 3.21: Set of probes showing mutually perpendicular directions

Figure 3.22 shows the frequency response of the EPR of the tower footing No. 2. As can be seen from the figure, the EPR magnitude is 9.5 V at 52 Hz and falls gradually with increasing in frequency up to 10 kHz. The frequency response of the tower impedance is shown in Figure 3.23.

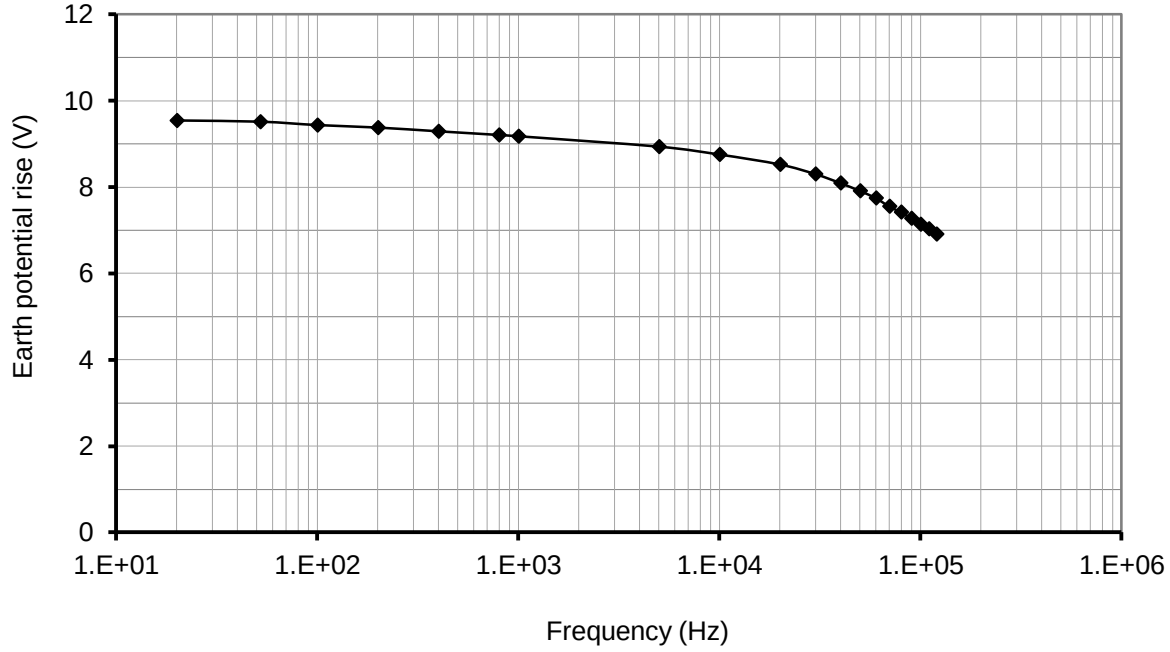

(a)

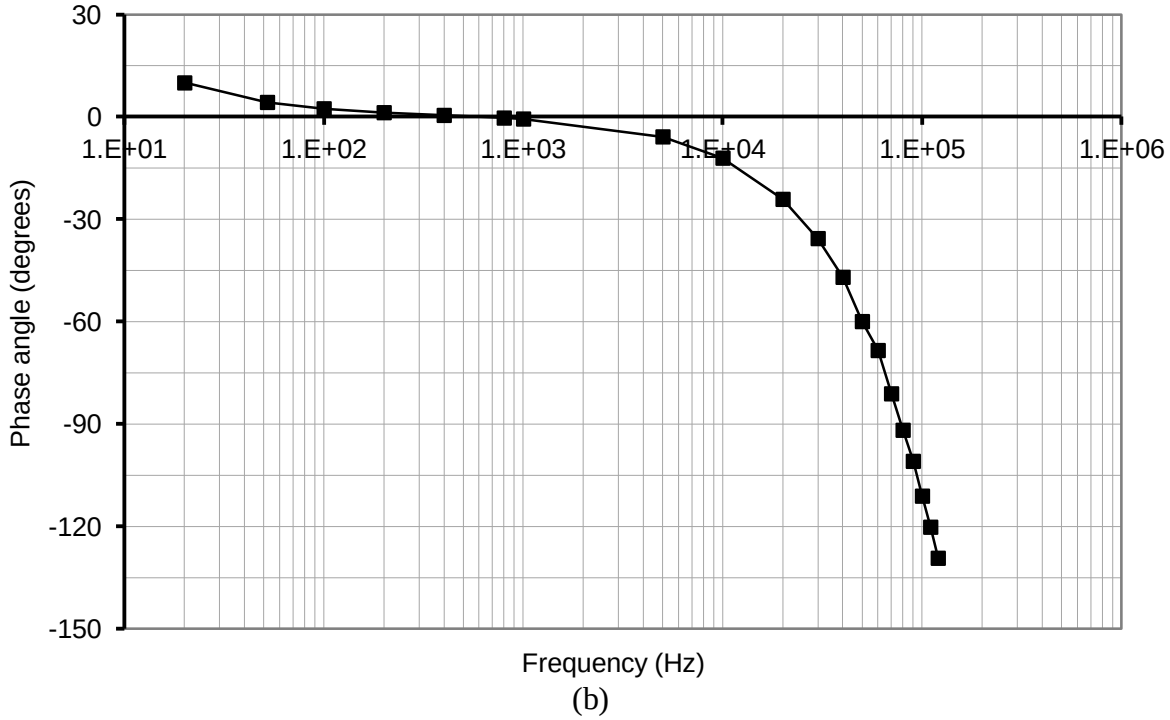

(b)

Figure 3.22: Frequency response of EPR of tower footing No2; showing (a) magnitude of EPR and (b) EPR phase angle

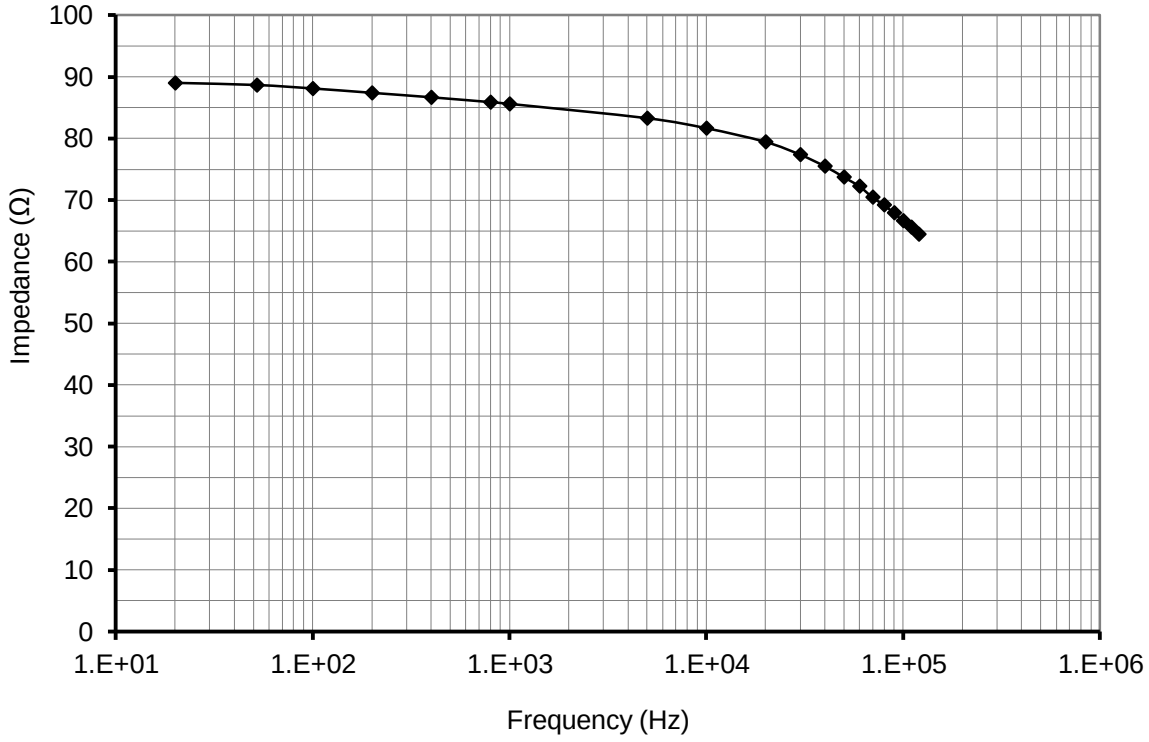

(a)

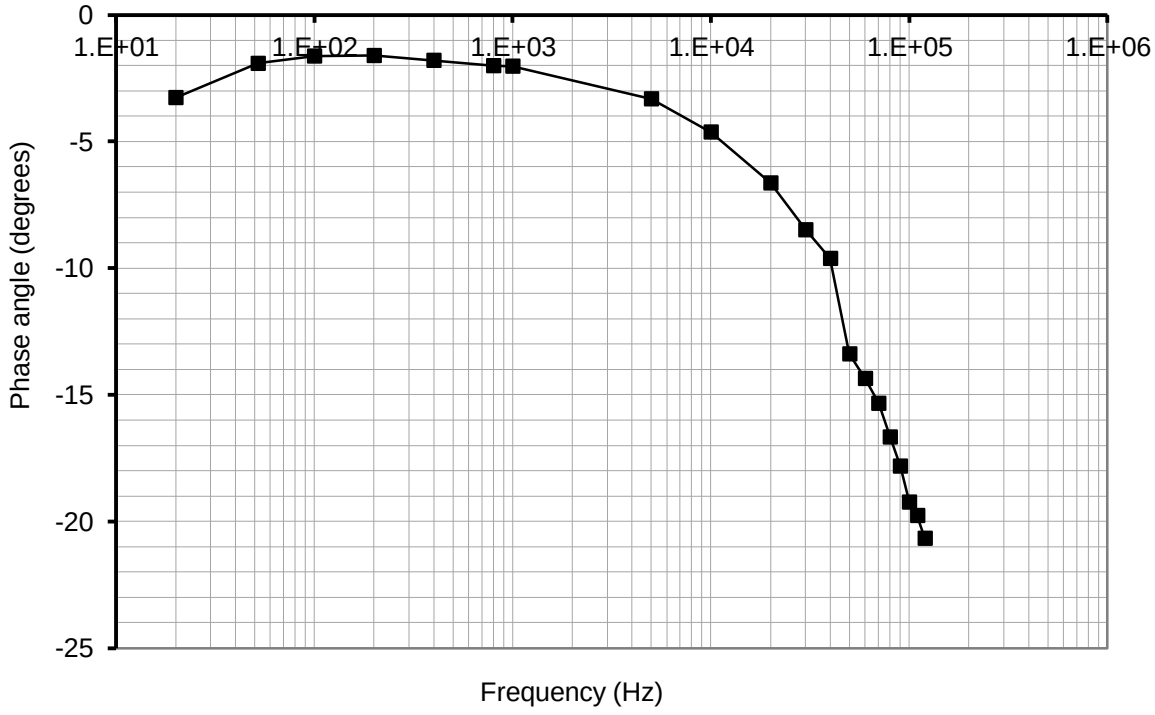

(b)

Figure 3.23: Frequency response of impedance of tower footing No. 2 showing (a) impedance magnitude (b) impedance phase angle

Figures 3.24-3.26 show the frequency response of each the three probes buried at different depths. Unlike the frequency response of ground potential measured by probes buried in the concrete footing, the frequency response of soil shows two main differences: (i) the potential (at low and high frequencies) measured by the three probes at the same depth are almost the same (ii) there is a slight upturn in potential at high frequencies rather than a down turn.

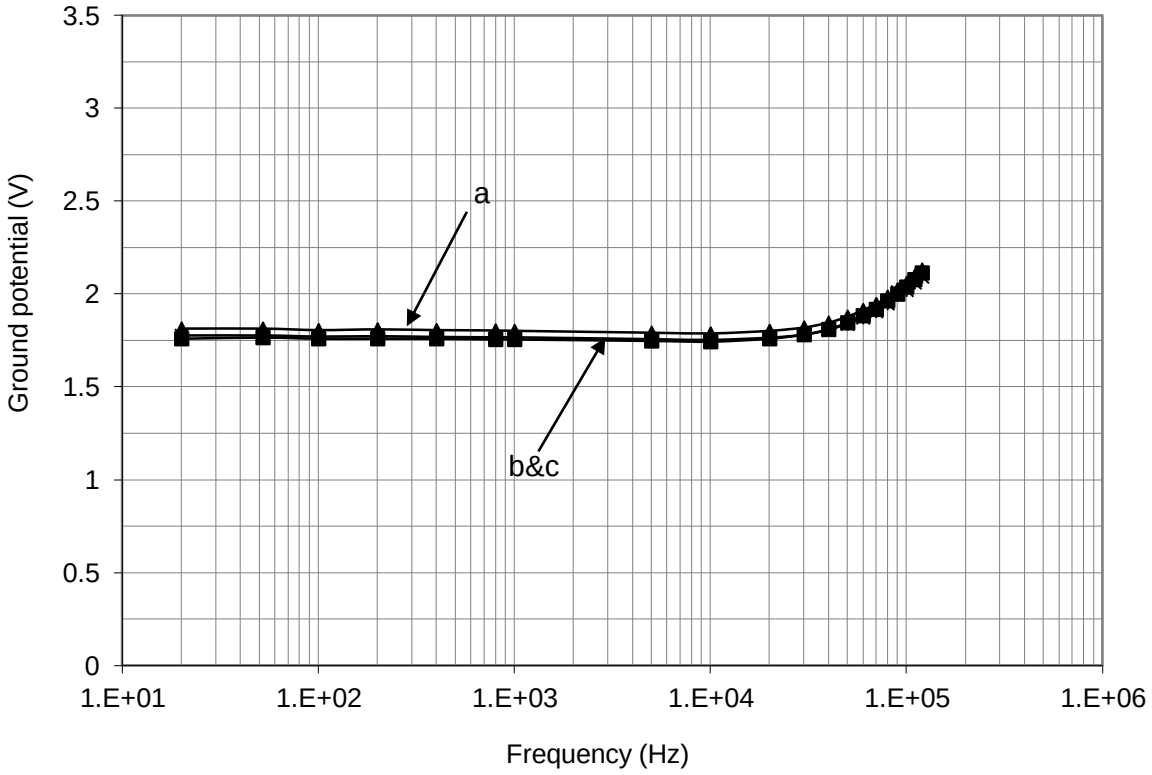

Figure 3.24: Frequency response of the magnitude of ground potential as measured by probes (a, b and c) at 1m depth

The results for the sets of probes buried at 2m and 3m show similar trends to those obtained for the probes buried at 1m. The potential decreased slightly with depth at low frequency as can be seen from Figures 3.25 and 3.26.

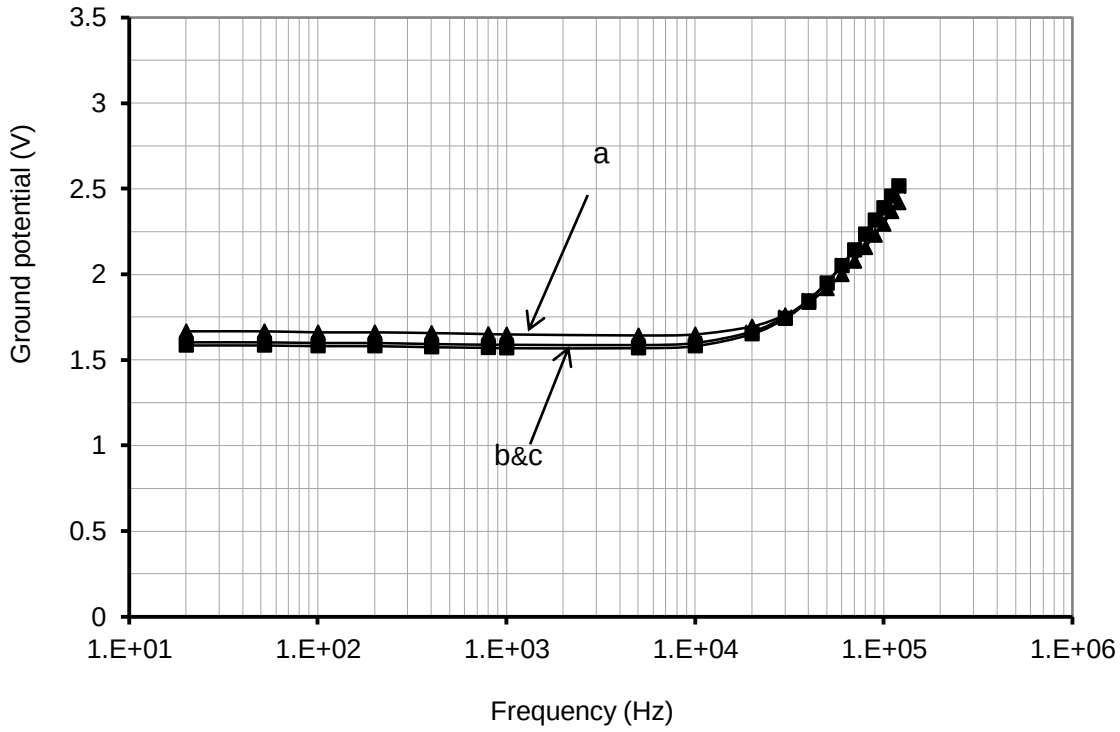

Figure 3.25: Frequency response of the magnitude of ground potential as measured by probes (a, b and c) at 2m depth

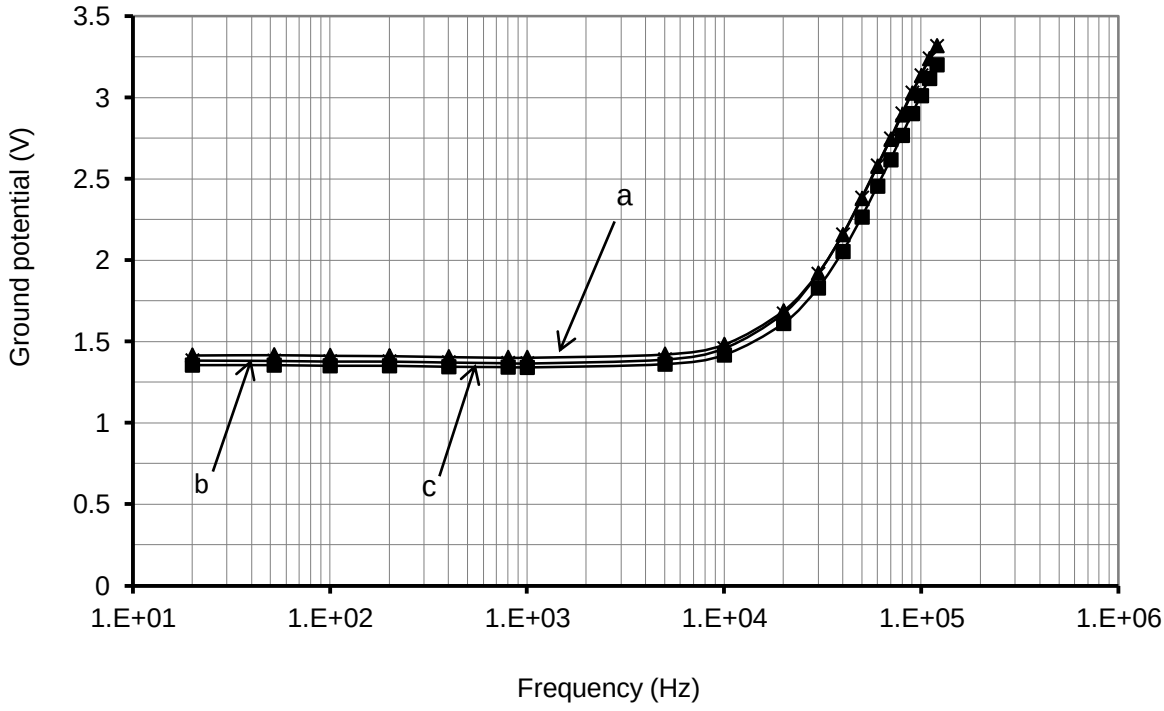

Figure 3.26: Frequency response of the magnitude of ground potential as measured by probes (a, b and c) at 3m depth

3.5.2.1 Ground potential measured by the probes in soil at different depths

The ground potential values recorded by individual probes (a, b and c) located at different depths are shown in Figures 3.27-3.29. Figure 3.27 presents the magnitude of ground potential at probe b located at 1 m, 2 m and 3 m. From the figure, the ground potential for the probe at 1 m is initially constant and higher than the corresponding values for probes at 2 m and 3 m, until the upturn frequency which appears to decrease with an increase in depth. For example, the upturn frequency for the probes at 1 m, 2 m and 3 m depth is 40 kHz, 20 kHz and 10 kHz, respectively. The deeper the probe the steeper the rate of increase of potential above the upturn frequency and at 120 kHz, the values of potential at 1m, 2m and 3m are 2.125V, 2.6V and 3.4V, respectively. This result indicates that the potential in soil increases with depth at the high frequencies range used in this field test. Similarly, the trend in Figures 3.28 and 3.29 for probes a and c show that at frequencies lower than the upturn frequency the effect of earth leakage resistance is dominant and the larger the depth is the lower the potential will be. However, above the upturn frequency, the potential for lower depths increases more rapidly than the potential at larger depths.

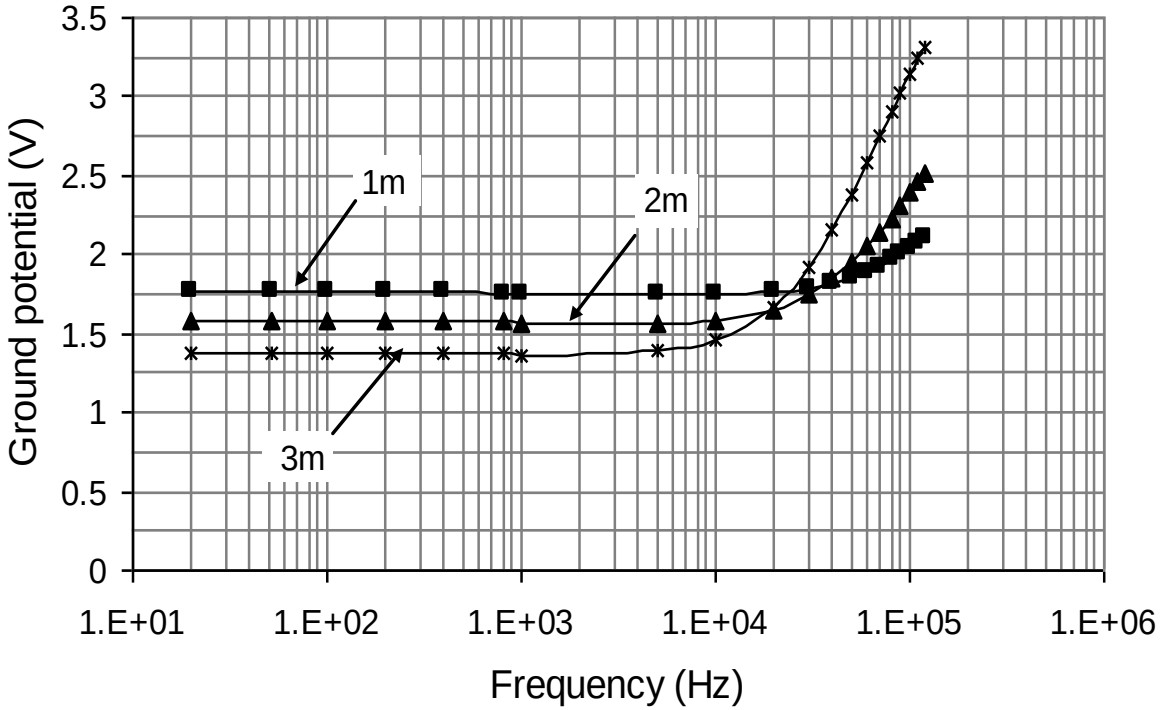

3.27: Frequency response of potential at probe b at different depths

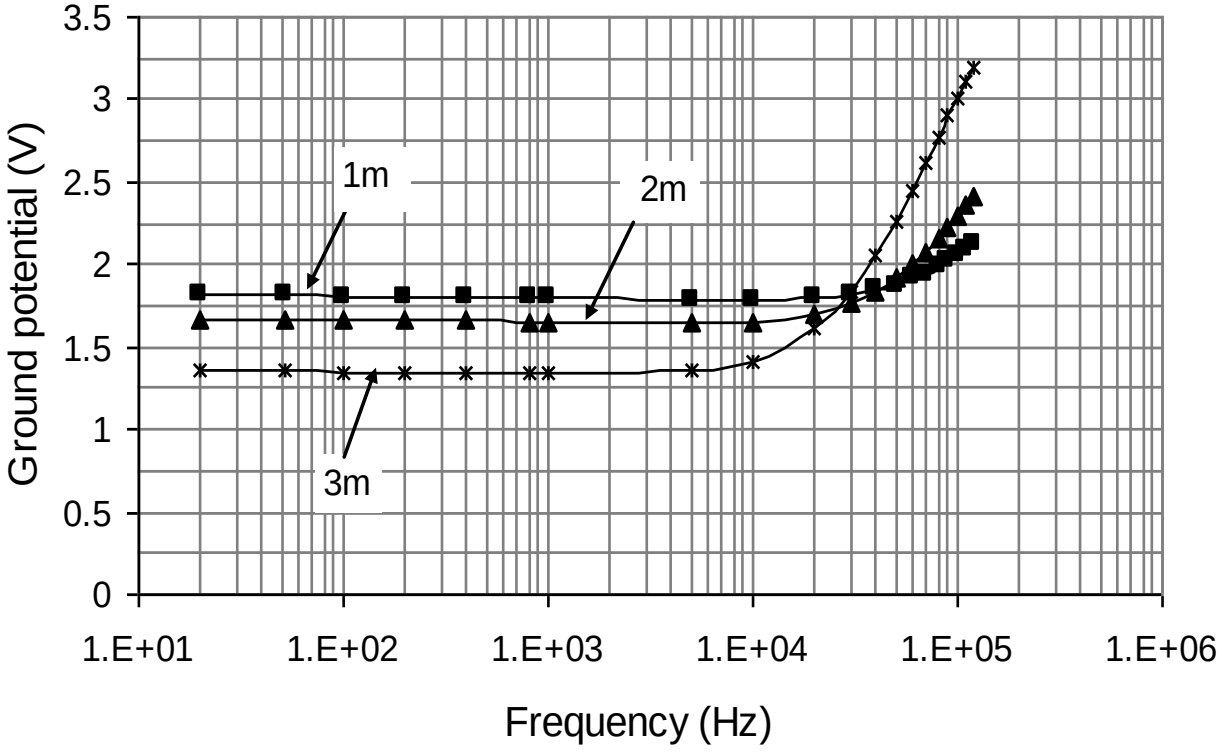

3.28: Frequency response of potential at probe a at different depths

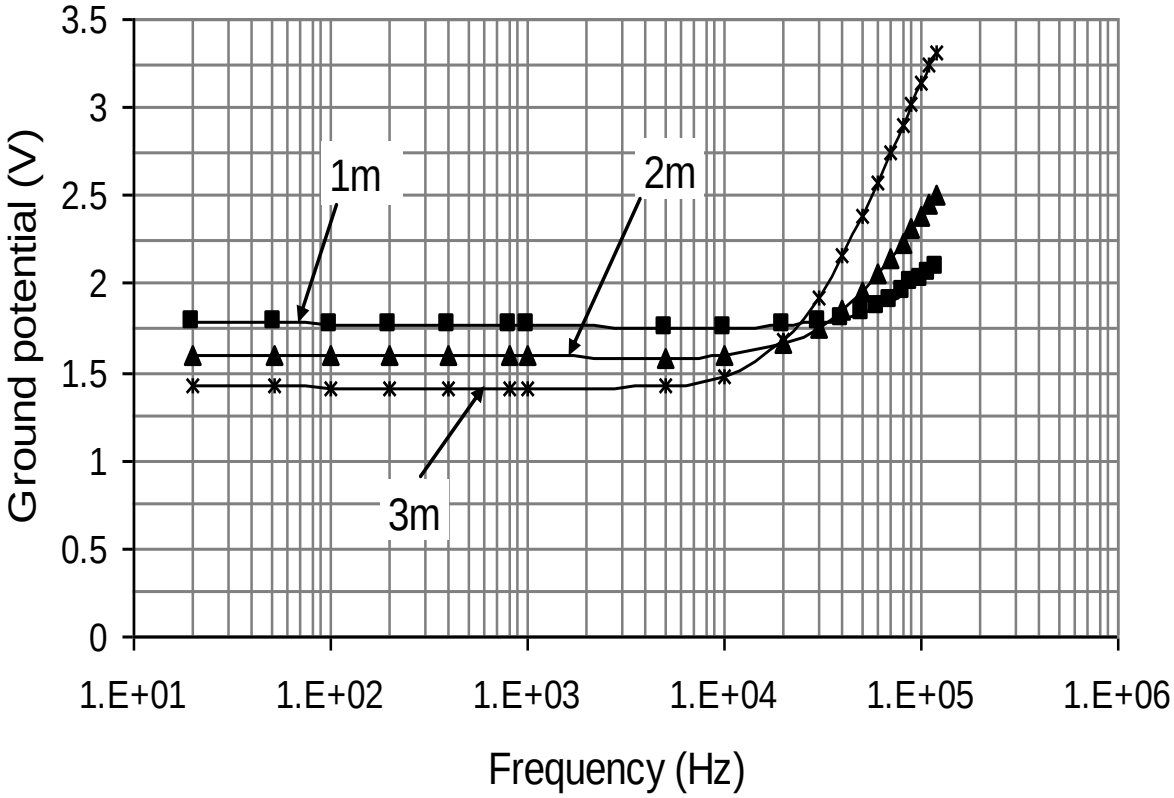

3.29: Frequency response of potential at probe c at different depths

3.6 DC resistance measurements of earthing test system

The resistance of individual 8 electrodes of the ring electrode shown in Figure 3.30, was measured. Furthermore, combinations of the electrodes connected with buried bare and insulated conductors were evaluated. The measurements were then compared with computed values.

To measure the earth resistance of the electrode of the various elements of the test circuit, the fall-of-potential test was used. In this method, see Figure 3.31, three electrodes are used. A current (I) circulates between the earth electrode under test (e.g. tower base) and an auxiliary electrode (C2) placed well away from the electrode under test. The voltage (V) between the electrodes under test and probe (P2) is measured [3.8]. The apparent resistance is given by the quotient V/I.

The distance, P, see Figure 3.31 of electrode ‘P2’ from the tower base is incrementally increased and a series of measurements are logged. The plot of voltage against (p) will contain a straight portion if the auxiliary electrode (C2) is placed at sufficiently distance [3.8]. Strictly, this distance should be sufficiently large that the straight portion of the curve contains the point (P), where (P=0.618C) [3.8], as this is the point on the curve which corresponds to the true earth resistance. Here, the (C2) probe was placed 100 m away from the tower base, and this distance was deemed sufficient that the true earth resistance could be determined from measurements made with the potential electrode (P2) positioned at a distance 61.8 m from the electrode under consideration (tower base).

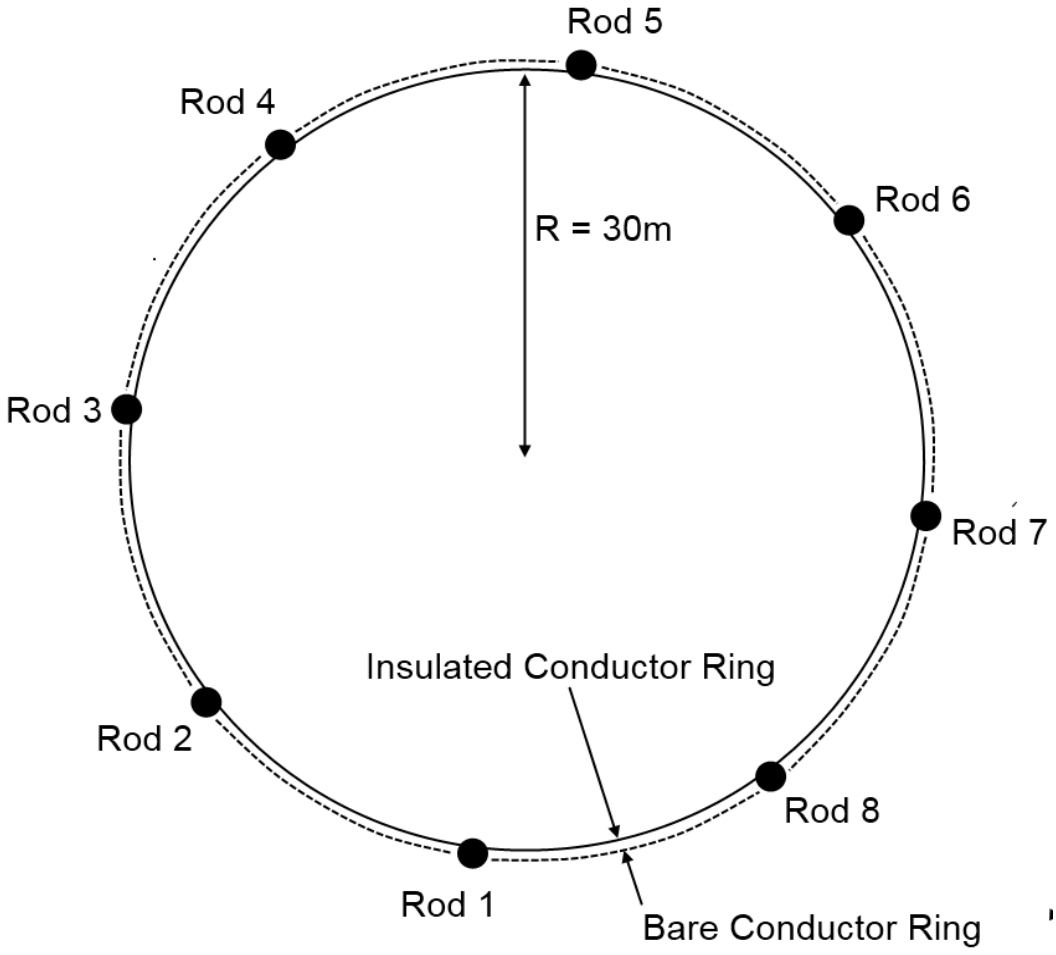

Figure 3.30: Ring electrode composes 8 rods and bare and insulated conductors

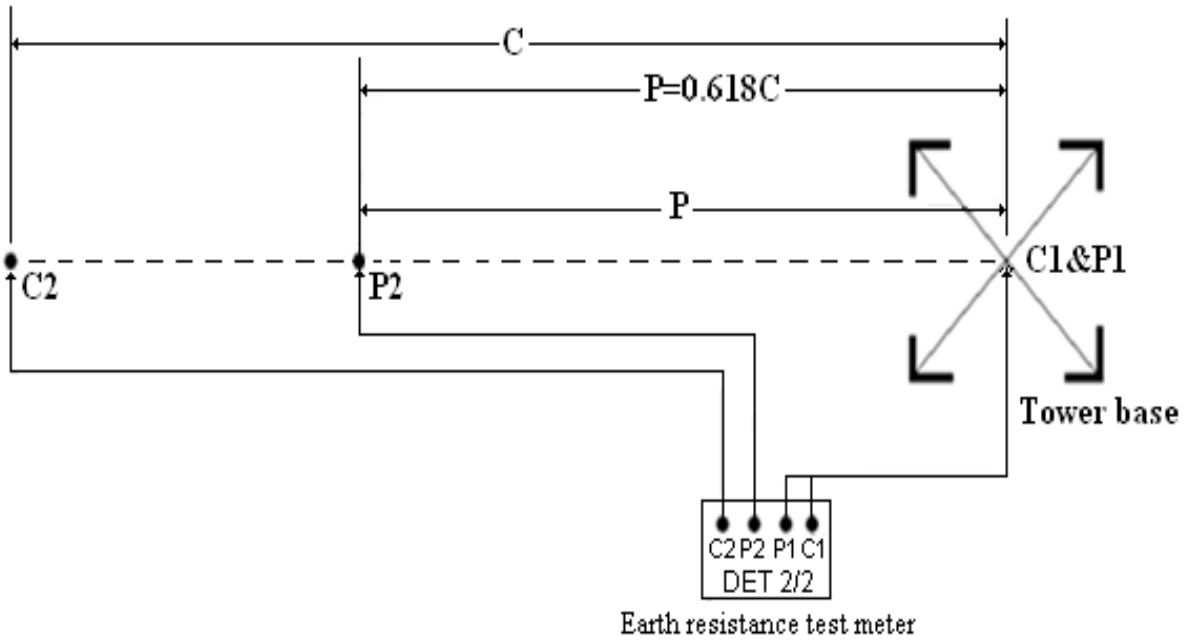

Figure 3.31: 61.8% method for measuring earth electrode resistance

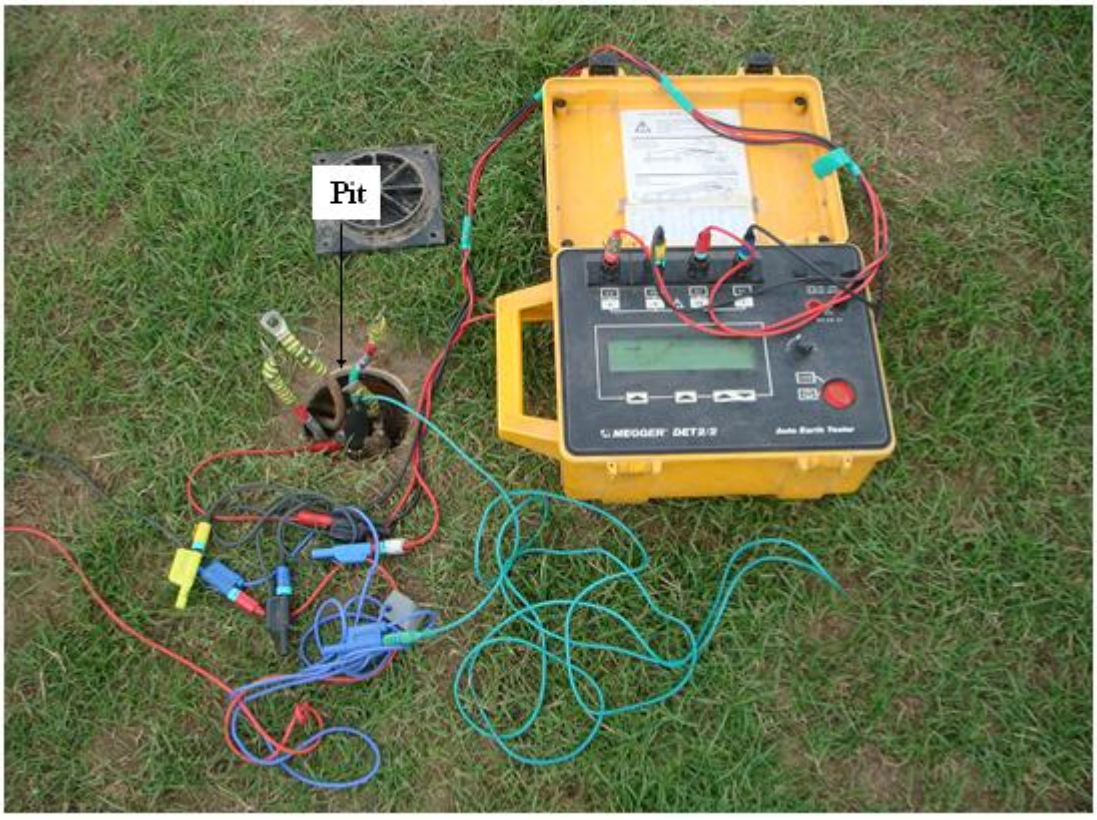

Figure 3.32: DET 2/2 instrument for DC earth resistance

The DC earth resistances of the individual rod electrodes were measured with the commercial DC earth resistance test meter (Megger DET 2/2) [3.9]. The measurements carried out on 23-09-2009 and are tabulated in Table 3.1. The earth resistance tester was placed beside one of 8 pits, where the insulated and bare conductors connect and disconnect to the earth rod to obtain different configurations of the ring electrode, as will be discussed later, is shown in Figure 3.32. These rods are of 16mm diameter, driven to 2.4m deep and arranged in a ring as shown in Figure 3.30. It is clear from the table that there are considerable differences in the magnitudes of measured earth resistances of the different rods. For example, the earth resistance of rod No. 1 is 79.6 Ω while it is 122 Ω for rod No. 8. The differences are attributed to the known lateral variation of the soil resistivity across the area occupied the rods in the local area.

The geometrical test configuration was simulated using the HIFREQ module of the CDEGS software [3.10]. The simulation requires all electrodes to be modelled as cylindrical conductors with radii much smaller than length. A two-layer soil model was used where the upper layer's soil resistivity is 200Ωm with depth of 9m and the bottom layer of soil resistivity is 30 Ωm. The computed results in the Table 3.1 shows large differences between the measured and computed values of the DC earth resistance of the rods which is ascribed to the simple soil resistivity model.

It was established that if a single vertical earth electrode inserted into the upper layer of a soil consisting of a two layers, where the ratio of the length of the vertical electrode to the thickness of the layer more than 0.25, so the influence of the bottom layer has to be taken into consideration [3.11].

The DC earth resistance of the earthing components can be calculated using well established formulae [3.8]. For a single vertical earth electrode inserted into the upper

layer of a soil consisting of a number of layers, the earth resistance was calculated using Equation (3.1).

$$R_1 = \frac{\rho_1}{2\pi l}\left[\ln\left(\frac{4L}{r}-1\right)+\sum_{n=1}^{\infty}\frac{k^n}{2}\ln\frac{nh/L+1}{nh/L-1}\right] \quad \text{..... (3.1)}$$

Where r is the radius of the electrode, L is the length, ρ_1 is the resistivity of the top layer of soil, k the reflection coefficient given by $(\rho_2-\rho_1)/(\rho_2+\rho_1)$, p_2 is the resistivity of the bottom layer of soil, and h is the depth of the upper soil layer. In this case ρ_1=200Ωm, ρ_2=30Ωm, h=9m. The results are added in Table 3.1 where the equation 3.1 was used to calculate the rod earth resistance and then tabulated in the table. The calculated value of rod earth resistance is 94Ω which lies in the range between the minimum and maximum measured values.

Table 3.1: DC earth resistance of vertical electrodes

	DC resistance (Ω)				
Earth electrode	**Measured**	**Calculated**	**CDEGS**	**Percentage error (%) calculated**	**Percentage error (%) CDEGS**
Rod No 1	79.6	94.0	61.5	18	22.7
Rod No 2	92.0	94.0	61.5	2.1	33
Rod No 3	88.7	94.0	61.5	5.9	30.6
Rod No 4	117	94.0	61.5	19.6	47
Rod No 5	88.6	94.0	61.5	6	30.5
Rod No 6	96.7	94.0	61.5	2.79	36.4
Rod No 7	105	94.0	61.5	10.4	41.4
Rod No 8	122	94.0	61.5	22.9	49.5

Table 3.2 also shows results of measured DC earth resistance for the rods interconnected by bare ring conductors with cross sectional area 0.2cm^2 and insulated ring conductors to form a ring electrode in various configurations is calculated by equation 3.3. As can be seen from the table, the DC earth resistance of the rods connected in parallel by the insulated conductor (13.4Ω) is five times as high as when they are connected by bare sections of a conductor. In the case of the bare conductor ring, the earth resistance is 2.95Ω and when interconnected with the rods, a slight decrease in the resistance of 10% was observed.

For the ring electrode, Equation (3.2) is used [3.8].

$$R_{ring} = \frac{\rho_1}{2\pi^2 D}\left(\ln\frac{8D}{d_o} + \ln\frac{4D}{2h_o}\right) \quad \text{..... (3.2)}$$

The value of ρ_1 in Equation (3.2) was taken as the resistivity of the top soil layer (200 Ωm).Where D is the ring diameter, h_o its burial depth and d_o the diameter of the wire. Equation 3.2 was used to calculate the earth resistance of the ring electrode and tabulated in Table 3.2. The DC resistance was calculated as 2.95Ω which is very close to the measured value. According to Tagg [3.8], the equivalent earth resistance of n rods arranged in a circle can be calculated using:

$$R_o = \frac{R_1}{n}\left(1 + 0.5\alpha + \alpha\sum_{s=1}^{s=(n/2-1)}\frac{1}{\sin\frac{s\pi}{n}}\right) \quad \text{..... (3.3)}$$

Where $\alpha = r/R$, R_1 is the resistance of a single rod calculated from Equation (3.1) with r radius of the earth electrode (r = 8 mm) and l = 2.4 m, and R is the radius of the ring. The calculated earth resistance of the ring and the 8 electrodes in parallel is shown in Table 3.2. As can be seen, there is good agreement between the calculated (11.76Ω)

and measured (13.4Ω) resistances. For a ring electrode with 8 rods at its periphery, the earth resistance is [3.13]:

$$R_c = \frac{R_{ring}R_o - R_m^2}{R_{ring} + R_o - 2R_m} \quad \text{..... (3.4)}$$

Where R_m is the mutual resistance between the ring electrode and the rods [3.13], given by:

$$R_m = \frac{\rho_1}{\pi^2 D} \ln \frac{4D}{\sqrt{\frac{2lh_o}{e}}} \quad \text{..... (3.5)}$$

The calculated value of the ring electrode with 8 rods at its periphery was 2.3Ω compared with the measured value of 2.67Ω, as shown in Table 3.2 where equation 3.4 was used to calculate the bare ring with 8 rods connected at its periphery. The tower footings resistance can be computed using Equation 3.1 for vertical earthing rods. In this case, it is assumed that each footing is represented by a cylinder with radius r and length *L* with a linear current source along its axis. For the tower base (4 footings in a square of side (s), the total earth resistance, R_T, is [3.13]:

$$R_T = R_1 \frac{1 + 2.707\alpha}{4} \quad \text{..... (3.6)}$$

$$\alpha = \frac{\rho_1}{2\pi\rho_2 s} \quad \text{..... (3.7)}$$

Where the equivalent radius r = 27.4 mm and *L* = 3 m. R_1 is the earth resistance of the single tower footing calculated by equation (3.1) where r in the equation replaced by the equivalent radius of the tower footing.

For all configuration of the ring earth electrode, a good agreement has been obtained between the measured and calculated DC resistance values. As regard to the computed values, the agreement was also obtained, but to a less degree.

Table 3.2: DC earth resistance of ring configurations

	DC resistance (Ω)				
Earth electrode	**Measured** 23-09-2009	**Calculated**	**CDEGS**	**Percentage error (%) calculated**	**Percentage error (%) CDEGS**
Bare ring	2.95	2.95	1.96	0	33.5
Bare ring with 8 rods	2.67	2.5	1.85	6.3	30.7
8 Rods in parallel connected with insulated conductor	13.4	11.76	9.78	12.2	27
Bare ring with 8 rods and insulated conductor	2.66	---	1.84	---	30.8

The DC earth resistance measurements were extended to the individual footings of the tower base and the tower base comprising the parallel connection of the footings. The results are shown in Table 3.3.

As in the case of the rods, the DC earth resistance of the individual footing varies considerably, from 64.2Ω for footing No. 4 to 117.6Ω for footing No. 1. The dimensions and construction of each footing are identical, and the differences are due to the variation in local soil resistivity around the footings.

The calculated results are given in Table 3.3. The differences between calculated and measured results are attributed to the variation in local resistivity of the soil surrounding each tower footing.

Table 3.3: DC earth resistance of tower footing

	DC resistance (Ω)				
Earth electrode	**Measured** 24-09-2009	**Calculated**	**CDEGS**	**Percentage error (%) calculated**	**Percentage error (%) calculated**
Footing No 1	117.6	63.0	55	46.4	53
Footing No 2	67.2	63.0	55	6.2	18
Footing No 3	80.7	63.0	55	21.9	31.8
Footing No 4	64.2	63.0	55	18.6	14.3
Tower base	20.9	21.9	15	4.7	28.2

3.6.1 Influence of seasonal variation on DC earth resistance

It is known that there are seasonal variations in soil resistivity and this affects the resistance of earth electrodes and potentials developed in their close vicinity. The influence of seasonal variation on the measured DC resistance of the test earth electrodes has been studied over a period of 13 months. DC measurements were made using the fall-of-potential method for individual legs, the tower base, eight rods in a circle connected by bare conductors and a single rod (rod 1). The results are plotted in Figures 3.33, 3.34 and 3.35 respectively.

Figure 3.33 shows the DC resistance measurements over a period of 13 months. As can be seen, the average DC earth resistance of the individual tower footings 1, 2, 3 and 4 over the period is 138.5Ω, 74.4Ω, 92.6Ω and 77.5Ω respectively.

Figure 3.33 shows the DC resistance measurements over a period of 13 months. As can be seen, the DC earth resistance varied over the year by more than 30% for tower footings 1, 3 and 4 and by 25% for tower footing 2. When the footings are connected in parallel to form the tower base, there was a variation of 22%.

The changes in DC earth resistance appear similar for all the electrodes and are due to variations in soil resistivity influenced by moisture content and temperature.

The figure depicts that the resistance being higher in the winter and lower in the summer. Since one of the major factors in the resistance is the resistivity of the bulk of the soil surrounding the electrode is liable to variations with moisture content and temperature among other things, such as, effect of vegetation and bacteriological activity, which is highest in the summer [3.12]. Further, however, the earth resistance in June 2010 shown lower resistance than the corresponding month in 2011.

.

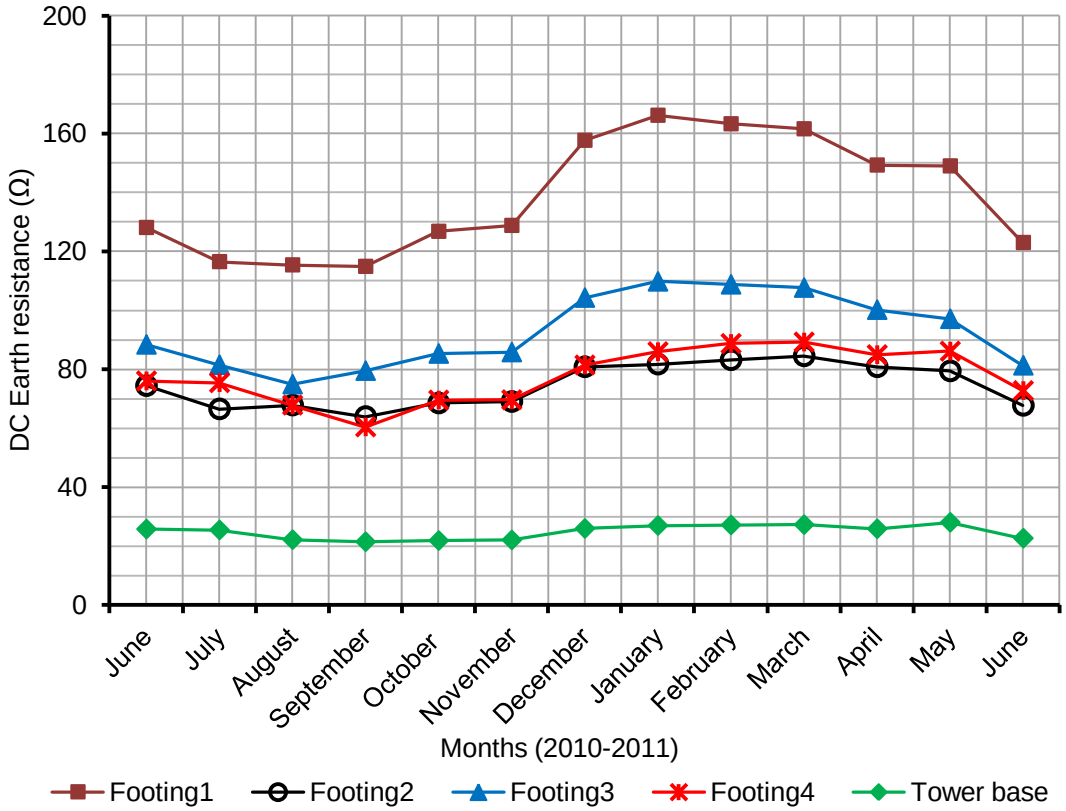

Figure 3.33: Seasonal variation on DC earth resistance of tower base test object

In the case of the current return electrode, the rods interconnected by bare conductors buried at a shallow depth of 30 cm showed considerably more variation in the DC resistance over the 14 months of the test. The maximum value was more than three times the minimum, as shown in Figure 3.34. This indicates that an earthing system buried in the soil layer near the surface is more exposed to seasonal variation than deeper earthing systems. For a single rod (No. 1) driven to a depth of 2.4 m, there was very much less fluctuation in the DC earth resistance (Figure 3.35), and the average value over the 12 months period is 77%, and it shows very small variation in the measured DC resistance which is about 10% on either side of the mean value over the period.

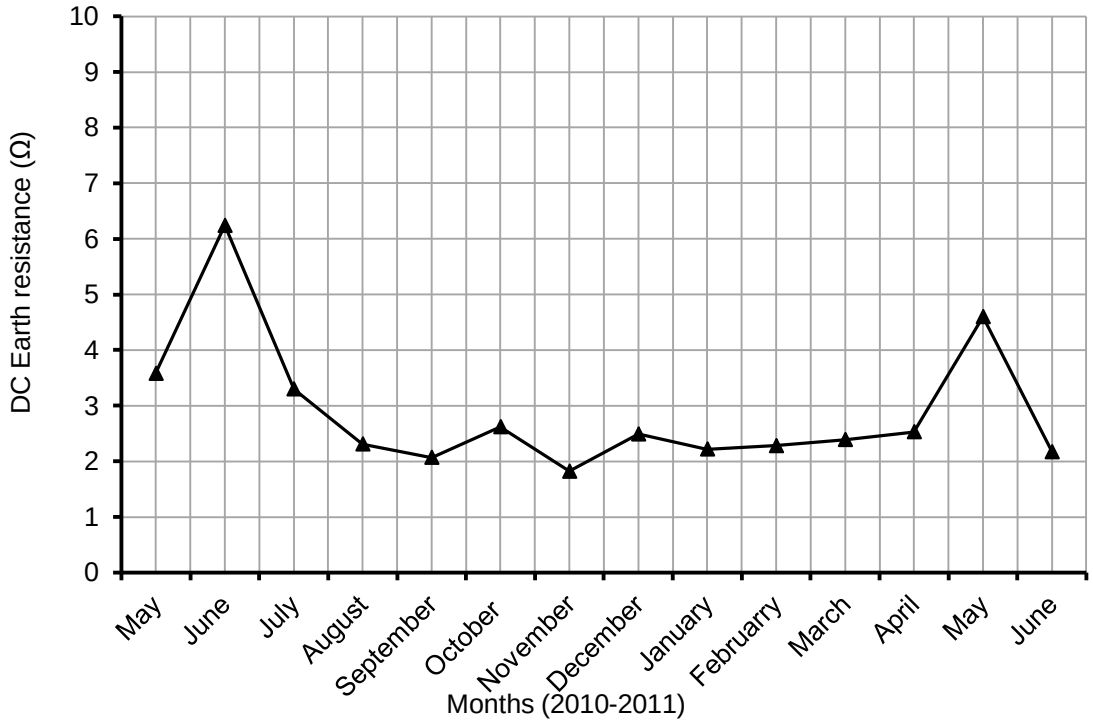

Figure 3.34: Seasonal variation of DC resistance of current return electrode bare ring with all 8 rods

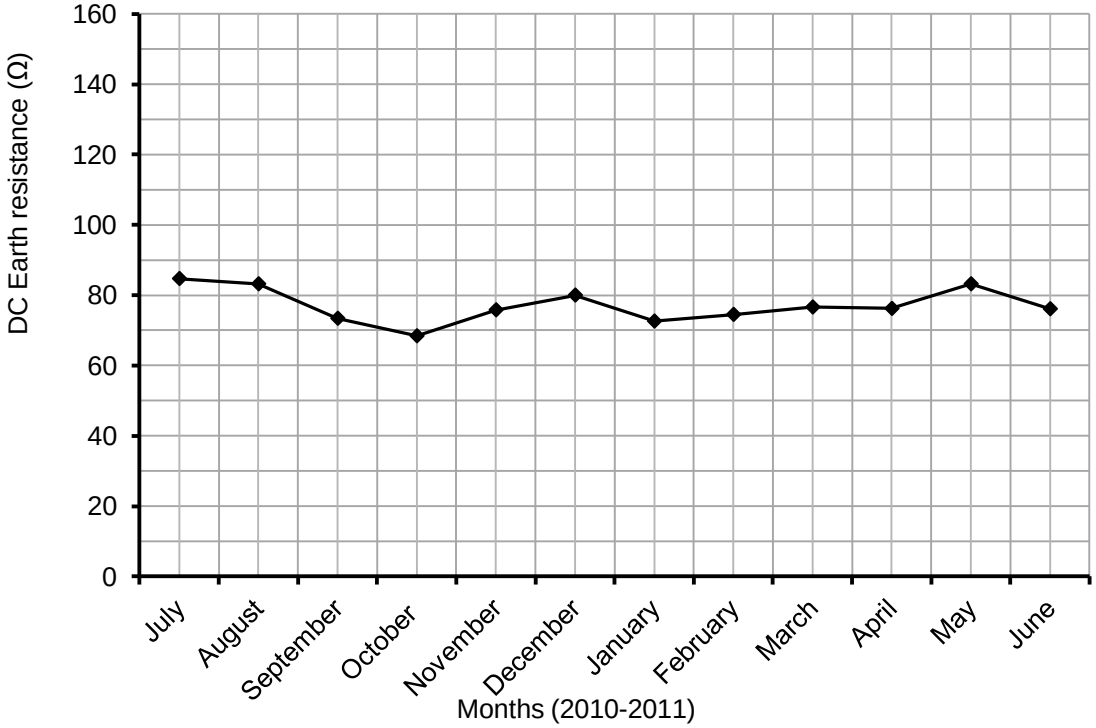

Figure 3.35: Seasonal variation of DC resistance for rod No. 1

3.7 Mitigation of hazards around transmission tower base

Previous work on the mitigation of safety voltage at transmission bases [3.14], has proposed a number of mitigation techniques to limit electrocution hazards in the vicinity of the transmission line tower bases. These techniques comprise potential grading, electrical insulation of tower legs, chemical treatment of soil, counterpoises, fencing, mesh and inclined rods.

In this section, investigations of control of potential gradient for both touch and step voltages are carried out.

For this study, the configuration of a 275kV L2-type tower base that was installed at Cardiff University's Llanrumeny site is adopted. The tower leg of cross section of 'L' shape of dimensions (123mm*10mm) was modelled as a circle of radius 27.4mm, as shown in Figure 3.36. A uniform soil model was used with different resistivity value of 10Ωm, 100Ωm, 1000Ωm and 10000Ωm.

In this study, the investigations are carried out on the tower base without and with potential gradient control rings.

3.7.1 Tower base with no mitigation rings

In this investigation, for each soil resistivity model, the earth potential rise (EPR) and earth surface potential (ESP) is computed at frequencies 50 Hz, 1 kHz, 500 kHz and 1 MHz, and 1A injection current throughout the investigation. The earth potential rise is computed at the tower injection point and the earth surface potential is computed along diagonal profiles of length 5m starting at a point 1m away from the tower leg in the outward direction. Figure 3.37 shows the plan view of the tower line model without any mitigation rings technique. The geometrical test configuration was simulated using the HIFREQ module of the CDEGS software [3.10]. The simulation requires all

electrodes to be modelled as cylindrical conductors with radii much smaller than length. The touch voltage was computed as the earth surface potential at 1m distance tower footing subtracted from earth potential rise at the leg. The step voltage is computed as a voltage difference between two points on the earth surface that are 1m apart.

Figure 3.38 illustrates the touch voltages which are given as percentage of the reference EPR for range of frequencies. From the figure, it can be seen that at 50Hz and 1000Hz, the touch voltage is 55% of the EPR for all different soil resistivities. It can be also seen from the figure that, at 500 kHz, the touch voltage increased sharply at 10Ωm up to nearly 90% of EPR. For the higher frequency of 1MHz, an increase in touch voltage as much as 93% and 66.5% of EPR for low soil resistivity of 10Ωm and 100Ωm respectively. In the case of higher soil resistivity a marginal change has been observed. Table 3.4 shows a summary of the EPR magnitudes of tower base and the corresponding touch voltage as a percentage of earth potential rises. As can be seen, the EPR increases with the soil resistivity.

As regard to step voltage, the results of computation of the step voltage as a percentage of EPR at 1m, 2m, 3m and 4m has been tabulated in Table 3.5. From the table, it can be seen that a higher step voltage as a percentage of EPR is obtained at 1m distance from the tower leg. This indicates that the potential on the ground surface is higher in the proximity of tower legs. The step voltage as a percentage of EPR forms 11.6% for frequencies of 50Hz and 1000Hz, independent of soil resistivity. For higher frequencies, 500 kHz and 1 MHz, the step voltage as a percentage of EPR increases with soil resistivity. The step voltage decreases as a result of increasing the distance from the tower leg.

a) Traversal view b) Equivalent area

Figure 3.36: Schematic diagram of leg of transmission tower base

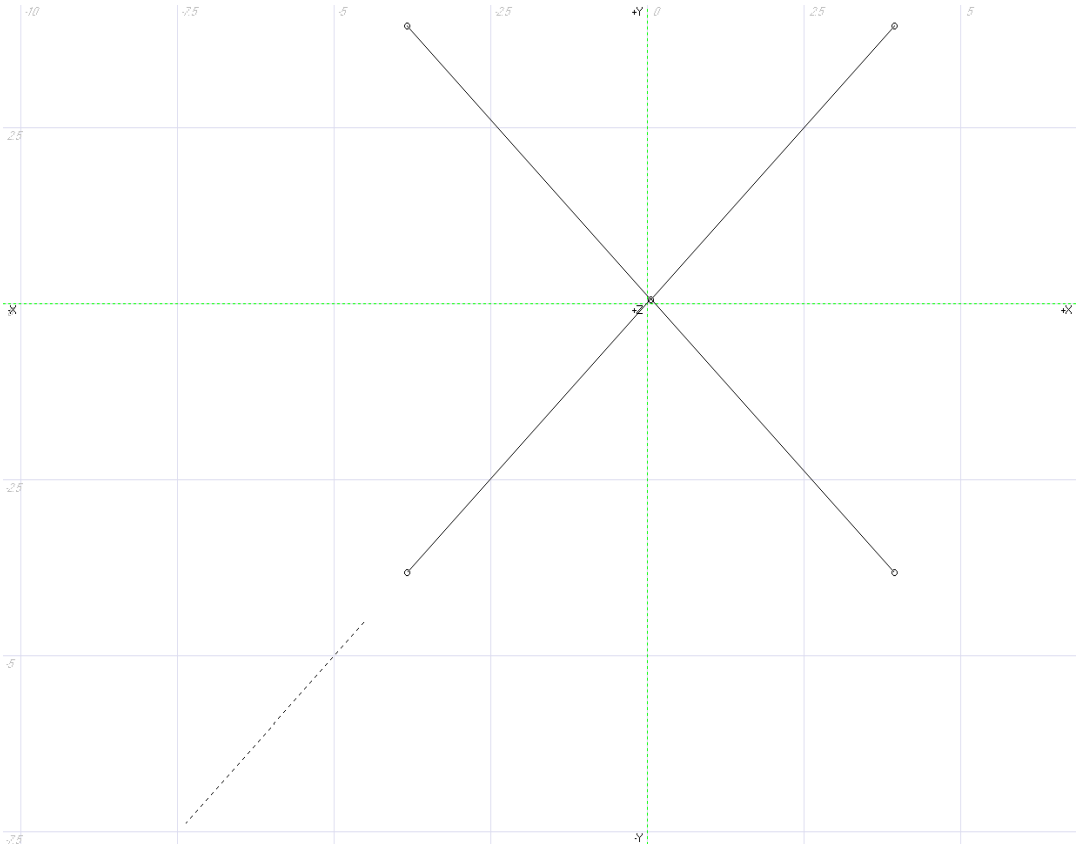

Figure 3.37: Tower base model with no mitigation

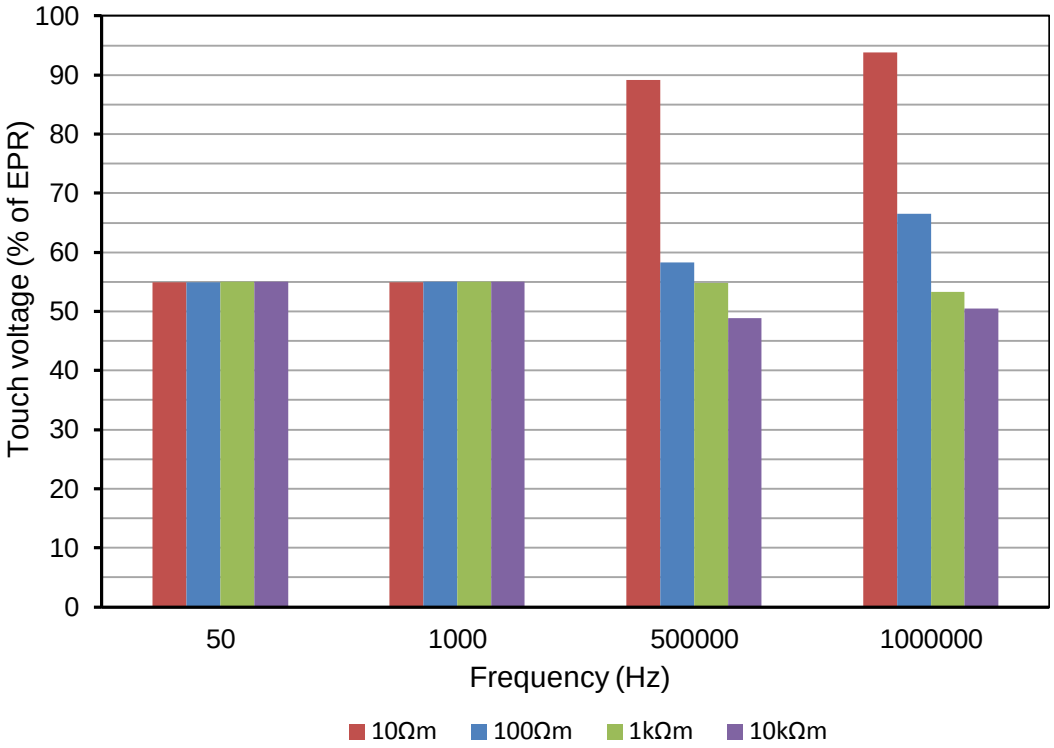

Figure 3.38: Touch voltage with no mitigation rings vs. frequency

Table 3.4: Computed EPR and touch voltage (% of EPR) at deferent frequency and resistivity

f (Hz)	Resistivity (Ωm)							
	10Ωm		100Ωm		1000Ωm		10000Ωm	
	EPR (V)	TV (% of EPR)	EPR (V)	TV (% of EPR)	EPR (V)	TV (% of EPR)	EPR (V)	TV (% of EPR)
50	0.823	54.96	8.23	54.98	82.32	54.98	823.2	54.98
1000	0.822	54.95	8.23	54.98	82.32	54.98	823.2	54.98
500000	4.11	89	8.9	58.28	79.2	54.79	559.8	48.82
1000000	7.95	93.8	11.28	66.5	74.42	53.35	430.9	50.45

Table 3.5: Computed EPR and step voltage (% of EPR) at deferent frequency and resistivity

SV	**1m**							
f (Hz)	Resistivity (Ωm)							
	10Ωm		100Ωm		1000Ωm		10000Ωm	
	EPR (V)	SV (% of EPR)	EPR (V)	SV (% of EPR)	EPR (V)	SV (% of EPR)	EPR (V)	SV (% of EPR)
50	0.823	11.6	8.23	**11.6**	82.32	11.6	823.2	11.6
1000	0.822	11.6	8.23	11.6	82.32	11.6	823.2	11.6
500000	4.11	2.7	8.9	10.6	79.2	11.8	559.8	12.2
1000000	7.95	1.6	11.28	8.6	74.42	12	430.9	11.7
SV	**2m**							
f (Hz)	Resistivity (Ωm)							
	10Ωm		100Ωm		1000Ωm		10000Ωm	
	EPR (V)	SV (% of EPR)	EPR (V)	SV (% of EPR)	EPR (V)	SV (% of EPR)	EPR (V)	SV (% of EPR)
50	0.823	6.2	8.23	**6.2**	82.32	6.2	823.2	6.2
1000	0.822	6.2	8.23	6.2	82.32	6.2	823.2	6.2
500000	4.11	1.5	8.9	5.8	79.2	6.3	559.8	6.4
1000000	7.95	0.9	11.28	4.6	74.42	6.4	430.9	6.4
SV	**3m**							
f (Hz)	Resistivity (Ωm)							
	10Ωm		100Ωm		1000Ωm		10000Ωm	
	EPR (V)	SV (% of EPR)	EPR (V)	SV (% of EPR)	EPR (V)	SV (% of EPR)	EPR (V)	SV (% of EPR)
50	0.823	4	8.23	**4**	82.32	4	823.2	4
1000	0.822	4	8.23	4	82.32	4	823.2	4
500000	4.11	1.27	8.9	3.7	79.2	4	559.8	4.46
1000000	7.95	0.88	11.28	3.12	74.42	4.1	430.9	4.29
SV	**4m**							
	Resistivity (Ωm)							
	10Ωm		100Ωm		1000Ωm		10000Ωm	
	EPR (V)	SV (% of EPR)	EPR (V)	SV (% of EPR)	EPR (V)	SV (% of EPR)	EPR (V)	SV (% of EPR)
50	0.823	2.8	8.23	**2.8**	82.32	2.8	823.2	2.8
1000	0.822	2.8	8.23	2.8	82.32	2.8	823.2	2.8
500000	4.11	0.7	8.9	2.6	79.2	2.8	559.8	3.2
1000000	7.95	0.4	11.28	2.15	74.42	2.9	430.9	3.15

3.7.2 Tower base with mitigation rings

In this work, a new approach to mitigate hazard voltages around the tower is proposed. It consists of a number of interconnected rings of increasing diameter and depth installed. In this investigation three rings of radius 1m, 2m and 3m buried in sequence at different depths were studied. Figure 3.39 shows the proposed configuration.

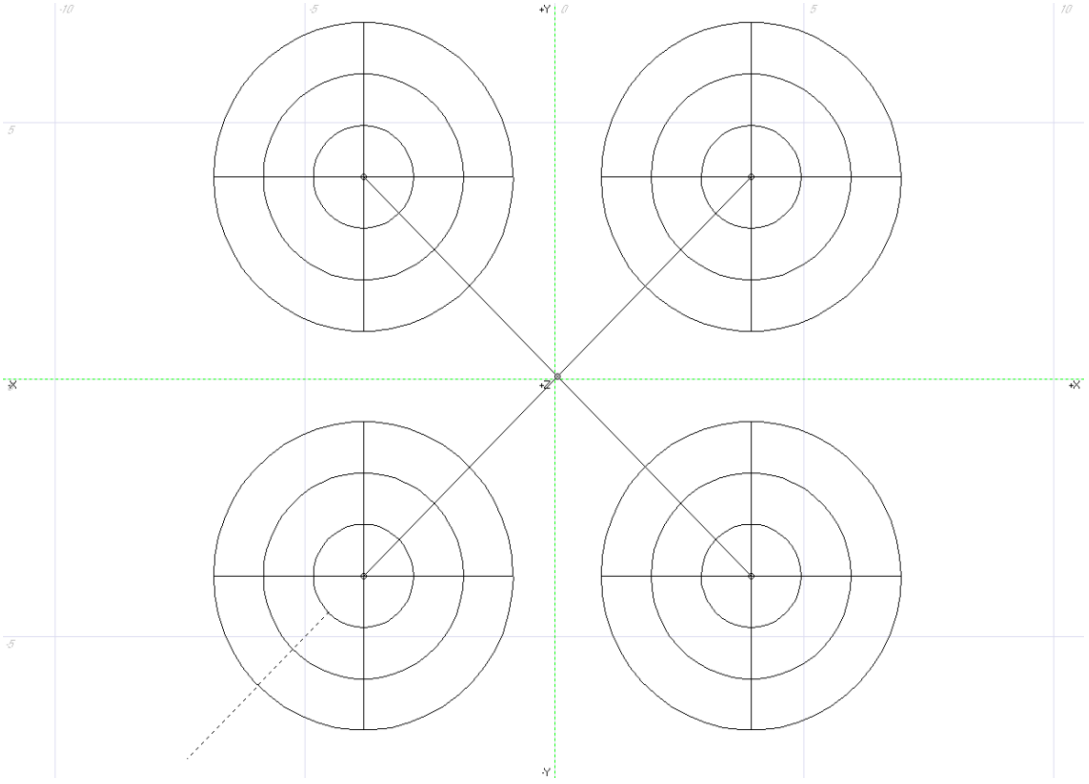

Figure 3.39: Tower base model with mitigation rings around each leg

3.7.2 .1 One mitigation ring around one leg

In order to examine the suitable depth at tower leg, a ring of radius 1m and cross sectional area 16mm^2 was placed at different depths in a soil resistivity of 100Ωm and at a frequency of 50Hz. These depths are 0.1m, 0.2m, 0.3m, 0.4m and 0.5m from the ground surface. Figure 3.40 shows the influence of depth on touch voltages as a percentage of earth potential rises. The figure reveals that as the depth of ring increases

steadily, the touch voltage increases. For example, the touch voltage at 0.1m depth is 1.1V corresponding to 14.85% of EPR, while at 0.5m depth the touch voltage is 1.92V corresponding to 26.29% of EPR.

Figure 3.41 illustrates the influence of the single ring at different depths on the step voltage. It is clear from the figure that the step voltage reduces gradually with depth for the step voltage at 1m distance away from the tower leg. For example, a ring buried at 0.1m depth at 1m distance from the tower leg, the step voltage is 2.8V, equivalent to 37.6% of EPR, whereas this voltage reduces to 24.3% at 0.5m depth.

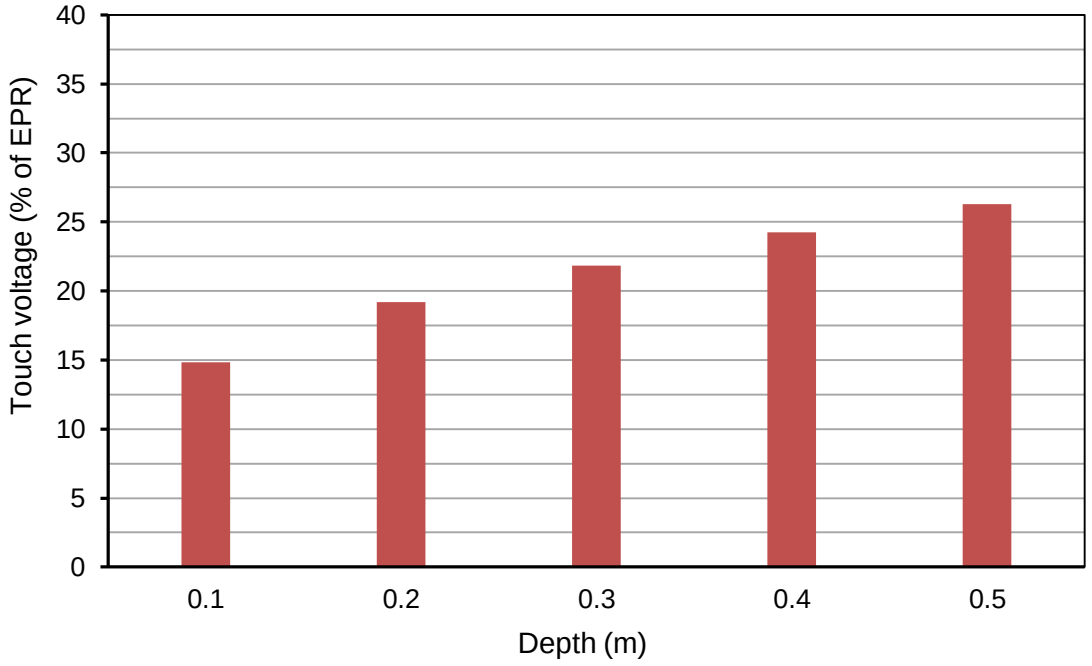

Figure 3.40: Effect of depth of single ring on touch voltage

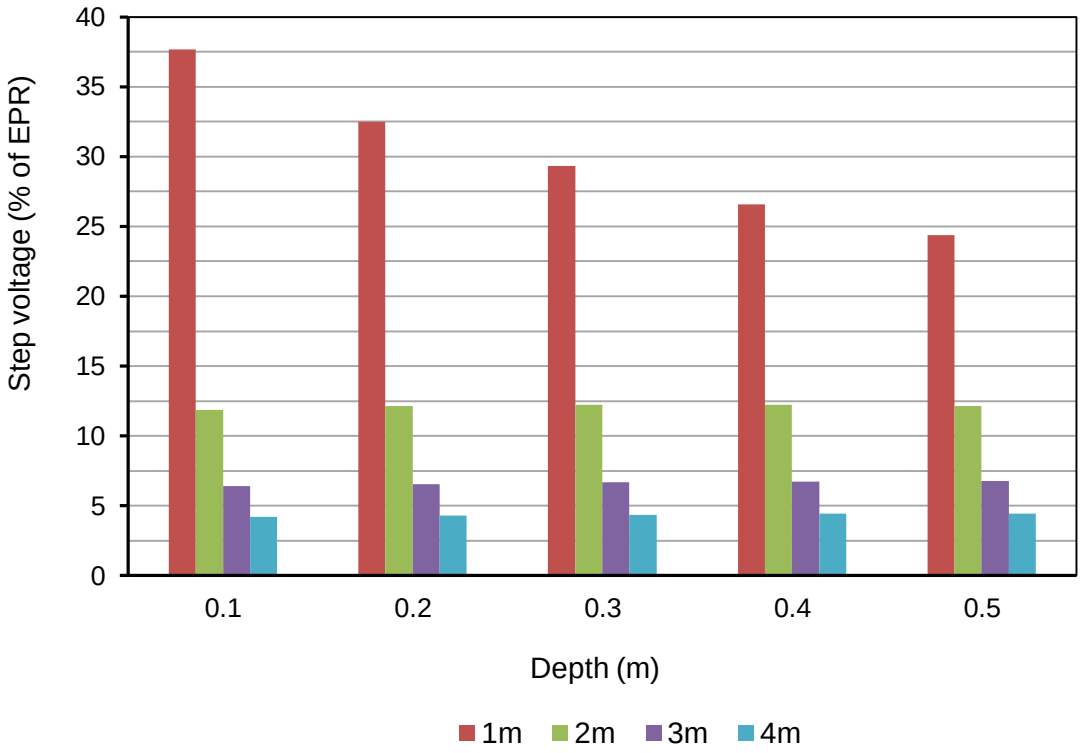

Figure 3.41: Effect of depth of single ring on step voltage at different distance from tower leg.

3.7.2 .2 Two mitigation rings around one leg

In this section, the inner ring was fixed depth of 0.1m, where the lowest touch voltage was obtained in the case of a single ring, as seen in the previous section. However, the outer ring (second ring) with a radius of 2m its depth is changing from 0.1m to 0.5m. Figure 3.42 shows the touch voltage (% of EPR) due to installing the two mitigation rings, where the outer one at a variable depth. It can be seen that the voltage reduces from 7% at 0.1m to 6.2% at 0.3m and then almost no noticeable reduction was observed afterward. Consequently, the second ring was buried at 0.3m. Comparing with the touch voltage when one ring installation (0.1m depth), the two rings (the outer one at 0.3m) proposal yields a 40% reduction. For the step voltage, it was observed that adding a second ring had a negligible influence.

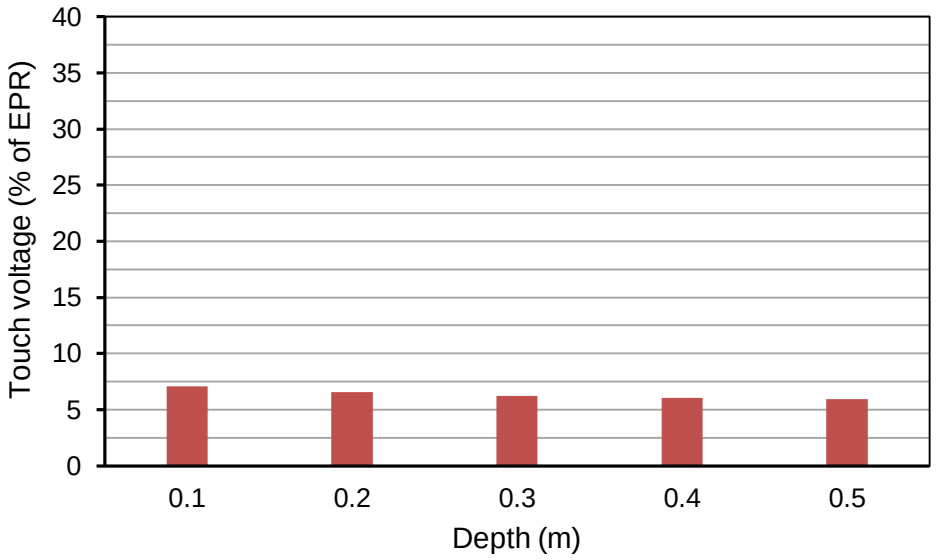

Figure 3.42: Effect of depth of two rings on touch voltage when the inner ring depth fixed at 0.1m and the outer one changing from 0.1m to 0.5m

3.7.2.3 Three mitigation rings around one leg

Third ring is installed with radius of 3m and depth changing from 0.3m to 0.5m. The inner ring (1m radius) and middle one (2m radius) are buried at 0.1m and 0.3m respectively. Figure 3.43 displays the touch voltage (% of EPR) as the outer ring buried at 0.3m, 0.4m and 0.5m which is 4%, 3.9% and 3.8 respectively. From the results, it can be seen that the depth of the third ring has little effect, but compared with the previous case (two rings), the touch voltage has been reduced by 40%.

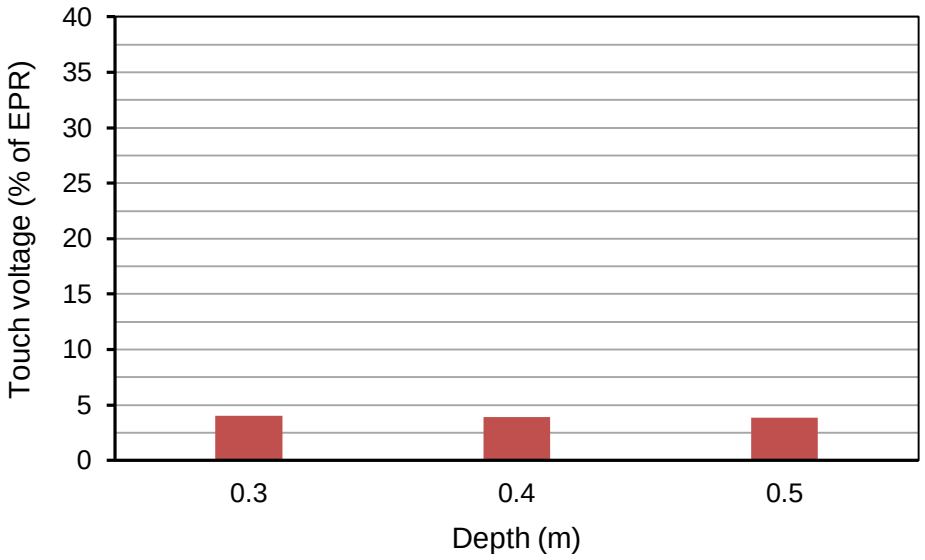

Figure 3.43: Effect of depth of three rings on touch voltage

3.7.3 Effect of soil resistivity on touch and step voltages

In this section, the studies are carried out on the tower base for power frequency condition and 1A current injection in which a uniform soil resistivities of 10Ωm, 100Ωm, 1kΩm and 10kΩm is assumed where the three interconnected mitigation rings are tied to 1 leg, 2 legs, 3 legs and 4 legs respectively. The effect of soil resistivity is found to be negligible on the % EPR value of the step and touch voltage. It was also found that the touch voltage (% of EPR) for mitigation rings around 1 leg, 2 legs, 3 legs and 4 legs is 4%, 3.4%, 3.2% and 2.9% respectively.

This comparison indicates that the mitigation rings at power frequency reduce the touch voltage to 97.8% of its value prior to installing any of the mitigation rings.

Table 3.6 summarizes the computed results of EPR and touch voltage for the various combinations of soil resistivity and number of tower legs having mitigation rings.

Table 3.6: Computed EPR and touch voltage (% of EPR) for mitigation rings at a number of legs

	Resistivity (Ωm)							
	10Ωm		100Ωm		1000Ωm		10000Ωm	
	EPR (V)	TV (% of EPR)	EPR (V)	TV (% of EPR)	EPR (V)	TV (% of EPR)	EPR (V)	TV (% of EPR)
1 leg	0.534	4	5.34	4	53.4	4	534	4
2 legs	0.43	3.48	4.3	3.48	43	3.48	430	3.48
3 legs	0.369	3.25	3.69	3.25	36.9	3.25	369	3.25
4 legs	0.324	2.9	3.24	2.9	32.4	2.9	324	2.9

3.8 Conclusions

The DC earth resistance measurements confirm that there is considerable variation of soil resistivity in the locality of the four legs (footings) of the test tower base, and this result in significant differences in the DC earth resistance of individual footings. The DC tests on the ring and rods' return electrode show that it is an effective low resistance electrode with a value about the tenth of the resistance of the test tower base. The seasonal variation of all the electrode components of the test circuit is significant and affects the shallow electrodes to a greater extent. The computations of the DC resistance of the electrode components agree reasonably well with the measured values. However, the differences, which are attributed to the simplified soil models used in both analytical formulae and computer simulations, reveal the limitations in accuracy when using laterally homogenous soil models.

The ground surface (52Hz) AC potential measurements along different profile across the tower base show that the highest potential gradients are along the diagonal profile passing through a footing. This confirms that the highest safety risk in terms of touch and step voltages will be close to an individual leg where the potential gradient is very high.

The simulated (52Hz) AC potential profiles almost agree with the measured values. The results of tests at higher frequencies (up to 120 kHz) show that a significant variation in profile shape, and hence ground surface potential gradient, around the test electrode.

The frequency response tests on individual footings measured by the probes buried at different depths and both within the concrete footing and adjacent to it indicate interesting results. There is a fall in ground potential with frequency in the concrete but a rise in probe potential with frequency outside the footing. The ground potential generally reduced with depth. These results, however, require further investigation.

CHAPTER FOUR: CHARACTERISATION OF TOWER BASE EARTHING UNDER LOW MAGNITUDE IMPULSE CURRENT

4.1 Introduction

Under power frequency fault conditions, the permissible values of step and touch voltages arising are specified for outdoor transmission and distribution substations [4.1, 4.2]. However, there are no internationally-agreed safety thresholds for voltages arising under impulse conditions. When lightning strikes a transmissions tower, the flow of current through the tower and adjacent towers may give rise to very high potentials, in excess of the tolerable power frequency voltage threshold values. Studies related to the step and touch voltages in high voltage installations under lightning conditions have been reported in the literature [4.3-4.6]. However, in the absence of absolute transient voltage limits, qualitative measures may be carried out to determine acceptable magnitudes of step and touch potentials, and this can be beneficial for tower locations where lightning strikes are relatively frequent.

Earth surface potentials developing near grounded structures under lightning and ac fault currents determine the magnitude of touch and step voltages in the immediate vicinity of the structure [4.7, 4.8]. These potentials may be of sufficiently high magnitude to endanger a person's life and extra measures will be needed to minimise their magnitudes when designing earthing systems.

This chapter is composed of two parts; (a) firstly; it reports earth surface potential (ESP) distribution near a full-scale 275 kV tower base for low impulse currents [4.9]. Experiments were carried out to study the influence of rise time on earth potential distribution. In addition, the influence of local resistivity around each individual footing on ESP and the consequent step and touch voltages are also investigated. The effect of various configurations of return electrode on these voltages is also examined.

(b) Secondly, it examines the ground potential into the tower footing and soil under impulse current conditions.

4.2 The experimental setup

In this test, the experimental setup for measurement of earth surface potentials is very similar to that discussed in the previous chapter which focused on AC conditions. Here, the study is designed to investigate the ESP arising under impulse conditions. A Haefely RSG 481 recurrent surge generator with the capability to generate an impulse with various rise times was used. In addition to the diagonal profile (P4) and the two median profiles (P5 and P6) introduced in the previous chapter, additional diagonal profiles passing through the other three footings (Profile 1, Profile 2, and Profile 3) have been studied, (see Figure 4.1). The potentials measurements along the profiles as well as the EPR of the tower base were measured with respect to a remote reference earth electrode placed 100m away.

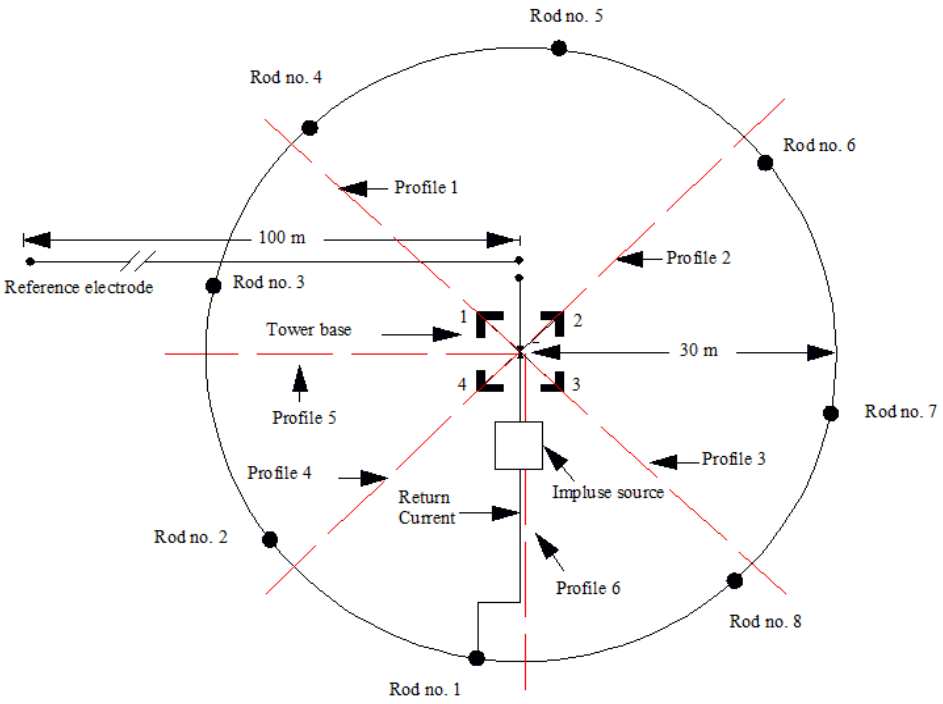

Figure 4.1: Experimental setup and detailed plan view of tower base foundation and arrangement of circular return ring electrode

4.3 Earth surface potential in the vicinity of transmission tower

Prior to the earth surface potential measurements, a test was carried out to measure the EPR of the tower base. The Haefely impulse generator produced a current of peak value 5.7 A with a rise time of 5.4μs and a time to half value of 25μs was injected into the tower base and produced an earth potential rise (EPR) of 126 V, see Figure 4.2. The impulse resistance, as defined by the ratio of peak voltage at the time of peak current to peak current was 22.2Ω.

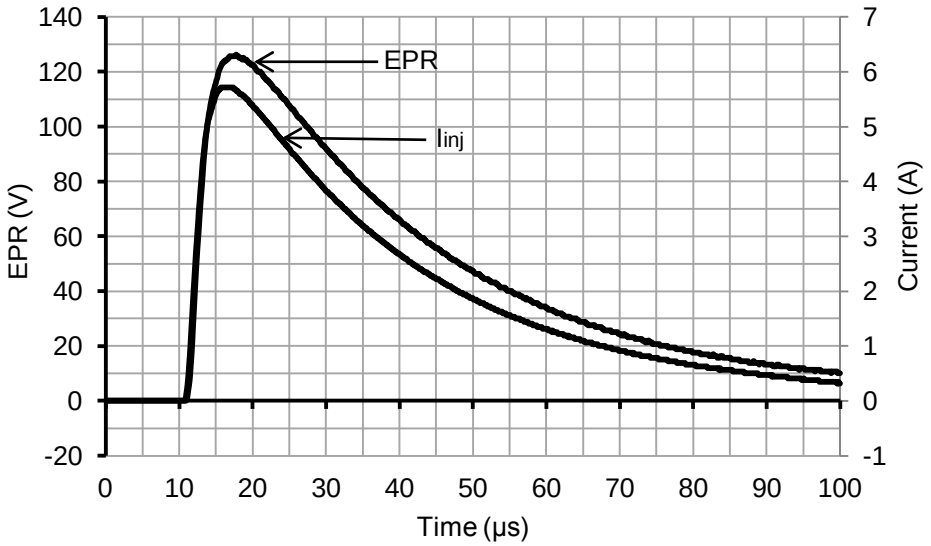

Figure 4.2: Current impulse of rise time 5.4μs and resulting EPR at injection point

4.3.1 Low voltage impulse profiles

The distributions of the ESP along profiles (P4, P5 and P6) under low-magnitude impulse current (5.7A) are shown in Figure 4.3. The peak potential due to the current pulse reaches a maximum value of 94.7% of the peak EPR measured 10 cm away from the tower footing. Potential gradients near to the tower footings on profile P4 are much higher than those on profiles P5 and P6, and their pattern is similar to those obtained under AC that current described in Chapter 3.

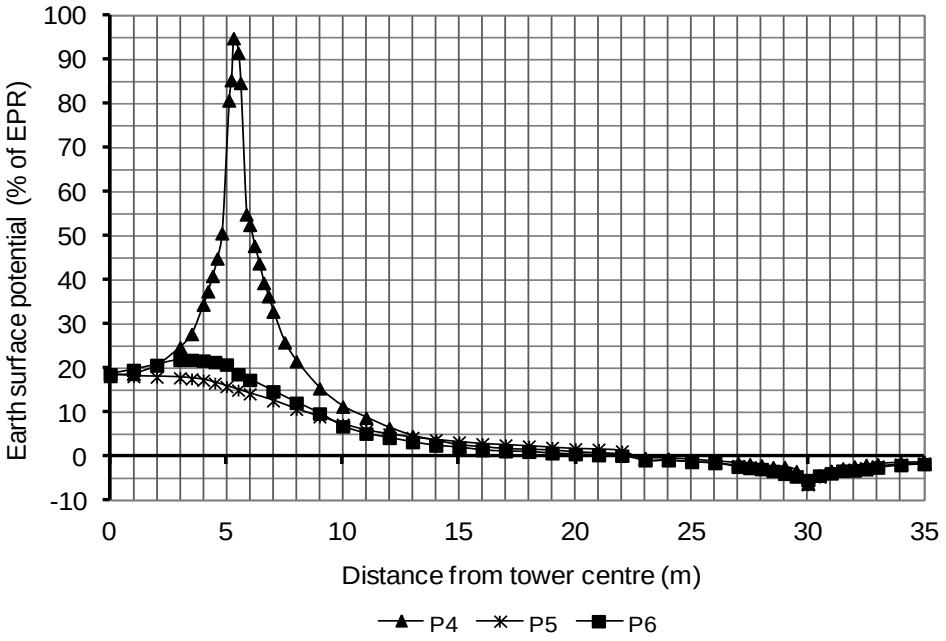

Figure 4.3: ESP distribution under impulse current for the three profiles

4.3.2 Comparison between AC and impulse profiles

Figure 4.4 shows the ESP developed due to AC (2.5A rms) and impulse currents (5.7A peak) along the critical diagonal profile P4. The magnitude of the ESP generated by the impulse is marginally higher than the low frequency AC generated voltage magnitude. The maximum values of both plots occur, as expected, directly along the footing. To assess the anticipated hazard for a person in the proximity of the transmission tower, the touch and step voltages were measured for both AC and impulse energisations where both are referred as a percentage of EPR.

Table 4.1: Step and touch voltages under AC and impulse conditions (profile 4)

Safety voltage	AC (I=2.5A)		Impulse (I=5.7A)	
	V	% of EPR	V	% of EPR
Touch	38.5	58.5	74.6	59.1
Step (10cm)	33.8	51.4	61.8	49
Step (20cm)	31.9	48.5	56.7	45
Step (30cm)	13.4	20.5	25.2	20

The worst case safety scenario is the touch voltage diagonally away from the tower leg and yielding, in this case, a touch voltage of almost 60% of the EPR. The safety voltage measurement results are shown in Table 4.1. As can be seen from the table, the AC and impulse energesations yield very similar step and touch voltages, with respect to the EPR.

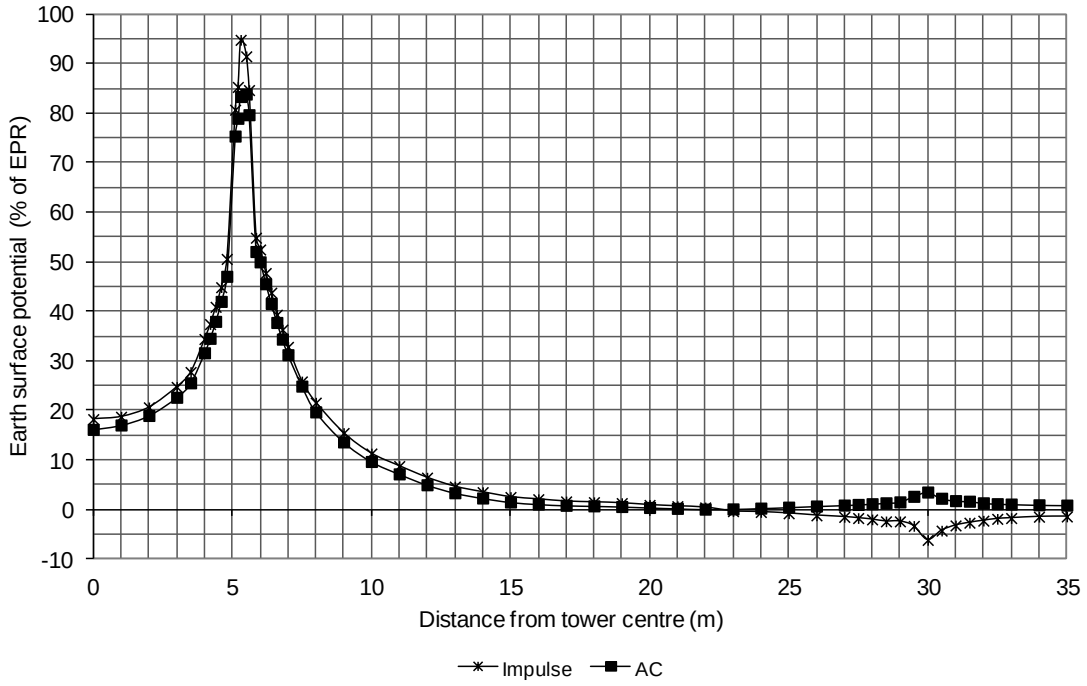

Figure 4.4: Comparison between ESP due to AC (rms) and impulse currents over critical profile P4

4.3.3 Effect of current rise time on ESP

Figure 4.5 shows the impulse ESP distribution along profile P4 for three different current rise times; 1.9μs, 5.4μs and 12.5μs. As can be seen from the figure, an impulse current with a fast rise time (1.9μs) gives rise to slightly higher voltages as a percentage of the EPR and similarities can be drawn with high frequency AC test results show in Figure 3.7 in Chapter 3.

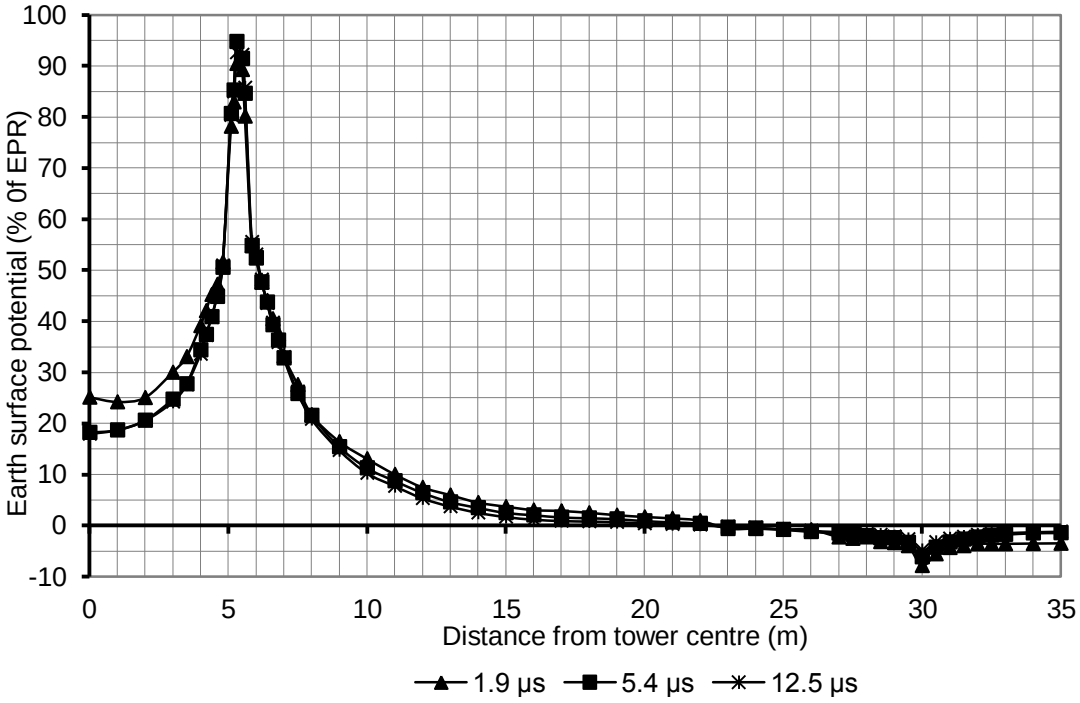

Figure 4.5: ESP profiles due to an impulse current of 5.7 A with different rise times

4.3.4 Comparison of ESP over diagonal profiles

Most studies concerning the calculation of tower base ESPs consider the transmission tower as a simple electrode and the surrounding soil to be homogeneous. This test has been carried out to understand the local ESP distribution and to assess step and touch voltages around each tower footing. Figure 4.6 shows the ESP distribution measured over the four profiles radiating outwards from the centre passing through each tower footing, and it can be seen that the ESP distribution is quite different for each profile with the lowest gradient. The ESP appears to be associated with the footing which has the lowest DC resistance (Footing No. 4), while the ESP with the steepest gradient occurs around the footing having the highest DC resistance (Footing No. 1). However, the difference in gradient may be due to the variation in soil resistivity both vertically and laterally. The touch and step voltages for the four profiles are shown in Table 4.2. The step voltage measured at 1m outward away from the tower leg on the profiles.

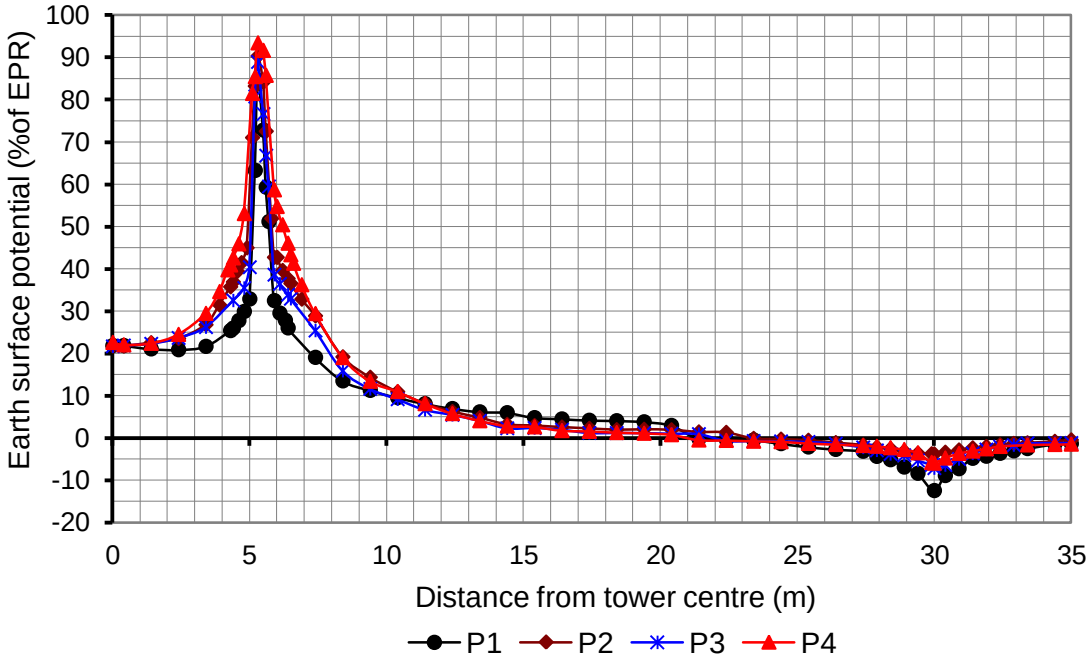

Figure 4.6: ESP profiles along the diagonal profiles under impulse current

The highest step voltage (V_S) was obtained along the profile which passes through the footing with lowest DC resistance, as summarised in Table 4.2. The step voltage 1 m away from Footing No. 4 in the outward direction is 16.6% of EPR whereas at the corresponding location of Footing No. 1, it is only 7.5% of ESP. The measured touch voltage (V_T) in terms of % EPR is also shown in Table 4.2. As expected, the highest touch voltage was obtained at the footing with the highest earth resistance (Footing No. 1), which forms 74.6% of EPR, while the lowest at Footing No. 4 that is corresponding to 54% of the EPR. The DC earth resistance of the tower footings is also listed in the table.

Table 4.2: Touch and step voltages around tower footings under impulse current

	DC Resistance (Ω)	V_T (% EPR)	V_S (% EPR)
Footing No. 1	117.6	74.6	7.5
Footing No. 2	67.2	62.3	8.8
Footing No. 3	80.7	66.5	8.5
Footing No. 4	64.2	54.0	16.6

The ESP along the four diagonal profiles (P1, P2, P3 and P4) was also measured using a DC source. Figure 4.7 shows the earth surface potential per unit current and the results were similar to those obtained for the impulse source. As can be seen in the figure, the maximum rate of rise or decrease near the tower footing occurs at footing No. 1, while the minimum rate of rise or decrease near the tower footing occurs at leg No. 4.

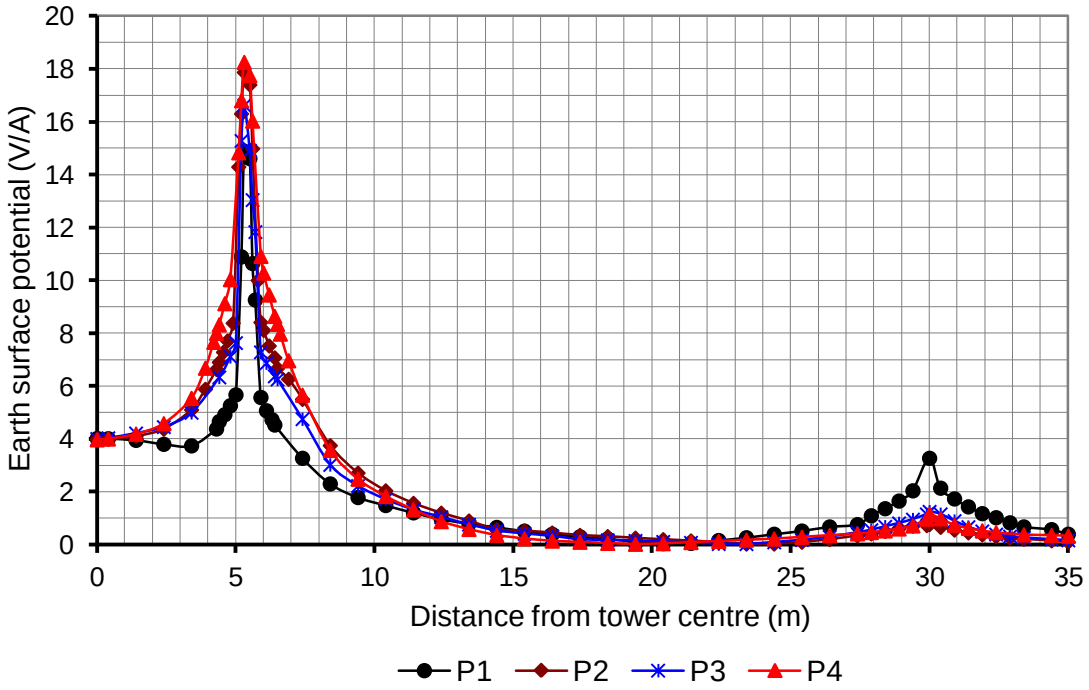

Figure 4.7: ESP profile over diagonal profiles under DC current

4.3.5 Effect of return electrode on ESP

This experiment was made to investigate the influence of the return earth electrode on ESP distribution along the diagonal profiles and consequent step and touch voltages. Four return electrode configurations were used: a bare ring electrode (Case 1), a bare ring electrode connected to eight vertical rods (Case 2), a bare ring electrode with eight vertical rods and an insulated ring conductor (Case3), and finally, the eight vertical rod electrodes connected in parallel by an insulated ring conductor (Case4). Figure 4.8 shows the ESP profiles for an impulse current magnitude of 5.7 A with rise time 5.4 μs. As can be seen from the figure, similar ESPs were measured for all cases. The measured touch voltages (V_T) for a particular footing were not significantly affected by the return electrode configuration, as can be seen in Table 4.3.

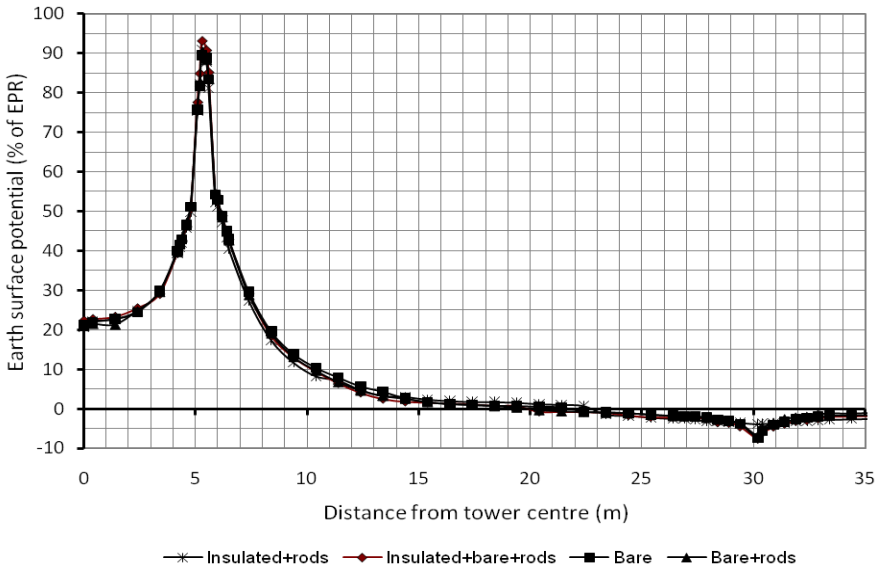

Figure 4.8: Influence of four different return electrode configurations on ESP

Table 4.3: Touch voltage around tower footings

Touch voltage (% of EPR)				
	Case 1	Case 2	Case 3	Case 4
Footing 1	75.6	76.0	76.9	76.9
Footing 2	62.1	63.9	63.6	63.7
Footing 3	65.7	66.9	67.0	67.3
Footing 4	55.0	54.7	54.8	56.6

4.4. Evaluation of direct and indirect methods of measurement for touch and step voltages

In section 4.3, the touch and step voltages were obtained indirectly by calculation. In the case of the touch voltage, the peak ESP at 1m away from the structure was subtracted from the peak EPR value. In the case of step voltage, t, the potential of two points on the ESP curve 1m apart was subtracted from each other. Because of errors in measurement due to induction in test leads and non-coincident peaks in voltage, a direct method of measurement of safety voltages was performed. In the direct method, and with reference to Figure 4.9(a), the touch voltage is measured directly between the leg (EPR) and 1m away (ESP) e.g. point ‘8’at footing No. 4.

Figure 4.9(b) shows the direct measurement method for step voltage where the voltage reading is taken across a 1m gap along the profile. In both cases, direct and non direct methods, the differential voltage probe can be placed very close to the point of measurement and the safety voltage can be transmitted using a fibre optic link to minimise coupling errors.

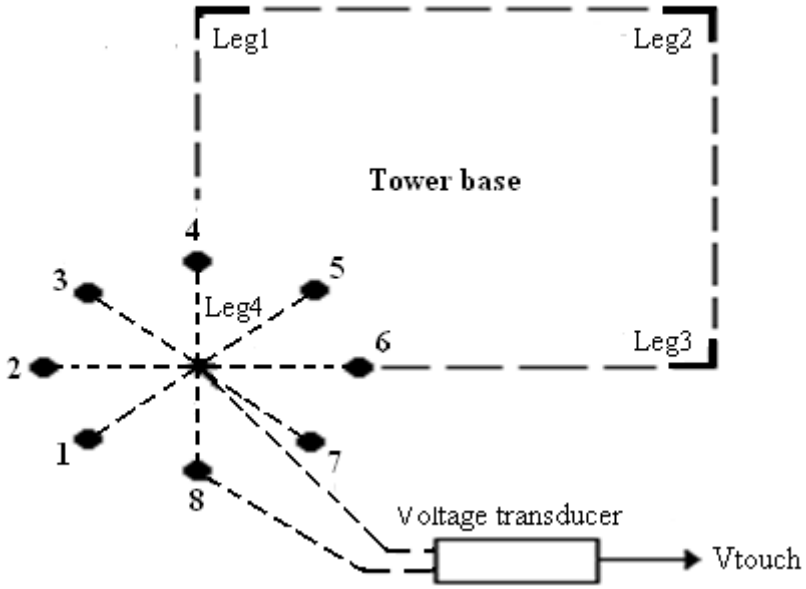

(a)

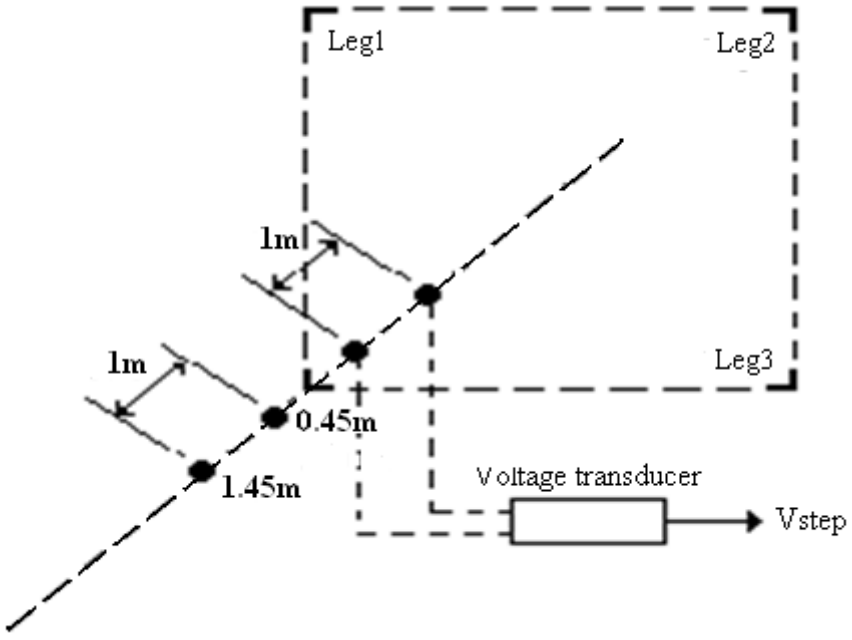

(b)

Figure 4.9: (a) Diagram illustrating touch voltage measurement method (b): Diagram illustrating step voltage measurement method (direct method)

4.4.1 Low-current impulse tests

Impulse current of peak 5.6A with rise time 5.5μs was injected into the tower base to evaluate the touch and step voltages. This developed an EPR of 107 V, as shown in Figure 4.10.

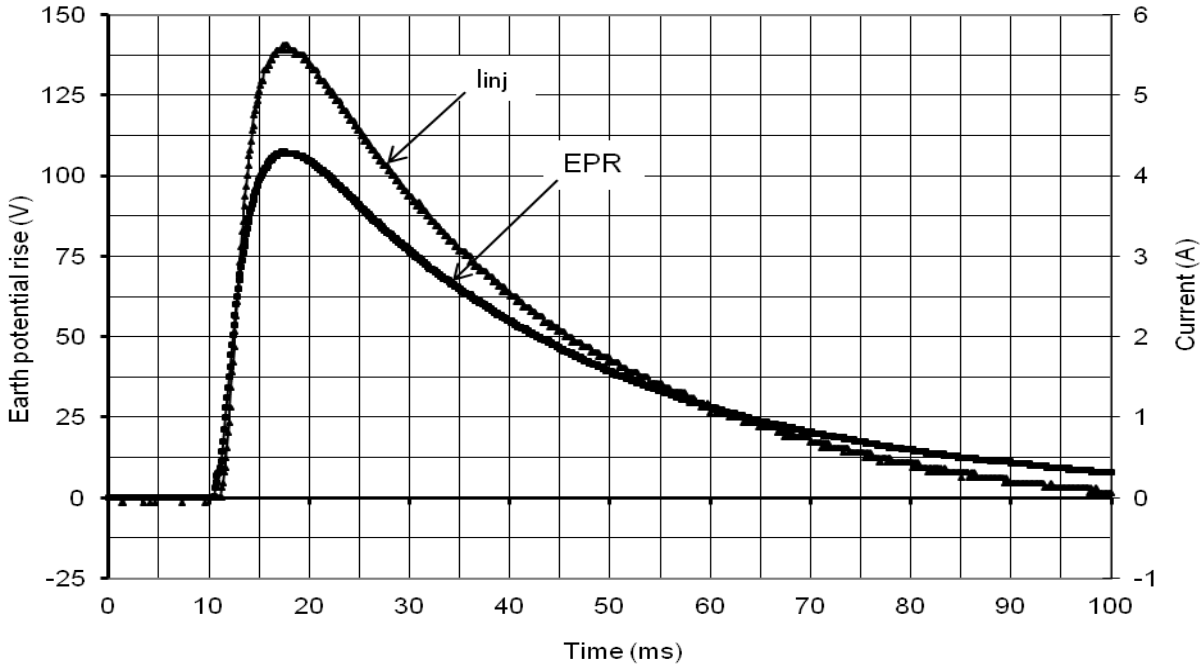

Figure 4.10: Impulse EPR with respect to reference point at 100m, and injected current of 5.6A.

4.4.2 Touch voltage

In order to investigate the touch voltage around the transmission line tower, a number of tests were carried out at each individual tower footing. The circuit configuration for this study had the impulse generator placed immediately at the tower base (the electrode under test) and the return current electrode was eight rods arranged in the peripheral a circle of 30 m radius at nearly same interval distance and then connected

in parallel (Figure 4.1). The impulse shape of the ESP at point 1 around tower footing No. 1 is shown in Figure 4.11 together with the EPR of the tower base.

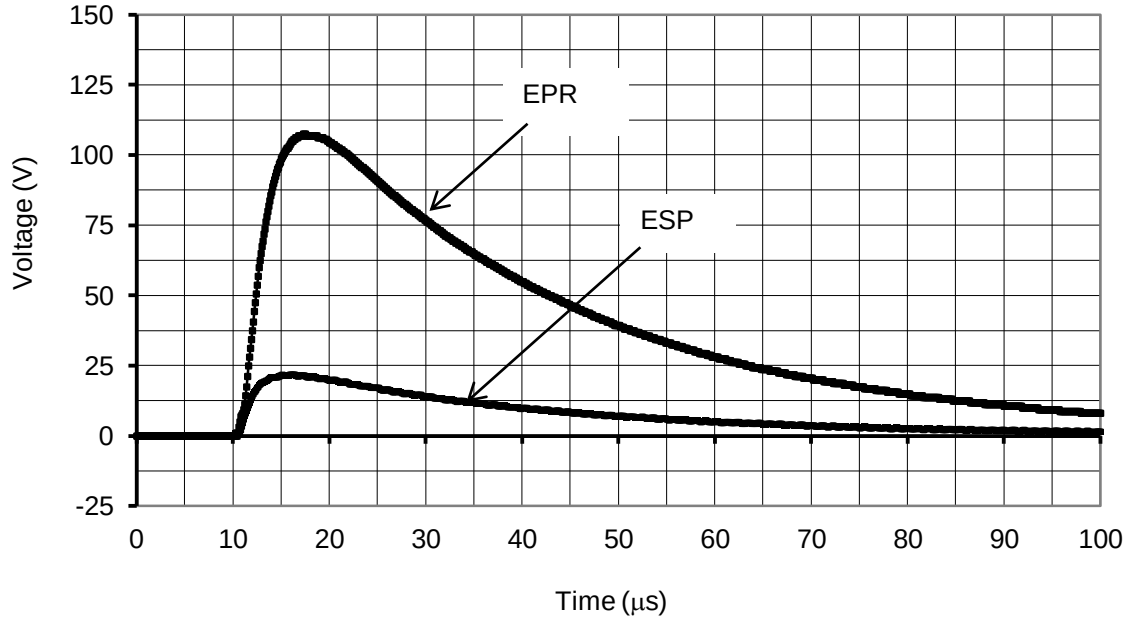

Figure 4.11: EPR of tower base and ESP at point 1 at footing No. 1.

Figure 4.12 shows the impulse shape of the touch voltage (V_T) measured by indirect and direct methods at point 1 at footing No. 1 as a result of injection of the impulse current of 5.6A with rise time 5.5μs. From the figure, the coincidence of the touch voltages measured by the two methods is excellent. Almost identical results were obtained for V_T at each of the 8 points around the four tower footings by direct and indirect methods as shown from the results in Figure 4.13. A similar result was obtained for the other footings.

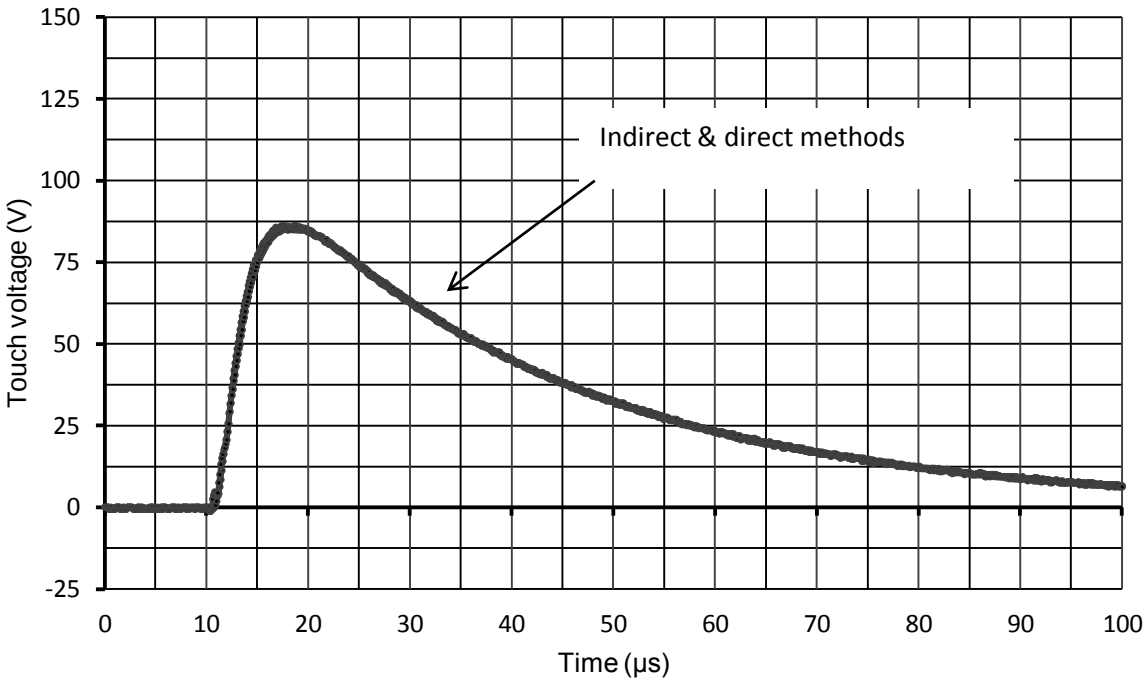

Figure 4.12: Touch voltage for current impulse for indirect and direct methods at point 1 at tower footing No. 1.

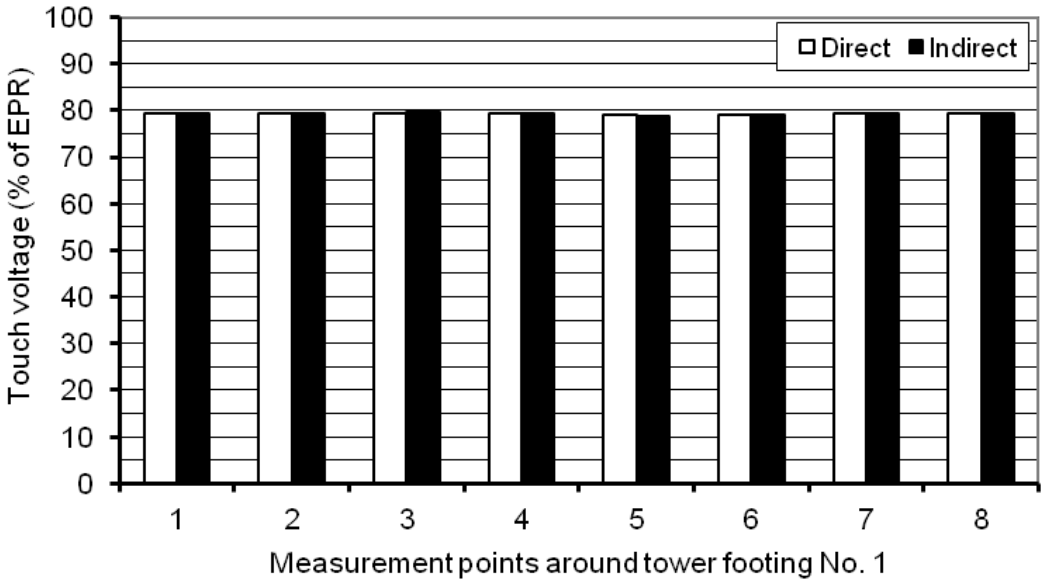

(a)

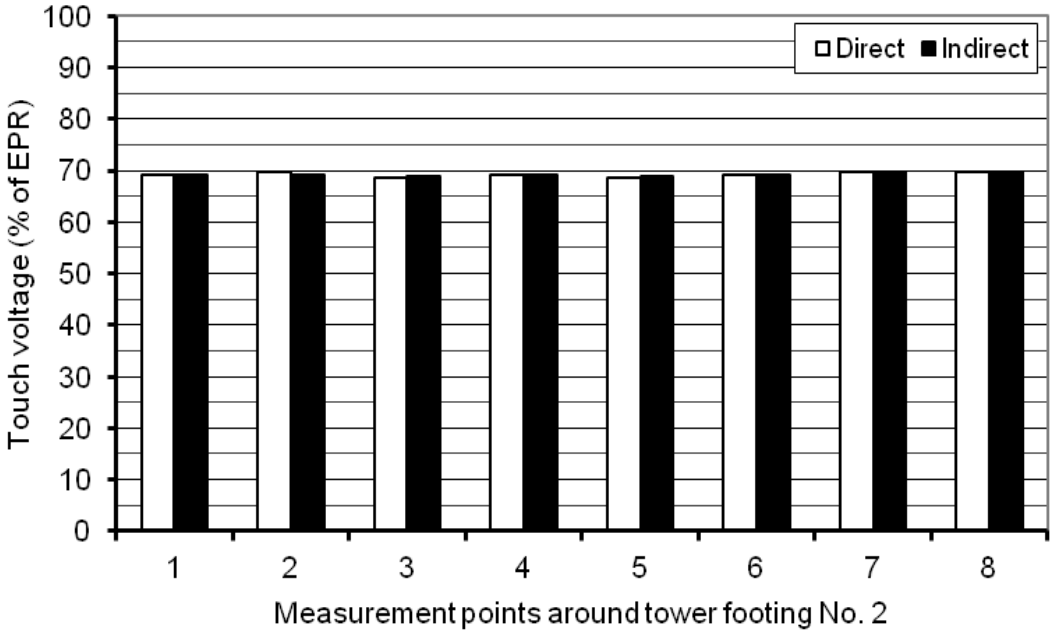

(b)

Figure 4.13: Touch voltage measured by indirect and direct methods around tower Footings No. 1 and footing No. 2

4.4.2.1 Effect of current rise time on touch voltage

In order to investigate the influence of the impulse shape on touch voltage around the transmission line tower footings, two current impulses with rise times of 2.8 µs and 5.4 µs were used. It was found that, for the impulse with the faster rise time, the touch voltage as a percentage of EPR was lower for both footing No 1 and footing No 4 as can be seen in Figure 4.14. This means that for the same current magnitude, the current with the faster rise time produces a lower touch voltage with respect to their EPR.

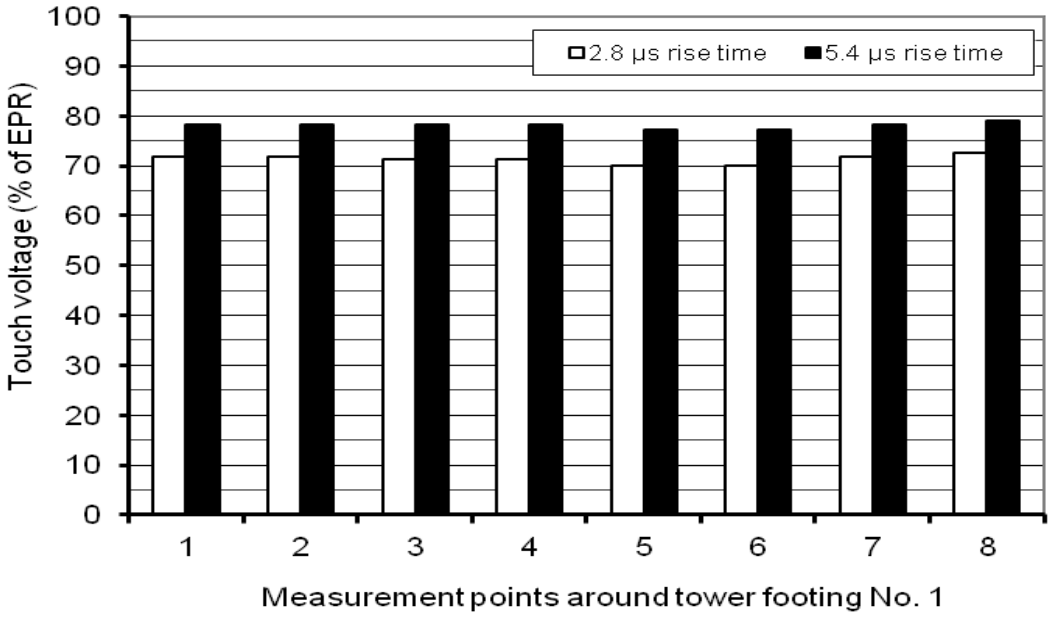

(a)

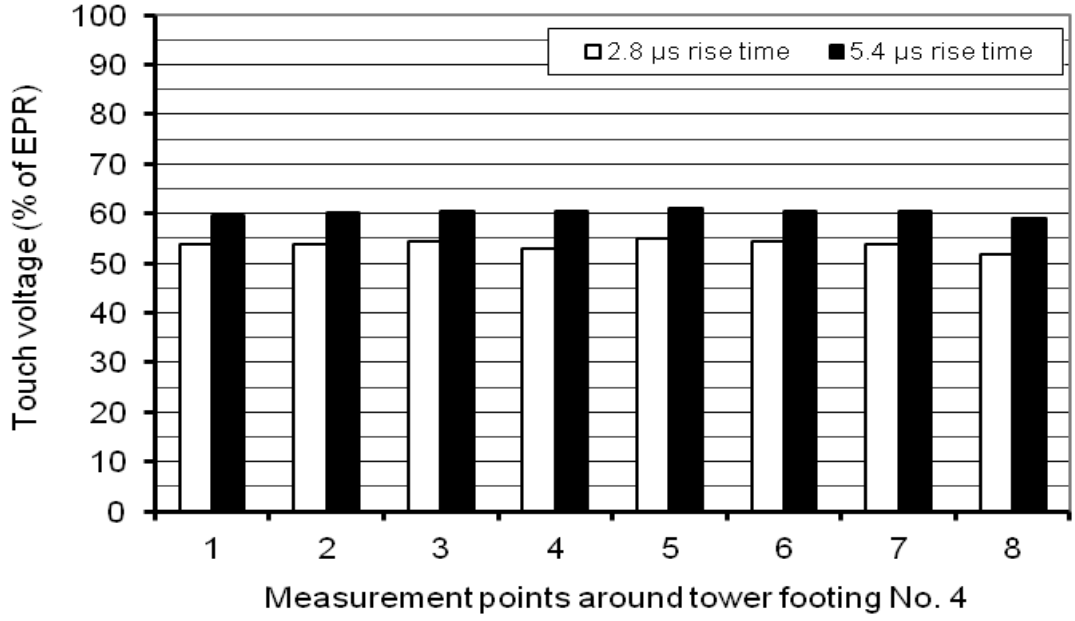

(b)

Figure 4.14(a): Touch voltage at footing No. 1 for impulse currents with different rise times (b): Touch voltage at footing No 4 for impulse currents with different rise times

4.4.2.2 Effect of injection point

To study the influence of the injection point on touch voltage around the transmission line tower footing, two strike points were examined; injection directly into the tower base and via transmission line. Although, the transmission line spans are around 330 m long, an injection via a transmission line of 30 m shows an effect on touch voltage. The set up for injection via a transmission line was that the impulse generator was placed beside Rod No.1 position. Figure 4.15(a) and (b) show that the measured touch voltage as a percentage of EPR is higher for the injection directly into the tower base than for injection via the transmission line. This is true for both tower footing No 3 and tower footing No. 4 by an average of nearly 1.5% and 1.0%, respectively.

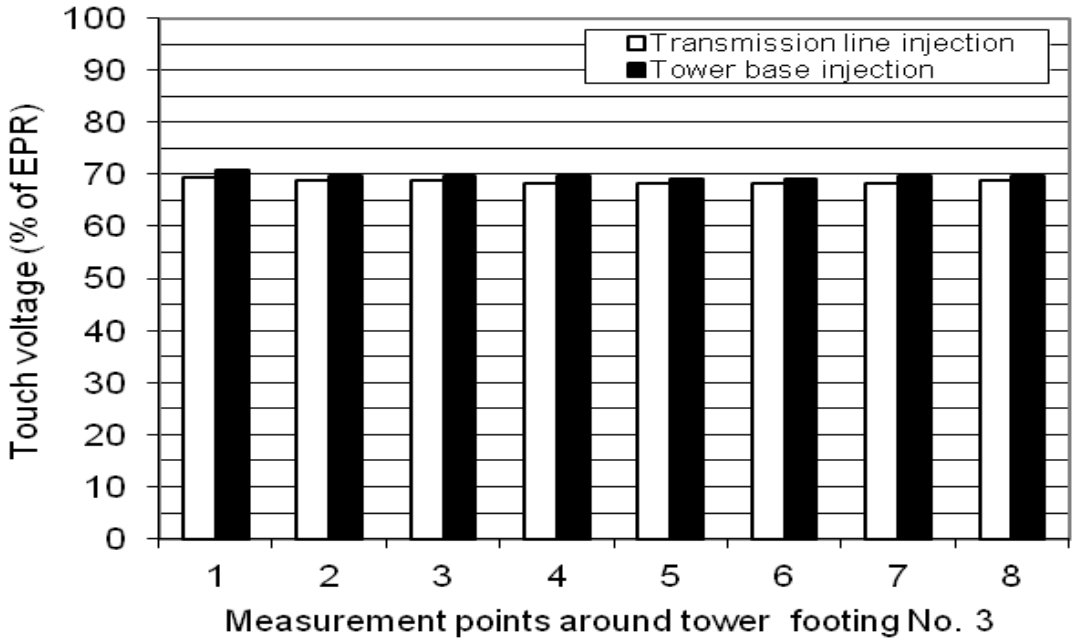

(a)

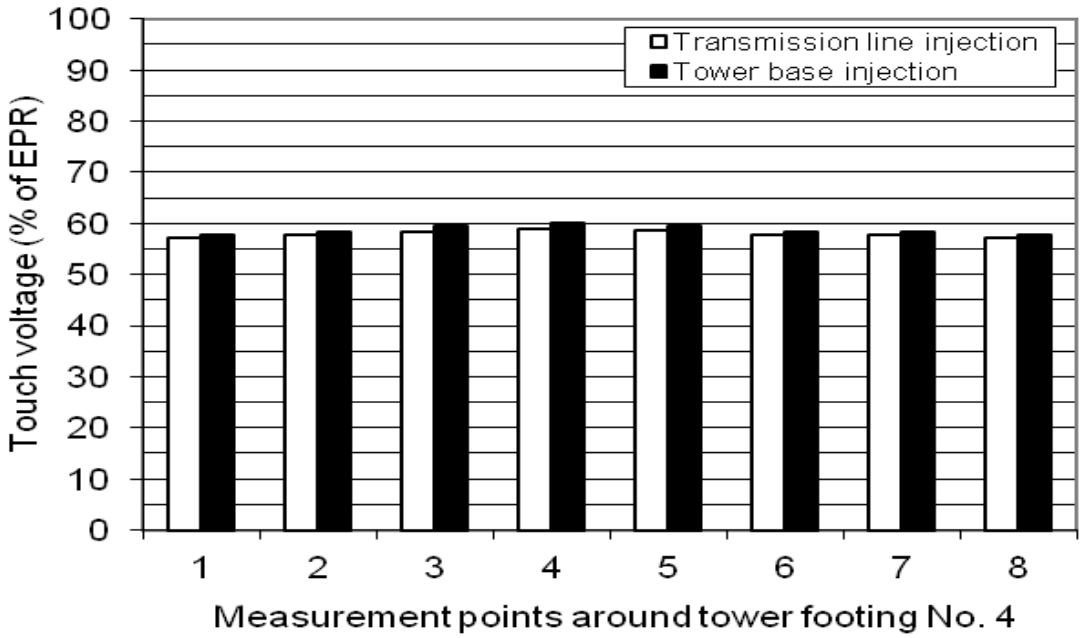

(b)

Figure 4.15(a): Effect of injection point on touch voltage around footing No. 3

(b): Effect of injection point on touch voltage around footing No. 4

4.4.3 Step voltages

Step voltage was measured along the diagonal profiles passing through the tower footings. Both direct and indirect methods, described earlier, were used to measure the step voltage. As can be seen from the results shown in Figure 4.16, the step voltage profile gradually follows the gradient of the ESP. The figure shows some small differences between direct and indirect methods. For footing No. 1, there appears to be no clear pattern to the differences.

Comparing Figures 4.16(a) and 4.16(b), it can be seen that the highest step voltage was measured at the tower footing with the lowest DC resistance and the lowest step voltage was obtained at the tower footing with the highest DC resistance. The step voltage at footing No. 4 is approximately three times that at footing No. 1.

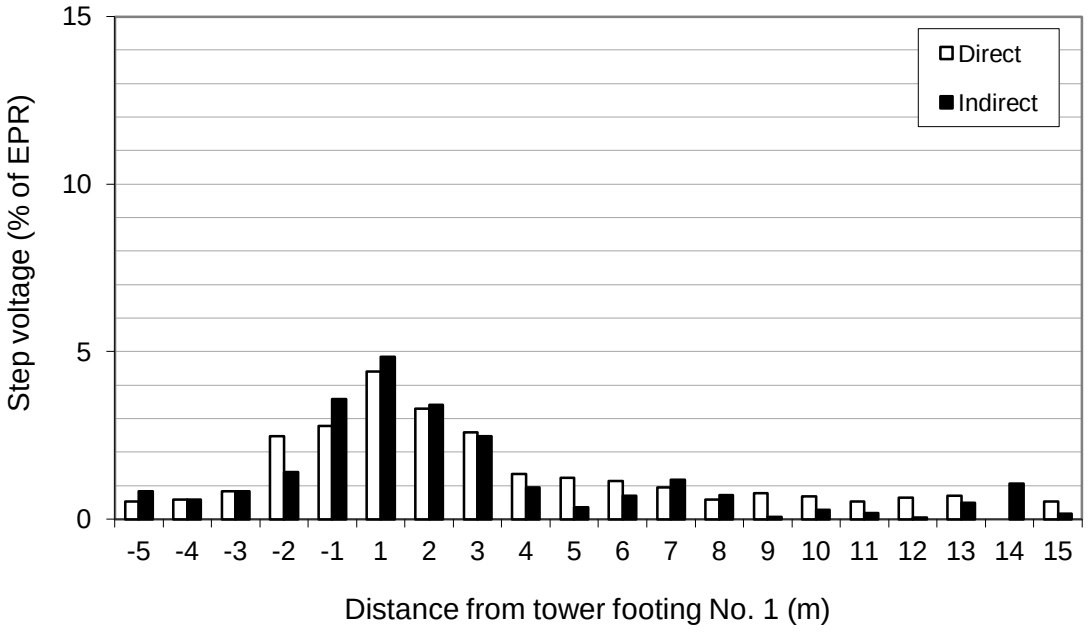

(a)

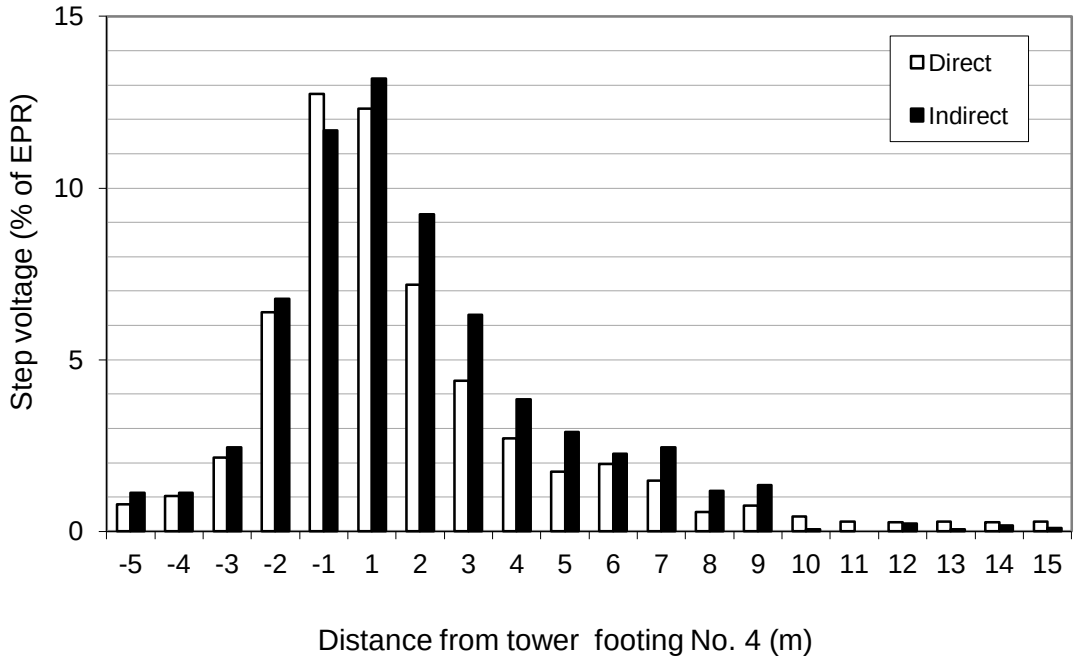

(b)

Figure 4.16: Step voltage along tower footing No.1 and tower footing No.4

4.5 Current distribution in the tower base

The current distribution between different footings of the tower base was investigated and with the aid of a CT buried at the bottom of the footing it was possible to examine current leakage from the base of a footing.

It should be recalled that when injecting a current into the tower base, the share of current of each tower footing is different which affects the levels of step and touch voltages appearing around each leg. Figure 4.17 shows the current distribution into the four footings of the tower base when a total impulse current of 6A is injected as shown in the experimental setup in Figure 4.1. Table 4.4 summarises the measured DC and impulse resistances and current share of each tower footing.

4.5.1 Current distribution into individual tower footings

Impulse tests were carried out with the four footings of the tower base connected in parallel. A current with a peak value of 6A, a rise time of 5.8 μs and a time to half value of 31.5 μs was injected into the tower base. The EPR was 106 V with respect to the remote earth. Figure 4.17 shows the current distribution between the four individual tower footings. From the figure, it can be seen that the highest current, approximately 2 A, equivalent to one third of the total current, flows into footing No 4, while only about 1A (16%) of the total current flows into footing No 1. Table 4.4 shows the measured DC resistances of the individual tower footings where it can be seen that footing No. 4 has the lowest DC resistance (55.3Ω) and footing No. 1, the highest (108.2Ω) the measured current distribution in accordance with the current distribution according to the calculated impulse resistance. The calculated impulse resistance values (see Table 4.4), show close agreement between the DC resistance and the calculated impulse resistance, R_i, as given by the following equation:

$$R_i = \frac{V_{@Ip}}{I_P} \tag{4.1}$$

Where I_p is the peak current and $V_{@Ip}$ is the voltage measured at the peak current.

Figure 4.17 shows I1, I2, I3 and I4 corresponding to current flow through footing 1, footing 2, footing 3 and footing 4.

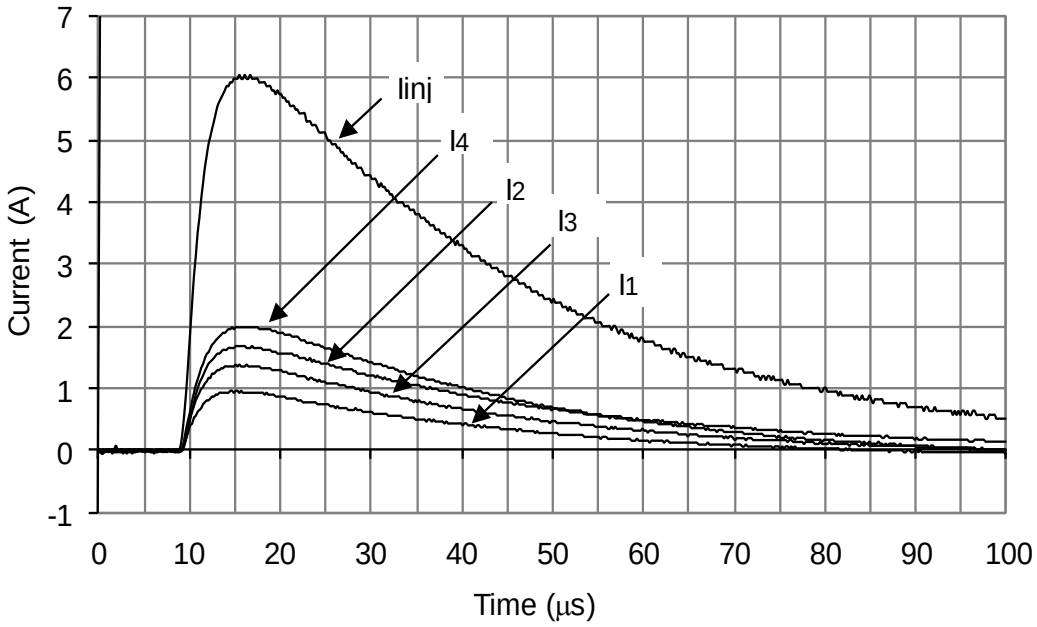

Figure 4.17: Current distribution between individual footings of tower base.

Table 4.4: Impulse and DC resistance of the individual tower footing

	Footing 1	Footing 2	Footing 3	Footing 4	Total
R_{DC} (Ω)	108.2	64.6	75.8	55.3	
$R_{Impulse}$ (Ω)	108.5	63.9	75.3	53.9	
Current (A)	0.978	1.66	1.41	1.97	6
% of total current	16	28	23	33	100

4.5.2 Current dissipation from the bottom-end of the tower footing

Here, a current transformer with sensitivity 0.1 A/V was buried underneath the foundation of one footing as shown in Figure 4.18. The CT was mounted around a short metal rod which was bonded to the bottom of the central metal channel of the tower footing as shown in Figure 4.18. To reduce interference during current measurements, the current signal was brought to the surface by means of a triaxial cable as shown in Figure 4.18. The side view of individual footing with current transformer is shown in Figure 4.19.

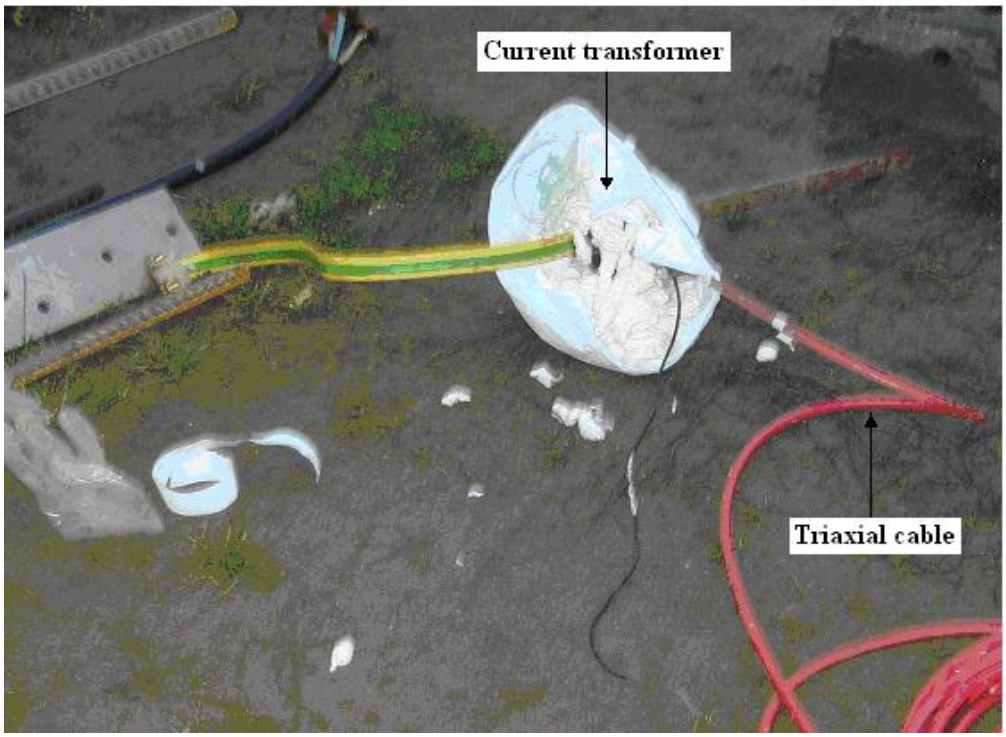

Figure 4.18: Current transformer buried underneath the tower footing (prior to burial)

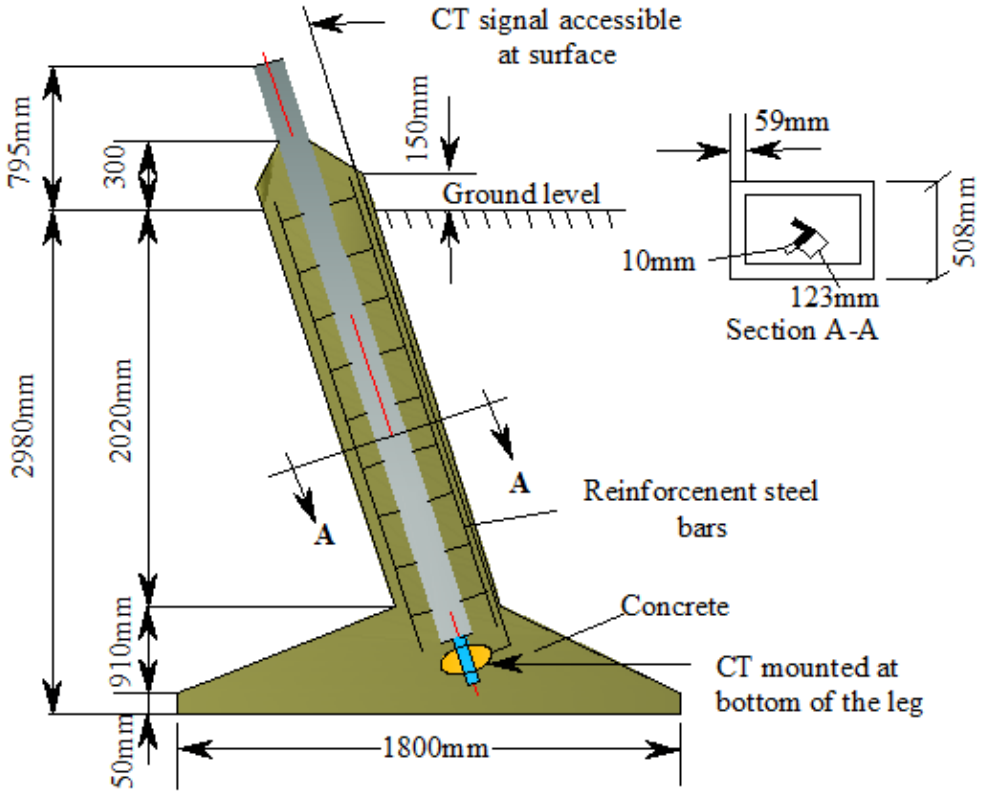

Figure 4.19: Side view of individual footing with current transformer

This experiment is conducted by injecting an impulse current with different rise times; 2.79 µs, 5.10 µs and 8.50 µs and with corresponding maximum rates 0.44 A/µs, 0.213 A/µs and 0.106 A/µs, respectively. For example, the impulse current of peak value 1.97 A with rise time 2.79 µs has been injected into tower footing No. 2 as shown in Figure 4.20. The Figure shows the injection current (I_{inj}) into the tower footing against the current (I_E) at the far end of the same foot. It is clear from the figure that the traces representing both I_{inj} and I_E have the same shape.

Figure 4.21 illustrates the relationship between the measured injected current for different rise times and magnitude against the measured current at the bottom of the tower footing No. 2. For instance, when a current of peak 2 A is injected, the corresponding currents for rise times of 8.5 µs, 5.1 µs and 2.79 µs are 120 mA, 130 mA and 140 mA, respectively. With reference to Figure 4.20, it can be seen that the

relationship between the total leg current and leakage current is linear for all rise times. The proportion of current leakage from the bottom of the leg (footing) ranges from 5.63% for a 8.5μs rise time to 6.83% for a 2.79μs rise time. The current dissipation in the tower footing against the rise time of the injected current impulse was plotted in Figure 4.21 which shows that the current dispersed in the foot for a rise time of 2.79 μs is nearly 93.17% while for a rise time of 8.5 μs is as high as 94.37%.

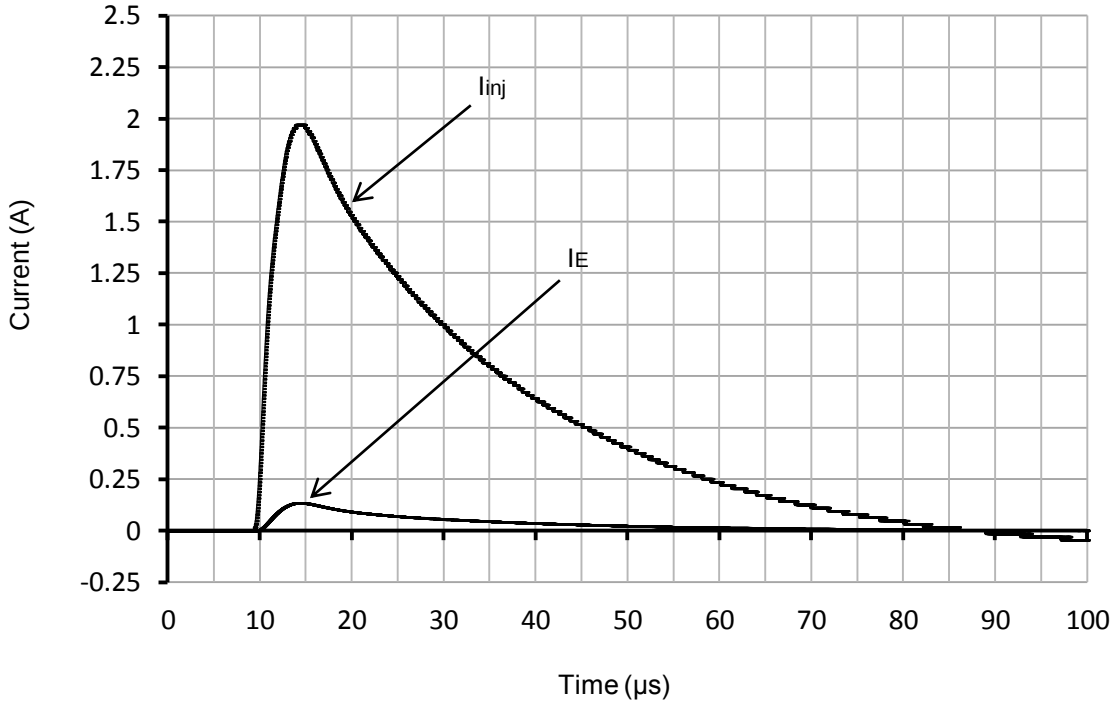

Figure 4.20: Current leakage from bottom of the tower footing as function of total leg (footing) current for injected

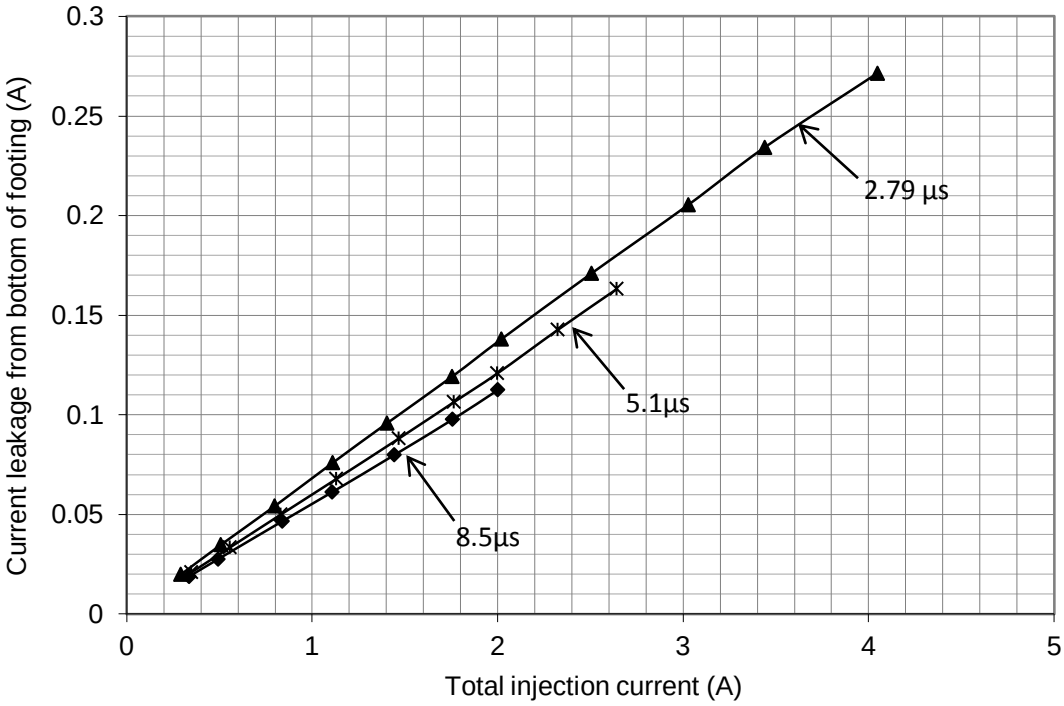

Figure 4.21: Current leakage from bottom of tower footing as function of total leg (footing) current.

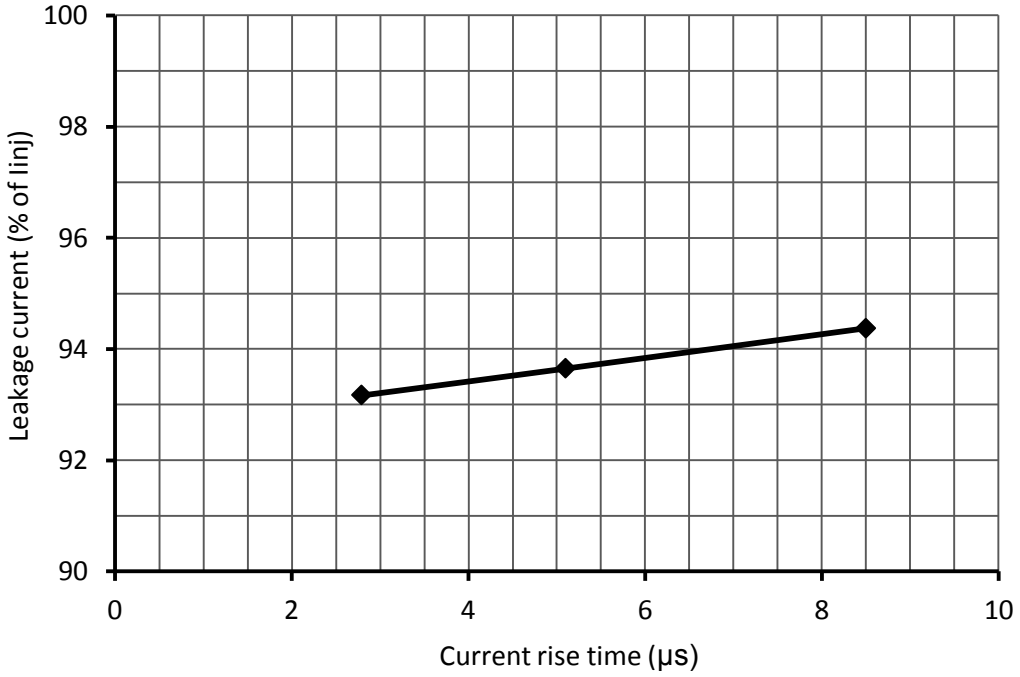

Figure 4.22: Current rise time against leakage current into tower footing.

4.6 Ground potential distribution inside the tower footing and soil

Using the sets of probes embedded in the concrete of footing No. 1 and in the soil adjacent to footing No. 2, and as described in detail in chapter 3, impulse tests were carried out to examine the potential distributions in the concrete and the adjacent soil.

The tower footing earth potential rise and ground potential at the probes locations were measured with respect to a rod electrode placed 100m away from the injection point.

4.6.1 Ground potential measured by the probes within concrete footing

The EPR of tower footing No. 1 as a result of injecting an impulse current of peak 869 mA and rise time 14 μs is shown in Figure 4.23. The EPR produced is 136 V and the impulse resistance is 156.5Ω, while the DC earth resistance is 169.4 Ω.

Figure 4.24 shows the ground potential at a depth of 1m into the tower footing measured by the three probes. A higher potential is observed at the probe a equal to 50% of the EPR compared with the other two probes c and b. A similar picture is obtained with the sets of probes at 2 m and 3 m depths. The measured results are summarised in Table 4.5. As can be seen from the table, there is a trend of decreasing potential with depth but there are large potential differences between the probes at the same depth.

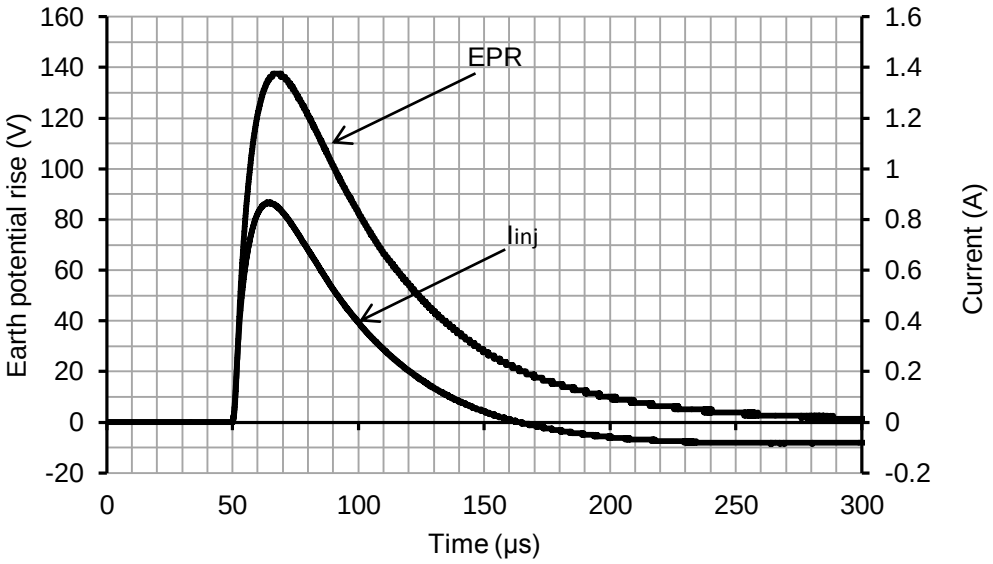

Figure 4.23: EPR and injection current with rise time 14 μs at tower footing

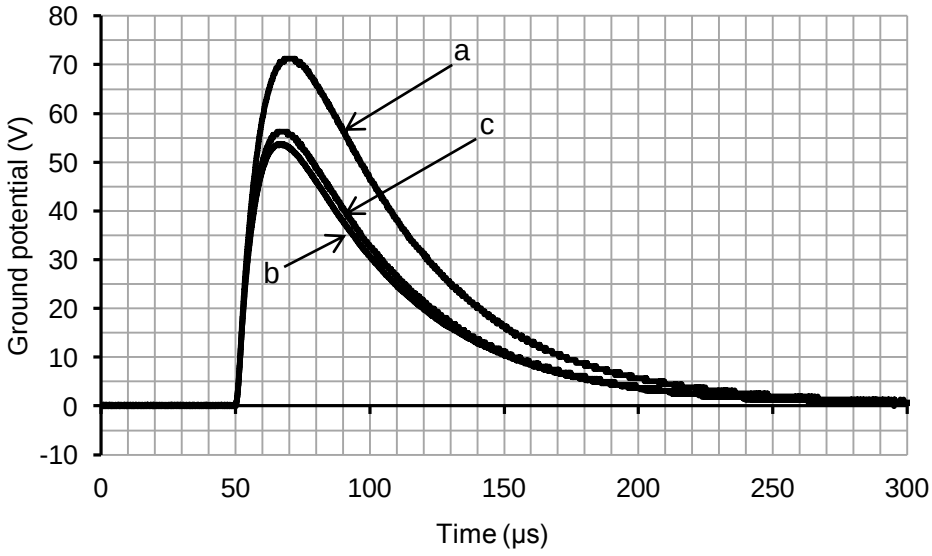

Figure 4.24: Ground potential in the concrete measured by probes (a, b, and c) at 1m depth

Table 4.5: Peak potential of probes buried at different depths in concrete of footing No. 1 as % of EPR

GP (% of EPR)	1 m	2 m	3 m
Probe b	39.48	27.13	28.23
Probe a	52.42	47.35	46.83
Probe c	41.3	34.26	31

4.6.2 Ground potential distribution in soil the adjacent to tower footing No. 2

The metal probes were described in section (3.5.2) and shown in Figures 3.20 and 3.21. Again, these were used to investigate the potential distribution in the soil under impulse conditions. An Impulse current of magnitude 1.75 A with rise time 8.5 μs was injected into tower footing No. 2, and the resulting EPR is shown in Figure 4.25. A peak EPR of 150 V was generated with respect to the reference electrode placed 100 m away.

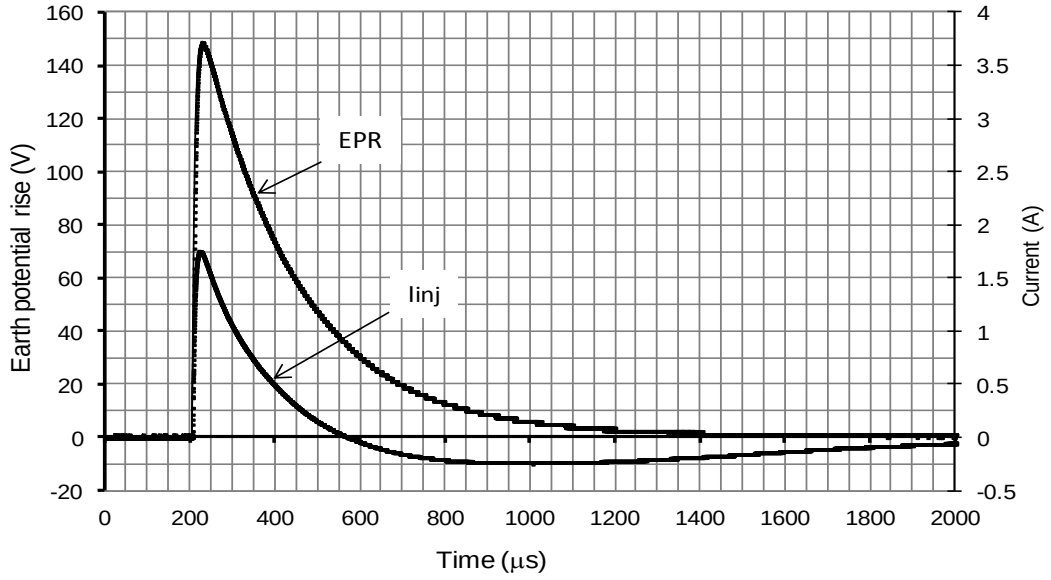

Figure 4.25: EPR and impulse current with rise time 8.5 μs injected at tower footing No. 2

The ground potential in Figure 4.26 shows the peak ground potential measured by the three probes at 1 m depth. As can be seen from the figure, similar potentials were measured with the three probes. A similar measurement is obtained for the sets of probes buried at 2m and 3m. A summary of the results is provided in Table 4.6.

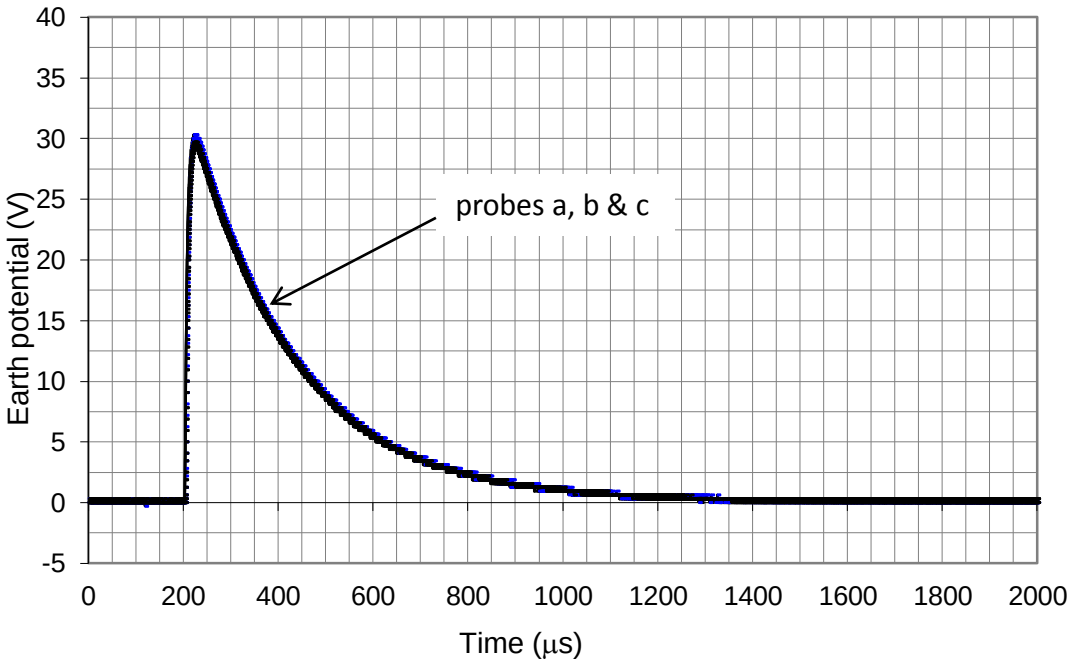

Figure 4.26: Measured ground potential using probes at 1 m depth

Table 4.6: Measured ground potential at different depths in soil adjacent to footing No. 2

	Probe depth		
	1 m	2 m	3 m
Probe b voltage (V)	29.4	26.2	24.7
Probe a voltage (V)	30.3	27.5	23.4
Probe c voltage (V)	29.7	26.6	24.7

4.7 Conclusions

The ground surface potential distribution under impulse current injection follows quite closely the distribution under AC injection. There is some evidence that impulse rise time affects the potential distribution, whereby, a small rise time leads to an increase of the ground surface potential inside the tower legs. The measured potential distribution varied significantly between the four diagonal profiles which yield different touch voltages at the corners of the legs. The differences are attributed to local variations in soil resistivity. Direct and indirect methods for measurement of step and touch voltages were evaluated, and it was found that there were only small differences between the results obtained from the two methods.

The amount of the current distribution among the footings under impulse injection depends on their DC resistance. By installing a CT at the bottom of the tower footing No. 2, it was established that a small proportion of current in an individual footing was dispersed from the bottom end. The tower footing dispersed the lowest amount of current when it injected with current with fastest rise time.

CHAPTER 5: EXPERMENTAL INVESTIGATION OF EARTHING CHARACTERSTICS OF A TOWER BASE UNDER HIGH IMPULSE CURRENT

5.1 Introduction

The design of transmission tower earthing systems, in common with other types of earthing systems, is based on performance under power frequency fault conditions in relation to the control of hazardous step and touch voltages. Studies relevant to impulse characteristics of tower and similar concentrated earthing systems, including the soil ionisation phenomena, are also available in the literature [5.1- 5.6], and these have been reviewed in Chapter 2. In these studies, the reduction in the electrode earth resistance under high impulse current is ascribed to the soil ionisation. According to the published literature, the degree of electrode earth resistance reduction depends on many factors such as electrode geometry, soil resistivity and the peak value of impulse current. Experimental studies specific to tower footings and tower bases can be classified into investigations under low current [5.5 and 5.6] and high current [5.4]. Many experimental studies on impulse response of earth electrodes have been confined to laboratory scale models with finite soil volumes forming a uniform medium. Such tests offer an ideal setting for controlling a variety of test parameters but may not be representative of full scale earthing systems where soil conditions are available. For example, in a bounded laboratory test system, the current path and potential distributions do not replicate realistic conditions associated with full scale, unbounded systems. Since only limited information on full-scale impulse testing of tower base earthing systems is available in the literature [5.4], measurements on full scale tower footings offer a valuable means of understanding their lightning behaviour and for validating theoretical models.

In this chapter, high impulse current tests up to 9kA are reported on the full-scale 275kV test tower base at Llanrumney University site. Non-linear soil conduction effects are confirmed and some breakdown characteristics of soil are explored.

5.2 Test setup

The high-current test set-up consisting of an impulse generator and a 30m-long overhead line suspended on wood poles of 1.7m height connecting the impulse generator to the test tower base is shown in Figure 5.1(a) and (b). Figure 5.2 shows the transportable impulse generator rated 400kV, and delivering currents up to 20kA at the test site together with the AC power supply generator. The impulse generator was located at the return electrode ring near Rod 1, where the current return point was connected to the earthing point of the generator. The earth potential rise (EPR) of the tower base was measured with reference to the current return point of the generator using a high voltage resistive divider having a ratio of 4700:1. The data acquisition system and generator control unit were placed at an equal distance of about 20m from both the generator and the voltage divider. The voltage measurement line is suspended on a second similar wood pole line in a direction perpendicular to the current line to minimise coupling. Prior to the high voltage tests, the DC and low-current impulse resistances of the tower base (R_T), the isolated footings ($R_{1,\ 2,\ 3\ and\ 4}$) and the ring electrode resistance (R_o) were measured using the low voltage Haefely recurrent surge generator and the DET 2/2 resistance meter. These measurements are summarised in Table 5.1.

Table 5.1: Measured DC resistance and low-current impulse resistance of test electrodes

	R_1	R_2	R_3	R_4	R_T	R_0
DC resistance (Ω)	108.2	64.6	75.8	55.3	18.5	1.9
R_{imp} (Ω)	109.4	63.9	75.3	53.9	17.5	1.8

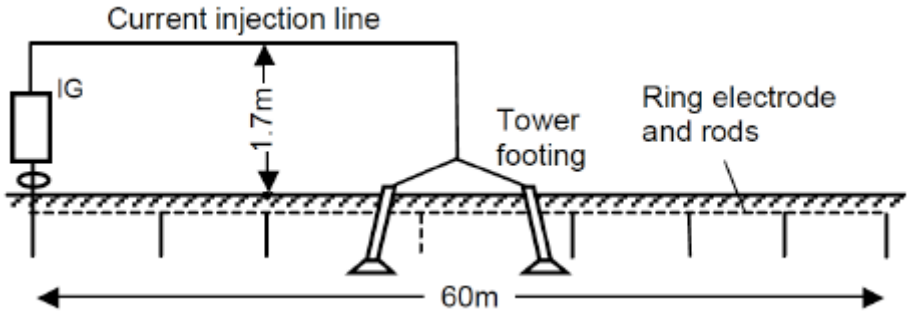

(a)

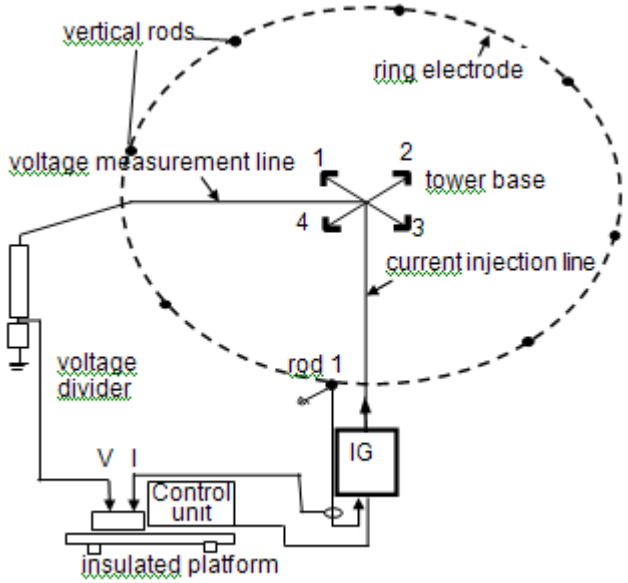

(b)

Figure 5.1: Experimental setup for high current tests a) elevated view

b) plan view

Figure 5.2: High voltage current generator at the field site

5.3 Tower base impulse resistance

A series of impulse tests were carried out on the tower base with currents of magnitudes ranging between 0.9kA and 5kA. Figure 5.3 shows selected recordings of injected currents and voltages measured between the tower base and the return electrode at Rod 1. For this particular set of tests, the current had a rise time of 4.5μs and a tail time of about 13μs. Using the peak values of the voltage and current waveforms, and given that these peaks coincide in time, the ratio Vp/Ip represents the combined impulse resistance of the tower base and the return earth electrode. The DC resistance of the return electrode is 1.9Ω which will be much smaller than that of the tower base, 18.5Ω, and therefore the measured impulse resistance is mainly indicative of the tower base component. The impulse resistance is plotted against the current peak values Ip in Figure 5.4 for two separate tests. As can be seen from the figure, the

impulse resistance decreases by about 15% over a current range from 900A to 5kA. It is recognised that soil ionisation is more likely to occur with electrodes of small surface area, high impulse currents and high resistivity soil. In the experimental study on a 500kV tower base reported in [5.4], the reduction in resistance with current was found to be negligible.

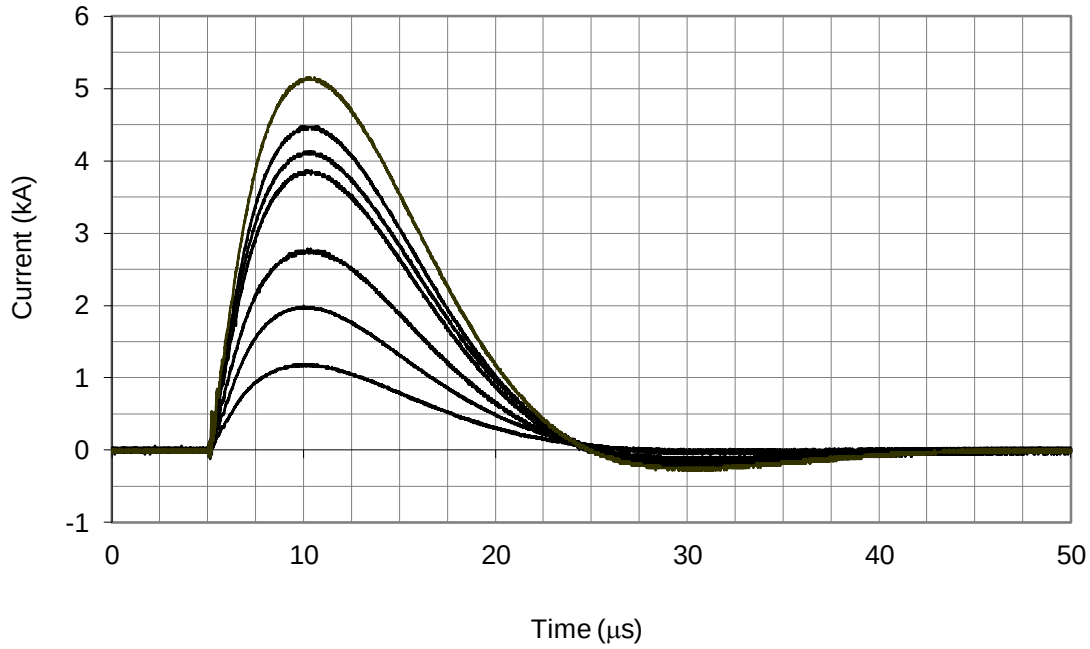

(a)

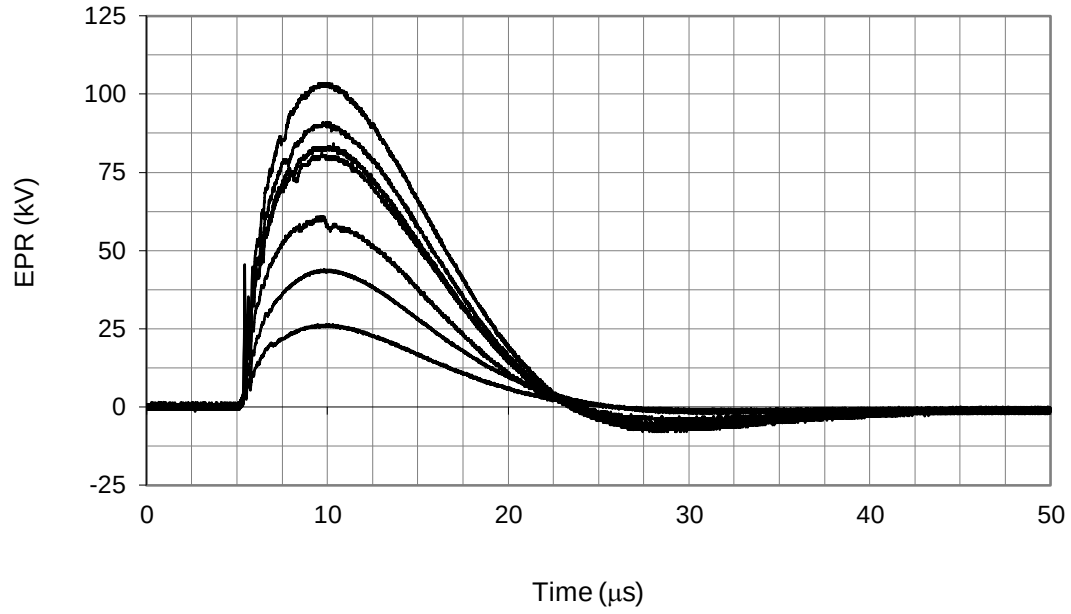

(b)

Figure 5.3: Corresponding recording of (a) current and (b) voltage for impulse tests of varying magnitude on the test tower base

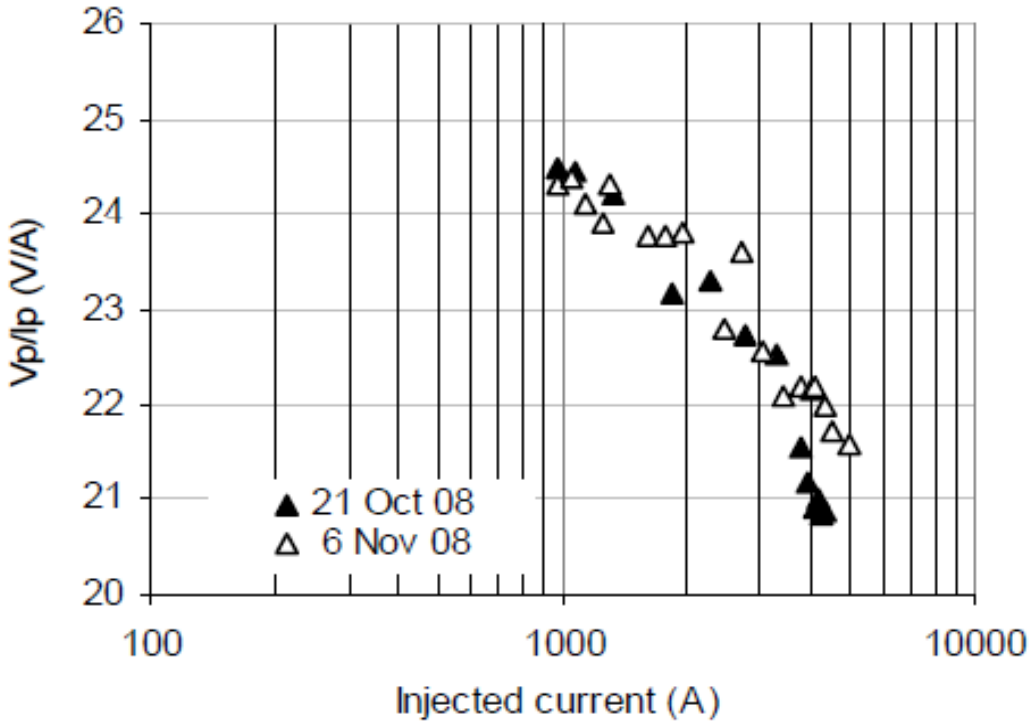

Figure 5.4: Tower base impulse resistance dependence on current magnitude

5.4 Assessment of individual and combination of tower footings

Similar tests were carried out on one of the tower footings (footing 1), and on the parallel combination of Leg 1 and Leg 4. Figure 5.5 shows the voltage and current recordings for the tests on tower Leg 1. From the figure, the characteristic signs of soil ionisation can be seen to occur at time Ti (inception time) and corresponding inception current Ii and voltage Vi. These characteristics were not seen for the tests on the combined tower base. After ionisation starts, an increase in current is accompanied by a sharp reduction in voltage, as shown in Fig. 5.5. At the inception of ionisation, the ratio Vi/Ii decreases by a relatively small amount from the DC value of 100Ω to about 94Ω with increasing applied current. The voltage recovers gradually and reaches a second peak value which is smaller than the voltage inception value. The amplitude of voltage reduction ΔV did not have a clear trend, but was found to vary between 4kV and 12kV, with an average value of 9kV.

Two resistances can be defined due to an existence of two peaks [5.7]. 1) the pre-ionisation resistance (R_1) that calculated by using equation (5.1) and 2) the post-ionisation resistance (R_2) that calculated by using equation (5.2). These resistances magnitudes were measured using the first and second peak currents and their corresponding instantaneous voltages. The pre-ionisation resistance corresponds to the resistance at the start of soil ionisation. The post-ionisation resistance corresponds to the maximum ionisation expansion. $V_{@Ip1}$ is the voltage at the first current peak and $V_{@Ip2}$ is the voltage at the second current peak.

$$R_1 = \frac{V_{@\,Ip1}}{I_{p1}} \quad \text{..... (5.1)}$$

$$R_2 = \frac{V_{@\,p2}}{I_{p2}} \quad \text{.....(5.2)}$$

From Figure 5.5 the first current peak appeared at 1.87μs from raise of the current trace and the second current peak occurred at 4.9μs from raise of the current trace. The pre-ionisation resistance was 94Ω, while the post-ionisation resistance was 69Ω.

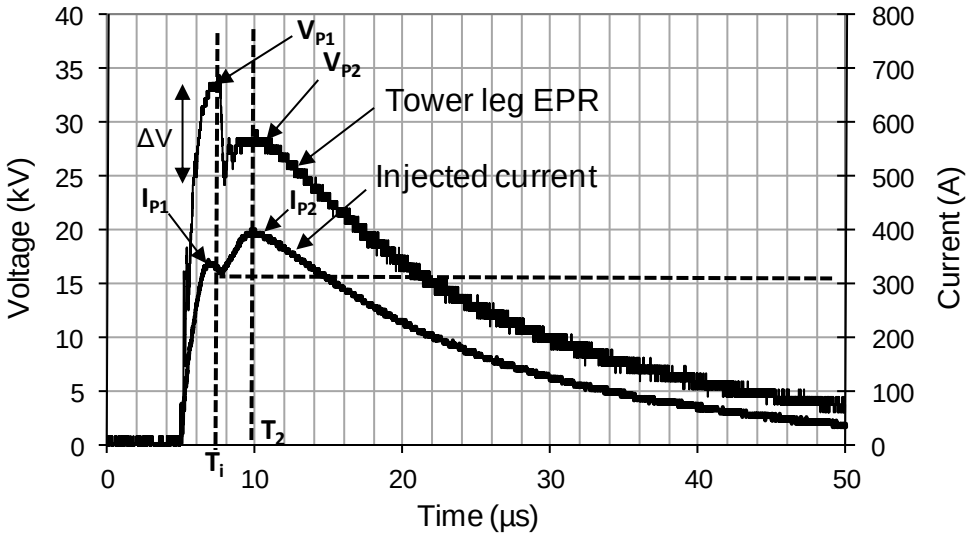

Figure 5.5: Tower leg impulse wave shapes

5.4.1 Ionisation inception current

The ionisation inception current was measured at the instant of first current change on the waveshape, and plotted against the current rate of rise. For simplicity, a linear rate of rise was assumed as defined by the ratio:

$$\frac{\Delta I}{\Delta T} = \frac{I_t}{T_i} \tag{5.3}$$

Figure 5.6 shows that the inception current increases approximately in proportion with the rate of rise of applied current. For a given impulse current shape, this means that for high currents, soil ionisation starts earlier on the waveshape but requires a higher inception current compared with low-magnitude currents. This dynamic property may be important when modelling soil ionisation, and will be further investigated. In most available models, the inception current or "critical current" is usually taken as a constant independent of time [5.6].

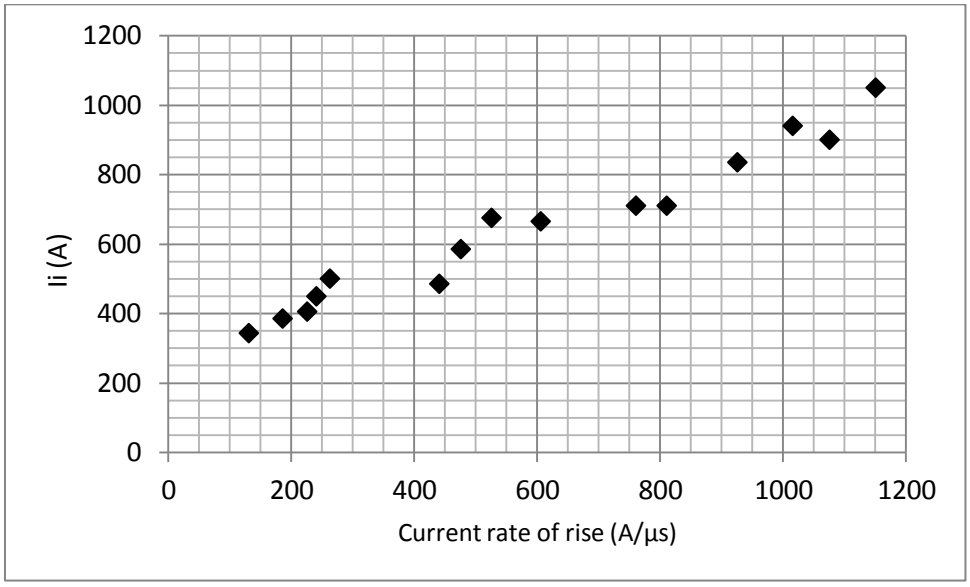

Figure 5.6: Relationship between current rate of rise and ionisation Current

5.4.2 Impulse resistance characteristics

The variation of the impulse resistance of a single leg and the combination of two tower legs with increasing impulse current are shown in Figure 5.7. A very large reduction in impulse resistance with applied current is observed for the single leg. For the range of applied currents used in this study, this reduction was 45% for the single leg and 20% for the combination of two legs. The time variations of the ratio of instantaneous voltage and current (dynamic resistance) Rimp(t) are shown in Figure 5.8, and can be used to explore the resistance characteristics of the tower legs. Prior to ionisation, the dynamic resistance takes a value of 100Ω, this is approximately equal to the DC resistance shown in Table 5.1 for tower leg no.1. Following ionisation, the resistance drops from its DC value by an amount which is dependent on the applied current. After the peak of the impulse current, the resistance remains at the new lower value for most of the duration of the impulse, indicating that ionisation may continue even if the applied current is falling which may be explained by a slower decay of the ionisation process. The dynamic resistance slowly increases with time as a result of the

diminution of the soil ionisation activity, and eventually recovers its DC value after extinction of ionisation. The minimum value of the dynamic resistance can be used to estimate the extent of the ionisation region around the tower leg if the latter is represented by an equivalent geometrical model. Models based on known geometries such as hemispheres and cylinders have been developed to compute the extent of the ionisation zone with injected current [5.8, 5.9]. By considering the critical soil ionisation field Ec and the critical ionisation current Ic, the field on the periphery of the ionisation zone of radial extent *rc* is as in equation 5.4 [5.10]:

$$E_c = \rho J_c = \rho \frac{I_c}{A(r_c)} \qquad (5.4)$$

where, J_c is the critical current density, ρ is the soil resistivity and $A(r_c)$ is the area of the ionisation zone at distance r_c from the electrode surface. Equation (2) can be used to determine r_c if the critical gradient and critical current are known, provided a suitable geometrical model is adopted.

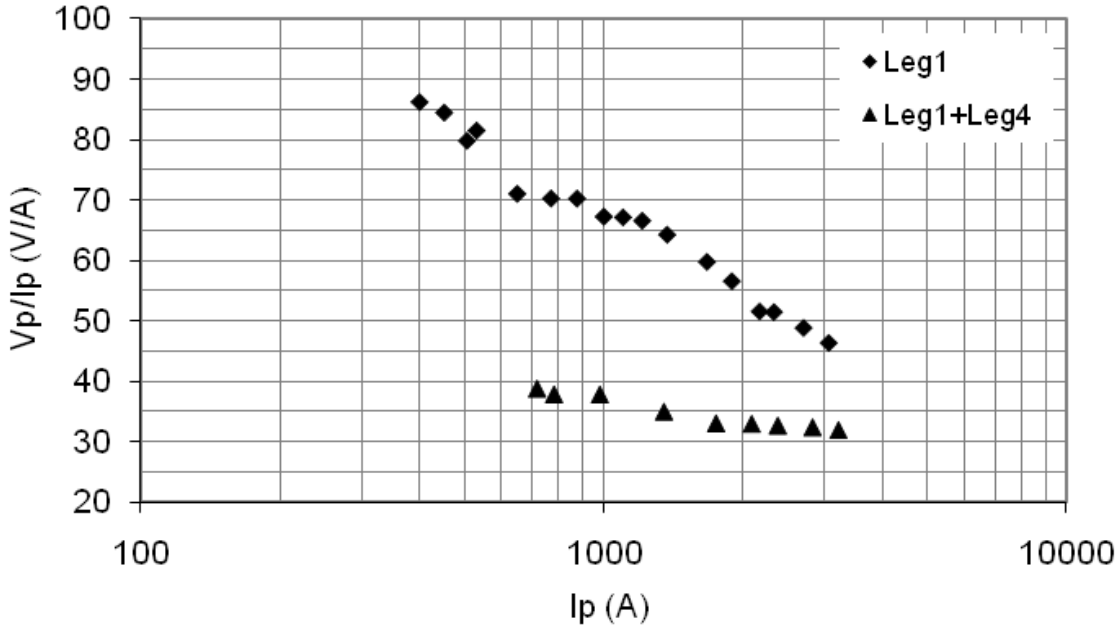

Figure 5.7: Impulse Resistance of Tower Legs

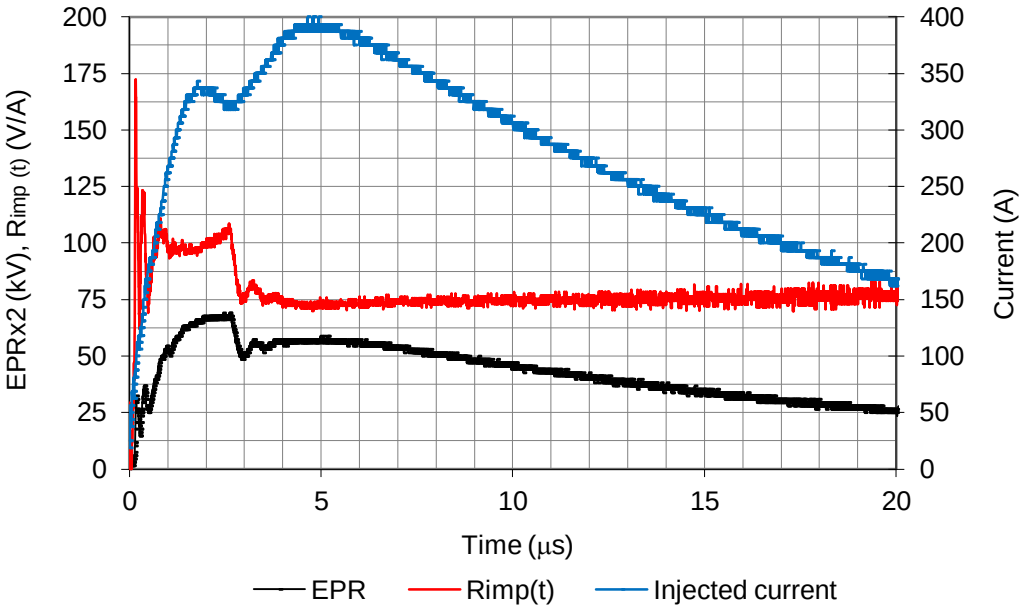

(a)

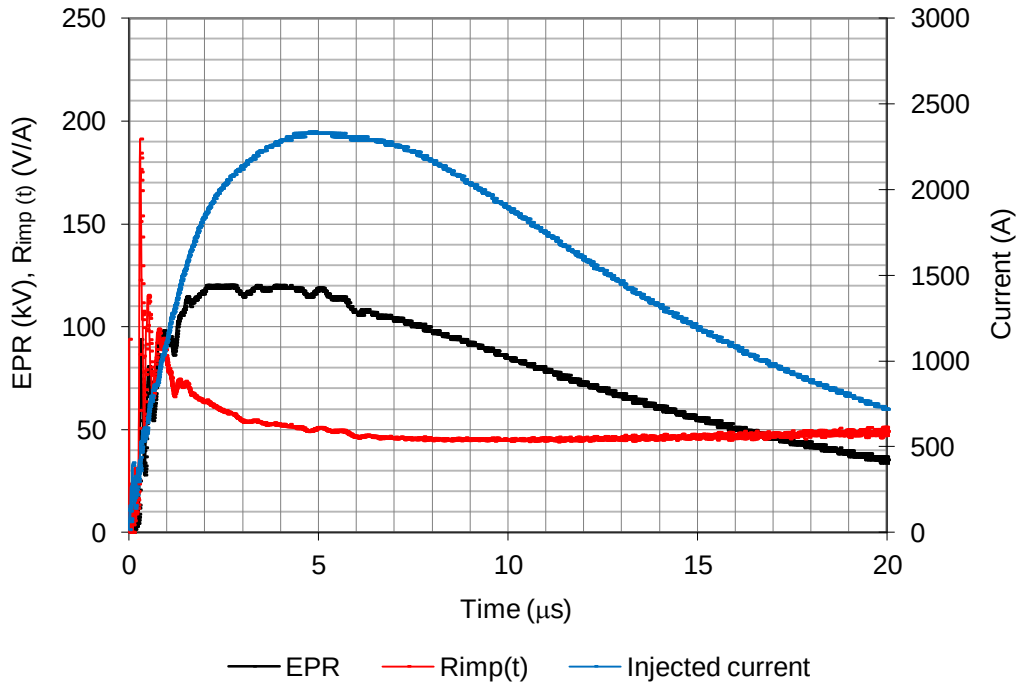

(b)

Figure 5.8: Time variations of tower leg impulse resistance.

(a) Ip=0.4kA, (b) Ip=2.32kA

5.5 Impulse tests at higher current magnitudes

This test is an extension of the previous tests on the tower base carried out in a previous investigation in 2009. Here, the range of currents is extended to between 0.4kA and 9kA with an impulse shape of 4.5/13, and the tested electrodes included the complete tower base and also every isolated tower footing.

Figure 5.9 shows the impulse resistance decreasing as a function of peak current magnitude for all tower footings. The highest reduction in resistance occurs with the footing having the highest DC resistance (Leg 1).

When the current increases from 600A to 6kA, the impulse resistances decreased by 47% for Leg 1, 40% for Leg 3, 22% for Leg 2 and 14% for Leg 4.

For the complete tower base, with all four legs connected in parallel, the percentage reduction in the impulse resistance is relatively small due to the current division between the legs which leads to limited ionisation progression around the individual legs. It is recognised that soil ionisation is more likely to occur with electrodes of small surface area, high impulse currents and in high resistivity soil.

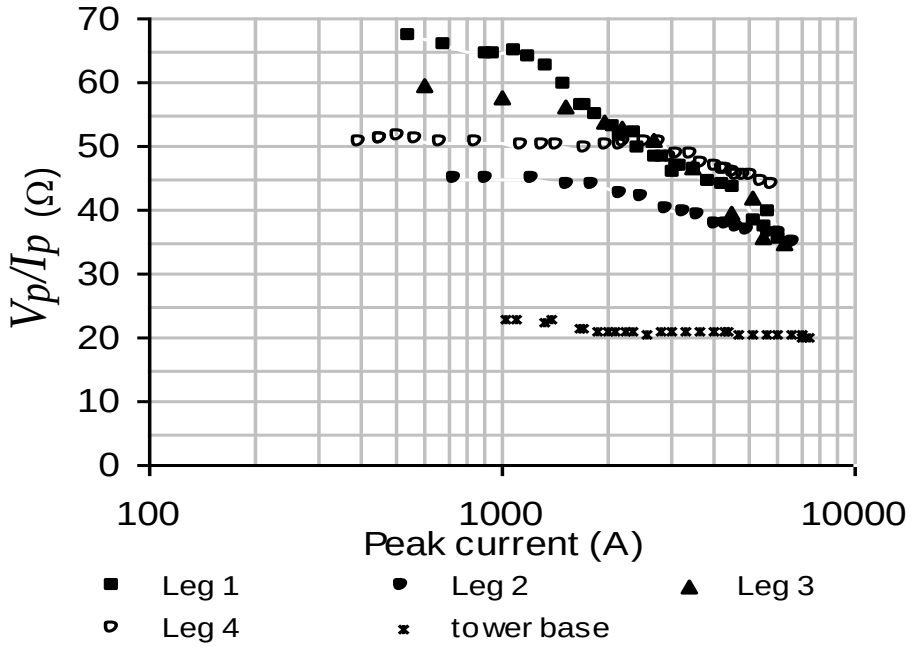

Figure 5.9: Variation of impulse resistance of tower footings with current magnitude

5.6 Conclusions

The characteristics of a full scale tower base under low and high-magnitude impulse currents have been investigated. For low currents, the impulse and DC resistances of the tower legs were found to have different values due to differences in localised soil conditions. The impulse resistance decreases with current magnitude due to soil ionisation. The largest reduction in impulse resistance occurred with the tower leg having the highest DC resistance, but the full tower base showed only a small reduction. The initial ionisation inception current was not constant but increased with the rate of rise of applied current. The time variations of the dynamic resistance showed that at high currents, the ionisation was characterised by two reductions in the resistance associated with simultaneous increase in current and reduction in voltage. The time and current dependence of the impulse resistance are, therefore, important parameters for modelling the performance of earthing systems under high impulse currents.

CHAPTER 6: CURRENT AND VOLTAGE DISTRIBUTION IN HORIZONTAL EARTH ELECTRODES UNDER IMPULSE CONDITIONS

6.1 Introduction

Earthing systems are designed to dissipate high magnitude fault current to ground and to provide safety for persons working or living near power system installations. In order to dissipate current efficiently under both power frequency and transient fault conditions, the earthing system should have a low impedance value.

For enhancing the earthing system of steel transmission lines, single earth rods or ring electrodes are used, in land with high soil resistivity, horizontal electrodes may also be used. The addition of horizontal earth electrodes will contribute to the reduction of the low-frequency earth impedance. However, under lightning conditions, these additional electrodes may not be effective in dissipating current because there is a limiting effective length of the electrode, which can be much lower than the physical length of the electrode.

This effective length depends on the electrode geometry, soil resistivity and the impulse characteristics, and this has been the subject of interest of many researchers [6.1-6.5]. The current and voltage distributions along a horizontal electrode have been analysed in [6.2] for a range of soil resistivity values and for low and high current magnitudes. Computation models based on distributed-parameter equivalent circuits have been proposed to determine the impulse response, the effective length and the impulse impedance of horizontal electrodes [6.3, 6.4].

6.2 Tests on the horizontal earth electrode

Figure 6.1 shows the aerial view of Cardiff University's Llanrumney site. The figure depicts the ring earth electrode which was used as the horizontal test electrode in this study. Figure 6.2 shows a diagram of the experimental setup used for the impulse tests. The test electrode, installed for this investigation, comprises, 88.5m-long conductor with cross-sectional area of $0.2cm^2$, buried at a depth of 30cm. The electrode is not a straight line but forms an arc of 30m radius of curvature as shown in Figure 6.2(a). It is divided into sections of different lengths with test pits located at the junctions to enable access for voltage and current measurements. These junctions are indicated by points A, B, C, D and E on the figure and the lengths of the conductor sections are given in Figure 6.2 (b). Current transformers of 0.1V/A and 0.01V/A sensitivities, and high-bandwidth differential voltage transducers were used for these measurements. The current was injected between one end of the electrode (point A) and the transmission tower base which was used as the auxiliary return current electrode. A low voltage recurrent surge generator was used for impulse current injection. The generator delivers double exponential impulse voltages, with the facility of varying the amplitude and shape by altering the generator circuit parameters. The electrode potential was measured with reference to a rod electrode placed of 100m away from the injection point.

An example of the applied impulse current and the resulting earth potential rise at the current injection location (point A) is shown in Figure 6.3. The current has a rise time of 5.8μs and a time to half value of 16 μs, with a peak value of 5.41 A. The corresponding peak EPR is 44.4 V. The significant influence of the electrode inductance is indicated by a sharp rise in electrode potential during the front of the impulse. A soil resistivity survey at the site gave a two-layer soil with a bottom layer of 30Ωm resistivity and a 200Ωm resistivity upper layer of about 8m depth.

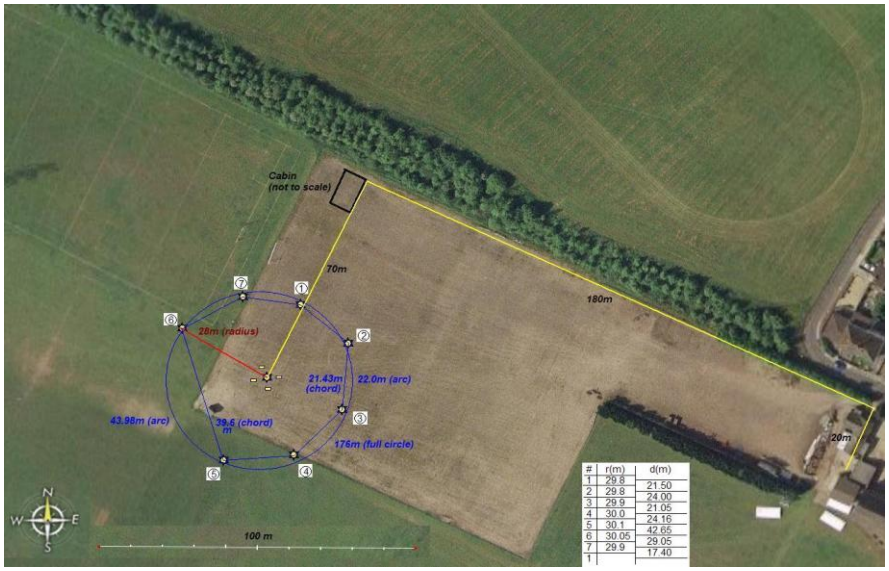

Figure 6.1: Aerial view of Cardiff University's Llanrumney site

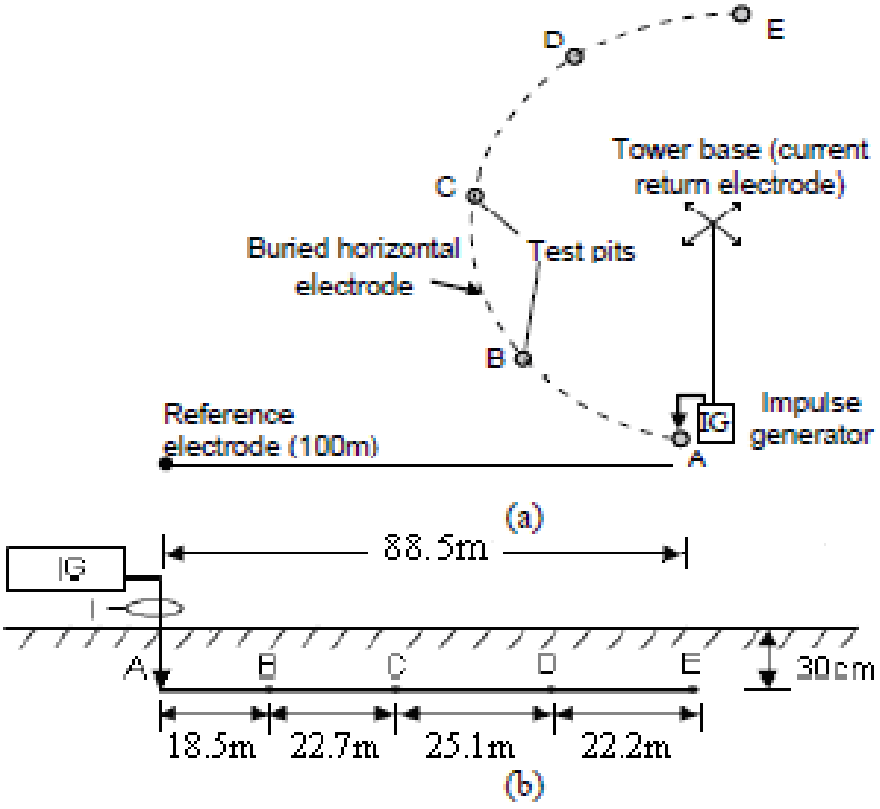

Figure 6.2: Experimental set-up, (a) top view (b) side view showing test electrode length and burial depth

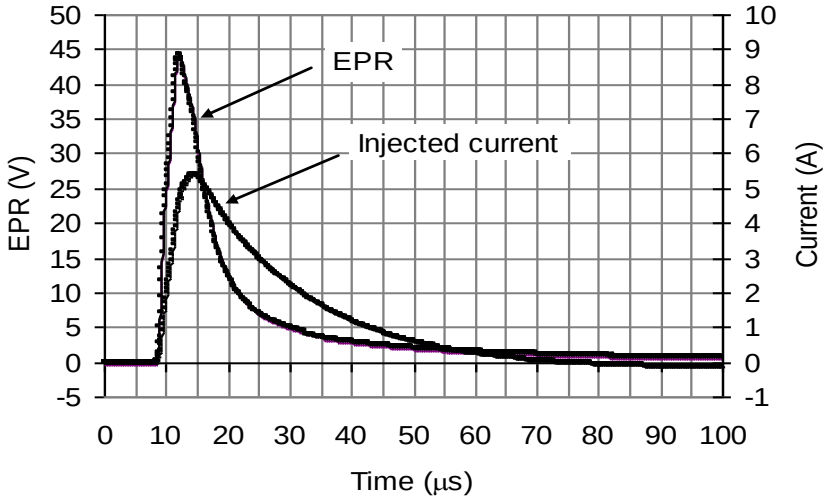

Figure 6.3: Voltage and current shapes at injection point (point A) of electrode 88.5 length

6.2.1 Current and voltage distributions along electrode

The impulse currents measured at points A, B, C and D of the horizontal electrode are shown in Figure 6.4, and the corresponding electrode voltages measured at these points and at the end point E are shown in Figure 6.5. As it travels along the electrode length, the current impulse undergoes an attenuation of its magnitude and a change in the rate of rise. This is attributed to the current leaking into the ground during propagation. The time delay observed on the current waveshapes measured at points B (18.5m), C (41.2m) and D (66.3m) is due to the surge travel time along the electrode. In the first 18.5m section of the horizontal electrode (section AB), 37% of the injected current is dissipated into the ground, whereas in the three sections AB, BC and CD together (66.3m of electrode length), the current dissipated is 85% of the injected current. It was found that the reduction in the peak magnitude of current is not uniform, with the highest proportion of current dissipated in the first section AB of the electrode which has the shortest length, compared with sections BC and CD.

Similarly, the magnitude of the voltage along the electrode shows a significant reduction with length, and there is a change in shape both on the front and tail of the impulse (Fig.6.5). The percentage reductions in EPR are 39% at point B, 62% at point C and 66% at points D and E.

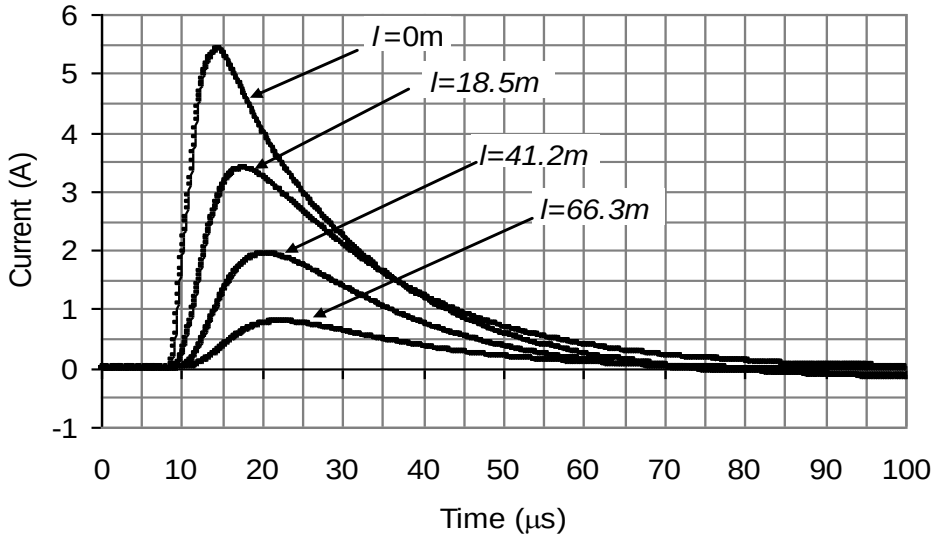

Figure 6.4: Measured impulse currents along the 88m electrode at distances 0m, 18.5m, 41.2m and 66.3m

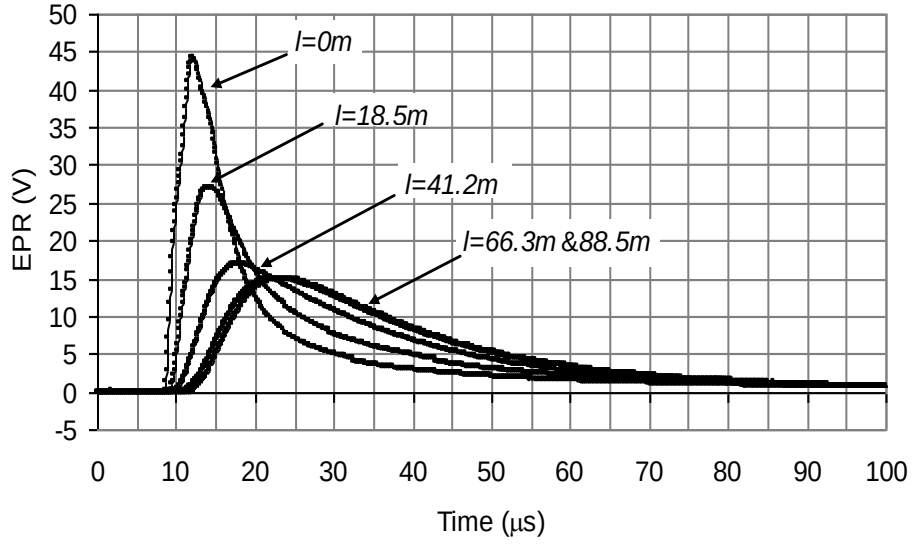

Figure 6.5: Measured impulse voltages along the 88m electrode at distances 0m, 18.5m, 41.2m, 66.3m and 88.5

The geometrical test configuration was simulated using the HIFREQ module of the CDEGS software [6.7]. The simulation requires all electrodes to be modelled as cylindrical conductors with radii much smaller than length. A two-layer soil model was used and both the current injection and voltage measuring leads were simulated as shown in Figure 6.6. The computation was performed by energising the electrode at point A using an impulse of the same magnitude and shape as the current in the field test. The frequency spectrum of the impulse current was then computed using an FFT routine before computing the individual frequency responses in the HIFREQ module. An inverse FFT routine was used to compute the time domain response of the electrode. Figure 6.7 shows the results of the computation of the electrode potentials at the specified points of the electrode coinciding with the measurement points A to D described. In Figure 6.7, the computed impulse shapes have slightly higher magnitudes than the measured traces. It should be noted, however, that the computer model is not an exact representation of the actual measurement set up. For example, the soil model used for computations is considerably simplified.

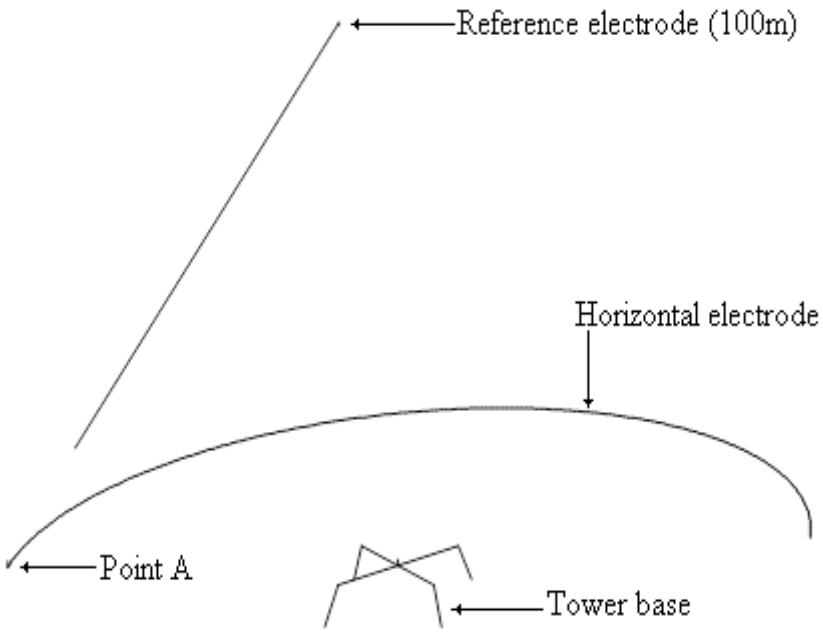

Figure 6.6: Horizontal earth electrode model

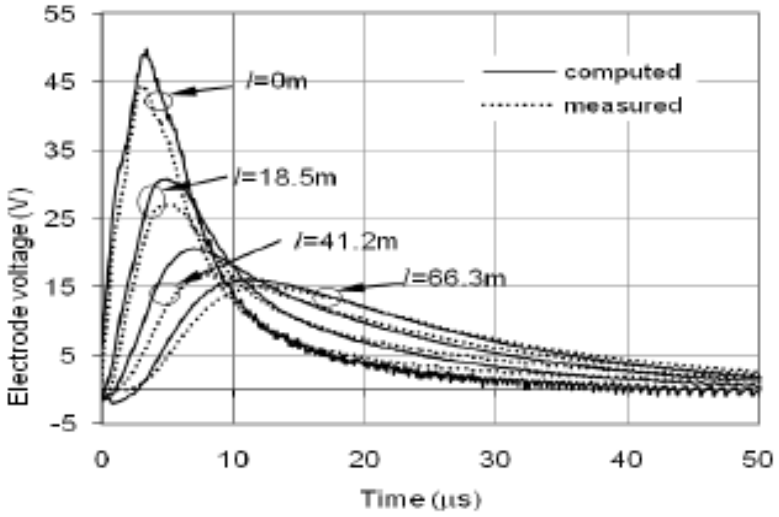

Figure 6.7: Computed and measured voltage waveshpes at different points on the 88.5m horizontal electrode

Figure 6.8 shows the peak current distribution along the electrode length normalised to the peak current at the injection point (*Iinj*), for injected impulse currents having peak values between 1A and 6A. Over this range of magnitudes, the current dissipation in the ground is independent of the magnitude of injected current. Also, the peak current reduction is quasi-linear. The corresponding EPR magnitudes normalised to the voltage at point A (V_A) are shown in Fig. 6.9, where no change in voltage occurs after 66.3m of the electrode length. As observed with the current, the relative reduction in voltage over the electrode length is independent of the magnitude of injected current for Iinj≥2A. For the smallest current Iinj=1A, the electrode voltage reduces with distance by slightly higher proportions compared with other current magnitudes.

Table 6.1 gives the peak values of current (*Ip*) and the corresponding voltages at the instant of current peak (*V(@Ip)*) at the test points along the electrode, for an injected current of 5.41A. The ratio *V(@Ip)/Ip* characterising the electrode impulse resistance was calculated to be 6.5Ω at the injection point of the electrode. This ratio remains approximately constant at this value over the first three sections of the electrode, and increases to more than three times towards the end of the electrode.

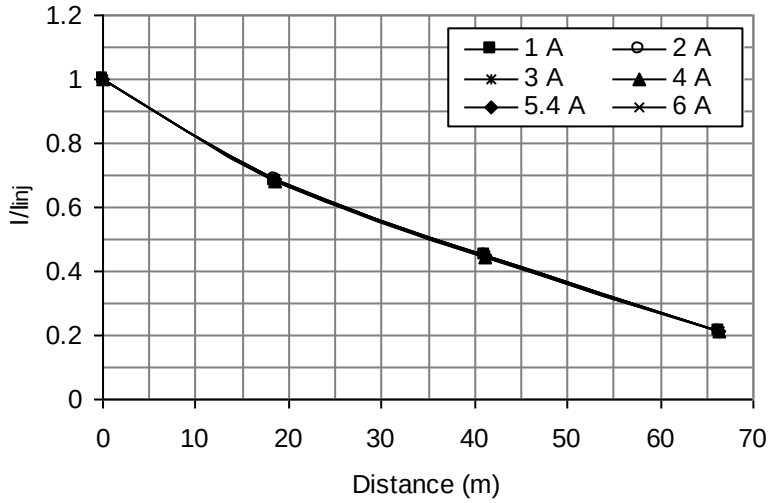

Figure 6.8: Normalised peak current distribution over electrode length

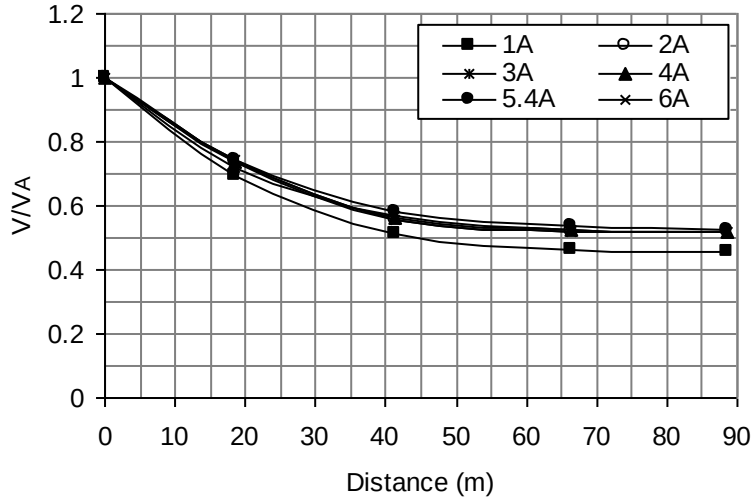

Figure 6.9: Normalised peak voltage distribution over electrode length

Table 6.1: Measured peak current and voltage along electrode

Distance (m)	0	18.5	41.2	66.3
Ip (A)	5.40	3.39	1.94	0.78
V(@Ip), (V)	35.4	21.9	16.2	14.6
V(@Ip)/Ip	6.5	6.46	8.36	18.54

6.2.2 Effect of current rise time on current and voltage distributions

In order to investigate the influence of the impulse shape on both current and EPR distributions over the electrode, two impulse current rise times were used; 5.8 μs and 3.5μs. It was found that for the impulse with the faster rise time, the reduction in current magnitude is larger than that observed with the slower rise time, as shown in Figure 6.10(a). This refers to a higher dissipation of current with faster rise time at the injection point. For voltage distribution along the horizontal electrode, a higher EPR was generated at the injection point for the current with faster rise time as shown in Figure 6.10(b). This means that for the same current magnitude, the fast rising current is dissipated into the ground more quickly than the slow rising current.

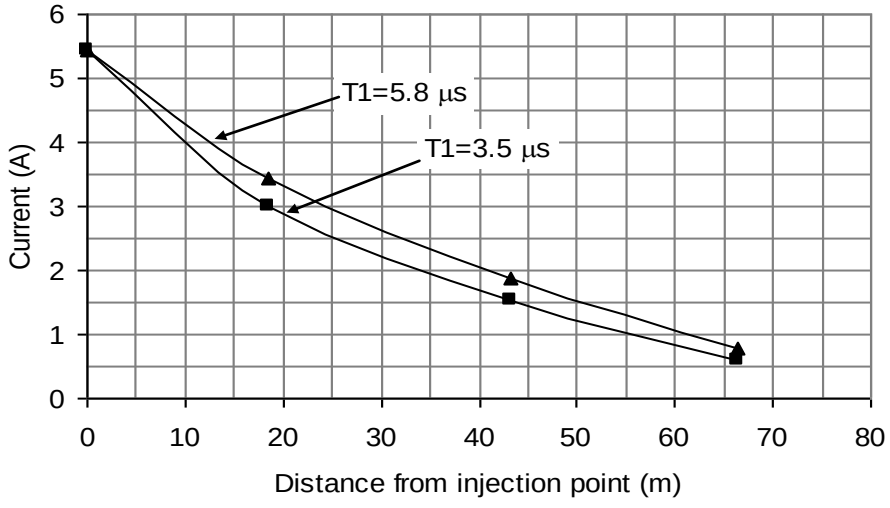

(a)

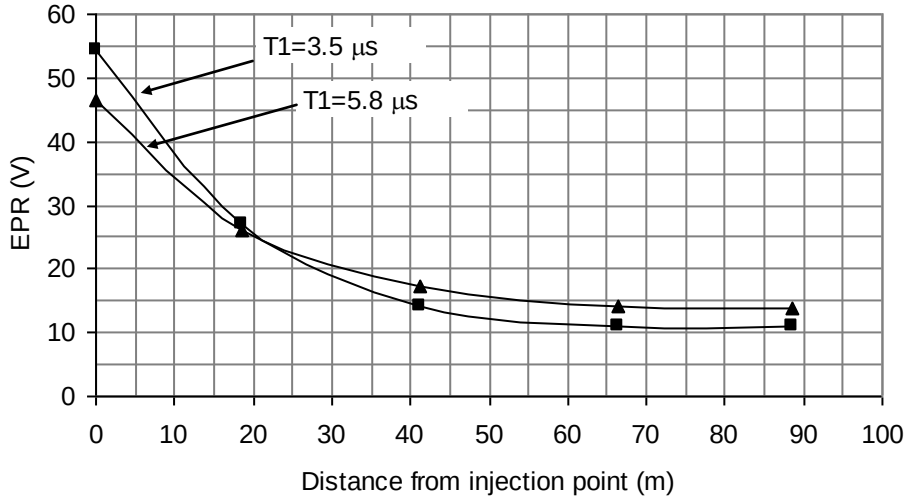

(b)

Figure 6.10: Effect of impulse current rise time on (a) distribution of current and (b) voltage over the electrode length.

6.2.3 Effect of current injection point

The current injection point has an important effect on the electrode impulse impedance and its effective length. In order to achieve minimum impulse resistance for a single electrode, injection at the centre point of the electrode is preferred. In this study, an impulse current of 4.5A was injected at various points of the electrode and the impulse voltage and current, measured at the point of injection, were used to calculate the electrode impulse resistance. Figure 6.11 shows the voltage at each point, and a summary of the measured electrode voltage and impulse resistance for different current injection points is tabulated in Table 6.2. As can be seen, the lowest impulse impedance is obtained at point C, which is at distances of 41.2m and 47.3m from the electrode start and end points respectively. Note that, although the injected current is the same, the impulse resistance measured at one end of the electrode is different from

that measured at the other end. This may be due to lateral soil resistivity variations which were found to occur within the site.

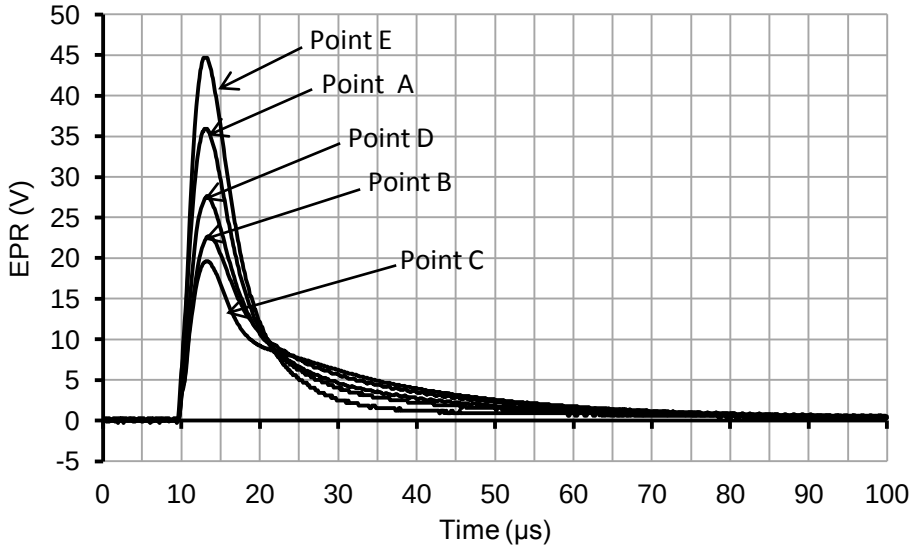

Figure 6.11: EPR due to injection current at different points

Table 6.2: Effect of current injection point on electrode impedance resistance

Current injection point	A	B	C	D	E
Ip	4.5	4.5	4.5	4.5	4.5
V (@Ip)	27.2	20.2	18.5	24.2	35.1
V(@Ip)/Ip	6.06	4.49	4.11	5.37	7.8

6.3 Effect of electrode length

Additional tests were carried out on individual and combined sections of the horizontal electrode. Initially, the current was injected onto the first section when isolated (section AB), and then the other sections were added in sequence to increase the electrode length. The current injected into the first section was 5A, and the current injected after adding all the other sections was 5.5A. Figure 6.12 shows the recorded

voltage waveshapes for increasing electrode length *l*. The EPR is reduced by 29%, when the conductor length is increased from18.5m to 41.2m, with no further reduction as additional sections are added. To determine the effective length of the electrode from these measurements, the impulse resistance R_i defined by the ratio *V(@Ip)/Ip* was calculated, and its variation with electrode length is plotted in Figure 6.13. The impulse resistance for an electrode length of 18.5m was 12.4Ω, which then decreases down to a value of 6.7Ω as the electrode length increases beyond 41.2m. This length can be taken as an indication of the effective length of the electrode since no significant reduction in impulse resistance is achieved by further increasing the electrode length. The DC resistance (Figure 6.13), in contrast, falls to a much lower value with electrode distance. As the electrode length is increased further, the impulse resistance remains constant while its DC resistance decreases, leading to values of DC resistance that decrease continuously in relation to impulse resistance with increasing electrode length. From these results, it can be deducted that substantial increase in electrode length may be effective in dissipating low frequency currents, but only a much more limited length is available for dissipating impulse currents. This result can be verified by comparing it to the following empirical formula (6.1) for calculating the effective length [6.8]:

$$l_{eff} = A(\rho\tau)^{0.5} \tag{6.1}$$

Where ρ is the soil resistivity, τ is the wave front time, and *A* is a constant which depends on the point of current injection, and is 1.4 for current injected at one end.

The calculated effective length using the present test data is 48m for a uniform soil resistivity of 200Ωm. However, since the soil at the test site consists of two layers and Equation 6.1 applies to uniform soil only, an equivalent uniform resistivity can be assumed to account for the lower layer resistivity. If this equivalent resistivity is taken

as the average of the upper layer and lower layer resistivities, the calculated effective length is 38m. Hence, the effective length of 41.2m is reasonably close to the value predicted by Equation (6.1).

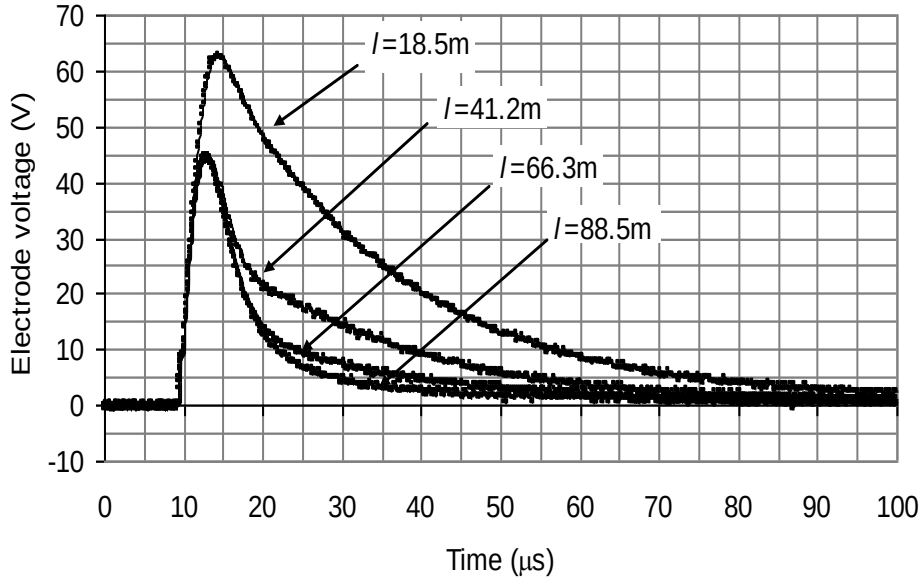

Figure 6.12: Measured voltage for different electrode lengths

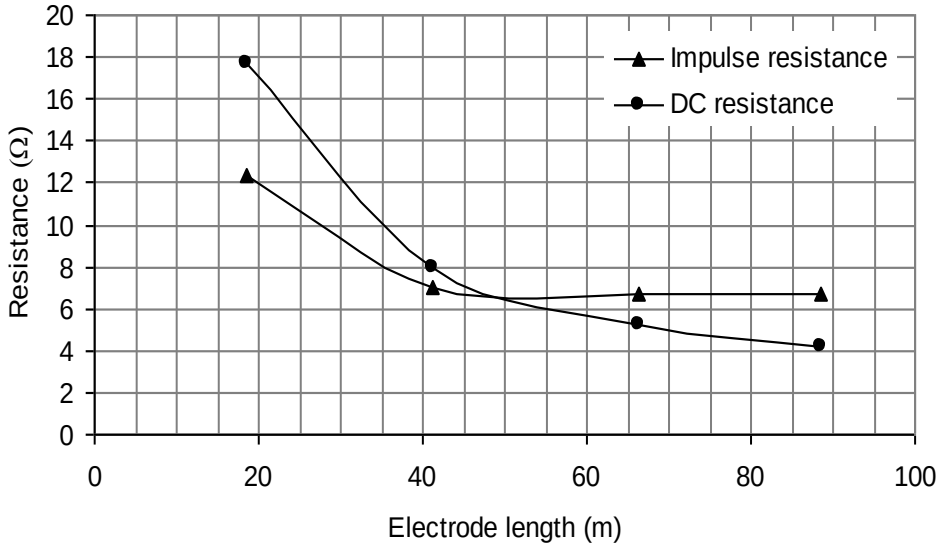

Figure 3.13: Variations of electrode impulse and DC resistance with length

6.4 Conclusions

Experimental tests on current and voltage distributions along a buried horizontal electrode under impulse currents were reported. The results show that a large proportion of the injected impulse current is dissipated into the ground along a length close to the injection point and that this proportion is greater for faster impulse rise times. The electrode potential reduces sharply with length starting from the injection point and then takes a constant value after a certain distance on the electrode. The effective length of the electrode was determined from the impulse resistance and was found to be comparable to that predicted using an empirical formula reported in literature. This effective length is dependent upon the soil properties and the impulse shape. The results also demonstrated that the impulse resistance was dependent on the current injection point and has a minimum value when current is injected near the centre point of the electrode. Computer simulations showed good agreement with measurement results.

CHAPTER SEVEN: CONCLUSIONS AND FURTHER WORK

7.1 CONCLUSIONS

A comprehensive review of the behaviour of earth electrodes under high impulse currents was carried out, and it revealed that the impedance characteristics of the electrodes are non-linear with injected current and that soil ionisation occurs above a critical electric field threshold value. Most of the previous work has been based on laboratory experiments, and there have been limited field tests on practical electrodes including tower base earthing systems. The earth resistance of tower base is important both with respect to the over voltage performance of shielded transmission lines and also for the safety of personal in the vicinity of tower structures due to the prospective high earth potential rise and the high potential gradients developed on the ground surface.

Accordingly, work was carried out to improve the understanding of the earth surface potential in the vicinity of a purpose installed test 275kV transmission tower base under variable frequency ac current. The field tests revealed that there are considerable differences between the earth resistances of the individual footings and that there is also a considerable seasonal variations. Satisfactory agreement was obtained between measured and computed values of tower footing resistances and the differences are attributed to limitations of the simplified soil models used in both analytical calculation and detailed computer simulations.

The same can be said about the prediction of ground surface potential distribution along profiles passing across the tower base: i. e., there is good general agreement between measured and computed values but the soil models used in the computations are restricted to laterally homogenous layers and hence are not able to replicate the

local variations in soil which produce different impedance associated with different legs. The results confirm that the maximum voltage gradients occur along the diagonal profiles. A similar picture emerges when the potential profiles were investigated using low voltage impulse energisation. These tests revealed that measured touch voltages were different for different legs and could be as high at 80% of the tower base EPR.

The earth surface potential has been measured due to injection a low-magnitude current. Both AC variable frequency and impulse current sources were used. The earth surface potential as a result of impulse current was measured along the four diagonal profiles. The measured current distribution in the tower legs under impulse confirmed that the current distribution governed according to the DC earth resistances of the individual legs. It was very interesting to know that quite a small proportion of current at the tower leg is dispersed from the bottom end of the leg. Investigation into the sub surface potential distribution, both inside the concrete footing and in the soil adjacent to the footing were achieved by sets of buried metal probes. The ac and impulse tests, which produced similar findings, showed that the potential ground reduced with depth and along the footing. There appear to be greater local variation in potential within the concrete footing compared with just outside the footing in soil.

High voltage impulse tests were conducted on a full scale tower base and its individual footings to examine non-linear behaviour under high current condition. The arrangement adopted for the high voltage impulse test allows the current to return through a number of rod electrodes connected by an insulated ring. Such a test method is different from the commonly used method, in which the return electrode is placed at a single location. The effect of localised high current density is minimised and the current is distributed in the ground in all directions. Consequently, it is argued that a better characterisation of the earthing will be achieved using this method, since it

involves a large volume of soil surrounding the tower base footings. The measurement results showed that the measured impulse resistance decrease with increasing surge current. The largest reduction of impulse resistance occurred with a tower footing having the highest magnitude of DC resistance. However, the full tower base showed only a small reduction compared with the footings as a result of low current density on the contact surface with soil. The initial ionisation inception current was found to be not constant but increases with the rate of the rise of applied current. The time variations of the dynamic resistance showed that at high currents, the ionisation is characterised by two reductions in the resistance associated with a simultaneous increase in current and a reduction in voltage. Therefore, the time and current magnitude dependence of the impulse resistance are important parameters for modelling the performance of earthing systems under high impulse currents. This behaviour of reduction in the resistance is attributed to non-linear conduction phenomena occurring in the soil (thermal conduction and soil ionisation).

Low voltage impulse currents were conducted on a circular counterpoise that could potentially be useful to enhance the earthing system of the tower base. It was shown that a large proportion of the injected impulse current is dissipated into the ground along a length close to the injection point. The electrode potential also falls sharply with length starting from the injection point and then settles at a constant value after a certain distance on the electrode. The effective length of the electrode was determined from the impulse resistance and was found to be comparable to that predicted by an empirical formula reported in literatur. This effective length is dependent upon the soil properties and the impulse shape. It was also experimentally demonstrated that the impulse resistance was dependent on the current injection point and has a minimum value when current is injected near the centre point of the electrode. The current rise time was found to have an effect on the amount of current dissipated; with the fast

rising impulse, more current was dissipated into the ground compared with the slow front impulse. Computer simulations showed good agreement with measurement results.

7.2 FUTURE WORK

Important areas of future research work on tower base earthing systems include (i) the installation a ring electrodes of different diameters and depths around each tower footing and (ii) further experimental studies to clarify the conduction mechanisms of earth electrodes under high magnitude impulse current. The objective of the experimental work on ring electrodes for controlling ground voltage gradient would be to mitigate step and touch voltages in the proximity of tower footings.

It is proposed that conduction mechanism investigations would be based on high voltage laboratory tests and high voltage tests on practical earth electrodes at the Cardiff University outdoor earthing test facility at Llanrumney.

REFERENCES

Chapter One

[1.1] H. Griffiths and N. Pilling, ‘‘Earthing,’’ in *Advance in High Voltage Engineering* A. Haddad and D. Warne, London: IET, 2004, pp. 349-413

[1.2] AIEE Committee Report: ‘‘Lightning Performance of 110- to 165-Kv Transmission Lines,’’ AIEE Transactions, vol. 58, pp. 249-306, 1939.

[1.3] BS EN 50522:2008: ‘‘Earthing of Power Installations Exceeding 1 kV a.c,’’ European Committee for Electrotechnical Standardisation (CENELEC), 2008.

[1.4] BS EN 62305-3:2011 ‘Protection against lightning part3: physical damage to structures and life hazard’European Committee for Electrotechnical Standardization (CENELEC)

[1.5] ENA TS 41-24: ‘‘Guidelines for the Design, Installation, Testing and Maintenance of Main Earthing Systems in Substations,’’ Energy Networks Association, Issue 1, 1992.

[1.6] BS 7430:2011: ‘‘Code of Practice for Protective Earthing of Electrical Installations,’’ British Standards Institution, 2011.

[1.7] IEEE Std. 80-2000 ‘Guide for Safety in Substation Grounding’ The Institute of Electrical and Electronic Engineers, New York, 2000.

[1.8] R. H. Golde, ‘‘Lightning Vol. 1: Physics of Lightning’’, Academic Press, London, ISBN 0-12-287801-9, 1977.

[1.9] Lightning and Insulator Subcommittee of the T&D Committee ‘Parameters of Lightning Strokes: a Review’ IEEE Transactions on Power Delivery, vol. 20, No. 1, January 2005.

Chapter Two

[2.1] Feng Zhenghua, Lu Ling and Feng Junzhong ‘‘Research on reducing grounding resistance of transmission line tower grounding grid,’’ The 2nd International Conference on Electrical and Control Engineering (ICECE), pp. 1216-1219, China, 2011.

[2.2] Takehiko Takahashi and Taro Kawase, ‘‘Calculation of earth resistance for a deep-driven rod in a multi-layer earth structure,’’ IEEE Transactions on Power De1ivery, vol. 6, No. 2, pp. 608-614, 1991.

[2.3] Akihiro Ametani, Tomohiro Chikaraa, Hiroshi Morii and Takashi Kubo, ‘‘Impedance characteristics of grounding electrodes on earth surface,’’ Electric Power Systems Research, vol. 85, pp. 38-43, April 2012.

[2.4] *IEEE Guide for the Application of Insulation Coordination*, IEEE Std 1313.2-1999, 1999.

[2.5] *IEEE Guide for Improving the Lightning Performance of Transmission Lines*, IEEE Std 1243-1997, 1997.

[2.6] Working Group on Estimating the Lightning Performance of Transmission Lines, ‘‘IEEE Working group report estimating lightning performance of transmission lines II-updates to analytical models,’’ IEEE Transaction on Power Delivery, vol. 8, No. 3, pp. 1254 – 1267,1993.

[2.7] James T. Whitehead, ‘‘Lightning performance of TV’s 500-kV and 161-kV transmission lines,’’ IEEE Transaction on Power Apparatus and Systems, vol. PAS-102, No. 3, pp. 752-768, 1983.

[2.8] W. A. Chisholm, Y. L. Chow and K. D. Srivastava, ‘‘Travel time of transmission Towers,’’ IEEE Transaction on Power Apparatus and Systems, vol. PAS-104, No. 10, pp. 2922-2928, 1985.

[2.9] Tomohiro Hayashi, Yukio Mizuno and Katsuhiko Naito, ‘‘Study on transmission-line arresters for tower with high footing resistance,’’ IEEE Transaction on

Power Delivery, vol. 23, No. 4, pp. 2456-2460, 2008.

[2.10] Khalifa M. 'High-Voltage Engineering Theory and Practice', Marcel Dekker Inc., 1990

[2.11] Makoto Takeuchi, Yoh Yasuda and Hidenobu Fukuzono, ''Impulse characteristics of a 500kV transmission tower footing base with various grounding electrodes,'' International Conference on Lightning Protection (ICLP), pp. 513-517, UK, 1998.

[2.12] *IEEE Guide for Protective Relay Applications to Transmission Lines*, IEEE Std C37.113, 1999.

[2.13] P. Chowdhuri, S. Li and P. Yan: ''Rigorous analysis of back-flashover outages caused by direct lightning strokes to overhead power lines,'' IEE Proceedings-Generation, Transmission and Distribution, vol. 149, No. 1, pp. 58-65, January 2002.

[2.14] Kosztaluk R., Loboda M., and Mukhedkar D.: ''Experimental study of transient ground impedances,'' IEEE Transaction on Power Apparatus and Systems, vol. PAS-100, No. 11, pp. 4653-4660, 1981.

[2.15] Harid N., A. Zanini, H. Griffths and A. Haddad: ''Characterisation of tower base earthing systems under impulse conditions,'' International Conference on Lightning Protection (ILCP), pp. 480-485, France, 2004.

[2.16] IEEE Fast Front Transient Task Force, ''Modeling guidelines for fast front transients,'' IEEE Transactions on Power Delivery, vol. 11, No. 1, pp. 493-506, 1996.

[2.17] Towne H. M.: ''Impulse characteristics of driven grounds,'' General Electric Review, vol. 31, No. 11, pp. 605-609, 1928.

[2.18] Bellaschi P. L.: ''Impulse and 60-cycle characteristics of driven grounds,'' AIEE Transactions, vol. 60, pp. 123-128, 1941.

[2.19] Bellaschi P. L., Armington R. E. and Snowden A. E.: ''Impulse and 60-cycle characteristics of driven grounds-II,'' AIEE Transactions, vol. 61, pp. 349-363, 1942.

[2.20] Liew A. C. and Darveniza M.: ''Dynamic model of impulse characteristics of concentrated earths,'' Proc IEE, vol. 121, No. 2, pp. 123-135, 1974.

[2.21] A. L. Vainer and V. N. Floru: ‘‘Experimental study and method of calculation of the impulse characteristics of deep earthings,’’ Elecktrichestvo, vol. 2, No. 5, pp. 18-22, 1971.

[2.22] Bewley L. V.: ‘‘Theory and tests of the counterpoise,’’ AIEE Transactions, vol. 53, No. 8, pp. 1163-1172, 1934.

[2.23] Geri A. and Garbagnati E., ‘‘Non-linear behaviour of ground electrode under lightning currents: computer modelling and comparison with experimental results,’’ IEEE Transactions on Magnetics, vol. 28,pp. 1442-1445, March 1992.

[2.24] S. Sekioka, H. Hayashida, T. Hara and A. Ametani, ‘‘Measurements of grounding resistances for high impulse currents,’’ IEE Proceedings-Generation Transmission Distribution, vol. 145, pp. 693-696, November 1998.

[2.25] Sonoda Toshio, Hidemi Takesus and Shozo Sekioka, ‘‘Measurement on surge characteristics of grounding resistance of counterpoise for impulse currents,’’ International Conference on Lightning Protection (ICLP), September 2000.

[2.26] K. Berger: ‘‘The behaviour of earth connections under high intensity impulse current,’’ CIGRE, vol.95, pp. 1-32, 1946.

[2.27] Petropoulos G. M., ‘‘The high-voltage characteristics of earth resistances,’’ Journal of the institution of Electrical Engineers Part II: Power Engineering, Vol. 95, pp. 59-70, February 1948.

[2.28] I. Cotton, ‘‘The soil ionization process,’’ ERA Conference, pp. 4.4.1-4.4.11, 2000.

[2.29] M. Victor, M. Cabrera, Stig Lundquist and Vernon Cooray, ‘‘On the physical properties of discharges in sand under lightning impulses,’’ Journal of Electrostatics, pp. 17-28, 1993.

[2.30] Schon J. M.: ‘Physical Properties of Rocks: Fundamentals and Principles of Petrophysics, (Handbook of Geophysical Exploration, Section 1, Seimic Exploration: Vol. 18),’ Oxford, UK, Elsevier Science Ltd, 1998.

[2.31] D. P. Snowden and Erler J. W: ‘‘Initiation of electrical breakdown of soil by water vaporization,’’ IEEE Transactions on Nuclear Science, vol. NS-30, No. 6, pp. 4568-4571, 1983.

[2.32] Vanlint V. A. J. and J. W. Erler, ‘‘Electric breakdown of earth in coaxial geometry,’’ IEEE Transactions on Nuclear science, vol. NS-29, No. 6, pp. 1891-1896, 1982.

[2.33] Srisakot S., H. Griffiths and A. Haddad, ‘‘Soil ionisation modelling under fast impulse,’’ Proceedings of the 36th Universities Power Engineering Conference (UPEC), UK, 2001.

[2.34] D. P. Snowden, G. C. Morries, Jr. and V.A.J. Van Lint: ‘‘Measurement of the dielectric constant of soil,’’ IEEE Transmissions on Nuclear Science, vol. NS-32, No. 6, pp. 4312-4314, 1985.

[2.35] T. M. Flanagan, C. E. Mallon, R. Denson and R. E. Leadon: ‘‘Electrical breakdown properties of soil,’’ IEEE Transmissions on Nuclear Science, vol. NS-28, No. 6, pp. 4432-4439, 1981.

[2.36] R. E. Leadon, T. M. Flanagan, C. E. Mallon and R. Denson: ‘‘Effect of ambient gas on ARC initiation characteristics in soil,’’ IEEE Transmissions on Nuclear Science, vol. NS-30, No. 6, pp. 4572-4576, 1983.

[2.37] Abdul M. Mousa: ‘‘The soil ionization gradient associated with discharge of high current into concentrated electrodes,’’ IEEE Transactions on Power Delivery, vol. 9, No. 3, pp. 1669-1677, 1994.

[2.38] N. Mohamad Nor, A. Haddad, and H. Griffiths: ‘‘Characteristics of Ionisation Phenomena in Soils under Fast Impulses,’’ IEEE Transactions on Power Delivery, vol. 21, No. 1, pp. 353-361, 2006.

[2.39] Junping Wang, Ah Choy Liew and Mat Darveniza: ‘‘Extension of dynamic model of impulse behaviour of concentrated grounds at high currents,’’ IEEE Transactions on Power Delivery, vol. 20, No. 3, pp. 2160-2165, 2005.

[2.40] M. E. Almeida and M. T. Correia de Barros: ‘‘Accurate modelling of rod driven tower footing,’’ IEEE Transactions on Power Delivery, vol. 11, No. 3, pp. 1606-1609, 1996.

[2.41] Pritindra Chowdhuri, *Electromagnetic Transients in Power Systems*. Exeter: Research Studies Press Ltd, 1996.

[2.42] E. E. Oettle: ‘‘A new general estimation curve for predicting the impulse impedance of concentrated earth electrodes,’’ IEEE Transaction on Power Delivery, vol. 3, No.

4 pp. 2020-2029, 1988.

[2.43] Loboda M. and Scuka V.: ‘‘On the transient characteristics of electrical discharges and ionisation processes in soil,’’ Proceedings of the 23rd International Conference on Lightning Protection (ICLP), pp. 539-544, Italy, 1996.

2.44 Srisakot S., H. Griffiths and A. Haddad ‘‘Soil Ionisation Modelling under Fast Impulse’’ Proceedings of the 36th Universties Power Engineering Conference (UPEC), Swansea (UK), 12-14 September 2001.

[2.45] Colin Bayliss, ‘‘Transmission and Distribution Electrical Engineering’’. Reed educational and professional publishing Ltd, Oxford, 1999, ISBN 0 706 4059 6.

[2.46] AIEE Committee Report, ‘‘Voltage gradients through the ground under fault conditions’’ American Institute of Electrical Engineers (AIEE), vol. 77, pp. 669-1043, 1958.

[2.47] *Effects of Current on Human Beings and Livestock-Part1:General Aspects*, IEC/TS 60479-1:2005, 2005.

[2.48] Charles F. Dalziel, Eric Ogden and Curtis E. Abbott, ‘‘Effect of frequency on let-go-Currents,’’ AIEE Transactions on Electrical Engineering, vol. 62, pp. 745-750, December 1943.

[2.49] Charles F. Dalziel and Thomas H. Mansfield, ‘‘Effect of frequency on perception currents,’’ AIEE Transactions on Electrical Engineering, vol. 69, pp. 1162-1168, 1950.

[2.50] Charles F. Dalziel, ‘‘Effect of wave form on let-go currents,’’ AIEE Transactions on Electrical Engineering, vol. 62, pp. 739-744, December 1943.

[2.51] Charles F. Dalziel and W. R. Lee, ‘‘Reevaluation of lethal electric currents,’’ IEEE Transactions on Industry and General Applications, vol. IGA-4, pp. 467- 476, September/October 1968.

[2.52] Charles F. Dalziel: ‘‘Threshold 60-cycle fibrillating currents,’’ AIEE Transactions On Power Apparatus and Systems, Part III, vol. 79, pp. 667-673, 1960.

[2.53] http://wiki.answers.com/Q/How_long_is_a_cardiac_cycle

[2.54] *Overhead Electrical Lines Exceeding AC 45kV- Part 1: General requirements – Common specifications*, BS EN 50341-1:2001 British Standard, 2001.

[2.55] *Earthing of power installations exceeding 1 kV a.c*, Draft BS EN 50522:2008, 2008.

[2.56] *IEEE Guide for Safety in AC Substation Grounding*, ANSI/IEEE Standard 80, 1986, 1986.

Chapter Three

[3.1] Dawalibi F. and Finney W.G.: "Transmission line tower grounding performance in non-uniform soil," IEEE Transaction on Power Apparatus and Systems, vol. PAS-99, No. 2, pp. 471-479, 1980.

[3.2] Romuald Kosztaluk, Dinkar Mukhedkar and Yvon Gervais: "Field measurements of touch and step voltages," IEEE Transaction on Power Apparatus and Systems, vol. PAS-103, No. 11, pp. 3286-3294, 1984.

[3.3] Safe Engineering Services, "Current distribution electromagnetic grounding analysis software (CDEGS)," Canada, 2006.

[3.4] Jones, P., ''Electrical measurement of large area substation earth grids,'' PhD Thesis, Electrical Division, Cardiff University, 2001.

[3.5] *IEEE Guide for Measurement Impedance and Safety Characteristics of Large, Extended, or Interconnected Grounding Systems*, IEEE Standard, 81.2-1991, 1991.

[3.6] *Overhead Electrical Lines Exceeding AC 45kV- Part 1: General requirements –Common specifications*, BS EN 50341-1:2001+A1:2009, 2001.

[3.7] Draft BS EN 50522:2008 "Earthing of Power Installations Exceeding 1 kV a.c'' European Committee for Electrotechnical Standardization, 2009

[3.8] G.F. Tagg: ''Earth Resistances,'' George Newnes Ltd, England, 1964.

[3.9] Megger DET2/2. Auto earth tester specification.AVO.

[3.10] Safe Engineering Services, "Current distribution electromagnetic grounding analysis software (CDEGS)," Canada, 2006.

[3.11] A. L. Vainer and V. N. Floru, ‘‘Experimental study and method of calculation of the impulse characteristics of deep earthings,’’ Elecktrichestvo, vol. 2, No. 5, pp. 18-22, 1971.

[3.12] Fawssett E., Grimmitt H. W., Shotter G. F. And Taylor H. G.: ‘‘Practical aspects of earthing,’’IEE Journal of Institution of Electrical Engineers, vol. 87, No. 526, pp. 357-390,1940.

[3.13] N. Harid H. Griffiths and A. Haddad: ‘‘Effect of Ground Return Path on Impulse Characteristics of Earth Electrodes’’ 7th Asia-Pacific International Conference on Lightning (APL), pp. 686-689, China, 2011.

[3.14] High voltage group, Cardiff University, ‘‘Understanding of earthing associated with transmission tower bases,’’ National grid research report, 2004.

Chapter Four

[4.1] *IEEE Guide for Safety in AC Substations*, ANSI/IEEE Standard 80, 2000.

[4.2] *Effects of Current on Human Beings and Livestock, Part 1: General aspects,* IEC TS 60479-1:2005, 2005.

[4.3] Meliopoulos A.P.S.: "Lightning: safety and protection," Lightning Protection of Wind Turbines IEE Half-Day Colloquium, pp. 711-717, UK, 1997

[4.4] M. Nayel, J. Zhao, J. He, Z. Cai and Q. Wang: “Study of step and touch voltages in resistive/capacitive ground due to lightning stroke,” The 4th Asia-Pacific Conference on Environmental Electromagnetics (CEEM), vol. 2, pp. 56-60, China, 2006.

[4.5] E. Cherney, K. Ringler, N. Kolcio and G. Bell: “Step and touch potentials at faulted transmission towers,” IEEE Transaction on Power Apparatus and

Systems, vol. PAS-100, No. 7,pp. 3312-3321, 1981.

[4.6] Working Group on Transmission Line Structure Grounding, Towers, Poles and Conductors Subcommittee: "Background and methodology for analysing step and touch potentials near transmission structures part I background," IEEE Transactions on Power System, vol. PWRD-1, No. 2, pp. 150-157, 1986.

[4.7] Dawalibi F. and Finney W.G.: "Transmission line tower grounding performance in non-uniform soil," IEEE Transactions on Power Apparatus and Systems, vol. PAS-99, N. 2, pp. 471-479, 1980.

[4.8] R. Kosztaluk, D. Mukhedkar and Gervais: "Field measurements of step and touch voltages," IEEE Transactions on Power Apparatus and Systems, vol. PAS-103, No. 11, pp. 3286-3294, 1984.

[4.9] N. Harid, N. Ullah, M. Ahmeda, H. Griffiths and A. Haddad: "Experimental evaluation of potential rise and step and touch voltages at high voltage tower under Lightning Impulse ", ISH, pp. 1651- 1656, South Africa, 2009.

Chapter Five

[5.1] P. L. Bellaschi: ''Impulse and 60-Cycle Characteristics of Driven Grounds,'' AIEE Transactions, Vol. 60, No. pp. 123-128, 1941.

[5.2] P. L. Bellaschi, R. E. Armington and A. E. Snowden: ''Impulse and 60-Cycle Characteristics of Driven Grounds-II,'' AIEE Transaction, Vol. 61, pp. 349-363, 1942.

[5.3] A. C. Liew: 'Dynamic Model of Impulse Characteristics of Concentrated Earths' IEE, Vol. 121,No. 2, pp. 123-135, 1974.

[5.4] Takeushi, M., Yasuda Y., Fukuzono, H., Kawabata, K., Hara, T., and Sekioka, S.: ''Impulse Characteristics of a 500kV Transmission Tower Footing Base

with Various Grounding Electrodes,'' International Conference on Lightning Protection (ICLP), pp. 513-517, UK, 1998.

[5.5] R. Koztaluk, M. Loboda and D. Mukhedkar: ''Experimental Study of Transient Ground Impedances,'' IEEE Transactions on Power Apparatus and Systems, Vol. PAS-100, No. 11, pp. 4653-4660, 1981

[5.6] Korsunscev A. V.: ''Application of the Theory of Similitude to the Calculation of Surge Characteristics of Concentrated Earth Electrodes,'' Electrichestvo, No.5, pp. 31-35, 1958.

[5.7] N. Mohamad Nor, A. Haddad, and H. Griffiths: ''Characteristics of Ionisation Phenomena in Soils under Fast Impulses,'' IEEE Transactions on Power Delivery, vol. 21, No. 1, pp. 353-361, 2006.

[5.8] Meliopoulos A. P. S.: ''Lightning: Safety and Protection,'' Lightning Protection of Wind Turbines IEE Half-Day Colloquium, pp. 711-717, UK, 1997

[5.9] Mohamad Nayel, Jie Zhao, Jinliang He, Zongyuan Cai and Qi Wang: ''Study of Step and Touch Voltages in Resistive/Capacitive Ground Due to Lightning Stroke'' 4th Asia-Pacific Conference on Environmental Electromagnetic (CEEM'2006), vol. 2, pp. 56-60, China, 2006.

[5.10] Vernon Cooray, ''*Soil Ionization*,'' in *Lightning Protection* Vernon Cooray, London: IET, 2010, pp. 531-551

Chapter Six

[6.1] Mazetti C. and Veca G.M.: ''Impulse behavior of grounding electrodes,'' IEEE Transaction Power Apparatus and Systems, vol. PAS-102, No. 9, pp.

3148-3154, 1983.

[6.2] S Ghosh, S Munshi, and J R Biswas: "Computer aided analysis of surge behaviour of an earthing counterpoise discharging impulse current to ground," Journal of the Institution of Engineers India, vol. 77, pp.128-132, 1996.

[6.3] J. He, Y. Gao, R. Zeng, J. Zou, X. Liang, B. Zhang, J. Lee and S. Chang: ''Effective length of counterpoise wire under lightning current,'' IEEE Transaction on Power Delivery, vol. 20, No.2, pp. 1585-1591, 2005.

[6.4] A. K. Mishra, A. Ametani, N. Nagaoka and S. Okabe: ''Non-uniform characteristics of a horizontal grounding electrode,'' IEEE Transaction On Power Delivery, Vol. 22, No. 4, pp. 2327 2334, 2007.

[6.5] J., He, R. Zeng, C. Sheuiming, S. Li, and W. Weihan: "Impulse characteristics of grounding systems of transmission-line towers in the regions with high soil resistivity," International Conference on Power System Technology Proceedings (powercon), vol. 1, pp. 156-162, China, 1998.

[6.6] Tagg, G. F. 'Earth Resistance', George Newnes Ltd, London, 1964.

[6.7] Safe Engineering Services, "Current distribution electromagnetic grounding analysis software (CDEGS)," Canada, 2006.

[6.8] B. P. Gupta and B. Thapar: ''Impulse characteristics of grounding electrodes,'' Journal of the Institution of Engineers India, vol. 64, no.4, pp. 178-182, February 1981.